

## ABSTRACT

Title of Document: Expanding the Range of Polyolefins through  
Living Coordinative Chain Transfer  
Polymerization

Jia Wei, Doctor of Philosophy, 2012

Directed By: Professor Lawrence R. Sita  
Department of Chemistry and Biochemistry

The strategy, termed living coordinative chain-transfer polymerization (LCCTP), has been explored to boost the efficiency and versatility of polyolefin synthesis by coupling a reversible chain-transfer process with living coordination polymerization. LCCTP strategy not only overcomes the “one-chain-per-metal” limit on polymerization yield, but also provides opportunities to flourish the architectural, compositional and functional flexibility of polyolefin-based materials.

A new strategy, named ternary living coordinative chain-transfer polymerization (t-LCCTP), extends the LCCTP methodology through employing the rapid and reversible chain-transfer process under living conditions between an active transition-metal propagating species, a primary surrogate  $\text{AlR}_3$ , and a catalytic amount of  $\text{ZnEt}_2$  as a secondary surrogate and chain-transfer mediator. This strategy

provides a cost-effective, scalable process for the production of precision hydrocarbons, such as the low-molecular-weight oligomers from propene and  $\alpha$ -olefins under near-ambient conditions. Having the advantage of using  $\text{AlR}_3$  and  $\text{ZnR}_2$  as surrogate chain-growth sites, block and end-group functionalized polyolefin-based materials have been synthesized directly through chemical reactions of the Al-C/Zn-C bonds.

Rapid and reversible chain-transfer between “tight” and “loose” ion pairs has been used to modulate the relative reactivities of ethene and 1-hexene or cyclopentene in a programmed fashion for LCCTP. Thus, different grades of a monodisperse polyolefin copolymer, such as the poly(ethene-*co*-1-hexene), have been obtained with a single cationic transition-metal catalyst. Through employing long chain  $\alpha$ -olefins as co-monomers, a novel class of polyethene-based waxes has been synthesized with precisely tunable side-chain crystalline sizes.

The discovery of a fundamentally novel Group 4 transition-metal binuclear catalyst has achieved the highly challenging goal of making ethene/propene (E/P) multi-block copolymers through steric-control over the “regional” and “local” hindrance around the binuclear catalyst molecule. Structural, thermal, surface morphological and mechanical characterizations of these E/P blocky materials unambiguously reveal their blocky nature and unique physical properties regarding to the traditional E/P random copolymers. Finally, LCCTP has been successfully coupled with this binuclear catalyst to provide a variety of polyethene-based blocky copolymers under chain-transfer conditions.

EXPANDING THE RANGE OF POLYOLEFINS THROUGH LIVING  
COORDINATIVE CHAIN TRANSFER POLYMERIZATION

By

Jia Wei

Thesis submitted to the Faculty of the Graduate School of the  
University of Maryland, College Park, in partial fulfillment  
of the requirements for the degree of  
Doctor of Philosophy  
2012

Advisory Committee:  
Professor Lawrence R. Sita, Chair  
Professor Bryan W. Eichhorn  
Professor Jeffery T. Davis  
Professor Andrei Vedernikov  
Professor Robert M. Briber

© Copyright by  
Jia Wei  
2012

## Acknowledgements

First of all, I would like to thank my advisor, Dr. Lawrence R. Sita for his continuous support of both my research and personal life. His profound knowledge in the area of organometallics and polymer science helped me build up the foundation of a chemist. His enthusiasm in chemistry constantly encouraged me. The skills that I learned while in his research group will benefit my career forever.

Secondly, I will extend my gratitude to my committee, Dr. Eichhorn, Dr. Davis, Dr. Vedernikov and Dr. Briber, for their great help both in my classes and on my research. Without their support, this work would not have been possible.

I also want to thank all the previous and present members in the Sita group who worked with me for their help and friendship. Special thanks to Dr. Wei Zhang, Rennisha Wickham, Brendan Yonke, Wonseok Hwang, Cathryn Blakley and Kaitlyn Crawford for useful discussion and the time we have experienced in the laboratory.

Moreover, I thank my wife, Lulu Xu and my daughter, Qianqian Wei for their invaluable love and confidence. Also thanks to my parents, Shaoyu Wei and Houjing Ding and parents-in-law, Xuening Xu and Xiaoling Hou, for their love and indispensable support to my family.

Finally, I am thankful to the Ann G. Wylie Dissertation Fellowship from the Graduate School at the University of Maryland to support my thesis writing.

# Table of Contents

Acknowledgements.....	ii
Table of Contents.....	iii
List of Abbreviations .....	viii
List of Numbered Compounds.....	ix
List of Tables .....	x
List of Figures.....	xi
List of Schemes.....	xiv
Chapter 1: Introduction.....	1
1.1 A Brief History of Coordination Polymerization .....	1
1.1.1 Heterogeneous Ziegler-Natta polymerization.....	1
1.1.2 Homogeneous metallocene and post-metallocene catalysts .....	2
1.2 Living Coordination Polymerization .....	6
1.2.1 Living polymerization.....	6
1.2.2 Living coordination polymerization.....	8
1.2.3 An example of stereospecific living polymerization of 1-hexene .....	11
1.2.4 Living degenerative group-transfer coordination polymerization .....	12
1.3 Living Coordinative Chain-Transfer Polymerization (LCCTP).....	15
1.3.1 Coordinative chain-transfer polymerization (CCTP).....	15
1.3.2 Living coordinative chain-transfer polymerization (LCCTP) .....	18
1.3.3 An example of chain shuttling polymerization .....	21
1.3.4 Challenges and opportunities in the area of LCCTP .....	22
Chapter 2: Ternary Living Coordinative Chain-Transfer Polymerization of Propene and Higher $\alpha$ -Olefins.....	23

2.1 Background.....	23
2.1.1 Aufbaureaktion and chain-growth on aluminum process .....	23
2.1.2 Catalyzed polypropene chain-growth on aluminum .....	24
2.2 Ternary Living Coordinative Chain-Transfer Polymerization (t-LCCTP).....	26
2.2.1 Proposed mechanism of t-LCCTP .....	26
2.2.2 t-LCCTP of propene using mixed $\text{AlR}_3$ and $\text{ZnEt}_2$ .....	29
2.2.3 Study on the induction period of $\text{AlR}_3$ mediated t-LCCTP .....	34
2.2.4 t-LCCTP with catalytic amount of $\text{ZnEt}_2$ relative to $\text{AlR}_3$ .....	36
2.3 Scalable Production of Precision Hydrocarbons from $\text{AlR}_3$ via t-LCCTP.....	38
2.4 t-LCCTP Copolymerization of Propene with 1-Octene .....	40
2.5 Conclusions.....	42
Chapter 3: Preparation of Block and End-Group Functionalized Precision Polyolefins through LCCTP .....	23
3.1 Background.....	43
3.1.1 End-group functionalization through living coordination polymerization	43
3.1.2 Coordinative chain-transfer strategy for end-group functionalization.....	45
3.2 Preparation and Stability Study on $\text{Zn}(\text{polymeryl})_2$ Stock Solution.....	47
3.3 Ring-Opening Polymerization of $\epsilon$ -Caprolactone from $\text{Zn}(\text{O-polyolefin})_2$ .....	49
3.3.1 Synthesis and characterization of <i>aPP-block-PCL</i> .....	49
3.3.2 Synthesis and characterization of <i>PE-block-PCL</i> .....	51
3.4 Synthesis of Iodo-Terminated Polyolefins from $\text{Zn}(\text{polymeryl})_2$ .....	52
3.4.1 Synthesis and characterization of 1-iodo- <i>aPP</i> .....	52
3.4.2 Synthesis of 1-iodo-terminated ethene-based copolymers .....	54
3.5 Ethene and Propene Block Copolymer Synthesis and Integrity Study.....	55
3.5.1 E/P block copolymer via $\text{Zn}(\text{PE})_2$ .....	55
3.5.2 E/P block copolymer via $\text{Zn}(\text{aPP})_2$ .....	59
3.6 Synthesis and Characterization of 1-Lithio- <i>aPP</i> and its Derivatives.....	61
3.6.1 Synthesis and characterization of 1-lithio- <i>aPP</i> .....	61
3.6.2 Synthesis of 1-carboxy- <i>aPP</i> and 1-hydroxymethyl- <i>aPP</i> .....	63
3.7 Conclusions.....	66

Chapter 4: Modulation of Copolymer Compositions through Reversible Chain-Transfer between “Tight” and “Loose” Ion Pairs .....	67
4.1 Background .....	67
4.2 Study on Anion Exchange between “Tight” and “Loose” Ion Pairs .....	70
4.3 Proposed Strategy of Chain-Transfer between “Tight” and “Loose” Ion Pairs .....	73
4.4 Copolymerization of Ethene with $\alpha$ -Olefins in Toluene Solution.....	74
4.4.1 Kinetic studies on LCCTP using mixed ion-pair initiators.....	74
4.4.2 Modulation of 1-hexene incorporation levels .....	76
4.4.3 Modulation of propene incorporation levels .....	79
4.5 Copolymerization of Ethene with 1-Hexene in Neat 1-Hexene .....	81
4.5.1 Synthesis of poly(E- <i>co</i> -H) materials.....	81
4.5.2 Compositional characterization of poly(E- <i>co</i> -H) materials.....	84
4.5.3 Thermal analysis of poly(E- <i>co</i> -H) materials.....	87
4.6 Copolymerization of Ethene with Cyclopentene .....	88
4.6.1 Synthesis and characterization of 1-iodo-poly(E- <i>co</i> -CPE) materials .....	88
4.6.2 MALDI-TOF-MS analysis of 1-iodo-poly(E- <i>co</i> -CPE) materials.....	90
4.7 Conclusions.....	92
Chapter 5: Preparation of Precision Polyolefin Waxes through LCCTP	
Copolymerization of Ethene with Long Chain $\alpha$ -Olefin Co-monomers .....	93
5.1 Background.....	93
5.2 LCCTP Copolymerization of Ethene with 1-Hexadecene.....	95
5.2.1 Synthesis of poly(E- <i>co</i> -HDE)s with varying molecular weights.....	95
5.2.2 Structural and thermal analysis of poly(E- <i>co</i> -HDE)s .....	97
5.3 Modulation of Side-Chain Lengths.....	100
5.3.1 Synthesis of copolymers with varying side-chain lengths .....	100
5.3.2 Influence of side-chain length on polyolefin wax property .....	102
5.3.3 A scaled-up copolymerization to produce poly(E- <i>co</i> -ODE) wax.....	103
5.4 Modulation of Co-monomer Incorporation Levels.....	104
5.4.1 Synthesis of poly(E- <i>co</i> -HDE)s with varying HDE incorporation levels .	104
5.4.2 Influence of HDE incorporation level on wax property .....	106

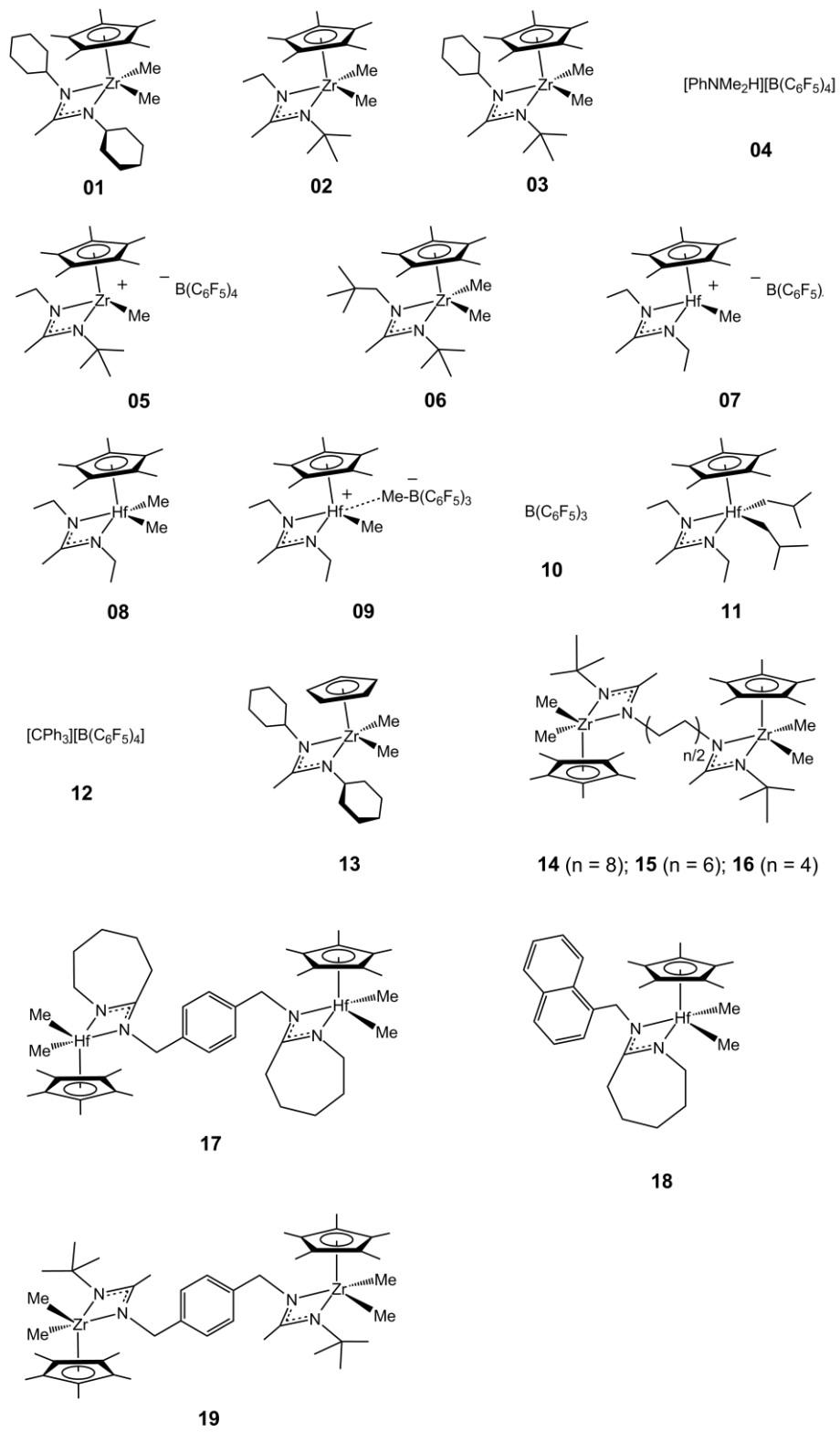
5.5 ODE-based Homo-, Co- and Ter-polymers and Diblock Copolymers.....	107
5.5.1 Synthesis of ODE-based homo-, co- and ter-polymers .....	107
5.5.2 WAXD study on ODE-based homo-, co- and ter-polymers .....	110
5.5.3 Synthesis and characterization of ODE-based diblock copolymers .....	111
5.6 Conclusions.....	113
Chapter 6: Synthesis and Characterization of Ethene/Propene Multi-Block Copolymers through “Regional” Steric-Control Mechanism using a Binuclear Hafnium Catalyst.....	
6.1 Background.....	115
6.1.1 Polyolefin-based Block Copolymers .....	115
6.1.2 Multi-nuclear olefin polymerization catalyst systems .....	116
6.2 A Novel Binuclear Catalyst and Proposed Steric-Control Mechanism.....	118
6.2.1 Design and synthesis of a hafnium binuclear catalyst .....	118
6.2.2 Proposed steric-control mechanism for block copolymer synthesis.....	120
6.3 Mechanistic Study using E/H Polymerization System .....	122
6.4 Copolymerization of E/P using Binuclear and Mononuclear Catalysts .....	125
6.4.1 Synthesis and characterization of E/P copolymers .....	125
6.4.2 Study on monomer sequence distributions and relative reactivities .....	128
6.4.3 Binuclear catalyst generality study .....	130
6.5 Characterization of E/P Block and Random Copolymers .....	130
6.5.1 Structural characterization of <i>b</i> -E/P and <i>r</i> -E/P copolymers.....	130
6.5.2 Surface morphological characterization of <i>b</i> -E/P and <i>r</i> -E/P copolymers	133
6.5.3 Mechanical property characterization of <i>b</i> -E/P and <i>r</i> -E/P copolymers ...	135
6.6 LCCTP Copolymerization of E with $\alpha$ -Olefins using Binuclear Catalysts....	137
6.6.1 LCCTP copolymerization of E with P.....	137
6.6.2 LCCTP copolymerization of E with $\alpha$ -olefins.....	139
6.7 Conclusions.....	141
Chapter 7: Conclusions.....	142
Appendix: Experimentals .....	144

References: ..... 156

## List of Abbreviations

CCTP	coordinative chain-transfer polymerization
LCCTP	living coordinative chain-transfer polymerization
t-LCCTP	ternary living coordinative chain-transfer polymerization
ATRP	atom transfer radical polymerization
RAFT	reversible addition–fragmentation chain transfer
ROMP	ring-opening metathesis polymerization
Cp	cyclopentadienyl ( $\eta^5$ -C <sub>5</sub> H <sub>5</sub> )
Cp*	pentamethylcyclopentadienyl ( $\eta^5$ -C <sub>5</sub> Me <sub>5</sub> )
CpAm	monocyclopentadienyl monoamidinate
PE	polyethene
PP	polypropene
<i>iso</i> PP	isotactic polypropene
<i>a</i> PP	atactic polypropene
<i>s</i> PP	syndiotactic polypropene
PH	poly(1-hexene)
PO	poly(1-octene)
PHC	precision hydrocarbons
$M_n$	number average molecular weight
$M_w$	weight average molecular weight
PDI	polydispersity index ( $M_w / M_n$ )
$T_m$	melting temperature
$T_c$	crystallization temperature
$T_g$	glass transition temperature
GPC	gel permeation chromatography
DSC	differential scanning calorimetry
AFM	atomic force microscopy
WAXD	wide-angle X-ray diffraction
MALDI-TOF	matrix-assisted laser-desorption time-of-flight

## List of Numbered Compounds



## List of Tables

<i>Table 1.</i> LCCTP and t-LCCTP of propene .....	29
<i>Table 2.</i> t-LCCTP copolymerization of propene with 1-octene .....	40
<i>Table 3.</i> Kinetic studies of LCCTP copolymerization of ethene with 1-hexene .....	75
<i>Table 4.</i> LCCTP copolymerization results of ethene with 1-hexene in toluene .....	78
<i>Table 5.</i> LCCTP copolymerization results of ethene with propene in toluene .....	80
<i>Table 6.</i> LCCTP copolymerization of ethene with 1-hexene in neat 1-hexene .....	82
<i>Table 7.</i> Diads analysis and calculated relative reactivities of ethene and 1-hexene .	84
<i>Table 8.</i> Results of the 1-iodo-poly(E-co-CPE) materials .....	88
<i>Table 9.</i> Results of LCCTP copolymerization of ethene with 1-hexadecene .....	96
<i>Table 10.</i> Results of LCCTP copolymerization of ethene with long chain $\alpha$ -olefins .....	101
<i>Table 11.</i> Modulation of HDE incorporation levels .....	105
<i>Table 12.</i> Results of homo-, co- and ter-polymer based on ODE.....	107
<i>Table 13.</i> Mechanistic study on binuclear and mononuclear catalyst systems.....	123
<i>Table 14.</i> Copolymerization of E/P using binuclear and mononuclear catalysts .....	126
<i>Table 15.</i> Results of diads analysis, relative reactivities and average sequence lengths of E/P copolymers .....	128
<i>Table 16.</i> Large scale synthesis of <i>b</i> -E/P and <i>r</i> -E/P copolymers.....	131
<i>Table 17.</i> LCCTP copolymerization of E and P using binuclear and mononuclear catalysts .....	137
<i>Table 18.</i> Results of thermal and structural analysis of E/P copolymers through LCCTP .....	138
<i>Table 19.</i> LCCTP copolymerization of E and $\alpha$ -olefins using binuclear catalyst <b>17/04</b> .....	140
<i>Table 20.</i> Results of thermal and structural analysis of E/ $\alpha$ -olefin copolymers .....	140

## List of Figures

<i>Figure 1.</i> Relationship of isotactic PP material property with the melting temperature and concentration of <i>rr</i> defects of stereoregularity. ....	4
<i>Figure 2.</i> Examples of highly active post-metallocene olefin polymerization catalysts .....	5
<i>Figure 3.</i> Examples of Group 4 precursors for living coordination polymerization ..	10
<i>Figure 4.</i> Structures of three Cp*ZrMe <sub>2</sub> [N(R <sup>1</sup> )C(Me)N(R <sup>2</sup> )] catalyst precursors .....	11
<i>Figure 5.</i> Molecular weight distributions for PPs obtained with varying amount of ZnEt <sub>2</sub> .....	20
<i>Figure 6.</i> <sup>1</sup> H NMR spectra of a 1 : 1 ratio Al <i>i</i> Bu <sub>3</sub> and ZnEt <sub>2</sub> mixture (top), pure Al <i>i</i> Bu <sub>3</sub> (middle) and pure ZnEt <sub>2</sub> (bottom).....	28
<i>Figure 7.</i> Molecular weight distributions for aPPs of entry 2.05, 2.06, 2.07 (from left to right) of Table 1 and a polystyrene standard (dotted line) .....	31
<i>Figure 8.</i> <sup>13</sup> C NMR spectrum and structural drawings of aPP from entry 2.06 of Table 1 .....	32
<i>Figure 9.</i> <sup>13</sup> C NMR spectrum and structural drawings of aPP from entry 2.07 of Table 1 .....	33
<i>Figure 10.</i> AlMe <sub>3</sub> complexation with dimethyl zirconocene during activation process	34
<i>Figure 11.</i> Molecular weight distributions for aPP products obtained from the LCCTP (red dashed curve) and t-LCCTP (blue solid curve) of propene.....	37
<i>Figure 12.</i> A new PHC-based aPP oil prepared by scaled-up t-LCCTP (left) and the photos of polymerization reaction flask at 0 h (middle) and 72 h (right).	39
<i>Figure 13.</i> Molecular weight distributions for poly(P- <i>co</i> -O) materials made from t-LCCTP (blue curve) and LCCTP (red curve).....	41
<i>Figure 14.</i> Stability study through <sup>1</sup> H NMR spectroscopy of Zn(aPP) <sub>2</sub> /toluene stock solution.....	48
<i>Figure 15.</i> <sup>1</sup> H NMR spectra of aPP- <i>block</i> -PCL (bottom) and ε-caprolactone (top) ..	51
<i>Figure 16.</i> <sup>1</sup> H NMR spectra and resonance assignments of 2-methyl-ω-iodo-PE .....	52
<i>Figure 17.</i> <sup>1</sup> H NMR spectrum and resonance assignments of 1-iodo-aPP.....	53
<i>Figure 18.</i> <sup>13</sup> C { <sup>1</sup> H} NMR spectrum and resonance assignments of 1-iodo-aPP.....	54
<i>Figure 19.</i> <sup>13</sup> C { <sup>1</sup> H} NMR spectra and resonance assignments of poly(P- <i>block</i> -E) ..	57
<i>Figure 20.</i> <sup>1</sup> H NMR spectra and resonance assignments of 1-iodo-poly(P- <i>block</i> -E).	58
<i>Figure 21.</i> <sup>13</sup> C { <sup>1</sup> H} NMR spectra and resonance assignments of 1-iodo-poly(P- <i>block</i> -E).....	59

Figure 22. $^1\text{H}$ NMR end-group analysis of blocky integrity of poly(E- <i>block</i> -P) .....	61
Figure 23. $^{13}\text{C}$ { $^1\text{H}$ } NMR spectra and resonance assignments of 1-deuterio- <i>a</i> PP ....	63
Figure 24. $^1\text{H}$ NMR spectrum and resonance assignments of 1-carboxy- <i>a</i> PP .....	64
Figure 25. $^{13}\text{C}$ { $^1\text{H}$ } NMR spectrum and resonance assignments of 1-carboxy- <i>a</i> PP. 64	
Figure 26. $^1\text{H}$ NMR spectrum and resonance assignments of 1-hydroxymethyl- <i>a</i> PP 65	
Figure 27. $^{13}\text{C}$ { $^1\text{H}$ } NMR spectrum and resonance assignments of 1-hydroxymethyl- <i>a</i> PP .....	65
Figure 28. Transition metal complex ion pairs.....	67
Figure 29. Sketch structures of (1,2-Me <sub>2</sub> Cp) <sub>2</sub> ZrMe <sup>+</sup> MeB(C <sub>6</sub> F <sub>5</sub> ) <sub>3</sub> <sup>-</sup> (left) and Cp* <sub>2</sub> ThMe <sup>+</sup> -B(C <sub>6</sub> F <sub>5</sub> ) <sub>4</sub> <sup>-</sup> (right) .....	69
Figure 30. Plots of $M_n$ vs. $t_p$ (▲) and 1-hexene incorporation levels vs. $t_p$ (●) .....	76
Figure 31. Plot of H molar percentage vs. loose ion pair concentration .....	79
Figure 32. Molecular weight distributions of poly(E- <i>co</i> -H) samples of entries 4.17 to 4.22 (from right to left) of Table 6.....	82
Figure 33. H incorporation levels vs. loose ion pair concentrations .....	83
Figure 34. Co-monomer relative reactivities, $r_H$ and $r_E$ vs. loose ion pair concentrations .....	85
Figure 35. $^{13}\text{C}$ NMR triads analysis of poly(E- <i>co</i> -H) samples in Table 6 .....	86
Figure 36. Photos of poly(E- <i>co</i> -H)s of entries 4.17 to 4.22 (from left to right) of Table 6 .....	86
Figure 37. DSC traces for poly(E- <i>co</i> -H) materials of entry 4.17 to 4.22 of Table 4..	87
Figure 38. $^{13}\text{C}$ { $^1\text{H}$ } NMR analysis of 1-iodo-poly(E- <i>co</i> -CPE) of entry 4.24 in Table 8.....	89
Figure 39. MALDI-TOF-MS spectra of the $\alpha$ -[I][Ph <sub>3</sub> P]-poly(E- <i>co</i> -CPE) materials described in Table 8, a) entry 4.25, b) entry 4.24, and c) entry 4.23 .....	90
Figure 40. DSC traces for 1-iodo-poly(E- <i>co</i> -CPE) materials .....	91
Figure 41. Molecular weight distributions of poly(E- <i>co</i> -HDE) samples of Table 9..	97
Figure 42. $^{13}\text{C}$ { $^1\text{H}$ } NMR spectrum and assignments of poly(E- <i>co</i> -HDE) of entry 5.03 in Table 9 .....	98
Figure 43. DSC thermograms of poly(E- <i>co</i> -HDE) of entry 5.03 in Table 9.....	99
Figure 44. DSC thermograms of entries 5.06 to 5.10 in Table 10 .....	103
Figure 45. Poly(E- <i>co</i> -ODE) wax stars of entry 5.11 in Table 10.....	104
Figure 46. DSC thermograms of samples in Table 11 .....	106

<i>Figure 47.</i> DSC thermograms of samples in Table 12 .....	108
<i>Figure 48.</i> $^{13}\text{C}$ $\{^1\text{H}\}$ NMR spectrum and assignments of poly(ODE) of entry 5.17	108
<i>Figure 49.</i> $^{13}\text{C}$ $\{^1\text{H}\}$ NMR spectrum and assignments of poly(E-co-ODE) of entry 5.18.....	109
<i>Figure 50.</i> $^{13}\text{C}$ $\{^1\text{H}\}$ NMR spectrum and assignments of poly(E-co-H-co-ODE) of entry 5.19 .....	109
<i>Figure 51.</i> WAXD Data of ODE-based homo-, co- and ter-polymers of Table 12 .	110
<i>Figure 52.</i> DSC thermograms of 1 <sup>st</sup> block (top) and diblock (bottom) of poly(ODE)-block-poly(E-co-ODE).....	112
<i>Figure 53.</i> Structure of binuclear compounds <b>14–16</b> .....	117
<i>Figure 54.</i> Structures of binuclear compound <b>17</b> and mononuclear analogue <b>18</b> ....	118
<i>Figure 55.</i> Molecular weight distributions of PHs using mononuclear catalyst <b>18/04</b> (top) and binuclear catalyst <b>17/04</b> (bottom) .....	123
<i>Figure 56.</i> Molecular weight distributions of sequential monomer addition of E followed by H using mononuclear catalyst <b>18/04</b> (top) and binuclear catalyst <b>17/04</b> (bottom) .....	124
<i>Figure 57.</i> Triads analysis of E/P copolymers made from binuclear catalyst <b>17/04</b> (top) and mononuclear catalyst <b>18/04</b> (bottom).....	129
<i>Figure 58.</i> $^{13}\text{C}$ NMR spectrum of <i>b</i> -E/P copolymer (entry 6.13 of Table 16).....	132
<i>Figure 59.</i> $^{13}\text{C}$ NMR spectrum of <i>r</i> -E/P copolymer (entry 6.14 of Table 16) .....	132
<i>Figure 60.</i> AFM images of <i>r</i> -E/P (entry 6.14, top) and <i>b</i> -E/P (entry 6.13, bottom).	134
<i>Figure 61.</i> Photo images of <i>r</i> -E/P (left clear film) and <i>b</i> -E/P (right opaque film) ...	134
<i>Figure 62.</i> Plot of storage modulus vs. temperature of <i>r</i> -E/P (red diamond) and <i>b</i> -E/P (blue circle) materials .....	135
<i>Figure 63.</i> Plot of $\tan \delta$ vs. temperature of <i>r</i> -E/P (red diamond) and <i>b</i> -E/P (blue circle) materials .....	136

## List of Schemes

<i>Scheme 1.</i> Cossee mechanism for Ziegler-Natta polymerization .....	2
<i>Scheme 2.</i> Proposed MAO activation processes for metallocenes .....	3
<i>Scheme 3.</i> Mechanisms of propagation and chain transfer in coordination polymerization .....	8
<i>Scheme 4.</i> Synthesis of block copolymers with a vanadium catalyst .....	10
<i>Scheme 5.</i> Synthesis of <i>iso</i> PH- <i>block</i> -PMCP- <i>block-iso</i> PH triblock copolymer .....	12
<i>Scheme 6.</i> Mechanism of stereoerror incorporation that occurs under living degenerative methyl group-transfer conditions .....	13
<i>Scheme 7.</i> Synthesis of <i>iso</i> PP- <i>block-a</i> PP- <i>block-iso</i> PP stereoblock elastomer .....	14
<i>Scheme 8.</i> Mechanism of coordinative chain-transfer polymerization (CCTP) .....	16
<i>Scheme 9.</i> Iron complex catalyzed PE chain-growth on zinc .....	17
<i>Scheme 10.</i> CCTP of propene using cationic <b>07</b> with ZnEt <sub>2</sub> as surrogate .....	19
<i>Scheme 11.</i> Mechanism of chain-shuttling copolymerization of ethene and 1-octene	21
<i>Scheme 12.</i> Aufbaureaktion and Alfen Process .....	23
<i>Scheme 13.</i> Ternary living coordinative chain-transfer polymerization (t-LCCTP) of propene .....	26
<i>Scheme 14.</i> t-LCCTP of propene with mixed AlR <sub>3</sub> and ZnEt <sub>2</sub> surrogates.....	30
<i>Scheme 15.</i> Synthesis of compound Cp*Hf( <i>i</i> Bu) <sub>2</sub> [N(Et)C(Me)N(Et)] ( <b>11</b> ).....	35
<i>Scheme 16.</i> Modified procedure of t-LCCTP of propene to avoid induction period..	36
<i>Scheme 17.</i> Synthesis of end-group functionalized polypropene with a vanadium catalyst.....	44
<i>Scheme 18.</i> Versatile pathways for in situ polyolefin functionalization with heteroatoms .....	45
<i>Scheme 19.</i> Mechanism of the initiation step for coordination–insertion ring-opening polymerization.....	49
<i>Scheme 20.</i> One pot synthesis of <i>a</i> PP- <i>block</i> -PCL .....	50
<i>Scheme 21.</i> Synthesis of 1-iodo-poly(E- <i>co</i> -MCP), 1-iodo-poly(E- <i>co</i> -VCH) and 1-iodo-poly(E- <i>co</i> -CPE).....	55
<i>Scheme 22.</i> Synthesis of poly(P- <i>block</i> -E) and 1-iodo-poly(P- <i>block</i> -E) via Zn(PE) <sub>2</sub> .	56
<i>Scheme 23.</i> Synthesis of 1-iodo-poly(E- <i>block</i> -P) via Zn( <i>a</i> PP) <sub>2</sub> stock solution (with 1-iodo- <i>a</i> PP as a byproduct) .....	60

<i>Scheme 24.</i> End-group functionalized PP materials from 1-iodo- <i>a</i> PP .....	62
<i>Scheme 25.</i> Synthesis of “loose” and “tight” ion-pair initiators .....	71
<i>Scheme 26.</i> Copolymerization of ethene with 1-hexene using mixed “loose” and “tight” ion pairs and GPC analysis of the resulting copolymers .....	72
<i>Scheme 27.</i> Proposed mechanism of LCCTP between “tight” and “loose” ion-pair initiators .....	73
<i>Scheme 28.</i> LCCTP copolymerization of E with H using mixed loose and tight ion pairs in the presence of ZnEt <sub>2</sub> .....	77
<i>Scheme 29.</i> LCCTP copolymerization of E with long chain $\alpha$ -olefins .....	95
<i>Scheme 30.</i> Synthesis of poly(ODE)- <i>block</i> -poly(E- <i>co</i> -ODE) .....	111
<i>Scheme 31.</i> Proposed mechanism of urea hydrolysis into carbon dioxide and ammonia mediated by the urease enzyme .....	116
<i>Scheme 32.</i> Two-step synthesis of binuclear compound <b>17</b> .....	119
<i>Scheme 33.</i> Proposed “regional” and “local” steric-control mechanism of copolymerization of ethene with propene using binuclear precatalyst <b>17</b> .....	121

# Chapter 1: Introduction

## 1.1 A Brief History of Coordination Polymerization

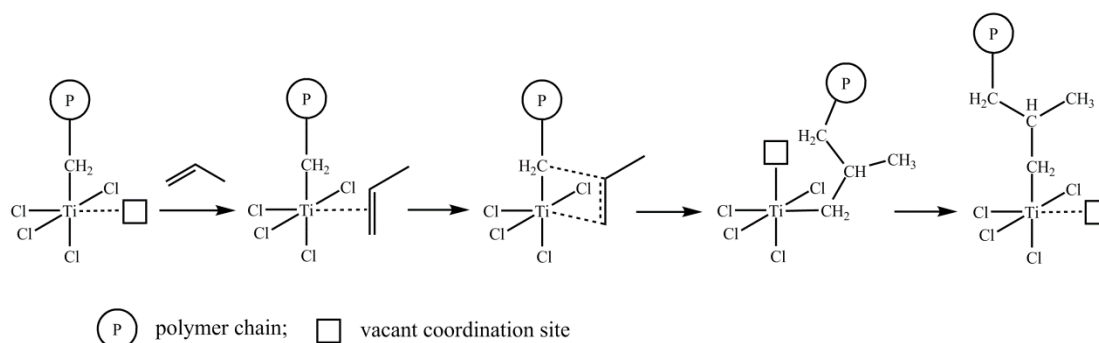
### 1.1.1 Heterogeneous Ziegler-Natta polymerization

Coordination polymerization is also known as Ziegler-Natta polymerization to memorialize the revolutionary work by the 1963 chemistry Nobel laureates, Karl Ziegler and Giulio Natta.<sup>1, 2</sup> In the early 1950s, Karl Ziegler<sup>3</sup> in Germany discovered that certain combinations of transition metal compounds and organometallic compounds, such as  $\text{TiCl}_4$  and  $\text{AlEt}_2\text{Cl}$ , polymerized ethene at low temperatures and pressures to give polyethene (PE) that has an essentially linear structure. Now referred to as high-density polyethene (HDPE), the product is denser, tougher, and higher melting than the branched low-density polyethene (LDPE), and is used for bottles, pipes, film, wires etc. Following close on the heels of Ziegler's discovery was the recognition by Giulio Natta<sup>4</sup> in Italy that the same type of catalysts was capable of polymerizing propene to yield stereoregular isotactic polypropene (PP) that is also crystalline. Ziegler-Natta polymerization is usually referred to a heterogeneous system such as that discovered by Ziegler and the  $\text{MgCl}_2$ -supported  $\text{TiCl}_4$  system discovered by Kashiwa.<sup>5, 6</sup> Coordination polymerization usually represents a homogeneous single-site metallocene or post-metallocene system which will be discussed later.

Unlike free radical or ionic initiators, the Ziegler-Natta polymerization catalysts are not consumed in the polymerization. Therefore, the active chain propagation species is referred to as a "catalyst", not an "initiator", to emphasize the fundamental catalytic event of

monomer enchainment (in some cases, initiator is also used to emphasize the chain-growth process). The most widely accepted polymerization mechanism was proposed by Cossee and Arlman.<sup>7, 8</sup> As shown in Scheme 1, Cossee mechanism occurs as follows: 1) olefin side-on coordination to a vacant site which activates the C–C double bond; 2) migratory insertion of the  $\delta$ -coordinated polymer chain to the  $\pi$ -coordinated olefin *via* a four-member ring transition state; 3) the polymer chain is lengthened by one monomer unit, and a new vacant site is produced which was originally occupied by the polymer chain. This Cossee process can be repeated while the polymer chain keeps growing.

*Scheme 1.* Cossee mechanism for Ziegler-Natta polymerization

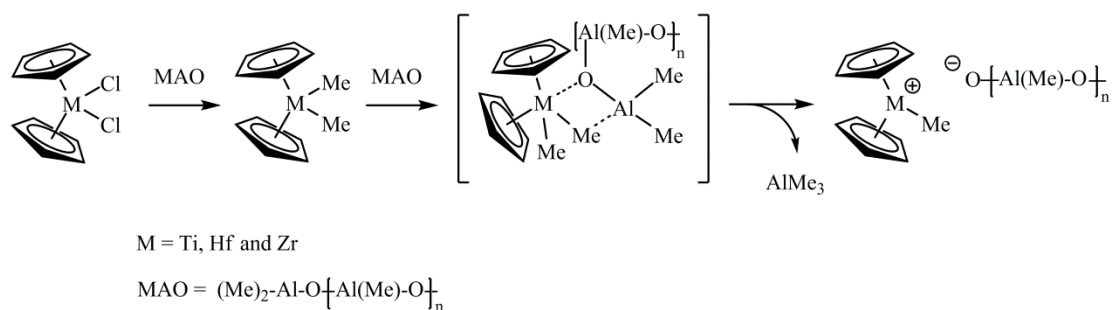


Ziegler-Natta polymerization is one of the most successful applications of transition metal catalysis. In 2005, 65 million tons of PE and 40 million tons of PP were produced worldwide, and the production has been increasing at the annual rate of 6% and 8% respectively.<sup>9, 10</sup> Polyolefins produced by Ziegler-Natta polymerization represent almost two-thirds of the major commodity thermoplastics used worldwide, and have numerous applications ranging from automotive parts to carpet fibers, household and food containers, toys, stretch film/shrink film, diapers and trash bags.<sup>11</sup>

### 1.1.2 Homogeneous metallocene and post-metallocene catalysts

A metallocene<sup>12</sup> is defined as a metal biscyclopentadienyl complex. Metallocene catalysts for coordination polymerization usually have a general structure of  $Cp_2MtX_2$  ( $Cp$  = cyclopentadienyl,  $Mt$  = metal,  $X$  = methyl or halide). Development of metallocene-based catalysts for olefin polymerization is a perfect example of the successful application of organometallic chemistry to homogeneous catalysis.<sup>13</sup> Olefin polymerization catalyzed by homogeneous metallocenes (e.g.,  $Cp_2TiCl_2/AlEt_2Cl$ ) has been studied since 1957.<sup>14, 15</sup> However only very low activity was achieved until the serendipitous discovery of the activating effect of small amounts of water<sup>16</sup> on the system  $Cp_2MtX_2/AlMe_3$  ( $X$  = Cl or alkyl group).<sup>17</sup> The subsequent study and controlled synthesis of methylalumoxane (MAO) by the group of Sinn and Kaminsky<sup>18, 19</sup> provided organometallic and polymer chemists with a potent cocatalyst able to activate Group 4 metallocenes, as well as many other transition metal complexes, toward the polymerization of virtually any 1-alkenes and several cyclic alkenes.<sup>20</sup>

*Scheme 2.* Proposed MAO activation processes for metallocenes

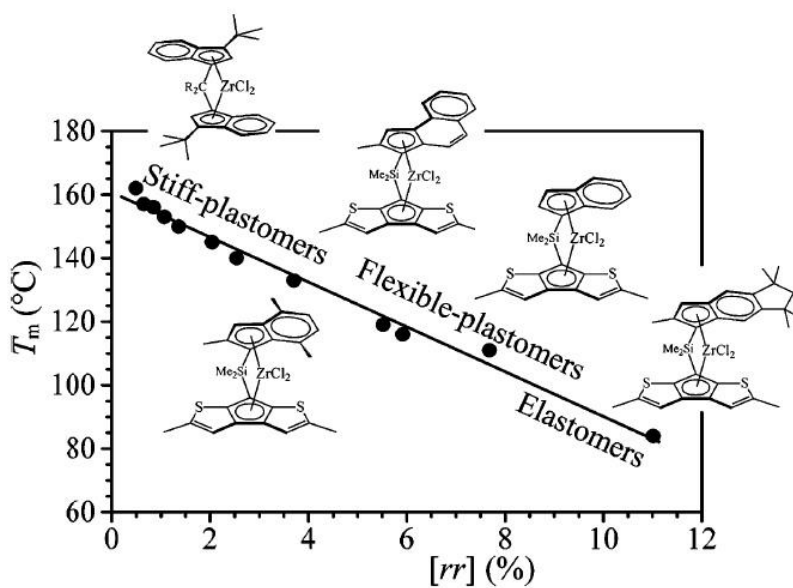


It was proposed that the metallocene dichloride compound was first methylated by MAO through a  $Cl-CH_3$  exchange process, and then the active cationic species was produced through a mechanism as shown in Scheme 2. The metallocenium cations, or more precisely the ion pairs, are the active chain propagation sites for coordination polymerization. Metallocene catalysts have had a revolutionary impact on the polymer industry because of

two main reasons. First, the synthetic versatility of different alkyl-substituted Cp ligands can induce on metallocene performances in olefin polymerization (the ligand effect).<sup>21, 22</sup> Second, the stereorigid, chiral metallocene catalysts can induce enantioselectivity in 1-alkene insertion, which in turn gives control of the physical properties of the final polymers.<sup>23-25</sup>

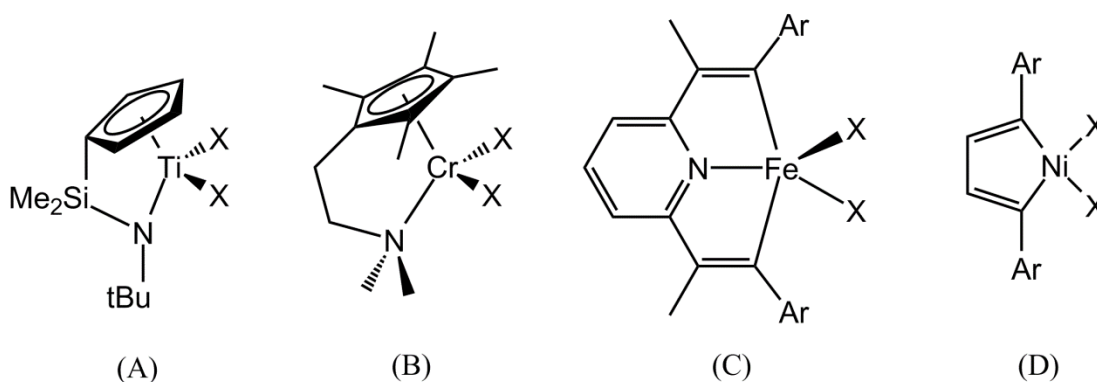
As an illustrative example, Figure 1 presents structure–property relationship data for several predominately isotactic polypropene (*iso*PP) materials that possess varying levels of *rr* stereoerror defects as a result of differing degrees of stereoselectivities from a series of closely related *ansa*-bridged metallocene-based catalysts.<sup>26</sup> The fine-tuning of the chain microstructure, achieved by a tailored design of new metallocene catalysts, has allowed production of new PP materials having desired properties, ranging from stiff plastics to semicrystalline flexible plastics to thermoplastic elastomers. This study reported by De Rosa, Resconi, and co-workers<sup>26</sup> beautifully epitomizes the present state-of-the-art for metallocene catalyst design and resulting polymeric property control.

Figure 1. Relationship of isotactic PP material property with the melting temperature and concentration of *rr* defects of stereoregularity.<sup>26</sup> Reproduced from Ref. (26).



Besides Group 4 metallocene catalysts, the related catalyst systems such as the half-sandwich amide or constrained-geometry catalysts have been at the forefront of olefin polymerization developments since 1980s.<sup>27</sup> Group 4 constrained-geometry catalysts (Figure 2A), developed by Dow and Exxon<sup>28-30</sup> by combining Cp ligands with an amide functionality  $[C_5^-, N^-]$ , are highly active toward commercialization and have good incorporation of 1-hexene co-monomer. Related to constrained-geometry systems, the Group 6 Chromium system<sup>31</sup> (Figure 2B) based on linked Cp–amine  $[C_5^-, N]$  ligands showed very high activities and has been studied as models for the trimerization of ethene to 1-hexene.

Figure 2. Examples of highly active post-metallocene olefin polymerization catalysts



bis(imino)pyridine ligand. The developments of homogeneous post-metallocene catalysts have greatly benefited the advances of living coordination polymerization which ensures better control over polymer structure as well as allows for the creation of virtually limitless types of new materials from a basic set of monomers.

## **1.2 Living Coordination Polymerization**

### **1.2.1 Living polymerization**

The potential applications of a polymer are determined by its physical and mechanical properties, which in turn greatly depend on the composition and architecture of the polymer. The discovery of the chain-growth polymerization methods that enable consecutive enchainment of monomer units without termination, known as living polymerizations<sup>35</sup>, has had tremendous impact on polymer and materials science.<sup>36</sup> It facilitated major developments not only in synthetic polymer chemistry but also in polymer physics as it allows the preparation of well-defined polymers with both precisely controlled molecular weight and a wide array of polymer architectures.<sup>37</sup> For example, block copolymers synthesized *via* sequential monomer addition by Szwarc et al.<sup>39</sup> more than 50 years ago have inspired a generation of polymer physicists to study their self-organization in bulk or solution.

The term *living polymer* was coined by Michael Szwarc<sup>38, 39</sup> to describe the products of the anionic polymerization of styrene initiated by electron transfer in tetrahydrofuran (THF). After that, extraordinary advances in living/controlled polymerization have been discovered by using anionic,<sup>40</sup> cationic,<sup>41</sup> and radical-based<sup>42-44</sup> polymerization. Recently, the developments in atom transfer radical polymerization (ATRP)<sup>45-47</sup>, reversible addition–fragmentation chain transfer (RAFT) polymerization<sup>48-49</sup> and ring-opening metathesis polymerization (ROMP)<sup>50</sup> have greatly flourished the polymeric materials produced by living

polymerization, which have also expanded their applications to high-technique and high-value areas.

Generally speaking, living polymerization is characterized by efficient initiation and chain termination/transfer rates that are negligible in comparison to the rate of propagation. Therefore, living polymerization should lead to a very narrow (Poisson) molecular weight distribution (MWD). More specifically, there are seven generally accepted criteria for a living polymerization:<sup>51</sup>

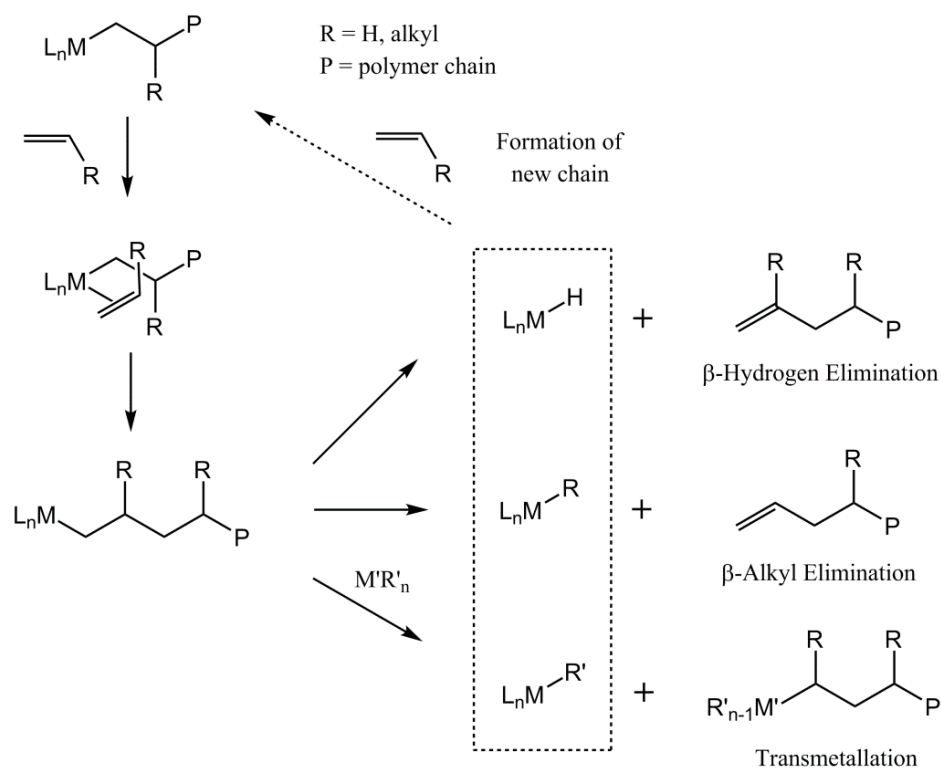
- 1) Polymerization proceeds to complete monomer conversion, and chain growth continues upon further monomer addition.
- 2) Number average molecular weight ( $M_n$ ) of the polymer increases linearly as a function of conversion.
- 3) The number of active centers remains constant during the polymerization.
- 4) Molecular weight can be precisely controlled through stoichiometry.
- 5) Polymers display narrow molecular weight distributions ( $M_w/M_n \sim 1$ ).
- 6) Block copolymers can be prepared by sequential monomer addition.
- 7) End-functionalized polymers can be synthesized.<sup>52</sup>

Few polymerization systems have been shown to meet all of these criteria. Many systems have claimed to be living as long as a substantial number of the key criteria have been met. Sometimes a process might proceed in a controlled fashion even if it obviously deviates from a living system, and the terms of controlled or quasi-living polymerization are commonly used.<sup>36, 53</sup>

## 1.2.2 Living coordination polymerization

Coordination polymerization systems have a significant advantage over their anionic, cationic, and radical polymerization counterparts with regard to stereochemical control, such as the stereoregularity control on *iso*PP material properties shown in Figure 1.<sup>26</sup> However, until ten years ago, these transition metal catalyzed insertion methods were inferior to ionic and radical mechanisms in the category of living polymerization. The main reason for this is that coordination polymerization catalysts often undergo irreversible chain transfer to metal alkyls and  $\beta$ -elimination reactions that result in the initiation of new polymer chains by the catalyst (Scheme 3).<sup>54</sup> When alkylaluminum cocatalysts are employed, an additional termination route is chain transfer to the aluminum centers.<sup>55</sup> Also, in many cases, the life time of the chain propagation is on the order of seconds, which makes it very difficult to synthesize block copolymers by sequential monomer addition.<sup>54</sup>

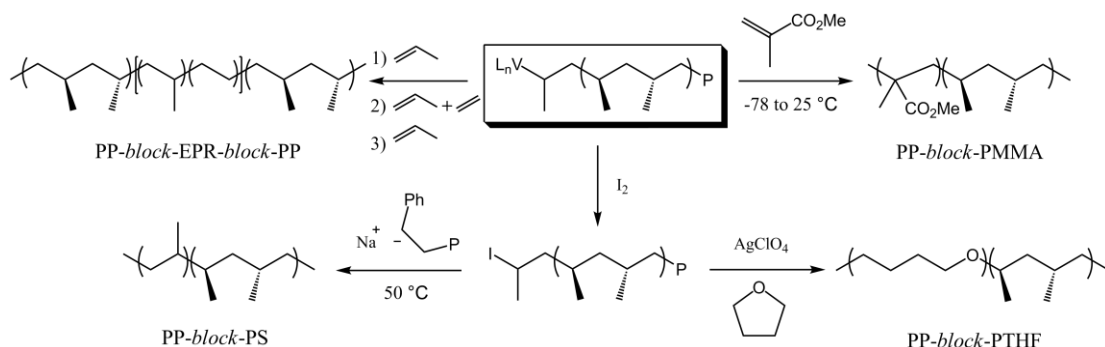
Scheme 3. Mechanisms of propagation and chain transfer in coordination polymerization



Several strategies have been devised to decrease the rates of chain terminations relative to that of propagation so that living systems can be formed. The first consideration is simply lowering the polymerization temperature, since the unimolecular  $\beta$ -hydrogen and alkyl elimination processes are more adversely affected than the bimolecular propagation process. However, the precipitation of polymers from solution at low temperature can hinder the control of polymerization.<sup>51</sup> The second strategy is to design new transition metal catalysts that favor propagation rather than chain termination processes at ambient temperature. A final consideration is to eliminate the use of alkylaluminum cocatalysts, such as trimethylaluminum ( $\text{AlMe}_3$ ) and triisobutylaluminum ( $\text{Al}i\text{Bu}_3$ ), which give the potential for chain transfer to aluminum reactions. In this regard, the development of weakly coordinating anions, such as perfluoroaryl borates, has made significant advances in living olefin polymerization possible.<sup>56</sup>

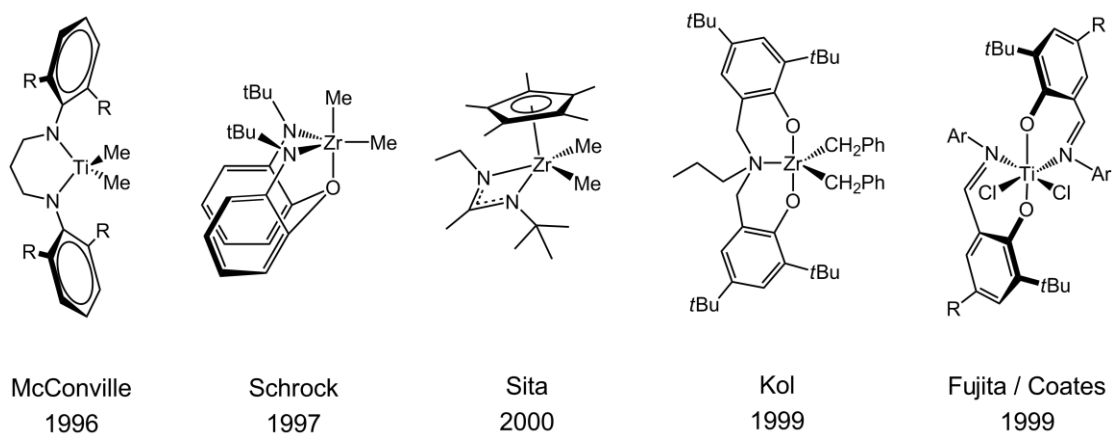
The first true living olefin polymerization system was reported by Doi et al.<sup>57</sup> in 1979 that satisfied all the requirements for a living polymerization. The catalyst,  $[\text{V}(\text{acac})_3]$ , when activated with  $\text{AlEt}_2\text{Cl}$ , produced partially syndiotactic PP (*s*PP) at  $-78\text{ }^\circ\text{C}$  with very narrow molecular weight distributions. Doi and co-workers have demonstrated the utility of the living vanadium catalysts through the synthesis of several end-group functionalized polymers from chemical reactions of the living chain end.<sup>58-62</sup> In order to produce well-defined block copolymers by sequential monomer addition, Doi and co-workers reported the synthesis of both AB- and ABA- type block copolymers from ethene and propene, such as PP-*block*-EPR-*block*-PP (EPR = ethene/propene rubber) (Scheme 4).<sup>63-64</sup> In addition to olefin-based nonpolar block copolymers, the vanadium catalysts have also been employed for the synthesis of block copolymers from polar monomers by transforming the living chain end to one capable of initiating a radical or cationic polymerization (Scheme 4).<sup>58, 65</sup>

Scheme 4. Synthesis of block copolymers with a vanadium catalyst



In the last decade, a significant number of advances have been reported and now there are abundant of metal catalysts across the transition series that feature living polymerization of ethene, propene, higher 1-alkenes, non-conjugated dienes and cyclic olefins, as well as precise control over all aspects of macromolecular architecture; especially chain composition, molecular weight, and stereochemistry.<sup>51, 54</sup> Group 4 transition metal catalyst systems have been well-known to exhibit living behavior at low temperatures by suppressing undesirable  $\beta$ -hydrogen or  $\beta$ -alkyl eliminations. As shown in Figure 3, systems developed by McConville,<sup>66-67</sup> Schrock,<sup>68-69</sup> Sita,<sup>70-71</sup> Kol<sup>72-73</sup> and Fujita<sup>74-75</sup>/Coates<sup>76-77</sup> have demonstrated not only living chain-growth characters to a variety of olefin monomers but also the control of stereochemistry in some cases.

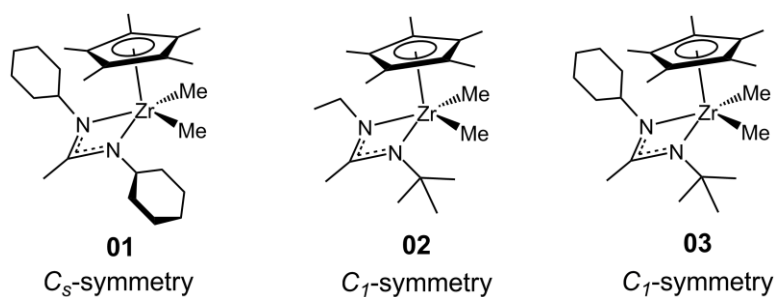
Figure 3. Examples of Group 4 precursors for living coordination polymerization



### 1.2.3 An example of stereospecific living polymerization of 1-hexene

Although the living vanadium catalysts developed by Doi and co-workers gave syndio-enriched PP, the first catalyst to simultaneously achieve the highly challenging goals of livingness and stereoselectivity was reported by Jayaratne and Sita in 2000.<sup>70</sup> As shown in Figure 4, a series of monocyclopentadienyl monoamidinate (CpAm) zirconium complexes,  $\text{Cp}^*\text{ZrMe}_2[\text{N}(\text{R}^1)\text{C}(\text{Me})\text{N}(\text{R}^2)]$  ( $\text{Cp}^* = \eta^5\text{-pentamethylcyclopentadienyl}$ ), were used as catalyst precursors (precatalysts) for the living polymerization of 1-hexene upon activation by a borate cocatalyst  $[\text{PhNMe}_2\text{H}][\text{B}(\text{C}_6\text{F}_5)_4]$  (**04**). Stereoselectivity was achieved by manipulating the steric bulk of the two N-amidinate substituents,  $\text{R}^1$  and  $\text{R}^2$ , which also determine the symmetry of the catalyst.

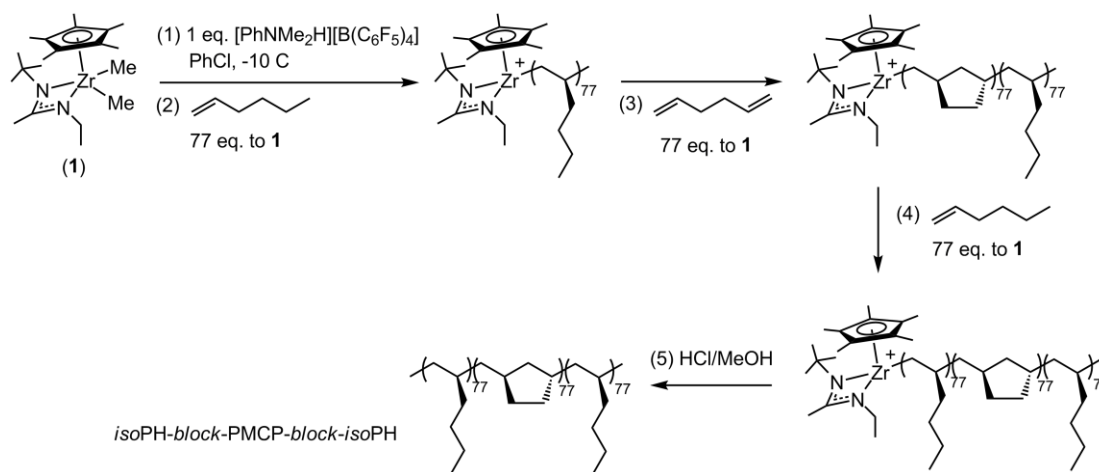
Figure 4. Structures of three  $\text{Cp}^*\text{ZrMe}_2[\text{N}(\text{R}^1)\text{C}(\text{Me})\text{N}(\text{R}^2)]$  catalyst precursors



When  $\text{R}^1 = \text{R}^2 = \text{cyclohexyl (Cy)}$ ,  $\text{C}_5$ -symmetric compound  $\text{Cp}^*\text{ZrMe}_2[\text{N}(\text{Cy})\text{C}(\text{Me})\text{N}(\text{Cy})]$  (**01**) was active towards 1-hexene polymerization, giving monodisperse atactic poly(1-hexene) material ( $M_n = 11.0$  kDa;  $M_w/M_n = 1.10$ ). When  $\text{R}^1 \neq \text{R}^2$ ,  $\text{C}_1$ -symmetric compound  $\text{Cp}^*\text{ZrMe}_2[\text{N}(\text{Et})\text{C}(\text{Me})\text{N}(\text{tBu})]$  (**02**) led the stereospecific living polymerization of 1-hexene and provided highly isotactic, high molecular weight materials with low polydispersities ( $[\text{mmmm}] > 0.95$ ;  $M_n = 32.6\text{--}69.5$  kDa;  $M_w/M_n = 1.03\text{--}1.10$ ). However,  $\text{C}_1$ -symmetric compound  $\text{Cp}^*\text{ZrMe}_2[\text{N}(\text{Cy})\text{C}(\text{Me})\text{N}(\text{tBu})]$  (**03**) displayed poor activity toward 1-hexene polymerization, probably due to the sterically encumbered nature of the complex.

The enormous potential of this living and stereoselective catalyst system based on compound **02** lies in its potential for the synthesis of well-defined olefin block copolymers with both crystalline and amorphous domains. With isotactic poly(1-hexene) (*iso*PH) block as amorphous domains well-established, catalyst system **02/04** was found to cyclopolymerize 1,5-hexadiene in a living fashion to yield poly(methylene-1,3-cyclopentane)s (PMCP) with high melting transitions ( $T_m = 98\text{--}99\text{ }^\circ\text{C}$ ) that could serve as crystalline domains.<sup>78</sup> Based on those results, a triblock copolymer *iso*PH-*block*-PMCP-*block-iso*PH were synthesized by sequential addition of monomers into a chlorobenzene solution of **02/04** at  $-10\text{ }^\circ\text{C}$  as shown in Scheme 5.<sup>78</sup> Atomic force microscopy (AFM) imaging of polymer thin films of the triblock material confirmed the microphase-separated cylindrical morphology consisting of hard cylinders of PMCP running parallel to the surface and surrounded by the more elastic *iso*PH domains.<sup>78</sup>

Scheme 5. Synthesis of *iso*PH-*block*-PMCP-*block-iso*PH triblock copolymer

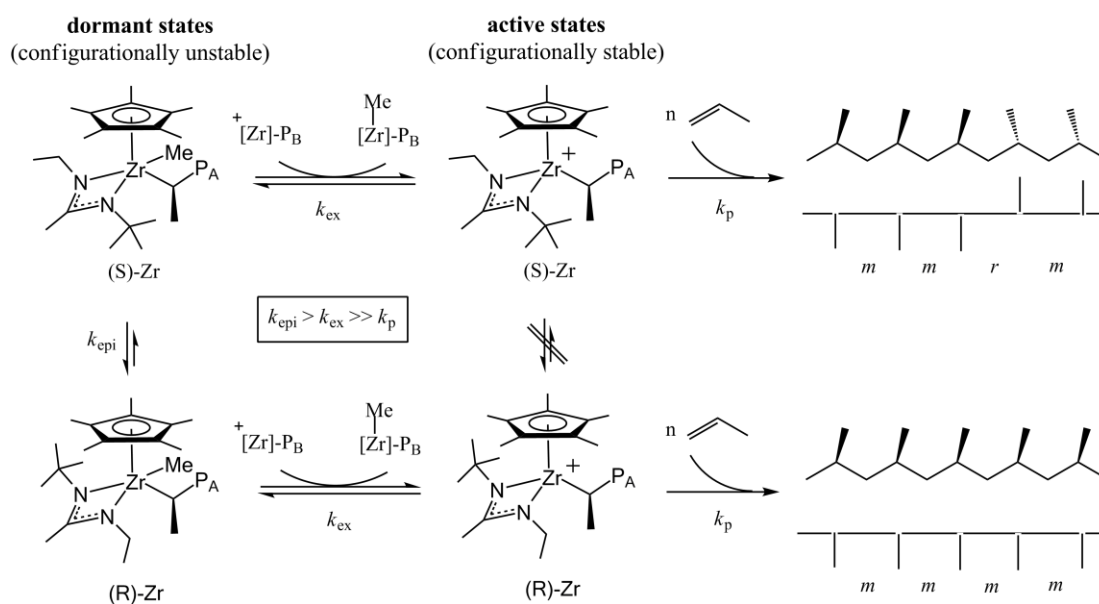


#### 1.2.4 Living degenerative group-transfer coordination polymerization

Later, it was found by Zhang and Sita<sup>79</sup> that the tacticity of poly( $\alpha$ -olefin)s formed using catalyst system **02/04** varied depending on the stoichiometry of borate cocatalyst **04**

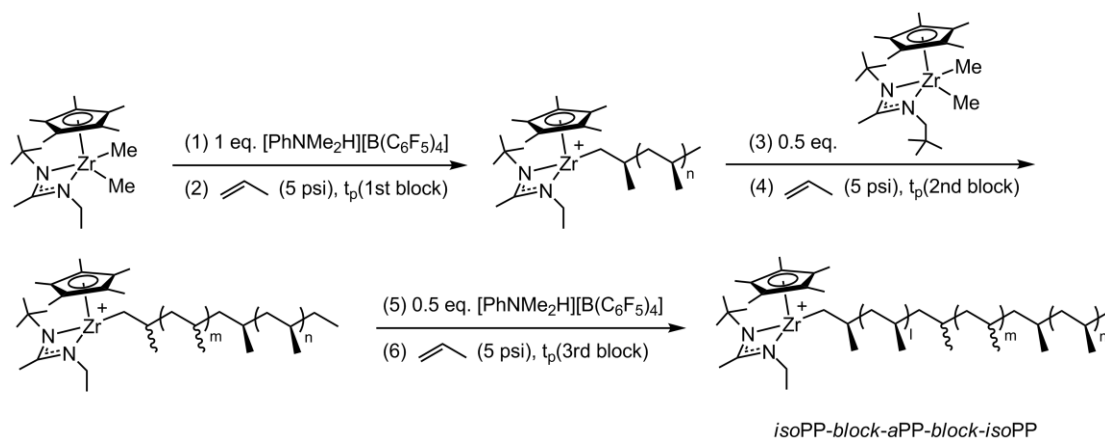
used. For example, when 0.5 equiv. of **04** was used relative to compound **02**, the resulting PH is considerably less isotactic with a *mm* diads content of 45–50%, while the resulting PP is completely atactic ( $[mm] = 0.267$ ,  $[mr] = 0.523$ ,  $[rr] = 0.210$ ).<sup>81</sup> The reason for this phenomenon was from a degenerate group-transfer mechanism<sup>79</sup> that is operating between a configurationally stable cationic active propagating species and a configurationally unstable neutral methyl, polymeryl dominant species. The rapid and reversible methyl-group exchange between the cationic (active) and neutral (dominant) species led to degradation in stereoselectivity due to the fast epimerization of the dormant metal centers (Scheme 6). Therefore, tacticity of the polymer is able to be modulated during the polymerization lifetime by alternatively turning the degenerative group-transfer "on" and "off" through partial methylation of cationic active species and full demethylation of neutral dormant species, respectively.<sup>80</sup>

*Scheme 6.* Mechanism of stereoerror incorporation that occurs under living degenerative methyl group-transfer conditions



As the best illustration of the application of this degenerative methyl group-transfer mechanism, isotactic-*block*-atactic-*block*-isotactic polypropylene (*isoPP-block-aPP-block-isoPP*) elastomeric materials have been synthesized with well-defined block lengths of each domain as well as controlled total molecular weights and narrow molecular weight distributions.<sup>81-83</sup> As shown in Scheme 7, the first *isoPP* block was made directly through stereoselective cationic species  $\{\text{Cp}^*\text{Zr}(\text{Me})[\text{N}(\text{Et})\text{C}(\text{Me})\text{N}(\text{tBu})]\}[\text{B}(\text{C}_6\text{F}_5)_4]$  (**05**) upon activation of precatalyst **02** with 1 eq. of cocatalyst **04**. The second *aPP* block was generated by turning the degenerative methyl group-transfer process “on” through addition of 0.5 eq. of  $\text{Cp}^*\text{ZrMe}_2[\text{N}(\text{Np})\text{C}(\text{Me})\text{N}(\text{tBu})]$  (Np = neopentyl) (**06**) as a methylation reagent. The final *isoPP* block was obtained by turning the degenerative methyl group-transfer process “off” through fully demethylation with an addition of 0.5 eq. of cocatalyst **04**. Length of each block and total isotactic content were simply modulated by manipulating the polymerization time ( $t_p$ ) of each block.

Scheme 7. Synthesis of *isoPP-block-aPP-block-isoPP* stereoblock elastomer



Extensive characterization by AFM, tensile testing, differential scanning calorimetry (DSC) and wide-angle X-ray diffraction (WAXD) techniques of the *isoPP-block-aPP-block-isoPP* materials with varying block lengths for each domain (isotactic contents) have been

taken out. The stereoblock PP sample with 18%-64%-18% (*iso-a-iso*) of  $M_n = 195$  kDa and  $M_w/M_n = 1.28$  showed the best elastomeric property with 15 MPa ultimate tensile strength at over 2500% strain and a recovery at break of 98.6%.<sup>83</sup> The results of these investigations serve to provide an important foundation to identify the best combination of stereoerror level incorporation within each domain in order to maximizing desirable elastomeric property and potential applications of those materials.

### **1.3 Living Coordinative Chain-Transfer Polymerization (LCCTP)**

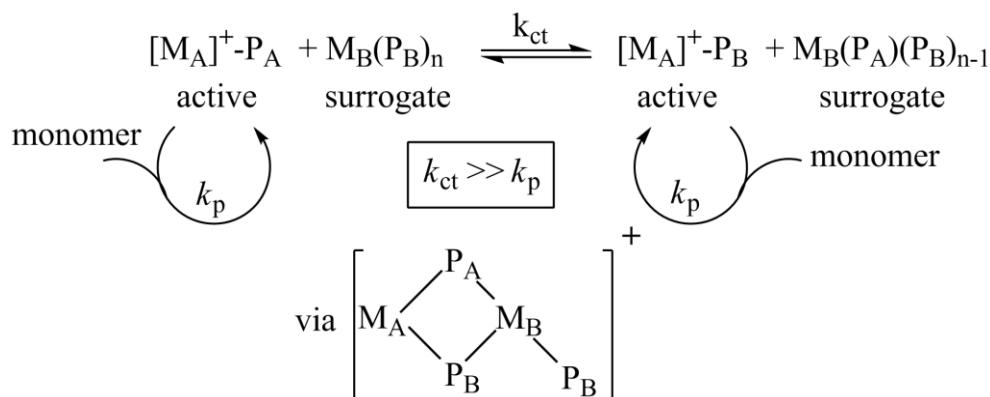
#### **1.3.1 Coordinative chain-transfer polymerization (CCTP)**

In Ziegler-Natta polymerization, polymer chains grow on the transition metal centers rather than main group metals, such as aluminum. In recent years, it was found that polymer chains could be transferred to the main group metal aluminum through a process named chain-transfer to aluminum.<sup>84</sup> This process is usually a chain termination reaction alongside with other chain-transfer reactions, such as  $\beta$ -hydrogen elimination (Scheme 3). However, if the chain-transfer to aluminum process is reversible and the rate is much faster compared to chain propagation rate, then the polymer chains will appear to be growing on aluminum centers.<sup>85</sup> This process can then reasonably be described as a transition metal catalyzed chain-growth reaction on aluminum or, using Ziegler's terminology, a transition metal catalyzed "Aufbaureaktion".<sup>86-87</sup>

Later, this fast and reversible chain-transfer to aluminum process, or transition metal catalyzed chain-growth on aluminum, was found to be very attractive in two main reasons. First, compared to the Aufbaureaktion process introduced by Ziegler, which requires very high pressure (e.g., 100 bar) and produces a pseudo-Poisson distributed long-chain linear hydrocarbons,<sup>86-87</sup> transition metal catalyzed chain-growth on aluminum process requires ambient conditions and produces Poisson distributed linear hydrocarbons with tunable

molecular weights. Second, the intrinsic “one-chain-per-metal” limit on efficiency of a living polymerization could be overcome by using the much cheaper and commercial available main group metals, such as aluminum, as the chain-growth sites.<sup>85</sup>

*Scheme 8.* Mechanism of coordinative chain-transfer polymerization (CCTP)



The strategy proposed based on this reversible chain-transfer between active transition metal centers and main group metals is referred to as coordinative chain-transfer polymerization (CCTP).<sup>85, 88-89</sup> According to Scheme 8, at the heart of CCTP is highly efficient and reversible chain (polymeryl group) transfer between active transition-metal propagating centers ( $M_A$ ) and inactive main-group metal species ( $M_B$ ) as chain-growth surrogates. Significantly, if the rate constant for chain-transfer exchange between the active and inactive metal centers,  $k_{ct}$ , is several times greater than the rate constant for propagation,  $k_p$ , then both the transition- and main-group metal centers will effectively appear to engage in chain-growth propagation at the same rate. Indeed, under these conditions, number-average degree of polymerization ( $X_n$ ) will be governed by both the quantity of monomer consumed and the total concentration of all polymeryl groups,  $P_A$  and  $P_B$ . For a living polymerization,  $X_n$  will be determined by eq. 1, where  $n$  is the number of equivalent polymeryl groups per main-group metal. The polydispersity index (PDI) will be approximately determined by the relative magnitudes of the rate constants for these two processes according to eq. 2 and be

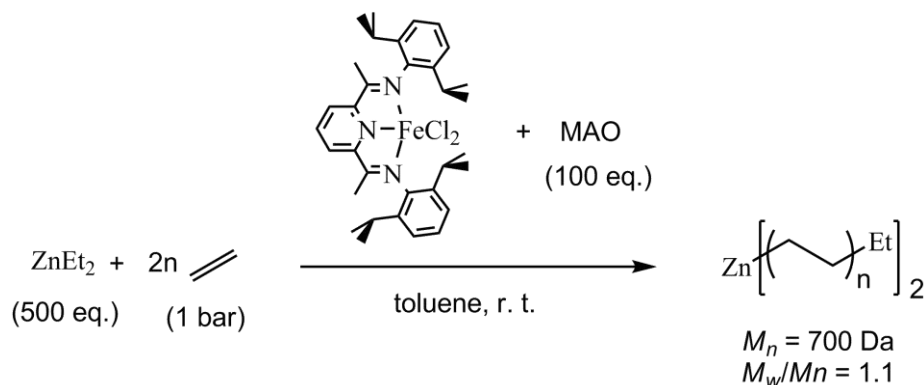
close to 1 when  $k_{ct} \gg k_p$ .<sup>100</sup> Finally, according to the mechanism depicted in Scheme 8, the quantity of polymer product is clearly no longer capped by the amount of transition-metal catalyst but rather the total molar equivalents of the much less expensive and readily available main-group metal alkyl that is employed.

$$X_n = \frac{[monomer]_0 - [monomer]_t}{[(M_A-P_A)^+ + n \cdot (M_B'-P_B)]_0} \quad (eq. 1)$$

$$PDI = \frac{M_w}{M_n} \approx 1 + \frac{k_p}{k_{ct}} \quad (eq. 2)$$

The CCTP strategy was first used to synthesize very narrowly distributed PE materials in the low molecule weight range ( $PDI < 1.1$  up to a  $M_n$  of about 4000 Da).<sup>85</sup> For example, in 2002 Gibson and coworkers<sup>84</sup> reported the first observation of a catalyzed chain-growth reaction on zinc using a MAO activated iron complex with a large amount of  $ZnEt_2$  as chain-transfer surrogate (Scheme 9). The PE oligomer obtained showed a Poisson distribution. Later, Gibson and coworkers studied more main group metal alkyls as chain-transfer surrogates, such as  $ZnR_2$  ( $R = Me, Et, iPr$ ),  $AlR_3$  ( $R = Me, Et, octyl, iBu$ ) and  $GaR_3$  ( $R = Et, nBu$ ).<sup>90</sup> Also, a comparative investigation of highly active catalyst systems across the transition series for CCTP of ethene was carried out by Gibson and coworkers in 2005.<sup>91</sup>

Scheme 9. Iron complex catalyzed PE chain-growth on zinc



Gibson rationalized the remarkably efficient iron catalyzed chain growth reaction for  $\text{ZnEt}_2$  compared to other metal alkyls on the basis of: (1) relatively low steric hindrance around the zinc center, (2) their monomeric nature in solution, (3) the relatively weak Zn-C bond, and (4) a reasonably close match in Zn-C and Fe-C bond strengths.<sup>90</sup> The coordination of Zn-C and Fe-C in the four member ring transition state for  $\delta$ -bond metathesis is also crucial for the success of CCTP. Very strong coordination of Zn-C and Fe-C will lead to no chain-growth, as Gibson observed from using  $\text{Zn}(\text{CH}_2\text{Ph})_2$  as chain-transfer surrogate,<sup>90</sup> since the concentration of the active transition metal species will be greatly decreased. Weak coordination of Zn-C and Fe-C will lead to no chain-transfer process but only transition-metal catalyzed chain-growth, as Gibson observed from using  $\text{ZnPh}_2$  as chain-transfer surrogate.<sup>90</sup>

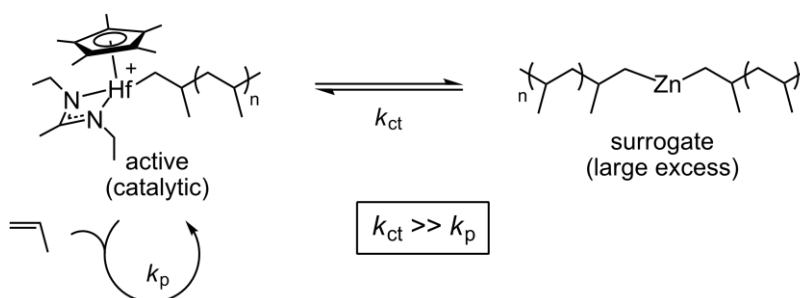
Other transition-metal- or lanthanide-catalyzed PE chain growth on main group metals employing the CCTP strategy include the yttrium/borates system with TIBAO (tetraisobutylalumoxane) developed by Kempe and coworkers in 2006,<sup>91</sup> the samarium system with *n*Bu-Mg-Et as both an activator and a surrogate studied by Mortreux, et al in 1996;<sup>92</sup> the system of  $\text{Cp}^*\text{Cr}(\text{PMe}_3)\text{Me}_2$  with  $\text{AlMe}_3$  or  $\text{AlEt}_3$  reported by Bazan and coworkers in 2000<sup>93-94</sup> and a neutral chromium catalyst [ $\text{Cp}^*\text{Cr}(\text{C}_6\text{F}_5)(\eta^3\text{-Bn})$ ] (Bn = benzyl) with  $\text{AlEt}_3$  designed by Gabba ĩ and coworkers in 2004.<sup>95-96</sup> However, none of those CCTP systems were claimed to be living, and the resulting polymers obtained through hydrolysis always had a certain amount of unsaturated chain-ends from  $\beta$ -hydrogen/ $\beta$ -alkyl eliminations.

### 1.3.2 Living coordinative chain-transfer polymerization (LCCTP)

Although CCTP strategy was proposed in the situation that chain-transfer to aluminum is the only chain-transfer process with absence of other chain termination reactions, CCTP has long been only successfully demonstrated in non-living fashion for ethene polymerization/oligomerization. In 2008, Zhang and Sita<sup>88</sup> reported the first living

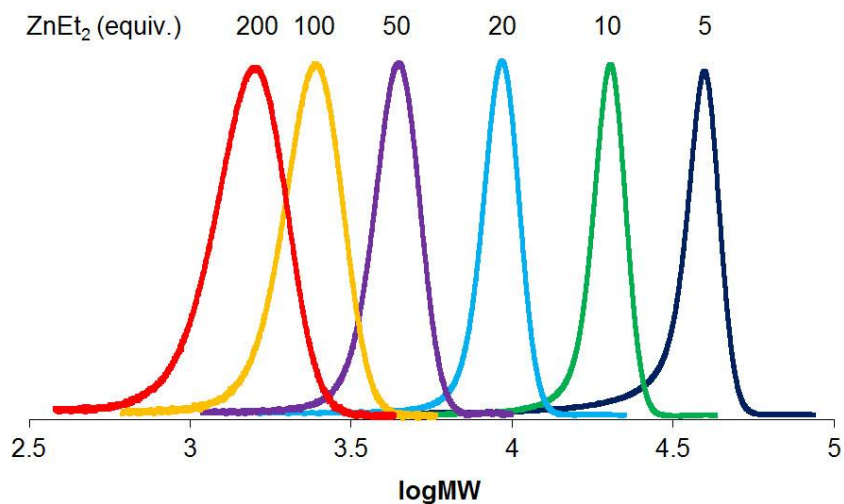
coordinative chain-transfer polymerization (LCCTP) of propene that achieved both truly living CCTP and transition metal catalyzed chain-growth of a higher  $\alpha$ -olefin on zinc. As shown in Scheme 10, a highly active *N,N*-diethyl hafnium cation,  $\{\text{Cp}^*\text{Hf}(\text{Me})\text{-}[\text{N}(\text{Et})\text{C}(\text{Me})\text{N}(\text{Et})]\}\text{[B}(\text{C}_6\text{F}_5)_4]$  (**07**) from equimolar amount of dimethyl precursor  $\text{Cp}^*\text{HfMe}_2[\text{N}(\text{Et})\text{C}(\text{Me})\text{N}(\text{Et})]$  (**08**) and the borate cocatalyst **04**, with an excess amount of  $\text{ZnEt}_2$  as chain-transfer surrogate were used to carry out the propene polymerization in nonpolar toluene at 0 °C. Kinetic study revealed the linear relationship of observed  $M_n$  and the inverse of total initial concentration of metal species ( $1/[\text{Hf} + \text{Zn}]_0$ ), which confirmed the livingness of this chain-transfer polymerization throughout the entire series.

Scheme 10. CCTP of propene using cationic **07** with  $\text{ZnEt}_2$  as surrogate



The advantages of LCCTP are that almost all the beneficial features of a living polymerization maintains, such as tight control over molecular weights and narrow polydispersities. As an illustration, molecular weights of the resulting PP materials were precisely tuned by varying amount of  $\text{ZnEt}_2$  (5–100 equiv. relative to **07**) used while keeping all the other conditions identical (Figure 5). Also the molecular weight distributions maintained narrow for all range of molecular weights. More importantly, LCCTP offers a very attractive solution to the intrinsic problem of “one-chain-per-metal” limit on polymerization scale, in which the use of expensive and synthetically difficult transition metal precatalysts and borate cocatalysts are greatly reduced.<sup>88</sup>

Figure 5. Molecular weight distributions for PPs obtained with varying amount of ZnEt<sub>2</sub>



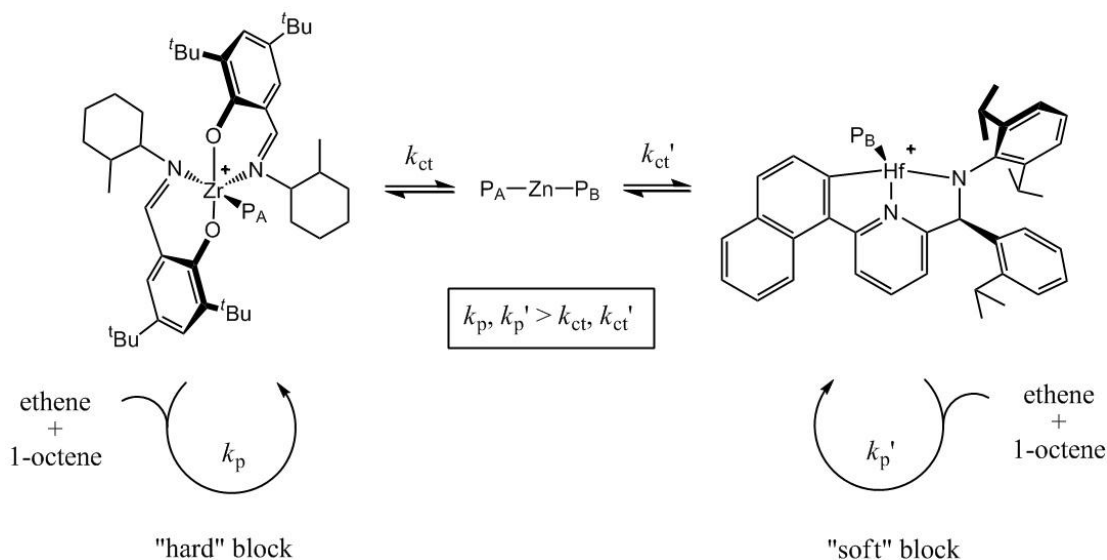
However, due to the non-selective  $\delta$ -bond metathesis nature of the chain-transfer process (Scheme 8), stereoselectivity was degraded during the LCCTP of  $\alpha$ -olefins. For example, when stereoselective cationic zirconium compound **05** was used as the active chain propagation species with ZnEt<sub>2</sub> (50 equiv. to **05**) for LCCTP of propene, *iso*-rich PP ( $[mmmm] = 0.253$ ) was obtained instead of *iso*PP products ( $[mmmm] = 0.694$ ) obtained from non-chain-transfer living polymerization.

Later, Zhang and Sita<sup>89</sup> have extended the LCCTP strategy to polymerize a broader range of monomers, such as ethene, higher  $\alpha$ -olefins (e.g., 1-pentene, 1-hexene and 1-octene), and  $\alpha,\omega$ -nonconjugated dienes (e.g., 1,5-hexadiene) using the cationic hafnium compound **07** with excess ZnEt<sub>2</sub> as a chain-transfer surrogate. Also, the LCCTP copolymerization of ethene with 1-hexene or 1,5-hexadiene using either hafnium compound **07** or  $\{\text{Cp}^*\text{Hf}(\text{Me})[\text{N}(\text{Et})\text{C}(\text{Me})\text{N}(\text{Et})]\}[\text{MeB}(\text{C}_6\text{F}_5)_3]$  (**09**), generated from **08** and a borane cocatalyst B(C<sub>6</sub>F<sub>5</sub>)<sub>3</sub> (**10**), have been taken out to yield poly(ethene-*co*-1-hexene) and poly(ethene-*co*-methylene-1,3-cyclopentane) with controlled molecular weights and narrow polydispersities.

### 1.3.3 An example of chain shuttling polymerization

In 2006, a team from Dow<sup>97</sup> reported a chain shuttling strategy to produce PE-based block copolymers with alternating semicrystalline and amorphous segments. In this system, a chain shuttling agent ( $\text{ZnEt}_2$ ) reversibly transfers growing chains between a zirconium bis(phenoxyimine) catalyst that produces ethene-rich “hard” poly(ethene-*co*-1-octene) block and a hafnium pyridylamide catalyst that gives 1-octene-rich “soft” poly(ethene-*co*-1-octene) block (Scheme 11). Since the polymer propagation rates,  $k_p$  and  $k_p'$ , are faster compared to chain-transfer rates,  $k_{ct}$  and  $k_{ct}'$ , the overall resulting copolymer has statistically distributed “hard” and “soft” blocks rather than randomly distributed copolymer our group made<sup>89</sup> in the situation when  $k_{ct} \gg k_p$ . The resulting multiblock copolymers have high melting temperatures and low glass transition temperatures, and therefore maintaining excellent elastomeric properties at high temperatures.<sup>98</sup> later, Hustad and coworkers reported a class of interesting photonic PE materials from self-assembled mesophases of polydisperse olefin block copolymers made based on this chain shuttling strategy.<sup>99</sup>

Scheme 11. Mechanism of chain-shuttling copolymerization of ethene and 1-octene



### 1.3.4 Challenges and opportunities in the area of LCCTP

Although developed recently, LCCTP has shown great power in the preparation of polyolefin-based materials with precisely controlled molecular weight and narrow molecular weight distribution. More importantly, through catalyzed chain-growth on main group metals, LCCTP can greatly reduce the cost of a scalable production. In the same time, there are still many issues that remain to be explored.

First of all, from a cost and safety perspective, the existing dependence of the current LCCTP process on  $\text{ZnEt}_2$  could prove to be an Achilles heel limiting the successful commercialization of precision polyolefin oligomers. In this respect, more prospective catalyzed chain-growth on aluminum process should be studied through investigating the nature of trialkylaluminum species as primary chain-transfer surrogates.

Secondly, as the immediate benefit of the LCCTP strategy, block and end-group functionalized polyolefin-based materials could be synthesized through chemically transformation of zinc/aluminum carbon bonds. Efficient and nearly quantitative reactions on the polyolefin chain-ends need to be discovered based on the coupling of known organic reactions and polymer behaviors in the solution.

Moreover, the opportunity of using the reversible chain-transfer process as a dynamic control to increase the grades of resulting polymers from a limited set of olefin monomers is very intriguing. Here the relative rates of chain-transfer process and chain propagation is the key to tune the final polymer structure and resulting physical property.

Finally, mechanistic study on coordination polymerization in combination with the design of suitable organometallic catalyst systems are always the fundamental driving force for novel polymeric materials with desired structure and property.

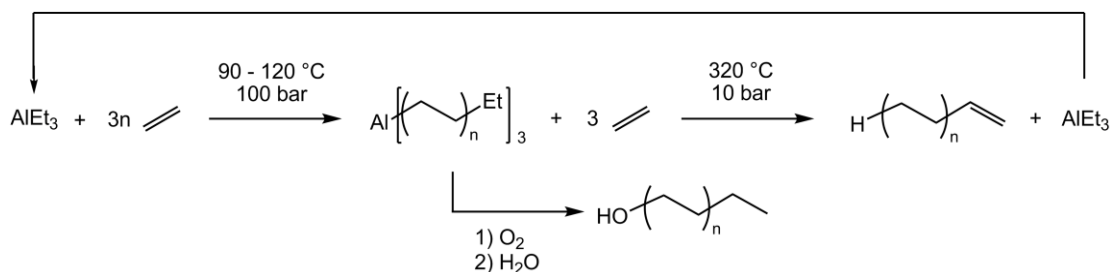
# Chapter 2: Ternary Living Coordinative Chain-Transfer Polymerization of Propene and Higher $\alpha$ -Olefins

## 2.1 Background

### 2.1.1 Aufbaureaktion and chain-growth on aluminum process

In 1952, Ziegler introduced a process for controlled oligomerization of ethene on triethylaluminum ( $\text{AlEt}_3$ ) named Aufbaureaktion.<sup>86-87</sup> In the Aufbaureaktion process, ethene is inserted into the aluminum carbon bond to produce long-chain alkylaluminums at high pressure but relatively low temperature (e.g., 100 bar, 120 °C). This chain-growth on aluminum process can be used for the synthesis of a pseudo-Poisson distributed long-chain linear  $\alpha$ -olefins of the general formula  $\text{H}_2\text{C}=\text{CH}(\text{CH}_2)_n\text{CH}_3$  ( $n = 1-15$ ) and the corresponding saturated terminal alcohols  $\text{HOCH}_2(\text{CH}_2)_{n+1}\text{CH}_3$  through direct chemical transformations of the  $\text{Al}[(\text{CH}_2)_{n+2}\text{CH}_3]_3$  intermediates (Scheme 12).<sup>101-103</sup>

Scheme 12. Aufbaureaktion and Alfen Process



This process is still commercially exploited today. In 2006 alone, global production of long-chain linear  $\alpha$ -olefins stood at four million metric tons, with 55% of this volume

being targeted for lubricants, plasticizers, detergents, additives, and fine chemical products.<sup>104</sup> Unfortunately, no Aufbaureaktion for the controlled oligomerization of propene or higher  $\alpha$ -olefins using  $\text{AlEt}_3$  or other trialkylaluminum ( $\text{AlR}_3$ ) species as chain-growth initiators has ever been developed.<sup>105-106</sup> Accordingly, the potential technological value of new classes of hydrocarbon-based products that might be available from such processes on a commodity volume scale remains unknown.

### 2.1.2 Catalyzed polypropene chain-growth on aluminum

In coordination polymerization, polypropene (PP) chain-transfer to aluminum is observed frequently as a chain termination pathway, which is irreversible and results in relative low molecular weight polymer and broader molecular weight distribution.<sup>107-113</sup> Very limited examples of reversible PP chain-transfer were reported. In 2002, Rieger and coworkers investigated the reversible chain-transfer to aluminum process during propene polymerization by three oxygen-substituted asymmetric zirconocene complexes.<sup>114</sup> The reversible chain-transfer process was proposed as the origin of stereoerror in the resulting PP. In 2006, Shiono reported that mono-distributed PP material was obtained with a titanium catalyst when activated by MMAO (modified MAO), and chain-transfer was observed in the presence of specific amount triisobutylaluminum ( $\text{Al}i\text{Bu}_3$ ).<sup>115</sup> In 2007, Busico and Stevens reported a PP chain shuttling process between an enantiomeric (pyridyl-amide) $\text{HfMe}_2$  complex with  $\text{AlMe}_3$ .<sup>116</sup> However, none of them achieved controlled/living PP chain-growth on aluminum as an analog of Aufbaureaktion process.

In 2008, our group have reported that the living coordinative chain-transfer polymerization (LCCTP) and copolymerization of ethene, propene, long-chain  $\alpha$ -olefins, and  $\alpha,\omega$ -nonconjugated dienes using *N,N*-diethyl hafnium cationic compound **07** as the active initiator for chain-growth propagation, along with multiple stoichiometric equivalents of

ZnEt<sub>2</sub> that serve as chain-growth surrogates.<sup>88-89</sup> The final yield of polyolefin product obtained through LCCTP is now depended upon the initial amount of ZnEt<sub>2</sub> employed, but the transport and handling of industrial volumes of ZnE<sub>2</sub> is still problematic, which limits the successful commercialization of precision polyolefin products. In this respect, AlEt<sub>3</sub> and Al*i*Bu<sub>3</sub>, which are produced on a commodity scale from aluminum metal, dihydrogen, and ethene and isobutene, respectively, are significantly less expensive and substantially less pyrophoric than ZnE<sub>2</sub>.<sup>117-119</sup> An additional advantage of these AlR<sub>3</sub> compounds over ZnEt<sub>2</sub> in terms of product yield is realized if all three alkyl groups on aluminum can equally engage in rapid and reversible chain transfer process.

Previously, Wei Zhang in our group has studied the LCCTP of propene using AlEt<sub>3</sub> as a chain-transfer surrogate under the same conditions as those using ZnEt<sub>2</sub> as a surrogate.<sup>88-89</sup> The polymerization rates were found to be depressed and molecular weight distribution of the resulting PP materials were significantly broader (PDI = 1.16–1.19) compared to those using ZnEt<sub>2</sub> as a surrogate (PDI = 1.02–1.07) under the same conditions. The broadness of the PDI was probably resulted from the slow chain-transfer rate between aluminum surrogate and the active hafnium initiator. To address that problem, Wei investigated a mixed surrogate of ZnEt<sub>2</sub> and AlEt<sub>3</sub> in the ratios of 1:1, 1:2, 2:1 and 1:4 to carry out LCCTP of propene. All four polymerizations yielded PP materials with much narrower molecular weight distributions (PDI = 1.02–1.04). Those results showed the potential to use a second main-group metal alkyl, such as ZnEt<sub>2</sub>, to facilitate the overall chain-transfer rate in the system where AlR<sub>3</sub> is the primary surrogate. If this hypothesis is true, living/controlled PP chain-growth on aluminum could be achieved for the first time after Ziegler's revolutionary discovery of Aufbaureaktion process 60 years ago to provide a class of precision hydrocarbons based on propene and higher  $\alpha$ -olefins.



Importantly, the third component  $\text{ZnEt}_2$  greatly enhances the overall rate of chain transfer between the active hafnium species and the primary surrogate aluminum centers by the mechanism proposed in Scheme 13. The key to the success of this proposal for t-LCCTP is that three different metal species must engage synergistically in ternary fashion. In other words, the relative rates ( $v$ ) and rate constants ( $k$ ) for polymeryl group exchange amongst all the metals, as well as that for chain-growth propagation at hafnium, must be of the following order:  $(v_{cb}, k_{ct})_{[\text{Zn,Hf}]}, (v_{cb}, k_{ct})_{[\text{Zn,Al}]} \gg (v_{cb}, k_{ct})_{[\text{Al,Hf}]} > (v_p, k_p)_{[\text{Hf}]}$ . Under this condition, similar approximate first-order relationships for number-average degree of polymerization  $X_n$  and polydispersity index PDI should be determined by eq. 3 and eq. 4, respectively, where  $k_{ct[\text{obs}]}$  is the overall apparent rate constant for chain transfer.<sup>100</sup>

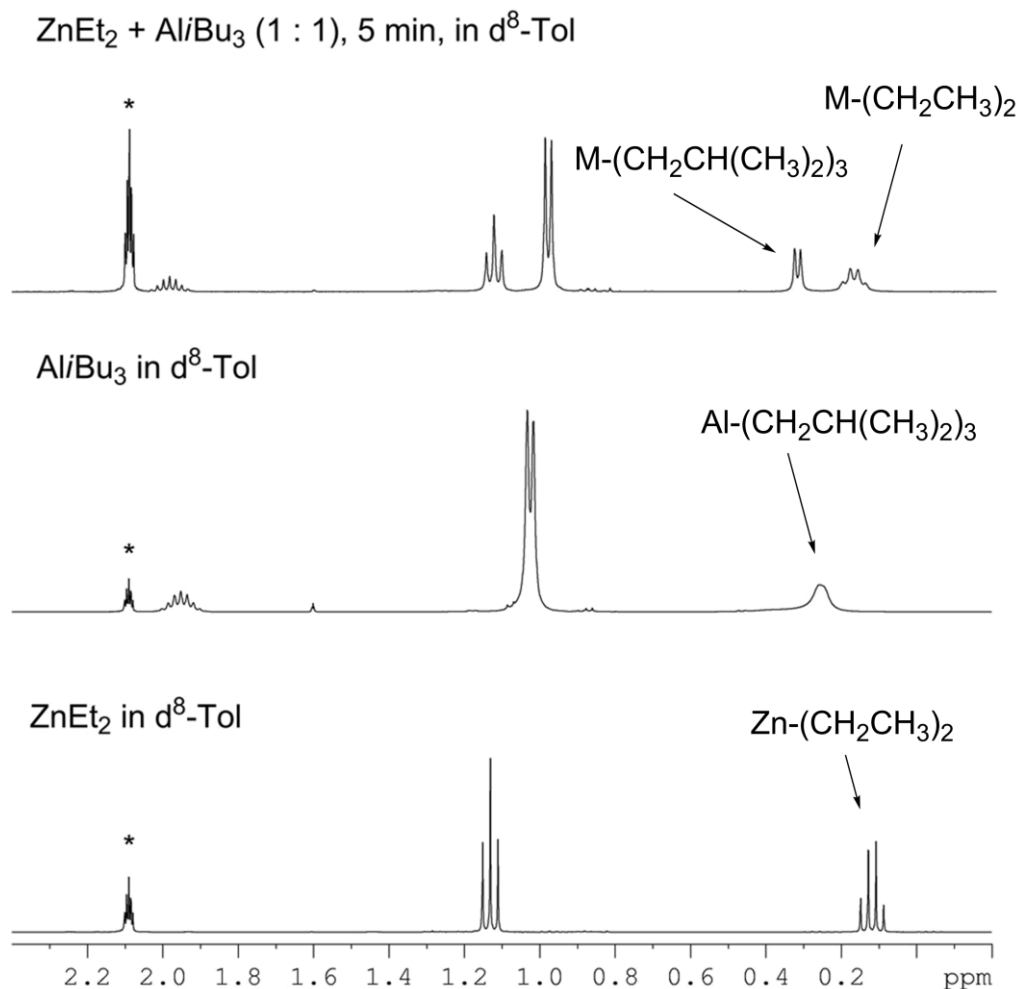
$$X_n = \frac{[\text{monomer}]_0 - [\text{monomer}]_t}{[(\text{Hf}) + 2x(\text{Zn}) + 3y(\text{Al})]_0} \quad (\text{eq. 3})$$

$$\text{PDI} = \frac{M_w}{M_n} \approx 1 + \frac{k_p}{k_{ct[\text{obs}]}} \quad (\text{eq. 4})$$

Polymerization results have demonstrated that the relative rates and rate constants for polymeryl group exchange between zinc and hafnium are much faster than those between aluminum and hafnium,  $(v_{cb}, k_{ct})_{[\text{Zn,Hf}]} \gg (v_{cb}, k_{ct})_{[\text{Al,Hf}]}$ .<sup>88-89</sup> The remaining question is whether the exchange rate between zinc and aluminum is also very rapid. First, there is ample evidence in support of rapid alkyl-group exchange in solution between two different main-group-metal alkyl species, such as between trialkyl borane compounds ( $\text{BR}_3$ ) and dialkyl zinc reagents ( $\text{ZnR}_2$ ),<sup>120-121</sup> as well as more specifically between  $\text{ZnEt}_2$  and  $\text{AlEt}_3$  in benzene.<sup>122</sup> Second,  $^1\text{H}$  NMR (400 MHz,  $\text{d}^8$ -toluene, 25 °C) experiments were carried out in order to study the alkyl group exchange rate between  $\text{ZnEt}_2$  and  $\text{AlR}_3$  without the presence of transition metal catalysts under our polymerization conditions. As shown in Figure 6, the chemical shifts of methylene protons on ethyl group (q,  $\delta = 0.18$  ppm, top) and methylene

protons on isobutyl group (d,  $\delta = 0.33$  ppm, top) in the 1 : 1 ratio of  $\text{Al}i\text{Bu}_3$  and  $\text{ZnEt}_2$  mixture changed compared to those from pure  $\text{ZnEt}_2$  (q,  $\delta = 0.12$  ppm, bottom) and pure  $\text{Al}i\text{Bu}_3$  (b,  $\delta = 0.25$  ppm, middle). Moreover, only one set of ethyl and one set of isobutyl resonances were observed in the  $\text{Al}i\text{Bu}_3$  and  $\text{ZnEt}_2$  mixture spectrum (top), indicating an average effect between zinc and aluminum metals. These results supported the much faster alkyl group exchange rate between  $\text{Al}i\text{Bu}_3$  and  $\text{ZnEt}_2$  relative to NMR time scale.

*Figure 6.*  $^1\text{H}$  NMR spectra of a 1 : 1 ratio  $\text{Al}i\text{Bu}_3$  and  $\text{ZnEt}_2$  mixture (top), pure  $\text{Al}i\text{Bu}_3$  (middle) and pure  $\text{ZnEt}_2$  (bottom). The methyl resonance of  $d^8$ -toluene is marked with an asterisk.



Finally, to the best of our knowledge, no data has yet been presented that might serve to either indicate or substantiate the possible existence of synergistic interactions for reversible coordinative chain-transfer polymerization of ethene, propene, or higher  $\alpha$ -olefins as mediated by two different main-group-metal alkyl species. Also, our intended use of  $\text{ZnEt}_2$  for t-LCCTP as both a secondary surrogate and as a CTM is mechanistically quite distinct from its role as a chain-shuttling agent for transferring a polymeryl group between two different active transition metal propagating species, as originally introduced by Arriola and co-workers<sup>97-98</sup> for the production of blocky poly(ethene-*co*-octene) by a nonliving process.

### 2.2.2 t-LCCTP of propene using mixed $\text{AlR}_3$ and $\text{ZnEt}_2$

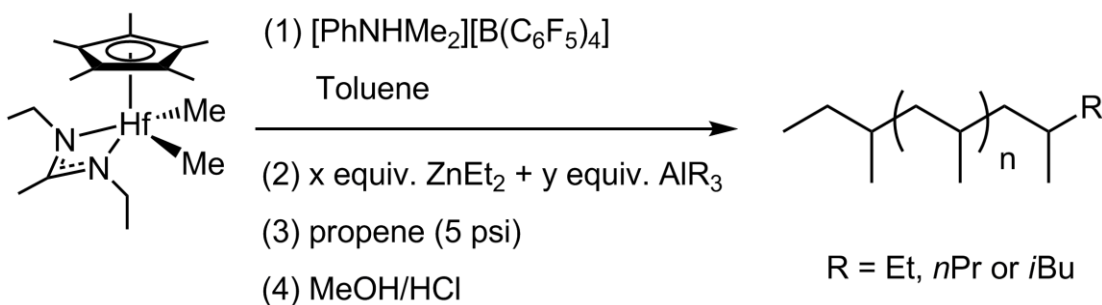
Table 1. LCCTP and t-LCCTP of propene

Entry	$\text{AlR}_3$ R	$\text{AlR}_3$ equiv. <sup>[a]</sup>	$\text{ZnEt}_2$ equiv. <sup>[a]</sup>	$t_p$ (h)	$T_p$ ( $^\circ\text{C}$ )	Yield (g)	$M_n$ <sup>[b]</sup> (kDa)	PDI
LCCTP								
2.01	-	-	20	2	0	4.2	8.75	1.04
2.02	Et	20	-	2	0	3.9	5.21	1.19
2.03	<i>n</i> Pr	20	-	4	20	2.7	3.42	1.20
2.04	<i>i</i> Bu	20	-	4	20	4.6	6.00	1.19
t-LCCTP								
2.05	Et	10	10	2	0	4.4	7.31	1.02
2.06	<i>n</i> Pr	10	10	2	0	2.0	2.88	1.05
2.07	<i>i</i> Bu	10	10	2	0	1.2	1.84	1.07
2.08	<i>i</i> Bu	18	2	4	20	3.1	4.53	1.04
2.09	<i>i</i> Bu	90	10	16	20	1.6	0.54	1.14
2.10	<i>i</i> Bu	18	2	20	-10	10.7	18.0	1.02
2.11	<i>i</i> Bu	190	10	72	20	88.0	0.58 <sup>[c]</sup>	1.10

[a] Molar equivalents relative to **07**. [b] Determined by GPC analysis. [c] Determined by NMR spectroscopic end-group analysis.

The upper half of Table 1 summarized the results of LCCTP of propene using active hafnium cation **07** and multiple equivalents of  $\text{ZnEt}_2$ ,  $\text{AlEt}_3$ ,  $\text{Al}n\text{Pr}_3$  and  $\text{Al}i\text{Bu}_3$  as chain-growth surrogates. Entry 2.01 served as a frame of reference in which compound **07** and 20 equiv. of  $\text{ZnEt}_2$  in toluene provided, after 2 h at 0 °C and 5 psi propene, an atactic polypropene (*a*PP) material for which the yield and  $M_n$  value were consistent with both ethyl groups of  $\text{ZnEt}_2$  being accessible and engaged in rapid and reversible chain transfer with the active transition-metal propagating species (e.g., PDI = 1.04). Upon replacing  $\text{ZnEt}_2$  with  $\text{AlEt}_3$  (entry 2.02),  $\text{Al}n\text{Pr}_3$  (entry 2.03) and  $\text{Al}i\text{Bu}_3$  (entry 2.04), similar results were obtained under identical conditions except the much broader molecular weight distributions (PDI = 1.19-1.21). The large PDI values were indicative of a smaller rate constant for hafnium–aluminum polymeryl group exchange relative to that for hafnium–zinc chain-transfer, or more specifically,  $k_{ct[\text{Zn,Hf}]} > k_{ct[\text{Al,Hf}]}$  according to Scheme 13.

Scheme 14, t-LCCTP of propene with mixed  $\text{AlR}_3$  and  $\text{ZnEt}_2$  surrogates

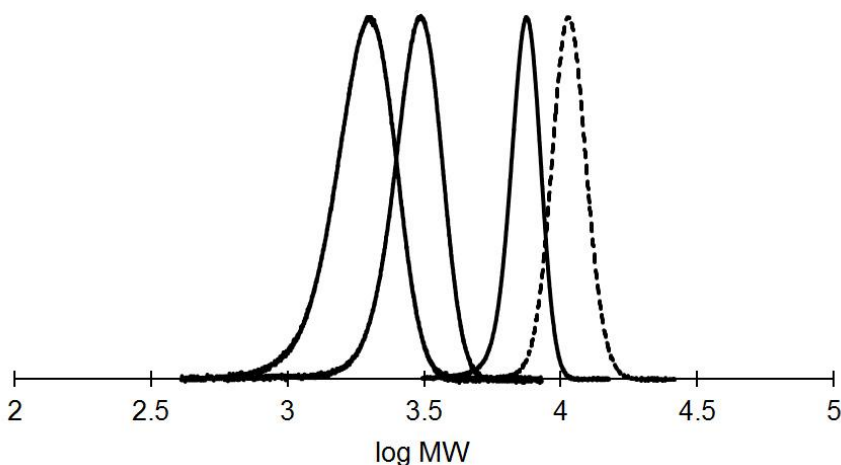


Wei Zhang has demonstrated that when 10 equiv. of each  $\text{AlEt}_3$  and  $\text{ZnEt}_2$  were employed, both the yield and  $M_n$  values of the resulting *a*PPs were found to be consistent with extremely rapid and reversible chain-transfer amongst all three metal species (entry 2.05). Remarkably, the polydispersity of this material was shown to be extremely narrow (PDI = 1.02). In order to explore the generality of t-LCCTP to a broad range of  $\text{AlR}_3$  compounds as primary chain-transfer surrogates,  $\text{Al}n\text{Pr}_3$  and  $\text{Al}i\text{Bu}_3$  were employed in

combination with  $\text{ZnEt}_2$  as CTM under the identical polymerization conditions shown in Scheme 14 and Table 1.

Gratifyingly, similar narrow molecular weight distributions were obtained when  $\text{AlnPr}_3$  and  $\text{Al}i\text{Bu}_3$  were employed as the primary surrogates with  $\text{ZnEt}_2$  as CTM in 1 : 1 ratio for t-LCCTP of propene (Figure 7). The PDI values decreased from 1.20 (entry 2.03) and 1.19 (entry 2.03) to 1.05 (entry 2.06) and 1.07 (entry 2.06) for t-LCCTP mediated by  $\text{AlnPr}_3$  and  $\text{Al}i\text{Bu}_3$ , respectively. Furthermore, end-group analysis of all the *a*PP samples by  $^1\text{H}$  NMR spectroscopy (600 MHz, 1,1,2,2- $\text{d}^2$ -tetrachloroethane, 90 °C) revealed the absence of terminal vinyl resonances owing to irreversible  $\beta$ -hydrogen transfer chain termination, thereby providing significant support for the living character of this t-LCCTP. The yields and  $M_n$  values decreased a little bit for t-LCCTP over LCCTP, which was due to the induction period at the early stage of polymerization probably raised from complexation between aluminum and hafnium complex. The preciseness of resulting polymers was maintained for both  $\text{AlnPr}_3/\text{ZnEt}_2$  and  $\text{Al}i\text{Bu}_3/\text{ZnEt}_2$  mediated t-LCCTP systems, which demonstrated the success of employing the t-LCCTP strategy to a broad selection of  $\text{AlR}_3$  as primary surrogates.

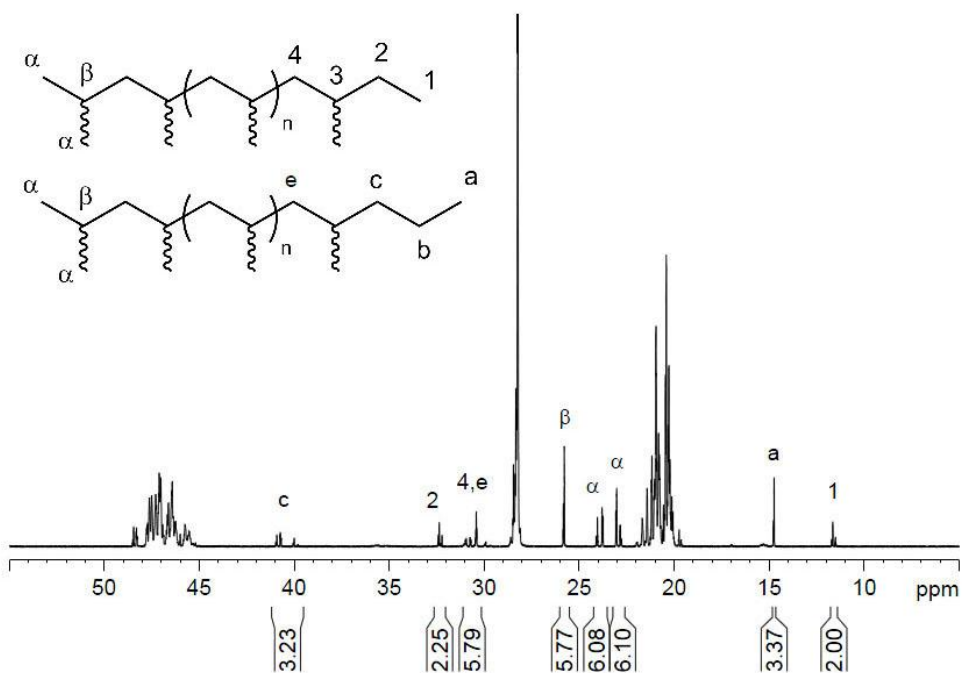
Figure 7. Molecular weight distributions for *a*PPs of entry 2.05, 2.06, 2.07 (from left to right) of Table 1 and a polystyrene standard (dotted line)



Moreover, end-group analyses by  $^{13}\text{C}$   $\{^1\text{H}\}$  NMR spectroscopy (150 MHz, 1,1,2,2- $\text{C}_2\text{D}_2\text{Cl}_4$ , 90 °C) were performed to investigate whether all three alkyl groups on aluminum were engaging in the t-LCCTP of propene. In the following experiments,  $\text{AlR}_3$  ( $\text{R} = n\text{Pr}$  and  $i\text{Bu}$ ) and  $\text{ZnEt}_2$  was used in a 1 : 1 ratio for easy integration and comparison. If all three alkyl groups on aluminum engaged in the chain-transfer process as both alkyl groups on zinc were, the chain-growth starting ends would have a 3 : 2 ratio of  $n$ -propyl/isobutyl to ethyl groups (the chain-termination ends would all be isobutyl groups from propene monomers).

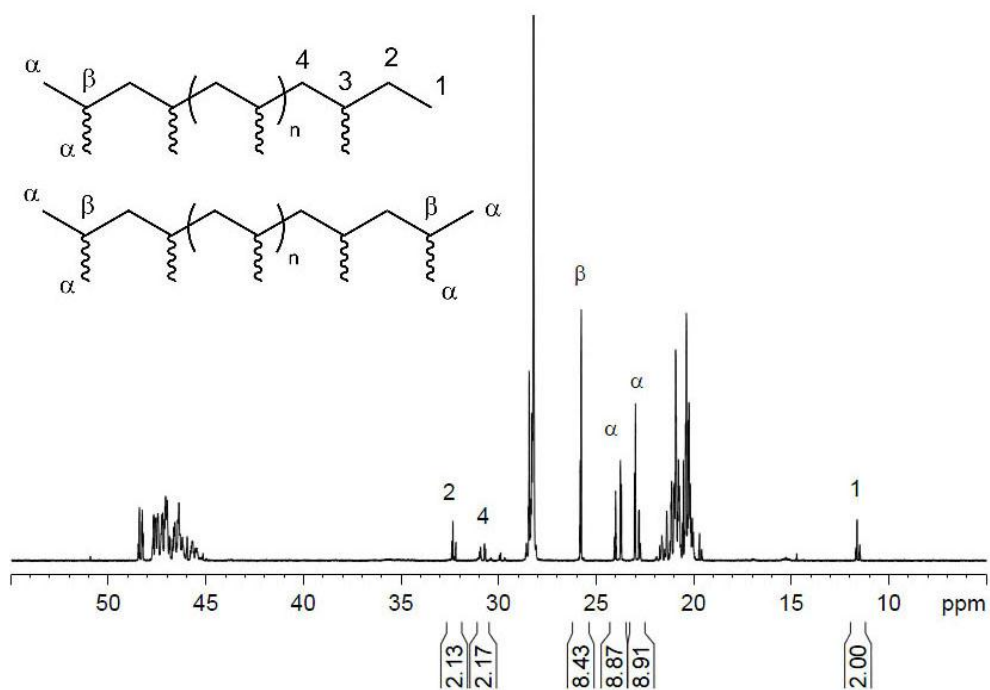
As shown by Figure 8, the structure assignments on the top represent  $a\text{PP}$  sample with an ethyl end-group from  $\text{ZnEt}_2$ , while structure assignments at the bottom represent  $a\text{PP}$  sample with a  $n$ -propyl end-group from  $\text{Al}(n\text{Pr})_3$ . Integrations of  $^{13}\text{C}$  NMR spectrum show that 3/10 of the polymer chain end-groups are  $n$ -propyl group, 1/5 end-groups are ethyl group, and 1/2 end-groups are isobutyl group, which perfectly agree with the theoretical ratio of a 1 : 1 mixture of  $\text{ZnEt}_2$  and  $\text{Al}(n\text{Pr})_3$ .

Figure 8.  $^{13}\text{C}$  NMR spectrum and structural drawings of  $a\text{PP}$  from entry 2.06 of Table 1



As shown by Figure 9, 4/5 of *a*PP end-groups are isobutyl groups and 1/5 end-groups are ethyl groups which again agree with the theoretical ratio of a 1 : 1 mixture of ZnEt<sub>2</sub> and Al(*i*Bu)<sub>3</sub>. Those results have unequivocally established that all three alkyl groups on AlR<sub>3</sub> (R = *n*Pr and *i*Bu) and both two alkyl groups on ZnEt<sub>2</sub> are incorporated into the respective *a*PP materials at the theoretical level and ratio in each case.

Figure 9. <sup>13</sup>C NMR spectrum and structural drawings of *a*PP from entry 2.07 of Table 1

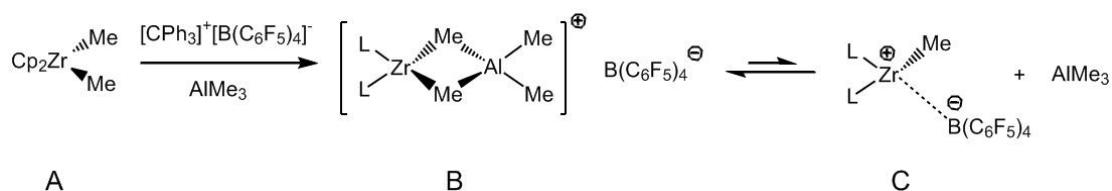


Finally, it can be noted that as the size of the R group in AlR<sub>3</sub> increased in the order Et < *n*Pr < *i*Bu, a commensurate decrease in the apparent overall rate of t-LCCTP that further tracks with a slight steady increase in PDI values was observed (entries 2.05-2.07 in Table 1). Although the origins of these trends are under further investigation, it is reasonable to presume that they arise from differences in the rates for initial chain transfer. That is to say, larger R group may lead to longer induction period before the onset of polymerization.

### 2.2.3 Study on the induction period of $\text{AlR}_3$ mediated t-LCCTP

For  $\text{AlR}_3$  ( $\text{R} = n\text{Pr}$  and  $i\text{Bu}$ ) mediated LCCTP and t-LCCTP, it was noted that long induction periods of at least one hour were always observed prior to the onset of polymerization. Induction period has no effect on the preciseness of resulting polymers, but it requires longer polymerization time to acquire similar yield and  $M_n$  values of the polymers compared to the polymerization without induction period. The possible origin of this phenomenon and solution to it are the subjects of the following investigations.

Figure 10.  $\text{AlMe}_3$  complexation with dimethyl zirconocene during activation process

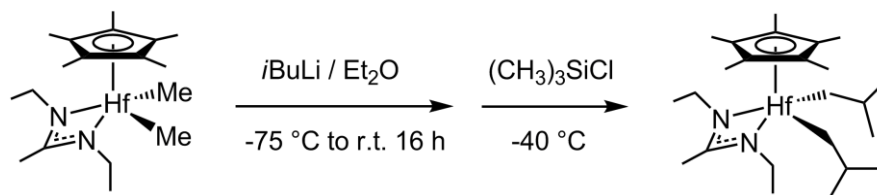


Bochmann reported that if sufficiently basic and sterically unhindered metal alkyls were present, such as  $\text{AlMe}_3$  (as a dimer of  $\text{Al}_2\text{Me}_6$ ), cationic heterobinuclear adduct B from the complexation of dimethyl zirconocene A and  $\text{AlMe}_3$  resulted (Figure 10).<sup>123-124</sup> The equilibration between active ion-pair chain propagation species C and B reduced the concentration of active C for polymerization, which might be the origin of the induction period we observed for  $\text{AlR}_3$ -mediated LCCTP and t-LCCTP.

Several strategies have been proposed to address the induction period problem. First, a diisobutyl hafnium precatalyst,  $\text{Cp}^*\text{Hf}(i\text{Bu})_2[\text{N}(\text{Et})\text{C}(\text{Me})\text{N}(\text{Et})]$  (**11**) was synthesized as an analogue to dimethyl compound **08** to check if isobutyl group will help to prevent the complexation of hafnium initiator with  $\text{AlR}_3$ . As shown in Scheme 15, diisobutyl compound **11** was made by reacting dimethyl hafnium compound **08** with  $i\text{BuLi}$  in diethyl ether at  $-75^\circ\text{C}$ , followed by quenching the excess  $i\text{BuLi}$  and resulting  $\text{MeLi}$  with trimethylsilyl chloride

(TMSCl) at  $-40\text{ }^{\circ}\text{C}$ . Final compound **11** was collected by recrystalling the crude product in pentane at  $-20\text{ }^{\circ}\text{C}$ . LCCTP of propene was carried using precatalyst **11** and cocatalyst **04** with 20 equiv. of  $\text{Al}i\text{Bu}_3$  in toluene at  $20\text{ }^{\circ}\text{C}$  for 4 h to give 4.5 g of *aPP* ( $M_n = 6.05\text{ kDa}$ ; PDI = 1.16). An induction period of 40 min was observed, which was less than that of using precatalyst **08** under same conditions (e.g., 1h induction period for entry 2.04 of Table 1). This showed that using bulkier isobutyl group help to reduce the length of induction period, but isobutyl group was not bulky enough.

*Scheme 15.* Synthesis of compound  $\text{Cp}^*\text{Hf}(i\text{Bu})_2[\text{N}(\text{Et})\text{C}(\text{Me})\text{N}(\text{Et})]$  (**11**)

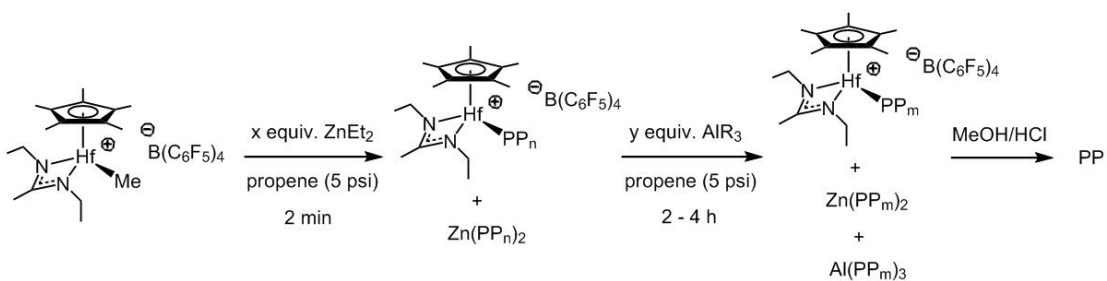


Second, we have investigated the possibility of using excess amount of borate cocatalyst (relative to precatalyst **08**) to drive the equilibrium to the dissociation of the Hf–Al binuclear complex that caused the induction period problem. When 3 equiv. of cocatalyst  $[\text{CPh}_3][\text{B}(\text{C}_6\text{F}_5)_4]$  (**12**) were used relative to **08**, both LCCTP of propene with  $\text{Al}i\text{Bu}_3$  and *t*-LCCTP of propene with  $\text{Al}i\text{Bu}_3/\text{ZnEt}_2$  showed immediate consumption of propene gas after initiation without any induction period. The actual reason behind this observation is not clear yet, but this offers a practical solution to eliminate the induction period. However, this solution is not ideal because it involves using multiple equivalents of a borate cocatalyst which is usually as expensive as the transition metal precatalyst, which contradicts our goal of reducing cost through LCCTP and *t*-LCCTP.

Finally, a third strategy has been developed, which did not require either synthesis of new transition metal compound or addition of extra amount of chemicals. In this method, we

only modified the procedure of polymerization as shown in Scheme 16. First, LCCTP was carried out using cationic compound **07** and  $\text{ZnEt}_2$  for a very short time (e.g., 2 min) to grow a short PP chain on hafnium metal that is long enough to prevent the complexation of  $\text{AlR}_3$  with hafnium compound. After that, a large amount of primary surrogate  $\text{AlR}_3$  was added to the polymerization system to ensure the ternary chain-transfer process, and the polymerization continued for a much longer time (e.g., 2 h). In this way, there was no induction period and the molecular weight distribution of the resulting polymer would be still monomodal because the lengths of the PP chains grown from first LCCTP step were negligible to the overall PP chain lengths. Satisfactorily, t-LCCTP of propene carried out using this method always shows narrow PDI values.

*Scheme 16.* Modified procedure of t-LCCTP of propene to avoid induction period

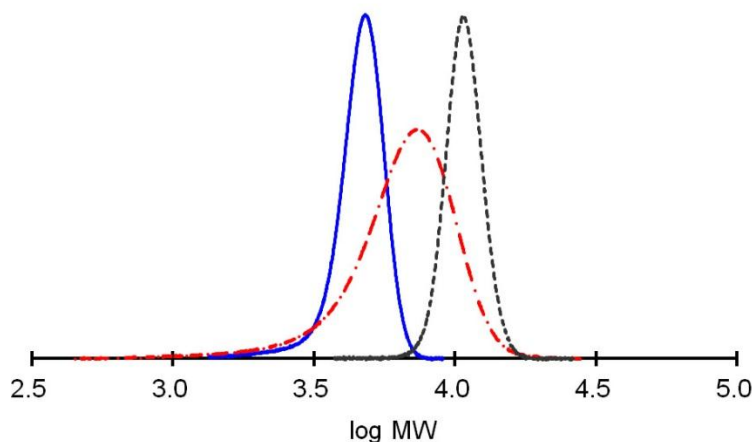


#### 2.2.4 t-LCCTP with catalytic amount of $\text{ZnEt}_2$ relative to $\text{AlR}_3$

With the success of expanding t-LCCTP primary chain-growth surrogates to a broad range of  $\text{AlR}_3$  ( $\text{R} = \text{Et}$ ,  $n\text{Pr}$  and  $i\text{Bu}$ ), we next sought to address the critical question of whether t-LCCTP could be achieved using only a minimal amount of  $\text{ZnEt}_2$ . This is directly related to our original goal of catalyzed PP chain-growth on aluminum metal instead of zinc. Compound **07** was used as initiator with 18 equiv. of primary surrogate  $\text{Al}i\text{Bu}_3$  and 2 equiv. of  $\text{ZnEt}_2$  as CTM in toluene at ambient conditions (20 °C, 5 psi) to produce *a*PP material of very narrow polydispersity ( $\text{PDI} = 1.04$ ). Figure 11 shows the comparison of molecular

weight distributions for *a*PP sample obtained from LCCTP of propene according to entry 2.04 (red dashed curve) and that from t-LCCTP of propene according to entry 2.08 (blue solid curve) of Table 1. The molecular weight distribution for a polystyrene standard ( $M_n = 11.3$  kDa; PDI = 1.02) is shown as the black dotted curve for comparison. Once again,  $^1\text{H}$  NMR spectroscopy further confirmed the living character of this t-LCCTP process. Therefore, all data conclusively demonstrated that with only 10 mol% (relative to total amount of surrogates)  $\text{ZnEt}_2$  serving as a CTM and secondary surrogate, the t-LCCTP of propene could be effectively and efficiently achieved.

*Figure 11.* Molecular weight distributions for *a*PP products obtained from the LCCTP (red dashed curve) and t-LCCTP (blue solid curve) of propene.



Further attempt of t-LCCTP of propene was carried out with 90 equiv. of primary surrogate  $\text{Al}i\text{Bu}_3$  and 10 equiv. of  $\text{ZnEt}_2$  (entry 2.09 in Table 1). After 16 h polymerization at 20 °C, 1.6 g of propene oligomer was obtained ( $M_n = 0.54$  kDa; PDI = 1.14), which was still very narrow compared with the polystyrene standard ( $M_n = 0.58$  kDa; PDI = 1.15). However, the polymerization yield was suppressed a lot because of the extremely long induction period (over 8 h) due to the large quantity of  $\text{Al}i\text{Bu}_3$  species. This experiment indicated that the

modified polymerization procedure shown in Scheme 16 would have to be employed in order to carry out t-LCCTP mediated with a large amount of  $\text{AlR}_3$ .

In order to study the temperature effect on the t-LCCTP of propene, polymerization was carried out at  $-10\text{ }^\circ\text{C}$  (entry 2.10 in Table 1) with other conditions same to those of entry 2.08. 10.7 g of *a*PP was obtained after 20 h of polymerization with  $M_n$  of 18.0 kDa and PDI value of 1.02. Lower PDI value was probably due to the reason that chain propagation rate constant,  $k_p$ , was more adversely affected by low temperature than observed chain-transfer rate constant,  $k_{ct[\text{obs}]}$ , based on the equation of  $\text{PDI} \approx 1+k_p/k_{ct[\text{obs}]}$ . The yield of 10.7 g after 20 h (entry 2.10) compared to that of 3.1 g after 4 h (entry 2.08) supported that lower activity and propagation rate at lower temperature.

### **2.3 Scalable Production of Precision Hydrocarbons from $\text{AlR}_3$ via t-LCCTP**

With conditions of t-LCCTP optimized for production of PHCs, our next attempt was to scale up the polymerization to make approximately 100 g of PP oligomers under near ambient conditions while using only a very small amount of transition-metal initiator and a catalytic amount (relative to  $\text{AlR}_3$ ) of  $\text{ZnEt}_2$  as CTM. The modified polymerization strategy shown in Scheme 16 was employed to minimize the influence of induction period in the presence of a large amount of  $\text{Al}i\text{Bu}_3$ .

As entry 2.11 of Table 1 and Figure 12 revealed, this living oligomerization of propene by t-LCCTP with catalyst **07** could be substantially and successfully scaled in volume by employing 190 equiv.  $\text{Al}(i\text{Bu})_3$  with as little as 5 mol% (10 equiv.)  $\text{ZnEt}_2$  in toluene at the room temperature and slightly above 1 atm (5 psi) to provide 88 g of the colorless oil represented by *a*PP with a targeted low molecular weight and very narrow polydispersity ( $M_n = 580\text{ Da}$ ;  $\text{PDI} = 1.10$ ). The PDI value (1.10) is even lower than the polystyrene standard with  $M_n$  value of 580 Da ( $\text{PDI} = 1.15$ ). Most telling regarding the

significance of this result is that, to obtain an equal quantity of this new PHC material through traditional living coordination polymerization, 64.7 g of transition metal precatalyst **08** (with 130.7 g of borate cocatalyst **12**) would have been required as compared to the 0.11 g of **08** (with 0.22 g of **12**) that was employed for t-LCCTP in the present example!

Equally important is the fact that this t-LCCTP of propene was carried out at ambient temperature over a period of 72 h with only a very slight increase in termination that is responsible for the small degradation in product polydispersity. A large excess of  $\text{Al}i\text{Bu}_3$  help to stabilize the active hafnium chain propagation initiators and made the polymerization robust at room temperature for several days. As shown by the middle and right photos in Figure 12, the limit of yield of this polymerization was actually the volume of the schlenk flask rather than the thermo-stability or turn over number of the transition metal catalyst.

*Figure 12.* A new PHC-based *a*PP oil prepared by scaled-up t-LCCTP (left) and the photos of polymerization reaction flask at 0 h (middle) and 72 h (right).



## 2.4 t-LCCTP Copolymerization of Propene with 1-Octene

With support of t-LCTPP of propene secured, we were curious to see if t-LCCTP strategy could be extended to the copolymerization of propene with higher  $\alpha$ -olefin monomers. Based on the reported results of LCCTP copolymerization of ethene with 1-octene using cationic catalyst **07** and ZnEt<sub>2</sub> as chain-transfer surrogate,<sup>89</sup> both LCCTP and t-LCCTP copolymerization of propene with 1-octene should be able to perform in a similar fashion, providing random copolymers. Also, incorporation of branches into the PP backbone could have influence on the rheology of the resulting polyolefin oligomers, which might lead to novel type of PHCs.

Table 2. t-LCCTP copolymerization of propene with 1-octene

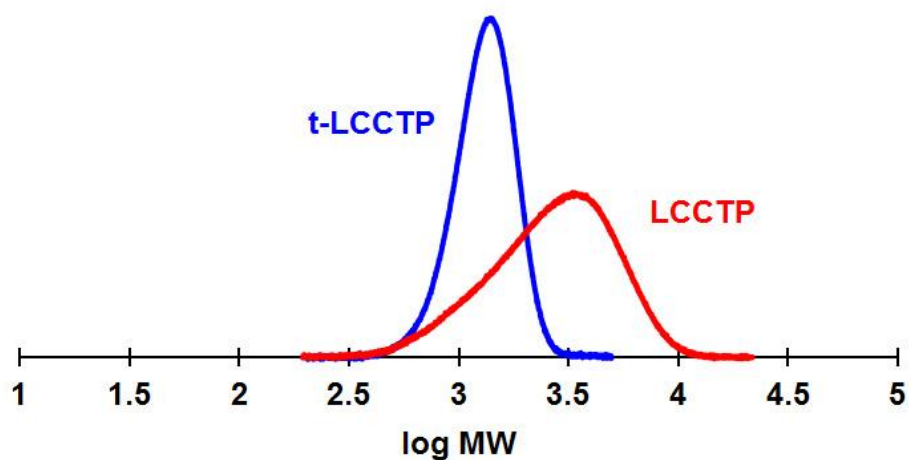
Entry	1-octene (equiv.)	Al <sub>i</sub> Bu <sub>3</sub> equiv. <sup>[a]</sup>	ZnEt <sub>2</sub> equiv. <sup>[a]</sup>	t <sub>p</sub> (h)	T <sub>p</sub> (°C)	Yield (g)	M <sub>n</sub> (kDa)	PDI	1-octene (mol%)
2.12	500	18	2	4	20	0.8	1.27	1.10	23
2.13	500	20	--	4	20	1.4	2.31	1.46	24

[a] Molar equivalents relative to precatalyst **08**.

Entry 2.12 of Table 2 served to establish that t-LCCTP could also be successfully extended to copolymerization of propene with 1-octene. In this case, 10 mol% (2 equiv. to precatalyst **08**) ZnEt<sub>2</sub> in combination with 18 equiv. Al<sub>i</sub>Bu<sub>3</sub> (relative to **08**) efficiently provided a random poly(propene-*co*-1-octene) (poly(P-*co*-O)) material comprised of a targeted low molecular weight of very narrow polydispersity ( $M_n = 820$  Da; PDI = 1.10). Once again, in the absence of ZnEt<sub>2</sub>, standard LCCTP provided a similar material, albeit one of inferior polydispersity (PDI = 1.46; entry 2.13 of Table 2). As shown in Figure 13, the copolymer made by t-LCCTP (blue curve) is more precise in molecular weight distribution when compared with material made by LCCTP (red curve), which agrees with the results of

homo-polymerization of propene. In both cases, 1-octene was incorporated at a level of approximately 23 to 24 mol% as determined by  $^{13}\text{C}$  NMR spectroscopic structural analysis. Actually, the usage of the main group metal alkyls as surrogates should not have influence on the co-monomer incorporation level, which is determined by the nature of the transition metal catalyst. In those copolymerizations, the yields and  $M_n$  values of t-LCCTP (entry 2.12) is lower than that of LCCTP (entry 2.13) and the reason is still under investigation. The complexation of  $\text{AlR}_3$  with transition metal complexes might lead to slightly decrease of the concentration of active chain propagation species during polymerization, which results in the lower yields.

*Figure 13.* Molecular weight distributions for poly(P-co-O) materials made from t-LCCTP (blue curve) and LCCTP (red curve)



## 2.5 Conclusions

In summary, the present results serve to validate the concept of t-LCCTP of propene and  $\alpha$ -olefins as a viable process for accessing a large variety of PHCs in scalable bulk quantities. Importantly, this process employs much less expensive and much less pyrophoric  $\text{AlR}_3$  (R = Et and *i*Bu) reagents that carry three alkyl chains as the primary surrogate chain-growth centers in combination with only a relatively small amount of  $\text{ZnEt}_2$  (e.g., 5 mol%). Polymerization procedure for t-LCCTP has been optimized to minimize the negative influence of the complexation of  $\text{AlR}_3$  with transition metal species on yield and polymerization time.

As the initial product of t-LCCTP before acidic quench is an  $\text{Al}(\text{polymeryl})_3$  species, a variety of simple chemical transformations can be envisioned to additionally yield a broad range of end-group-functionalized PHCs. In this respect, after a wait of nearly 60 years, a new Aufbaureaktion has been introduced for the practical and scalable living oligomerization of propene and longer-chain  $\alpha$ -olefins.

# Chapter 3: Preparation of Block and End-Group Functionalized Precision Polyolefins through LCCTP

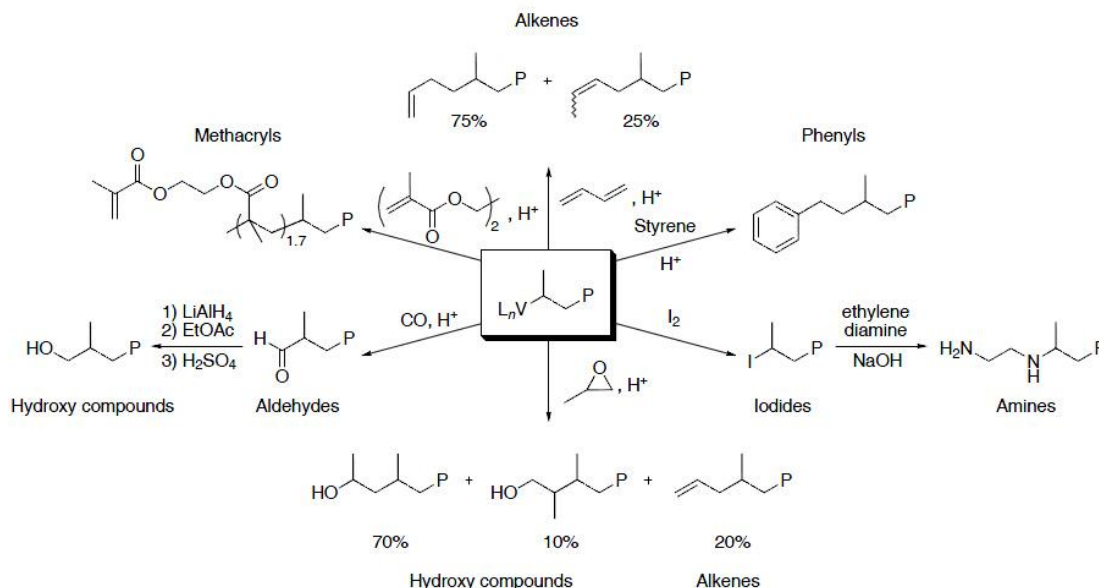
## **3.1 Background**

### **3.1.1 End-group functionalization through living coordination polymerization**

Functionalized polyolefins have many advantages and broader application range compared to non-functionalized polyolefins, including increased adhesion, paintability, and compatibility with diverse, more-polar materials, etc.<sup>125-127</sup> Two conventional pathways for polyolefin functionalization are post-polymerization modification and direct catalytic introduction of functional groups. Although the post-polymerization modification avoids the issues of catalyst functional-group tolerance, the unreactive nature of hydrocarbon polymers leads to difficult chemical modifications involving potentially harsh reaction conditions with a general lack of selectivity during the functionalization.<sup>128-129</sup> In contrast, selective and catalytic introduction of functional groups into polymerization processes offers the advantage of a controlled one-pot in situ synthesis.

One effective catalytic functionalization method involves in situ quenching a living coordination polymerization that has no/negligible chain-termination process. Therefore, the intermediate living polymers can provide a variety of well-defined end-group functionalized polyolefins with high efficiency through chemical reactions involving the reactive terminal metal-carbon bond.<sup>51,130-132</sup>

Scheme 17. Synthesis of end-group functionalized polypropene with a vanadium catalyst

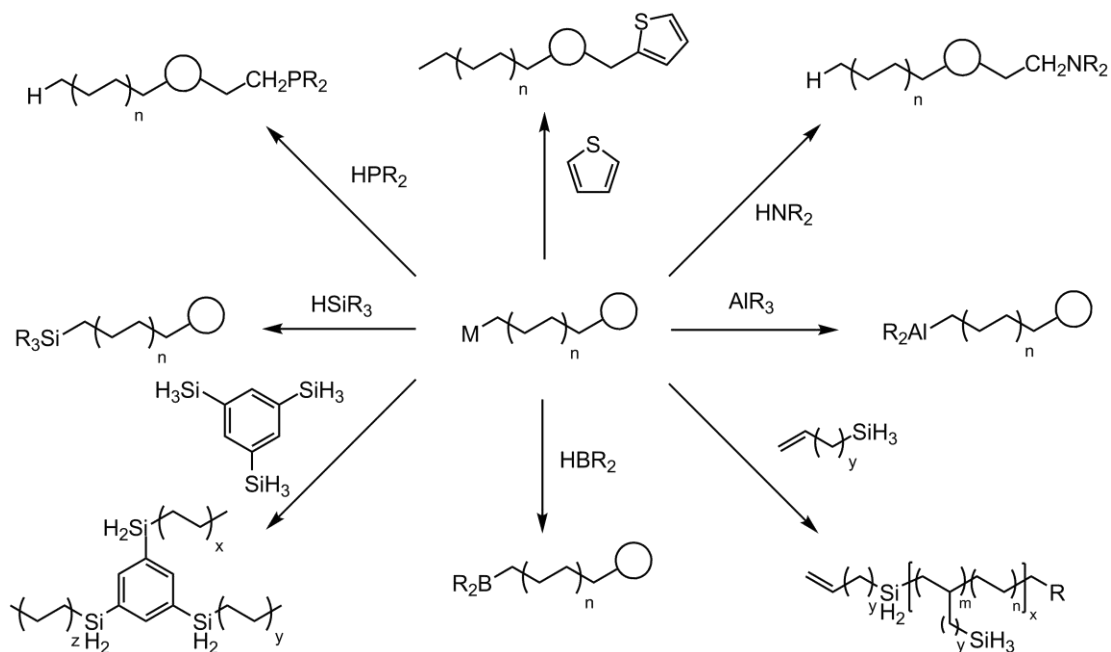


Doi and co-workers have demonstrated the utility of the living vanadium catalysts through the synthesis of polypropenes (PPs) with a wide variety of functional end-groups (Scheme 17).<sup>58-62</sup> In addition to providing important mechanistic information, these functional polymers display unique properties and have also been used as macro-initiators for the synthesis of block copolymers. First, the living vanadium-PP species was quenched with iodine at  $-78\text{ }^\circ\text{C}$  to yield a monodisperse iodine-functionalized PP ( $M_w/M_n = 1.15$ ).<sup>58</sup> Then this iodine-functionalized PP was used to prepare an amine-terminated PP by reacting the polymer with excess ethylenediamine in THF, followed by basic work-up.<sup>59</sup> Second, by reacting this vanadium-PP species with carbon monoxide, Doi et al. have prepared aldehyde-terminated PP.<sup>60</sup> This aldehyde functionality was used to prepare hydroxyl-functionalized PPs through reduction of the aldehyde with  $LiAlH_4$  in  $Et_2O$ , followed by acidic hydrolysis.<sup>61</sup> Third, PP macro-monomers containing methacryl functionality were prepared by addition of ethylene glycol dimethacrylate (EGDM) to a living chain end.<sup>62</sup> Finally, by quenching living PP with butadiene, PPs with alkenyl and phenyl end groups were prepared.<sup>61</sup>

### 3.1.2 Coordinative chain-transfer strategy for end-group functionalization

Chain-transfer is one of the most common processes in a polymerization as chain initiation, propagation and termination. Chain-transfer process represents highly effective chemical means to achieve selective, in situ transition metal catalyzed functionalization of polyolefins.<sup>133</sup> A diverse variety of electron-poor and electron-rich chain-transfer agents, such as silanes, boranes, alanes, phosphines, and amines, effect efficient chain transfer/termination with concomitant carbon-heteroatom bond formation during single-site olefin-polymerization processes (Scheme 18).<sup>125</sup> For example, Chung reported using 9-bora-bicyclononane (9-BBN) and other organoborane hydrides chain-transfer agents to prepare a series of boron-capped polyolefins. Further functionalization to a variety of end-group functionalized polyolefins, such as hydroxyl-terminated PP and diblock copolymer of PP-*block*-poly(methyl methacrylate) (PMMA), have also been achieved.<sup>134</sup>

*Scheme 18.* Versatile pathways for in situ polyolefin functionalization with heteroatoms<sup>125</sup>



Recently, researchers have explored and developed the concept of coordinative chain-transfer polymerization (CCTP) of ethene that utilizes an excess of an inexpensive main-group-metal alkyl as surrogate chain growth centers that arise from fast and reversible chain-transfer between the surrogate and the active transition metal propagating species.<sup>85</sup> In this way, chemical transformation of those main group metal carbon bond will bring functional group to the end of the polymer chains. Studies have been mainly focused on using aluminum<sup>135-137</sup>, zinc<sup>138-139</sup> and magnesium<sup>140-142</sup>-based chain-transfer surrogates. For example, D'Agosto and Boisson have investigated using a  $(\eta^5\text{-C}_5\text{Me}_5)_2\text{NdCl}_2\text{Li}(\text{OEt}_2)_2$  complex in conjunction with *n*butyloctylmagnesium (*n*Bu-Mg-Oct) as a chain-transfer surrogate to synthesize an array of end-group functional PE chains.<sup>141</sup> Hydroxyl-, thiol-, iodo-, azido- and porphyrine-end-group terminated PE materials have been synthesized and PE-*block*-poly(*n*-butyl acrylate) has been made *via* RAFT polymerization mediated by PE-SC(=S)S-*t*Bu as macro-initiator.

Our group's recent contribution to this field was to couple CCTP based on  $\text{ZnEt}_2$  with the living coordination polymerization and copolymerization of ethene, propene, and  $\alpha$ -olefin and  $\alpha,\omega$ -nonconjugated dienes that utilizes the cationic hafnium compound **07** as the active initiator in a process that we functionalized precision polyolefins that further proceeds with high chemical efficiency and yield. In chapter two, t-LCCTP has been successfully demonstrated to carry out PP and poly(P-*co*-O) chain-growth on aluminum metal by using a large amount of  $\text{AlEt}_3$  or  $\text{Al}i\text{Bu}_3$  as primary chain-transfer surrogate. One great advantage of t-LCCTP, as well as binary LCCTP, is the ease of functionalization of Zn-C/Al-C bonds to selectively add end-group functionality to the non-functional precision polyolefins. Also,  $\text{Zn}(\text{polymeryl})_2/\text{Al}(\text{polymeryl})_3$  and their derivatives could initiate another polymer chain-growth from polyolefins to make polyolefin-based block copolymers.

### 3.2 Preparation and Stability Study on Zn(polymeryl)<sub>2</sub> Stock Solution

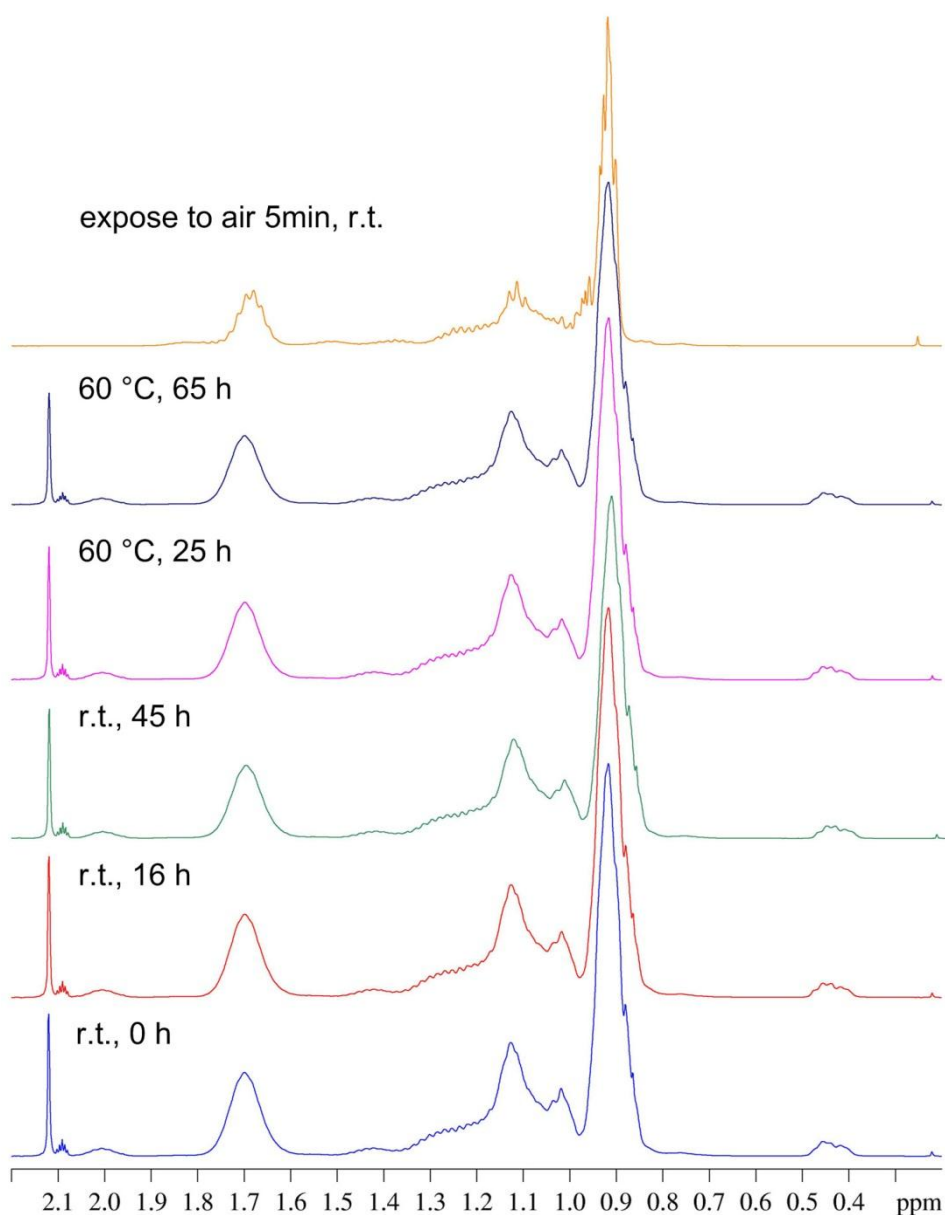
After executing either binary or ternary LCCTP, the principal products obtained are toluene solution of the main group metal polymeryl compounds, Zn(polymeryl)<sub>2</sub> and Al(polymeryl)<sub>3</sub>, respectively. A key question of both binary and ternary LCCTP is that, after removal of the olefin monomers *in vacuo*, could the stock solutions of Zn(polymeryl)<sub>2</sub> and Al(polymeryl)<sub>3</sub> in toluene be prepared and stored at low temperature for several days or months without any apparent decomposition. Using the stock solution has the advantage of avoiding performing a polymerization that usually takes several hours before each *in situ* end-group functionalization reaction. Also structures and properties of the end-group functionalized polymers, such as molecular weights and molecular weight distributions, are comparable from the same stock of starting materials.

First of all, a toluene solution of Zn(*a*PP)<sub>2</sub> was prepared through LCCTP of propene using cationic diethyl hafnium **07** with a large amount of ZnEt<sub>2</sub> (e.g., 200 equiv. relative to **07**) as surrogate in toluene at 0 °C. After the target molecular weight had been achieved, propene gas feed was terminated and the remaining propene in toluene was pumped down *in vacuo* for 30 min at 0 °C. The yellow Zn(*a*PP)<sub>2</sub>toluene solution was stocked at -20 °C under N<sub>2</sub> atmosphere.

<sup>1</sup>H NMR spectroscopy was used to probe the stability of Zn(*a*PP)<sub>2</sub> in toluene. 1 ml Zn(*a*PP)<sub>2</sub>/toluene solution was taken out and toluene was completely pumped down *in vacuo*. The remaining Zn(*a*PP)<sub>2</sub> was dissolved into dry d<sup>8</sup>-toluene under N<sub>2</sub> atmosphere for an immediate <sup>1</sup>H NMR experiment at room temperature. As shown in Figure 14, the broad resonance at 0.4 to 0.5 ppm stands for α-protons adjacent to zinc metal which confirmed the existence of Zn-C bond. A second and a third <sup>1</sup>H NMR experiments were carried out after 16 h and 45 h respectively, at room temperature. Same resonance at 0.4 to 0.5 ppm confirmed

the stability of  $\text{Zn}(\text{aPP})_2/\text{toluene}$  at room temperature up to 2 days. Then another  $\text{Zn}(\text{aPP})_2/\text{d}^8\text{-toluene}$  NMR sample was heated to 60 °C while sealed under  $\text{N}_2$  atmosphere. After 25 h and 65 h respectively, a fourth and a fifth  $^1\text{H}$  NMR experiments were carried out and results again demonstrated the stability  $\text{Zn}(\text{aPP})_2/\text{toluene}$  even at higher temperature for around 3 days without decomposition of Zn-C bond (Figure 14).

Figure 14. Stability study through  $^1\text{H}$  NMR spectroscopy of  $\text{Zn}(\text{aPP})_2/\text{toluene}$  stock solution



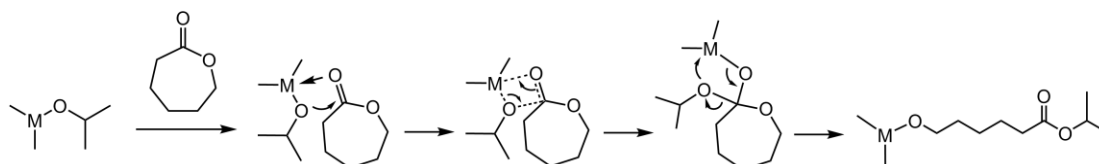
To test the stability/reactivity of  $\text{Zn}(a\text{PP})_2/\text{toluene}$  in the presence of  $\text{O}_2$ , a sixth sample was prepared by exposing  $\text{Zn}(a\text{PP})_2/\text{toluene}$  solution to air for 5 min before taking the  $^1\text{H}$  NMR in  $\text{CDCl}_3$ . As shown by the top spectrum in Figure 14, no resonance at 0.4 to 0.5 ppm was observed which indicated that  $\text{Zn-C}$  bond had been reacted in the presence of  $\text{O}_2$ . Those results demonstrated that  $\text{Zn}(a\text{PP})_2$  toluene solution was stable and not sensitive to temperature at  $\text{N}_2$  atmosphere for several days, while decomposed quickly in contact with air.

### 3.3 Ring-Opening Polymerization of $\epsilon$ -Caprolactone from $\text{Zn}(\text{O-polyolefin})_2$

#### 3.3.1 Synthesis and characterization of *aPP-block-PCL*

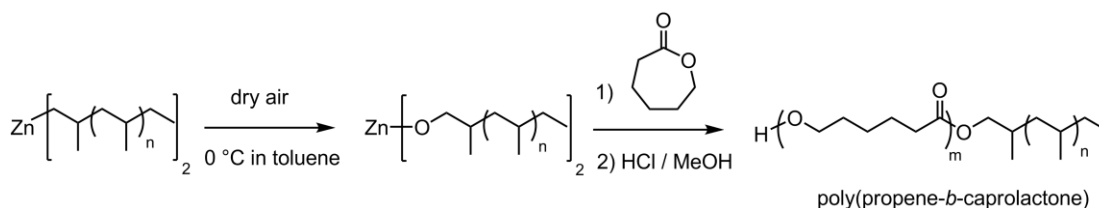
It is well-known that  $\text{Al}(\text{O-R})_3$  and  $\text{Zn}(\text{O-R})_2$  can initiate ring-opening polymerization of  $\epsilon$ -caprolactone through a coordination-insertion mechanism and generate poly( $\epsilon$ -caprolactone) (PCL).<sup>143</sup> As shown in Scheme 19, the propagation is proposed to proceed through the coordination of the monomer to the metal alkoxide compound and the insertion of the monomer into a metal-oxygen bond of the catalyst.<sup>144-145</sup> During propagation, the growing chain is attached to the metal through an alkoxide bond. R group from the metal alkoxide compound will remain at the end of PCL. Therefore, with the advantage of preparation the stock solution of  $\text{Zn}(\text{polyolefin})_2$ , it is interesting to see if we could couple the semicrystalline polyester to non-functional polyolefin as a diblock copolymer.

*Scheme 19.* Mechanism of the initiation step for coordination–insertion ring-opening polymerization



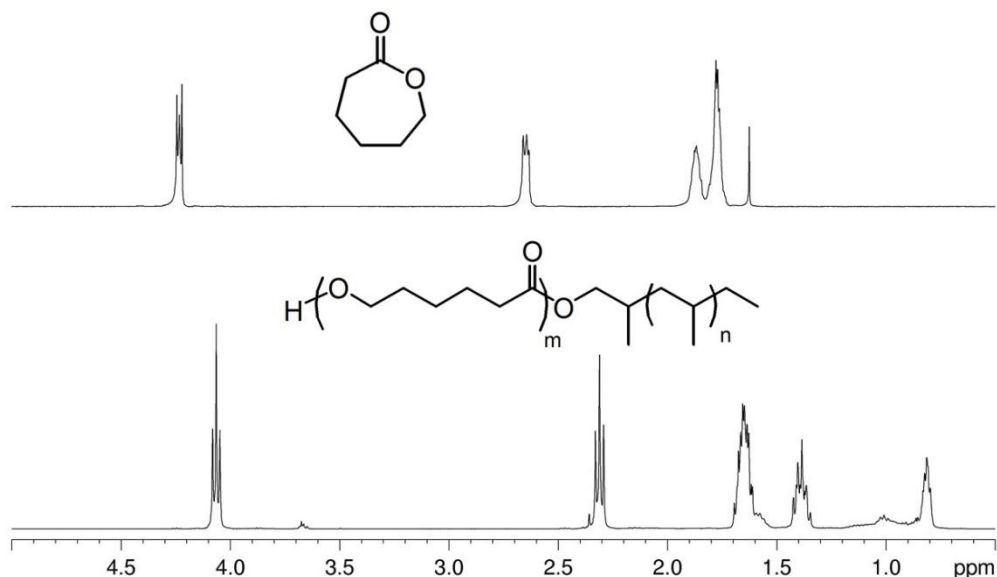
Based on the well-known reaction of  $ZnR_2$  compound with oxygen to generate  $Zn(O-R)_2$ , we have developed a method to generate  $Zn(O-aPP)_2$  in situ through blowing dry air into  $Zn(aPP)_2$ /toluene solution at 0 °C until the yellow color faded, followed by ring-opening polymerization of  $\epsilon$ -caprolactone at room temperature to yield poly(propene-*block*- $\epsilon$ -caprolactone) (*aPP-block-PCL*) diblock copolymer after hydrolysis as a one pot reaction (Scheme 20).

Scheme 20. One pot synthesis of *aPP-block-PCL*



*aPP-block-PCL* diblock has been synthesized with the length of the *aPP* block of 5 kDa and the length of the PCL of 21 kDa as determined by GPC analysis. The degree of polymerization for  $\epsilon$ -caprolactone was 160 and the percentage yield of PCL second block was over 80%. Unfortunately, there was less than 10% 1-hydroxyl-*aPP* left in the final diblock product determined by GPC analysis, which indicated that the initiation of chain-growth of PCL from  $Zn(O-aPP)_2$  was not quantitative. The *aPP-block-PCL* product was further characterized by  $^1H$  NMR spectroscopy to confirm the diblock structural integrity (Figure 15). Both proton resonances of *aPP* block and PCL block were presented in the spectrum, with the resonance of hydroxyl end-group at 3.67 ppm. The integration ratio of proton resonances from *aPP* and PCL were around 1 : 4, which agreed with the block lengths determined by GPC analysis. Finally, to study the thermal property of this amorphous-semicrystalline diblock, DSC analysis was carried out and only one melting endotherm was seen ( $T_m = 52.9$  °C), which agreed with literature value of 60 °C for the  $T_m$  of PCL.<sup>143</sup>

Figure 15.  $^1\text{H}$  NMR spectra of *aPP-block-PCL* (bottom) and  $\epsilon$ -caprolactone (top).



A kinetic study has been carried out for the ring opening polymerization of  $\epsilon$ -caprolactone as the second block initiated through  $\text{Zn}(\text{O-}a\text{PP})_2$ . After addition of  $\epsilon$ -caprolactone monomer to  $\text{Zn}(a\text{PP})_2/\text{toluene}$  solution at  $0\text{ }^\circ\text{C}$ , five aliquots were taken out after 30, 60, 90, 120 and 180 min for GPC and  $^1\text{H}$  NMR analyses. However, all the data showed that the ring opening polymerization of  $\epsilon$ -caprolactone finished within 30 min with the consumption rate over 80%.

### 3.3.2 Synthesis and characterization of PE-*block*-PCL

Using the same method, poly(ethene-*block*- $\epsilon$ -caprolactone) (PE-*block*-PCL) was synthesized from  $\text{Zn}(\text{PE})_2$  stock solution. Due to the solubility limit of linear PE in toluene, the length of the PE block has to maintain lower than 1.5 kDa to prevent  $\text{Zn}(\text{PE})_2$  from precipitation out of toluene. Although the material was designed to have a low molecular weight, it is enough to study the polymerization methodology through GPC and NMR analysis. Diblock PE-*block*-PCL was successfully synthesized according to the same method

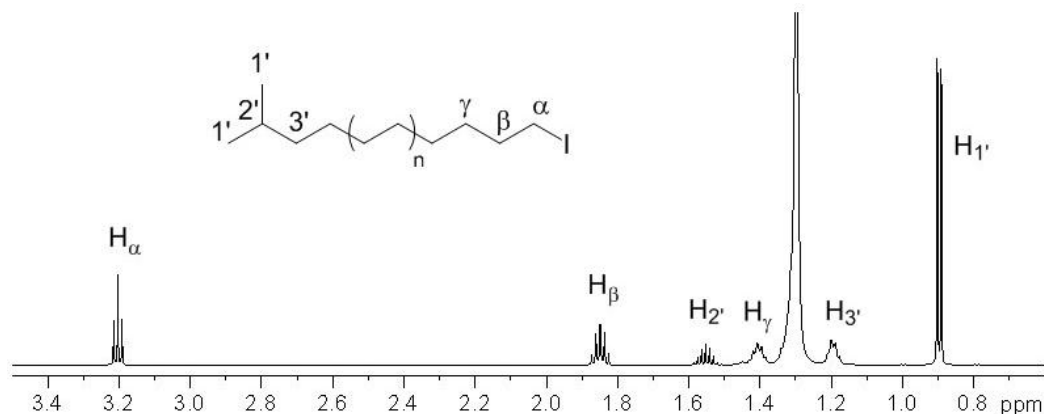
shown in Scheme 20 with complete initiation from  $\text{Zn}(\text{O-PE})_2$ . The degree of polymerization of PE block is 5 and the degree of polymerization of the PCL block is 54 as determined by  $^1\text{H}$  NMR spectroscopy. This diblock copolymer has poor solubility to carry out more characterizations because both PE and PCL blocks are semicrystalline. Finally, there were still around 10% of unreacted PE chains left in final product determined by GPC analysis.

### 3.4 Synthesis of Iodo-Terminated Polyolefins from $\text{Zn}(\text{polymeryl})_2$

#### 3.4.1 Synthesis and characterization of 1-iodo-*a*PP

Wei Zhang in our group has prepared  $\text{Zn}(\text{PE-CH}_2\text{CH}_3)_2$  and  $\text{Zn}(\text{PE-CH}(\text{CH}_3)_2)_2$  through LLCTP of ethene with surrogate  $\text{ZnEt}_2$  and  $\text{Zn}(i\text{Pr})_2$ , respectively.<sup>89</sup> Fortunately, both of these  $\text{Zn}(\text{polymeryl})_2$  species reacted with a toluene solution of  $\text{I}_2$ , which was titrated in until a slight persistent pink color was obtained, to provide the corresponding 1-iodo-terminated PE materials determined by  $^1\text{H}$  NMR spectroscopy (600 MHz,  $1,1,2,2\text{-C}_2\text{D}_2\text{Cl}_4$ , 90 °C). As proved by the spectrum of Figure 16, the reaction of  $\text{Zn}(\text{PE-CH}(\text{CH}_3)_2)_2$  with  $\text{I}_2$  quantitatively gave 2-methyl- $\omega$ -iodo-PE with the absence of ethyl group proton resonances from unreacted  $\text{PE-CH}(\text{CH}_3)_2$ .

Figure 16.  $^1\text{H}$  NMR spectra and resonance assignments of 2-methyl- $\omega$ -iodo-PE



Based on Wei's results on quantitative preparation of 1-iodo-terminated PE, it is interesting to see if other 1-iodo-terminated polyolefins could be synthesized quantitatively using the same method. First of all, 1-iodo-*a*PP has been synthesized by titration of yellow toluene solution of  $\text{Zn}(\text{aPP})_2$  using  $\text{I}_2$  until the pink color persisted. As shown in the Figure 17, two populations of resonances around 3.2 ppm were seen which were from the  $\text{H}_\alpha$  and  $\text{H}_\beta$  protons on the  $\alpha$ -carbon adjacent to iodine atom. Because of the atactic nature of this PP, both protons show multiple resonances from the randomly stereochemical position of the methyl groups close to the iodide chain-end.  $^{13}\text{C}$   $\{^1\text{H}\}$  NMR (150 MHz,  $1,1,2,2\text{-C}_2\text{D}_2\text{Cl}_4$ , 90 °C) spectrum shown in Figure 18 demonstrated that the reaction of  $\text{Zn}(\text{aPP})_2$  with  $\text{I}_2$  in toluene was quantitative, which was confirmed by the absence of isobutyl group as chain-ends. Meanwhile, the only type of hydrocarbon chain-end was ethyl group which was from  $\text{ZnEt}_2$  surrogate. Also, molecular weight and molecular weight distribution maintained the same before and after the end-group functionalization as determined by GPC analysis.

Figure 17.  $^1\text{H}$  NMR spectrum and resonance assignments of 1-iodo-*a*PP

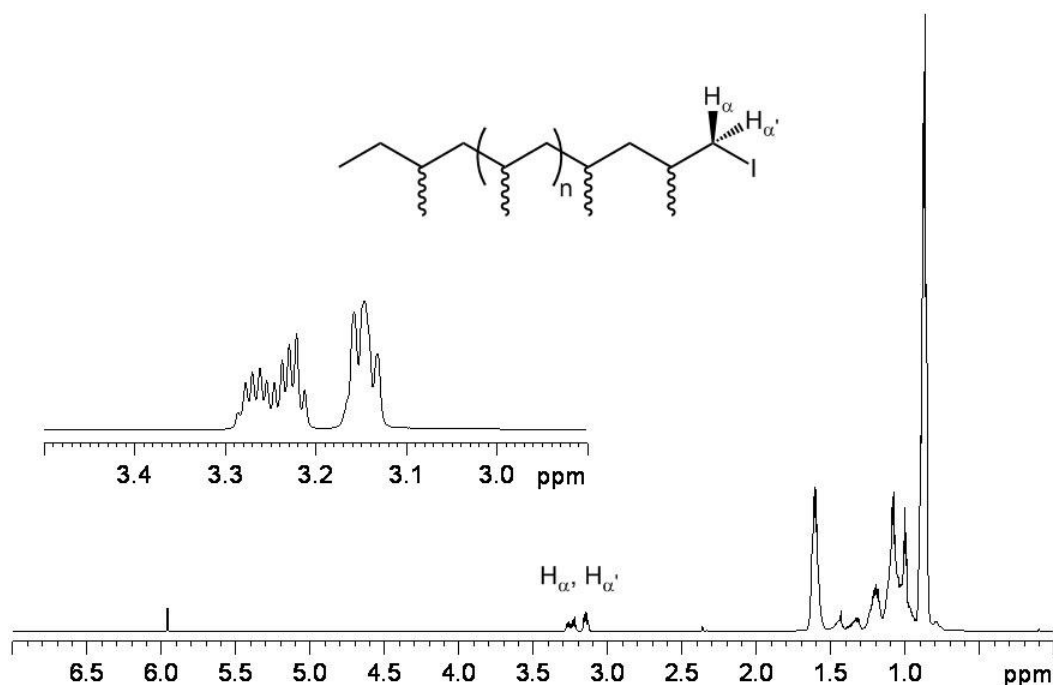
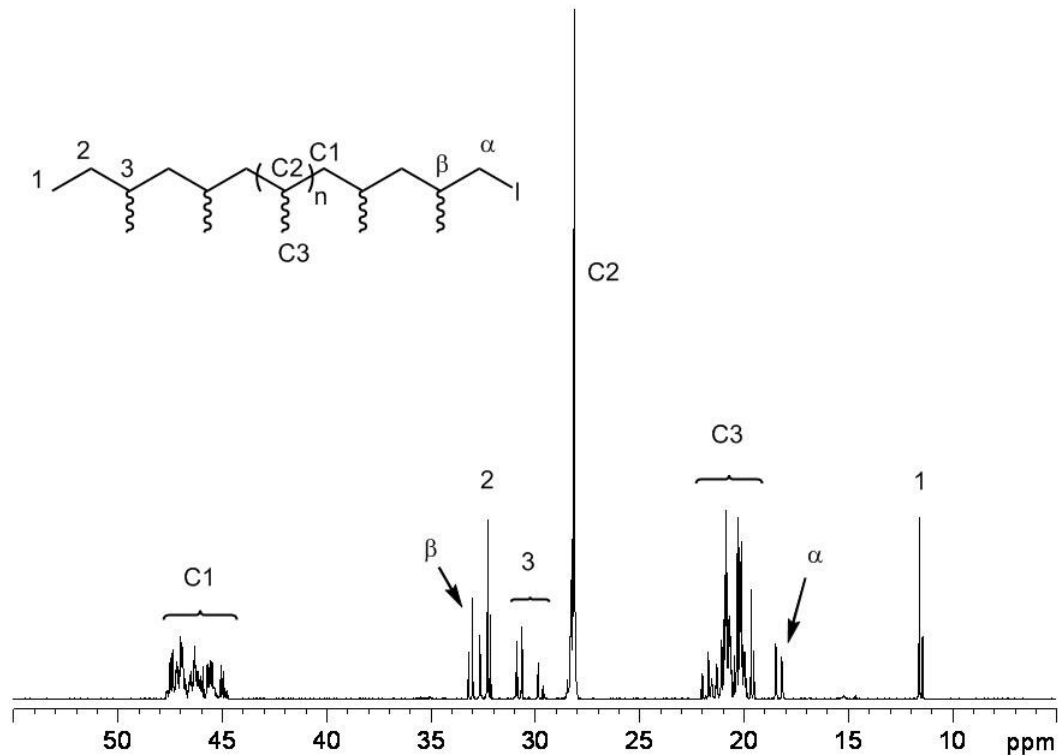


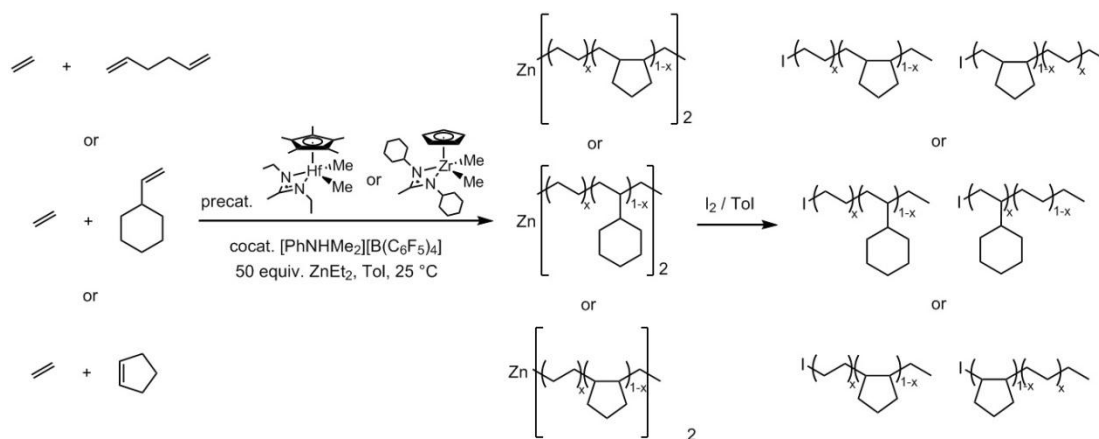
Figure 18.  $^{13}\text{C}$   $\{^1\text{H}\}$  NMR spectrum and resonance assignments of 1-iodo-*a*PP



### 3.4.2 Synthesis of 1-iodo-terminated ethene-based copolymers

With the success of quantitative synthesis of 1-iodo-terminated PE and PP materials, a series of 1-iodo-terminated ethene-based copolymers with cyclic co-monomers have been synthesized and characterized by GPC,  $^1\text{H}$  and  $^{13}\text{C}$  NMR measurements. First, LCCTP copolymerization of ethene and 1,5-hexdiene has been carried out using compound **07** with 50 equiv.  $\text{ZnEt}_2$  in toluene at 25 °C followed by in situ titration of  $\text{I}_2$  to yield 1-iodo-poly(E-*co*-MCP) (MCP = methylene-1,3-cyclopentane) (Scheme 21).  $^1\text{H}$  and  $^{13}\text{C}$  NMR spectra showed two different types of iodo-terminated end-groups; one was ethyl iodide end-group and the other was MCP iodide end-group. This demonstrated the random copolymer nature of this 1-iodo-poly(E-*co*-MCP) material.

*Scheme 21.* Synthesis of 1-iodo-poly(E-co-MCP), 1-iodo-poly(E-co-VCH) and 1-iodo-poly(E-co-CPE)



A more sterically open cyclopentadienyl derivative,  $\text{CpZrMe}_2[\text{N}(\text{Cy})\text{C}(\text{Me})\text{N}(\text{Cy})]$  ( $\text{Cp} = \eta^5\text{-C}_5\text{H}_5$ ,  $\text{Cy} = \text{cyclohexyl}$ ) (**13**), was used to carry out the living polymerization of sterically bulkier monomers, such as vinylcyclohexane (VCH) and cyclopentene (CPE). 1-iodo-poly(E-co-VCH) and 1-iodo-poly(E-co-CPE) were prepared through LCCTP copolymerization of ethene with VCH and CPE using precatalyst **13** and cocatalyst **04** with 50 equiv.  $\text{ZnEt}_2$  in toluene at 25 °C followed by in situ titration of  $\text{I}_2$  (Scheme 21). Both 1-iodo-poly(E-co-VCH) and 1-iodo-poly(E-co-CPE) showed two type of iodide end-groups, ethyl iodide and VCH/CPE iodide respectively, determined by  $^1\text{H}$  and  $^{13}\text{C}$  NMR spectroscopy. All those data have demonstrated that this method of synthesizing 1-iodo-terminated polyolefin materials could be extended to a variety of homo- and co-polymers.

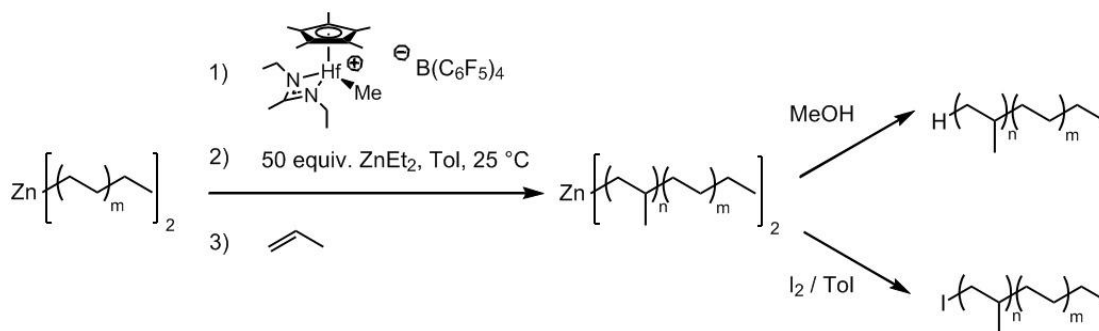
### 3.5 Ethene and Propene Block Copolymer Synthesis and Integrity Study

#### 3.5.1 E/P block copolymer via $\text{Zn}(\text{PE})_2$

With the success of using  $\text{Zn}(\text{polymeryl})_2$  as starting material for both ring opening polymerization and end-group functionalization, another intriguing question is whether it can

be used to as macro-surrogate to carry out the living coordination polymerization of a different olefin monomer to make polyolefin diblock copolymer, such as poly(ethene-*block*-propene) (poly(E-*block*-P)). The proposed mechanism is that the Zn/Al-C bonds are active and ready for reversible chain-transfer process with a new portion of transition metal initiators added to the stock solution in the presence of a different type of monomer. If the rate of the chain-transfer process is rapid and reversible compared to the chain propagation rate, then the growth of the second polyolefin block should be instantaneous and at a same rate. Therefore, the second polymerization is still living and the molecular weight distribution should still be monomodal and narrow.

Scheme 22. Synthesis of poly(P-*block*-E) and 1-iodo-poly(P-*block*-E) via  $\text{Zn}(\text{PE})_2$

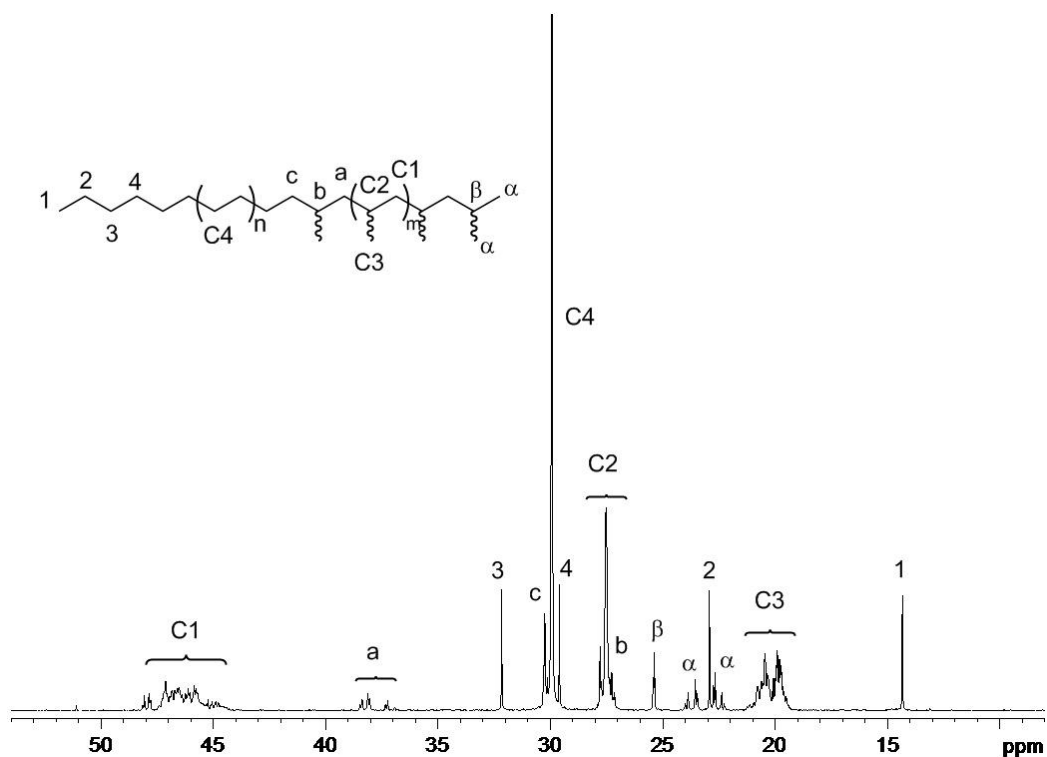


To test this proposal, synthesis of a poly(P-*block*-E) diblock was carried out from  $\text{Zn}(\text{PE})_2$  stock solution as shown in Scheme 22. First, LCCTP of ethene was taken out using active hafnium compound **07** with 200 equiv. of  $\text{ZnEt}_2$  in 40 mL toluene at 25 °C. After 30 min of polymerization, vacuum was applied the solution to remove excess of ethene, and an aliquot of the  $\text{Zn}(\text{PE})_2$  solution was taken out and quenched with MeOH for GPC analysis. The rest of the  $\text{Zn}(\text{PE})_2$  toluene solution was transferred to another glove box equipped with propene gas line. Then a new portion of compound **07** was added to the  $\text{Zn}(\text{PE})_2$  toluene solution and propene was pressurized at 25 °C for 2 h. Final product was obtained from quenching  $\text{Zn}(\text{aPP-}i\text{block-PE})_2$  toluene solution with acidic MeOH. GPC analysis of the

diblock copolymer gave monomodal distributed curve with  $M_n$  of 1.26 kDa and PDI of 1.09, which confirmed the living natures of both blocks.

GPC analyses of the aliquot of the first PE block and final poly(P-*block*-E) diblock confirmed the quantitative chain-growth from  $Zn(PE)_2$  with the absence of remaining PE molecular weight distribution curves. The degrees of polymerization of both PE first block and *a*PP second block were 19 determined by GPC. Furthermore,  $^{13}C \{^1H\}$  NMR (150 MHz, 1,1,2,2- $C_2D_2Cl_4$ , 90 °C) analysis of the poly(P-*block*-E) diblock unambiguously demonstrates the diblock nature of the material. On one hand, both PE and *a*PP resonances were observed in the spectra, as well as the *n*-butyl end-group from PE block and the isopropyl end-group from the *a*PP block. On the other hand, the resonances of the linkage between PE and *a*PP blocks (labeled as a, b and c in Figure 19) were seen in the spectrum which would not appear in neither PE nor *a*PP homopolymers.

Figure 19.  $^{13}C \{^1H\}$  NMR spectra and resonance assignments of poly(P-*block*-E)



Moreover, this  $\text{Zn}(\text{poly}(\text{P-}i\text{block-E}))_2$  stock solution was titrated with  $\text{I}_2$  to give 1-iodo-poly(*P-block-E*) materials according to Scheme 22. Both  $^1\text{H}$  and  $^{13}\text{C}$  NMR spectra again demonstrated the diblock integrity with only 1-iodo-*aPP* type of end group observed (Figure 20 and 21). The absence of 1-iodo-*PE* type of end-group confirmed the complete conversion of  $\text{Zn}(\text{PE})_2$  to  $\text{Zn}(\text{aPP-}i\text{block-PE})_2$ . Also the hydrolysis product, isopropyl end-group, was not seen in Figure 21, which further confirmed this quantitative 1-iodo-end-group functionalization reaction of the E/P block copolymer.

Figure 20.  $^1\text{H}$  NMR spectra and resonance assignments of 1-iodo-poly(*P-block-E*)

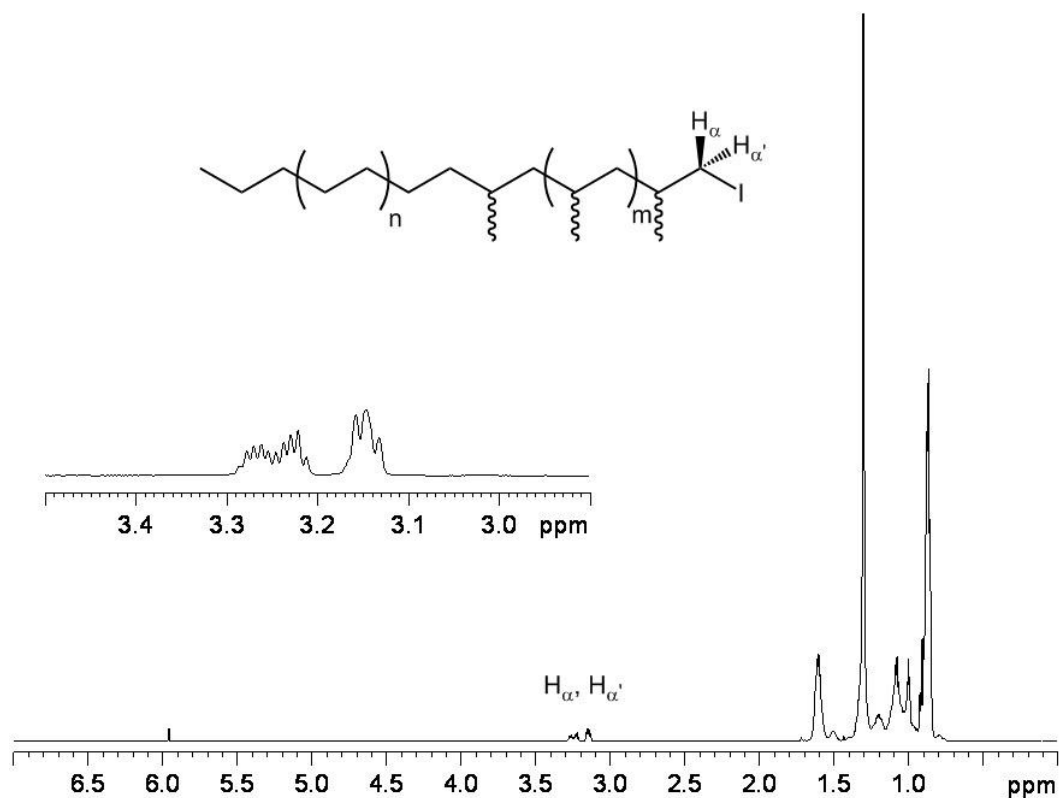
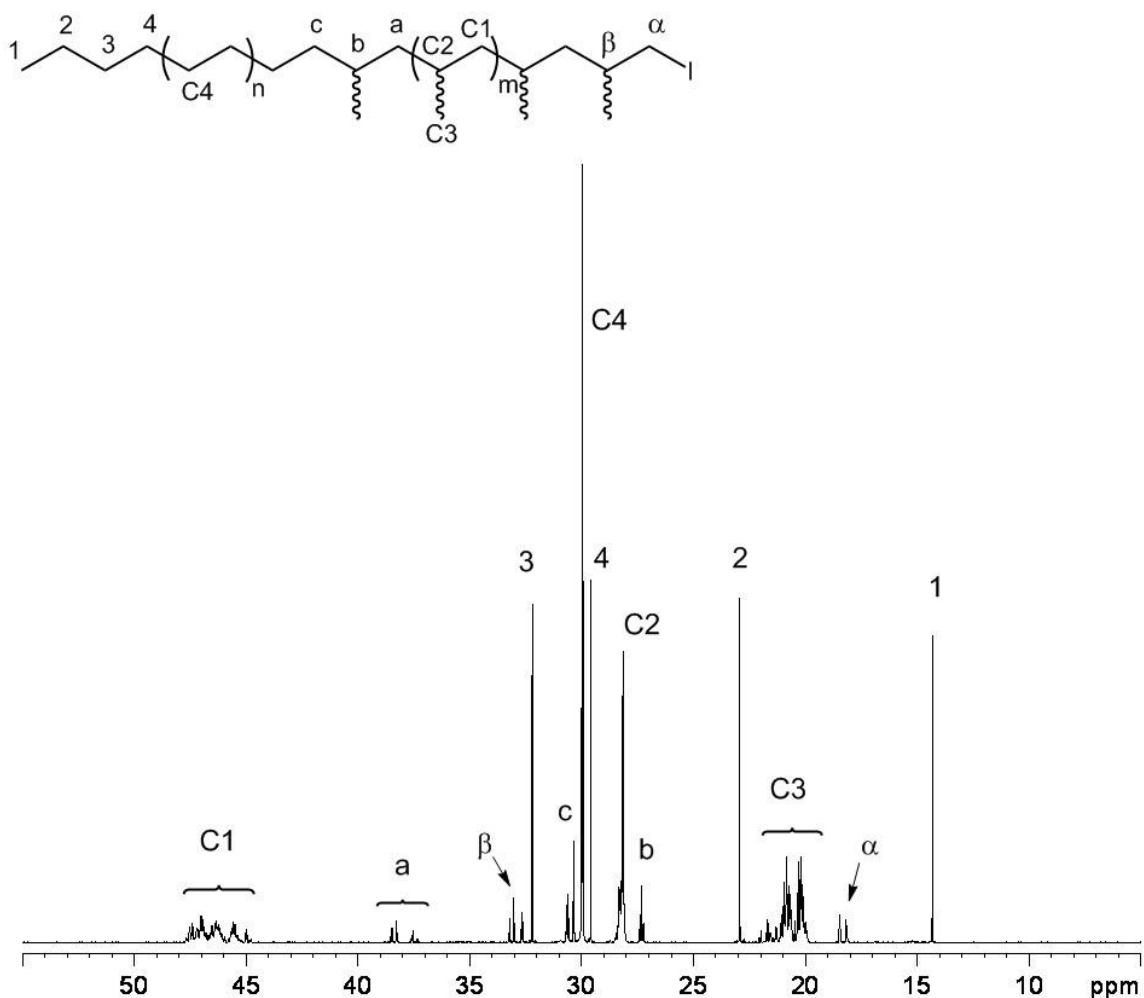


Figure 21.  $^{13}\text{C}$   $\{^1\text{H}\}$  NMR spectra and resonance assignments of 1-iodo-poly(P-*block*-E)



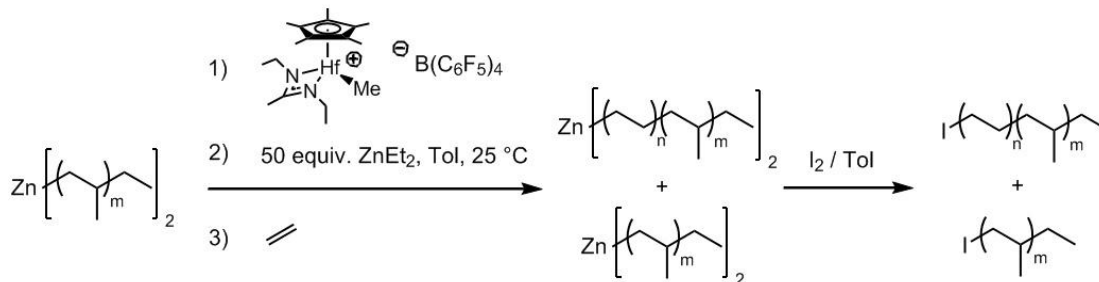
### 3.5.2 E/P block copolymer via $\text{Zn}(a\text{PP})_2$

However, when we were trying to prepare poly(E-*block*-P) diblock copolymer from  $\text{Zn}(a\text{PP})_2$  stock solution using the same method described before (Scheme 23), the resulting poly(E-*block*-P) always contained *a*PP as a byproduct. GPC analysis confirmed the partly formation of diblock with a bimodal molecular weight distribution curves.

To probe this problem, 1-iodo-poly(E-*block*-P) was synthesized according to Scheme 23. As a comparison,  $\text{Zn}(a\text{PP})_2$  stock solution was titrated with  $\text{I}_2$  to make pure 1-iodo-*a*PP as the reference for the first block.  $^1\text{H}$  NMR spectroscopy (600 MHz, 1,1,2,2- $\text{C}_2\text{D}_2\text{Cl}_4$ , 90 °C)

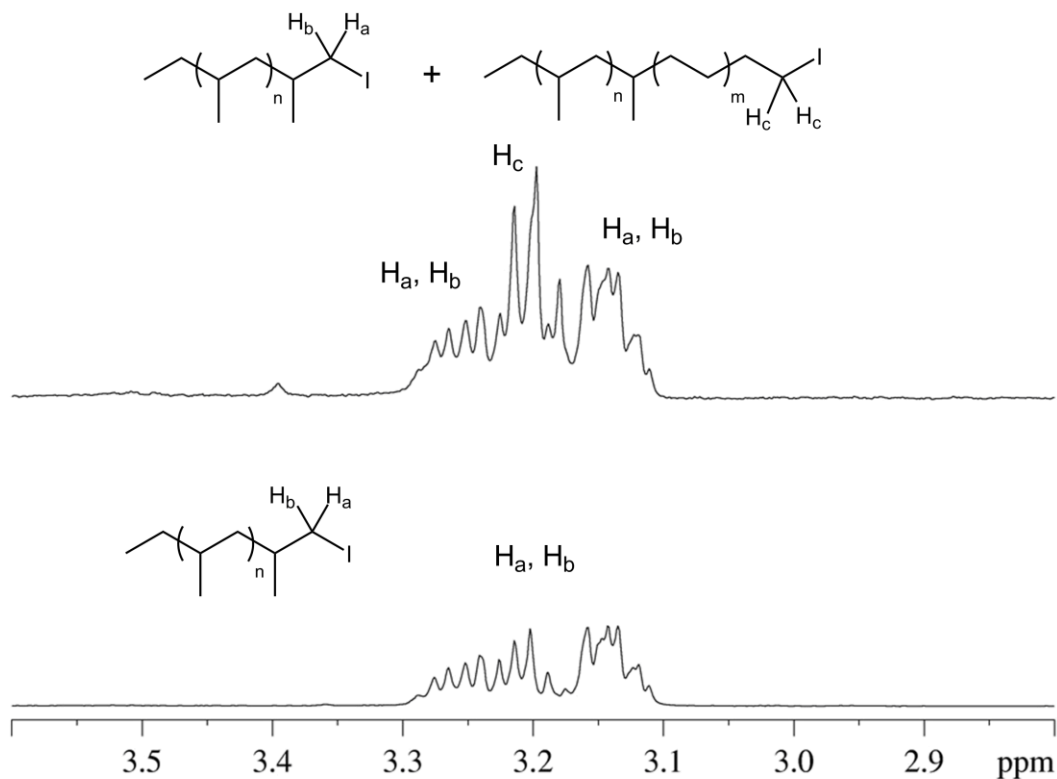
was used to study the iodide end-group functionalized products from the diblock synthesis (top of Figure 22) and the 1-iodo-*a*PP reference (bottom of Figure 22). Clearly, the top spectrum contained two types of iodo-end-groups; ethyl iodide end-group from the 1-iodo-poly(*E-block-P*) and isopropyl iodide end-group from the 1-iodo-*a*PP of the unreacted  $\text{Zn}(a\text{PP})_2$  left in the stock solution. NMR end-group analysis results agreed with the GPC data, indicating the incomplete PE chain-growth from  $\text{Zn}(a\text{PP})_2$  Stock solution.

*Scheme 23.* Synthesis of 1-iodo-poly(*E-block-P*) via  $\text{Zn}(a\text{PP})_2$  stock solution (with 1-iodo-*a*PP as a byproduct)



The detailed reason for this incomplete initiation of PE chain growth from  $\text{Zn}(a\text{PP})_2$  requires carefully mechanistic studies. However, based on the polymerization results and 1-iodo-end-group analysis, a hypothesis is proposed. When ethene monomers insert into the  $\text{Hf}^+$ -PP bond, the steric hindrance for insertion reduces because of the newly formed  $\text{Hf}^+$ -PE-PP active species. Thus, ethene will continue to insert into the  $\text{Hf}^+$ -PE-PP centers instead of the  $\text{Hf}^+$ -PP centers. As a result, it appears that PE chains prefer to grow on PE chains instead of PP chains so that  $\text{Zn}[\text{PE-block-}a\text{PP}]_2$  will keep propagating while the remaining  $\text{Zn}(a\text{PP})_2$  will not have a chance to grow the PE block in the chain-transfer system. In contrast, in the chain-growth of *a*PP from  $\text{Zn}(\text{PE})_2$ , there is no this issue because PP chains prefer to grow on less sterically hindered PE chains instead of PP chains, so that all  $\text{Zn}(\text{PE})_2$  species will propagate a second *a*PP block to quantitatively yield the  $\text{Zn}[a\text{PP-block-PE}]_2$  intermediate.

Figure 22.  $^1\text{H}$  NMR end-group analysis of blocky integrity of poly(E-block-P)



### **3.6 Synthesis and Characterization of 1-Lithio-aPP and its Derivatives**

#### **3.6.1 Synthesis and characterization of 1-lithio-aPP**

In order to expand the end-group-functionality on polyolefins to other interesting functional groups, such as hydroxyl and carboxyl groups, direct end-group functionalization was first carried out using the reaction of  $\text{Zn}(\text{polymeryl})_2$  with  $\text{O}_2$  followed by hydrolysis. However, beside the desired hydroxyl-terminated polyolefins, there were always unknown byproducts with higher molecular weights probably from free radical initiated homo-coupling of the polymeryl groups on zinc.

Furthermore, we have explored other synthesis pathways that involved iodide-terminated PP as the starting material. 1-iodo-aPP was first treated with 2 equiv. of *t*BuLi in

Et<sub>2</sub>O at -78 °C to yield 1-lithio-*a*PP as shown in Scheme 24. It was difficult to titration the concentration of the resulting 1-lithio-*a*PP due to the long *a*PP chain and the consequently low concentration of the lithium end-groups. Thus, to determine whether this reaction was close to complete conversion, an aliquot of the fresh 1-lithio-*a*PP was reacted with D<sub>2</sub>O followed by deuterio-end-group analysis through <sup>13</sup>C {<sup>1</sup>H} NMR spectroscopy (150 MHz, 1,1,2,2-C<sub>2</sub>D<sub>2</sub>Cl<sub>4</sub>, 90 °C) (Figure 23). According to the integration of the <sup>13</sup>C NMR spectrum, the nearly 1 : 1 ratio of 1-deuterio-methyl (CH<sub>2</sub>D) and methyl (CH<sub>3</sub>) on the isopropyl chain-end indicated that the conversion of 1-iodo-*a*PP to 1-lithio-*a*PP was at least nearly quantitative. Therefore, a variety of end-group functionalized *a*PPs could be synthesized based on the 1-lithio-*a*PP intermediate (Scheme 24).

Scheme 24. End-group functionalized PP materials from 1-iodo-*a*PP

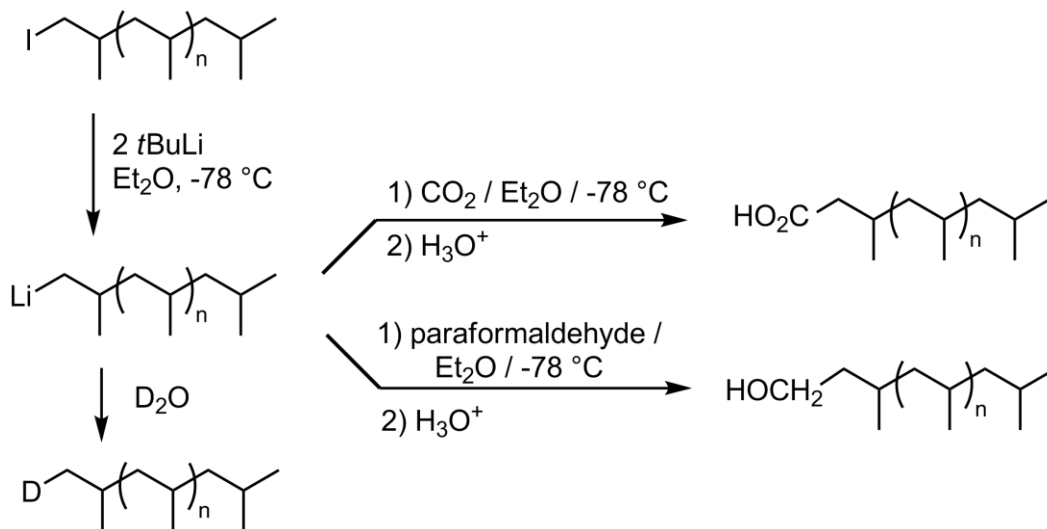
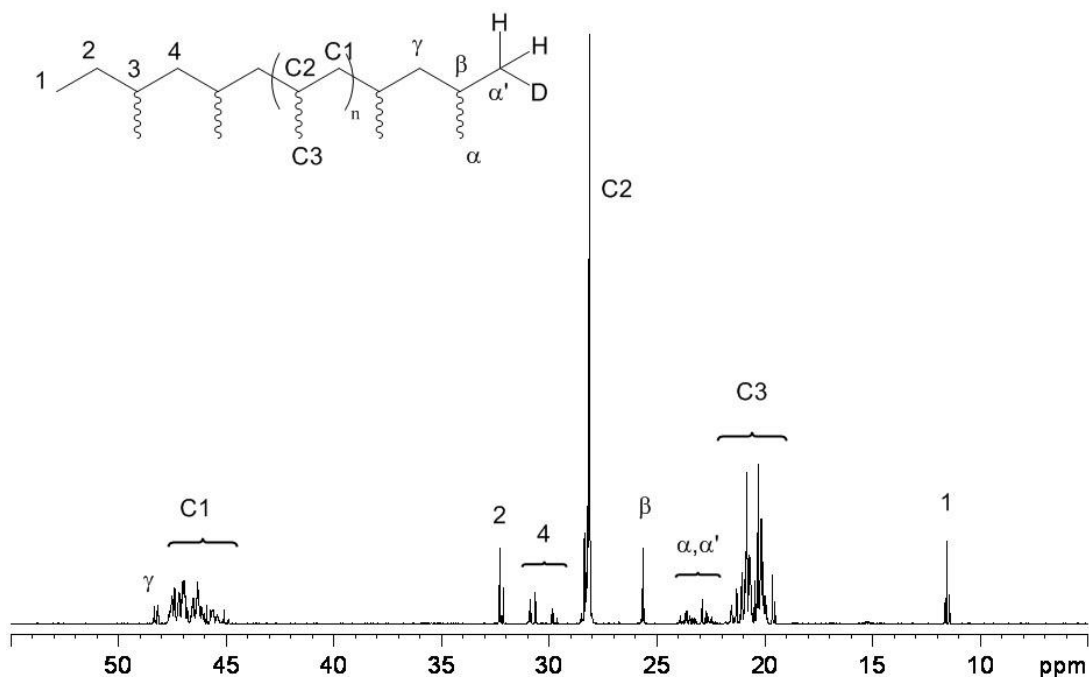


Figure 23.  $^{13}\text{C}$   $\{^1\text{H}\}$  NMR spectra and resonance assignments of 1-deuterio-*a*PP



### 3.6.2 Synthesis of 1-carboxy-*a*PP and 1-hydroxymethyl-*a*PP

This 1-lithio-*a*PP was then subsequently used to cleanly provide 1-carboxy-*a*PP and 1-hydroxymethyl-*a*PP through reaction with solid  $\text{CO}_2$  (dry ice) and paraformaldehyde  $[\text{H}_2\text{CO}]_x$ , respectively, followed by hydrolyses. Both reactions provided yields of greater than 70% and the quantitative nature of end-group functionalization was again unequivocally established from both  $^1\text{H}$  and  $^{13}\text{C}$  NMR spectra through the formation of carboxyl (Figure 24 and 25) and hydroxymethyl (Figure 26 and 27) end-groups. Furthermore, the absence of either isopropyl end-groups from hydrolysis or iodide end-groups from remaining starting material demonstrated the clean conversion and the advantage of using this method in preparation of precise polyolefin-based functional materials. Finally, for all the chemical transformations presented in Scheme 24, the polydispersities of the products remained very narrow and essentially unaffected from the *a*PP obtained through simple acid quench of the  $\text{Zn}(a\text{PP})_2$  starting material.

Figure 24.  $^1\text{H}$  NMR spectrum and resonance assignments of 1-carboxy-*a*PP

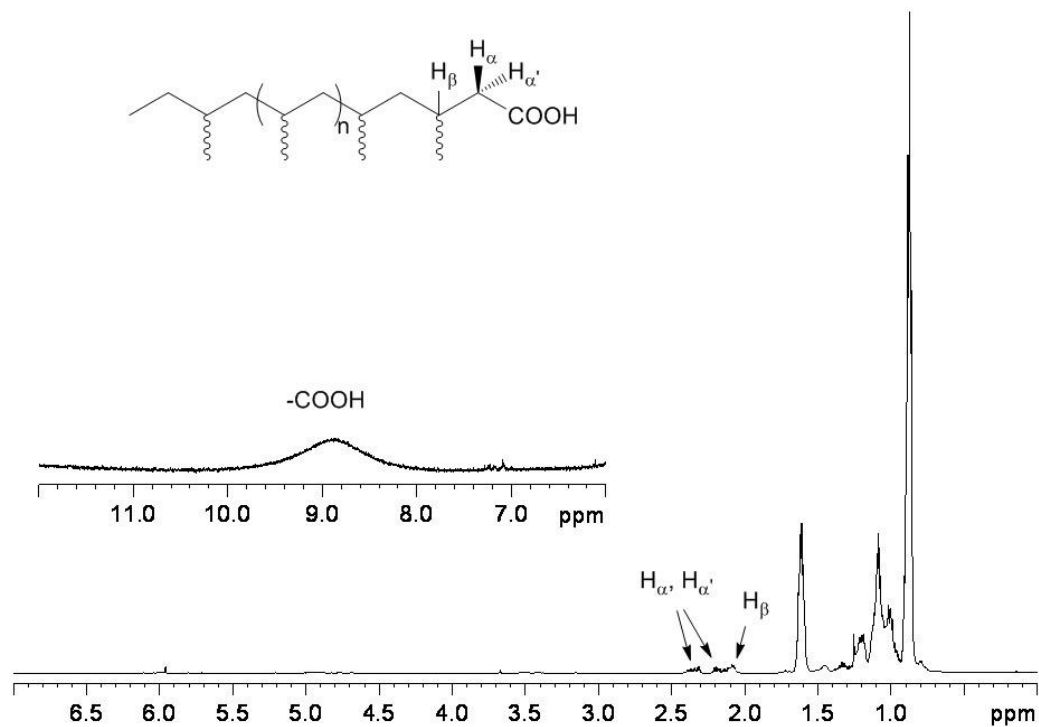


Figure 25.  $^{13}\text{C}$   $\{^1\text{H}\}$  NMR spectrum and resonance assignments of 1-carboxy-*a*PP

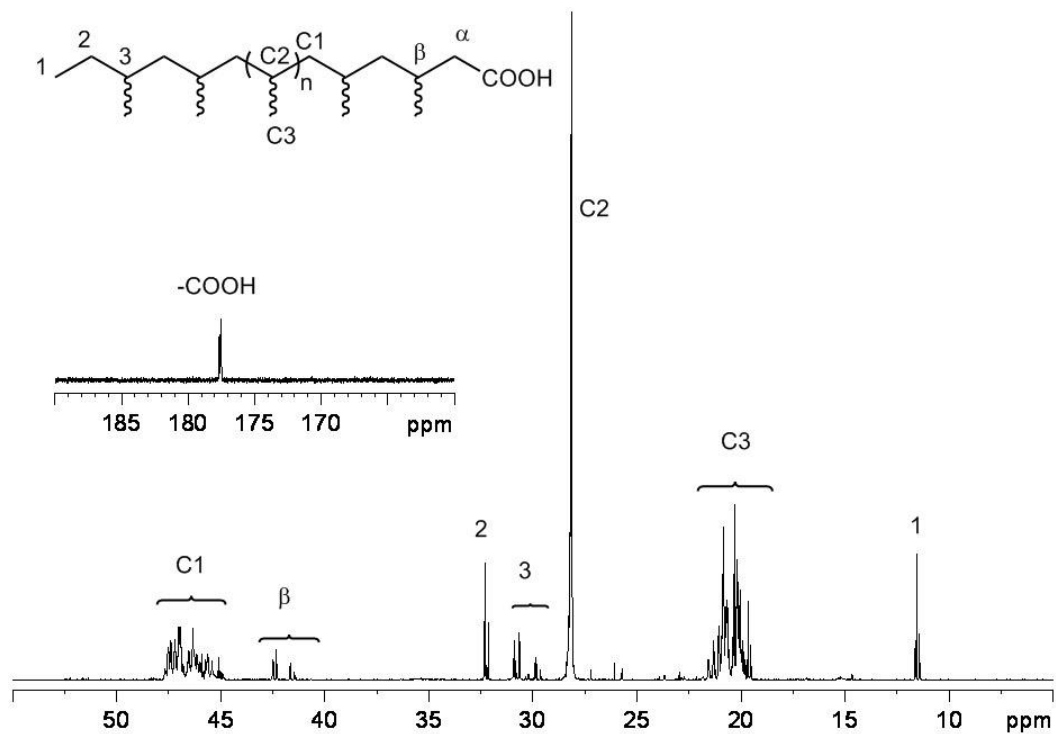


Figure 26.  $^1\text{H}$  NMR spectrum and resonance assignments of 1-hydroxymethyl-*a*PP

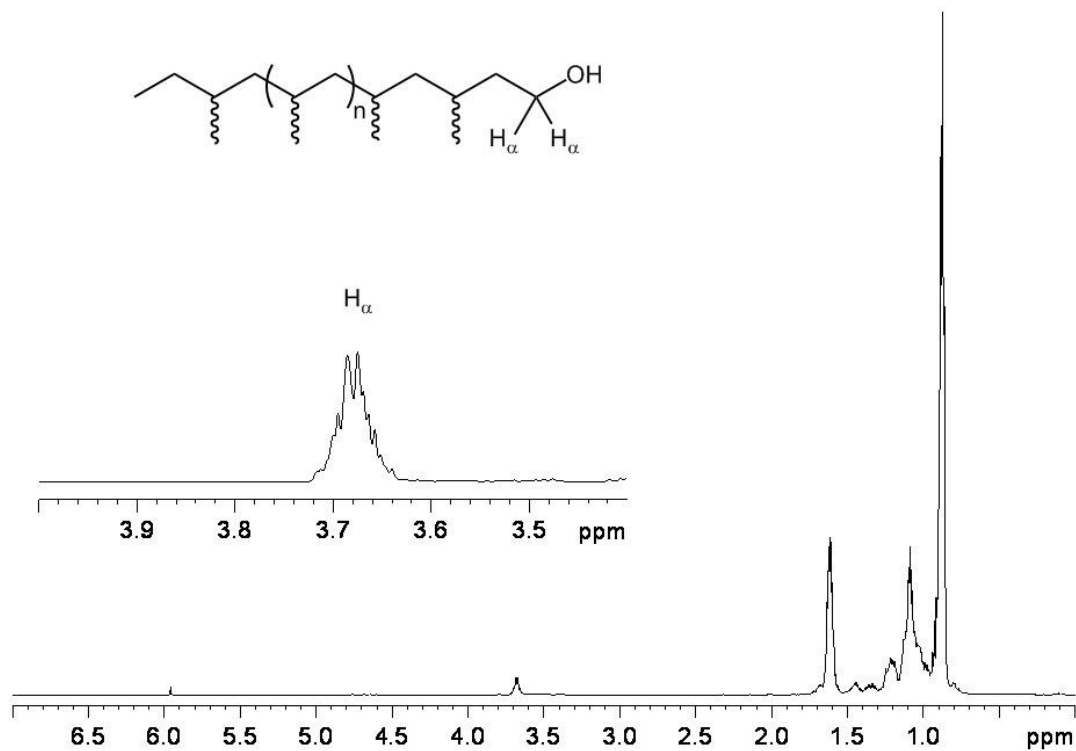
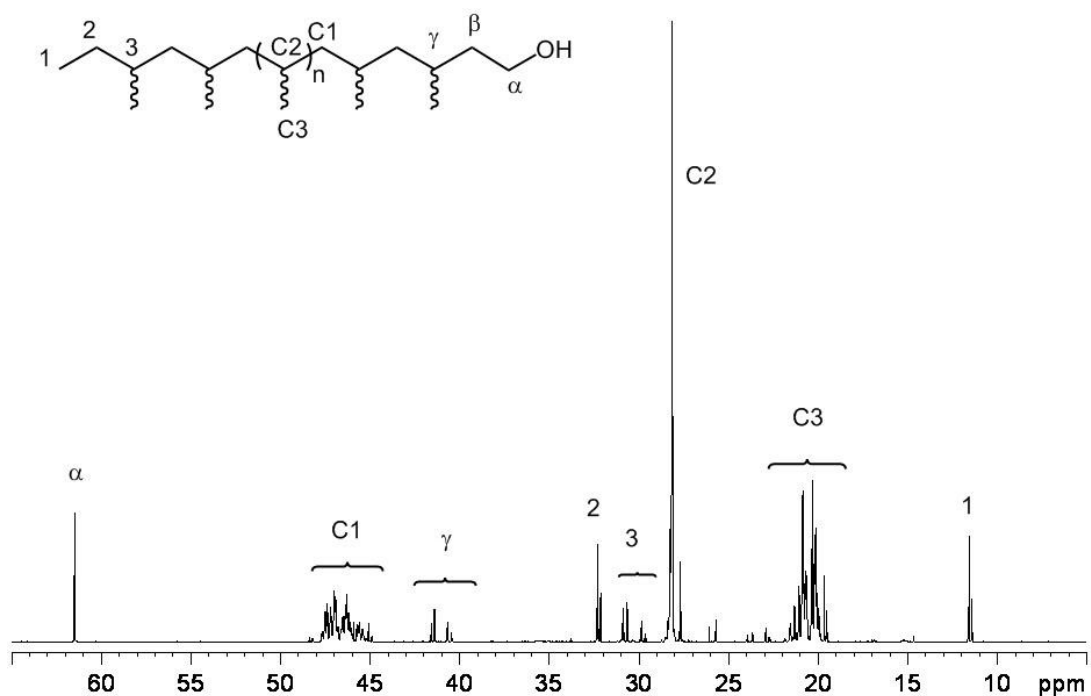


Figure 27.  $^{13}\text{C}$   $\{^1\text{H}\}$  NMR spectrum and resonance assignments of 1-hydroxymethyl-*a*PP



### **3.7 Conclusions**

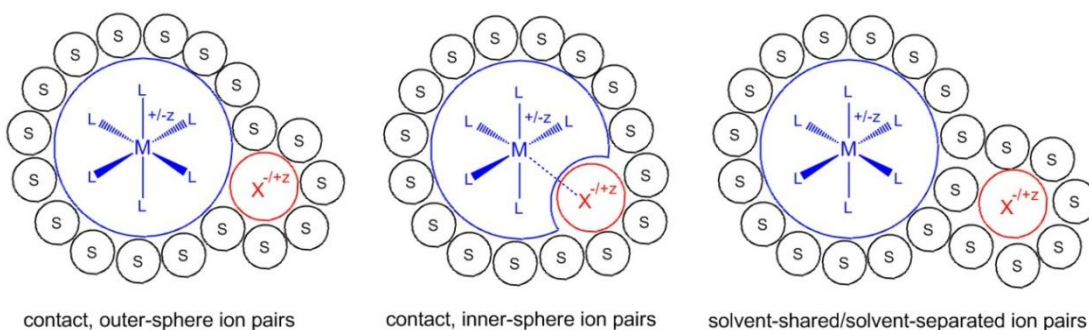
In the present work, the synthetic utility of  $\text{ZnEt}_2$  mediated LCCTP has been clearly demonstrated and exploited to prepare a number of different end-group functionalized precision polyolefins that are further characterized by having tunable molecular weights while maintaining very narrow polydispersities. Several of these new products are attractive as precursors to macro-monomers and macro-initiators, and accordingly, it can be anticipated that the availability of these new precision polyolefin materials can serve to foster and support the exploration of a large array of new polyolefin-based products. Importantly, either binary or ternary LCCTP process ensures that these new end-group functionalized materials can be readily obtained in bulk quantities in a relatively inexpensive manner. Further investigations of the full scope of end-group functionalized precision polyolefins that can be obtained, and of their subsequent use for material and polymer science and engineering is now in progress, the results of which will be reported in due course.

# Chapter 4: Modulation of Copolymer Compositions through Reversible Chain-Transfer between “Tight” and “Loose” Ion Pairs

## 4.1 Background

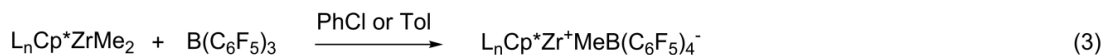
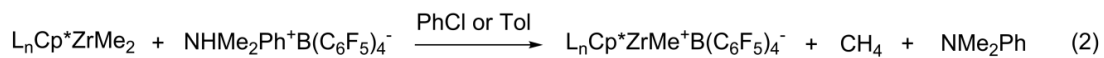
Ion pairs are defined as pairs of oppositely charged ions, with a common solvation shell, held together usually by Columbic forces.<sup>146-149</sup> For organometallic ion pairs, the moiety  $ML_n^{z}$  (M = metal, L = ligand) is usually considered as a whole ionic moiety. Based on the type and strength of anion-cation interactions, the transition metal complex ion pairs can be defined as several categories: contact outer-sphere ion pairs (left in Figure 28), contact inner-sphere ion pairs (middle), and solvent-shared/solvent-separated ion pairs (right). Contact ion pairs are more prevalent for transition metal complexes because the positive charge on the metal is decreased due to the formation of M-L bonds that are more covalent than for main-group metals.<sup>149</sup>

Figure 28. Transition metal complex ion pairs



It is now well known that the active catalyst (initiator) for coordination olefin polymerization is a transition metal cationic complex, or more precisely an ion pair.<sup>56, 150</sup> The ion-pair initiators can be generated from Group 4 metallocene dichlorides and MAO, or from metallocene or post-metallocene dialkyls and perfluoroaryl boranes. Due to the chemical robustness and resistance to hydrolysis of perfluoroaryl boranes,<sup>151</sup> their use in metallocene and post-metallocene polymerization catalysis lead to highly active catalyst systems that are also amenable to mechanistic studies. In many cases, the stereoselectivity of the ion-pair initiators are greatly depended on the structure of the counterion, as well as the cation-anion interactions.<sup>56</sup>

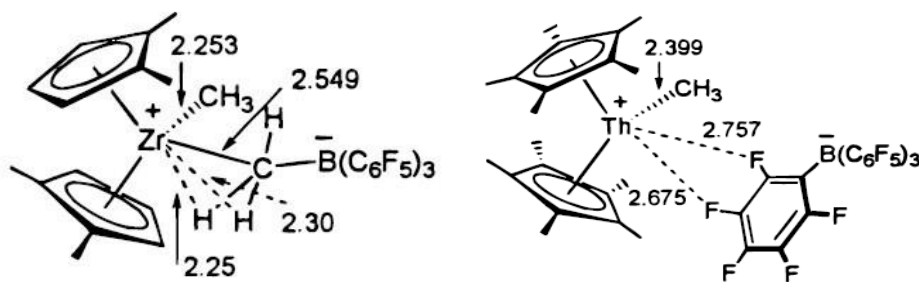
There are several activation processes involved in activating transition metal complex to generate ion-pair initiators for single-site olefin polymerization. For homogeneous single-site transition metal precatalysts, the activation usually involves reaction with perfluoroaryl boranes/borates such as  $B(C_6F_5)_3$  (**10**),  $[PhNMe_2H][B(C_6F_5)_4]$  (**04**) and  $[CPh_3][B(C_6F_5)_4]$  (**12**), as cocatalysts. Depended on the nature of perfluoroaryl boranes/borates, these are three pathways that are frequently used to activate transition metal complex precatalysts: oxidative and abstractive cleavage of M-R bonds by charged reagents (eq. 1), protonolysis of M-R bonds (eq. 2) and alkyl/hydride abstraction by neutral strong Lewis acids (eq. 3).<sup>56</sup> The activation usually involves quantitative reaction of precatalyst and cocatalyst in a 1 : 1 ratio.



Besides the research in studying the activation processes, particular interesting results have been obtained by Marks and co-workers in the characterization of isolable,

crystallographically characterizable metallocenium cation-anion pairs for studying the molecular basis of the polymerization catalysis.<sup>152-153</sup> For example, the solid-state structures of  $(1,2\text{-Me}_2\text{Cp})_2\text{ZrMe}^+\text{MeB}(\text{C}_6\text{F}_5)_3^-$  has been reported.<sup>152</sup> The charge-separated character of this complex is unambiguously established by the much longer Zr---CH<sub>3</sub> (bridging) distance (2.549 Å) than the Zr-CH<sub>3</sub> (terminal) distance (2.253 Å) and the relatively normal B-CH<sub>3</sub> distances. Another interesting feature of these metallocenium complexes is that the bridging methyl hydrogens exhibit relatively close contacts to Zr, indicative of  $\alpha$ -agostic interactions. Therefore, the structure of  $(1,2\text{-Me}_2\text{Cp})_2\text{ZrMe}^+\text{MeB}(\text{C}_6\text{F}_5)_3^-$  is more accurately described in the left sketch structure as shown in Figure 29.<sup>56</sup> The crystal structure of the thorium complex  $\text{Cp}^*_2\text{ThMe}^+\text{B}(\text{C}_6\text{F}_5)_4^-$  reveals that the anion is weakly coordinated to the cation through two Zr---F bridges as shown by the right sketch structure in Figure 29.<sup>153</sup> The relatively long Zr---F distances (2.757(4) and 2.675(5) Å, respectively) indicate that these interactions are very weak, as does the rapid interconversion of C<sub>6</sub>F<sub>5</sub> groups observed in the room-temperature <sup>19</sup>F NMR.

Figure 29. Sketch structures of  $(1,2\text{-Me}_2\text{Cp})_2\text{ZrMe}^+\text{MeB}(\text{C}_6\text{F}_5)_3^-$  (left) and  $\text{Cp}^*_2\text{ThMe}^+\text{B}(\text{C}_6\text{F}_5)_4^-$  (right)



Intense research activity has been focused on polymerization behaviors of those ion-pair initiators. It is now well-established that the strength of the ion-pairing interaction between a cationic transition-metal complex and a discrete counter-anion can have a

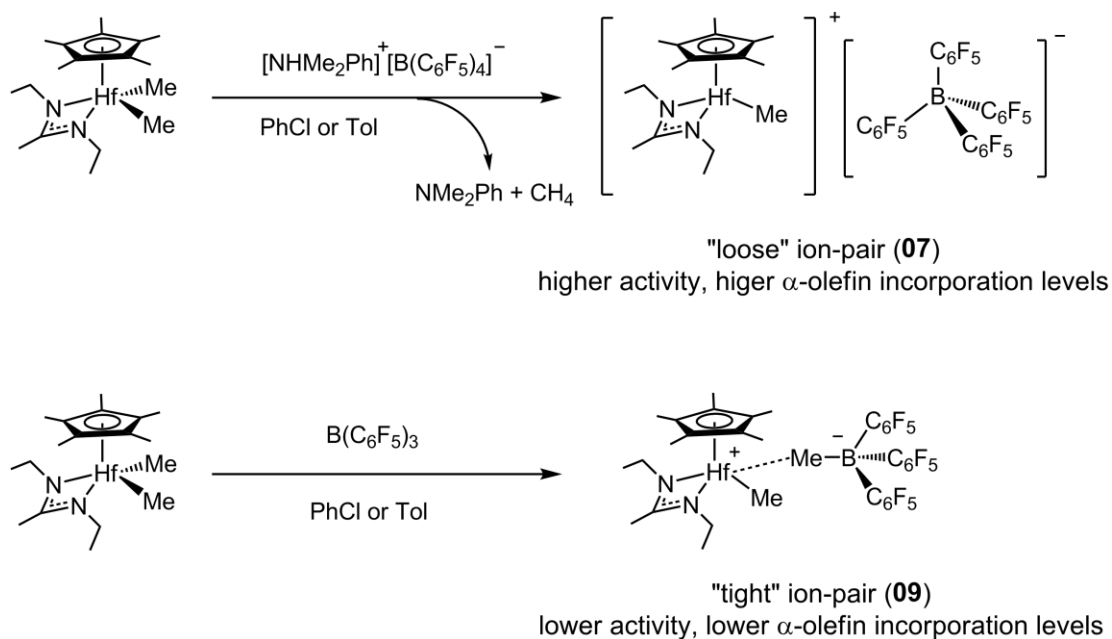
substantial influence on polymerization activity, stereoselectivity, and the extent of co-monomer incorporation.<sup>154-158</sup> Importantly, For ethene and 1-hexene copolymerization, Waymouth<sup>159</sup> found that activation of the  $C_5$ -symmetric amine bis(phenolate) zirconium dibenzyl complexes with MMAO yielded copolymers with 10% higher hexene incorporation than that observed upon activation with perfluoroaryl boranes/borates **04**, **10** and **12**. Also, Marks<sup>160</sup> has reported a case that using tris(2,2',2''-nonafluorobiphenyl) borane cocatalyst enhances co-monomer incorporation randomness of poly(ethylene-*co*-1-hexene) relative to using aluminate cocatalysts. However, to the best of our knowledge, there is no literature report regarding to the mechanism of modulating copolymer composition that take the advantage of different ion-pairing interactions. Therefore, in this chapter, we were trying to couple the “tight” and “loose” ion-pairing interactions with living coordinative chain-transfer polymerization (LCCTP) to achieve programmable modulation of co-monomer relative reactivities and thus control the compositions of ethene-based copolymers.

#### **4.2 Study on Anion Exchange between “Tight” and “Loose” Ion Pairs**

Diethyl hafnium precatalyst  $Cp^*HfMe_2[N(Et)C(Me)N(Et)]$  (**08**) is designed to have less sterical hindrance round the transition metal center in order to achieve higher activity towards copolymerization of ethene with  $\alpha$ -olefin co-monomers. When activated with different borate/borane cocatalysts,  $[PhNMe_2H][B(C_6F_5)_4]$  (**04**) and  $[B(C_6F_5)_3]$  (**10**), significant different values of activities, yields, molecular weights and co-monomer incorporation levels are observed under identical polymerization conditions (Scheme 25). Therefore, it is safe to propose that  $[Cp^*HfMe\{N(Et)C(Me)N(Et)\}][B(C_6F_5)_4]$  (**07**) generated from precatalyst **08** and cocatalyst **04** behaves as a “loose” ion pair, for which a more electropositive and more sterically accessible transition-metal center translates into a higher activity and degree of  $\alpha$ -olefin incorporation. Similarly, the active species

$[\text{Cp}^*\text{HfMe}\{\text{N}(\text{Et})\text{C}(\text{Me})\text{N}(\text{Et})\}][\text{MeB}(\text{C}_6\text{F}_5)_3]$  (**09**) derived from precatalyst **08** and cocatalyst **10** is assumed to propagate as a “tight” ion pair in which a closer (stronger) interaction of the metal center with the  $[\text{MeB}(\text{C}_6\text{F}_5)_3]^-$  counterion provides a greater barrier to  $\alpha$ -olefin incorporation, along with a decrease in activity.

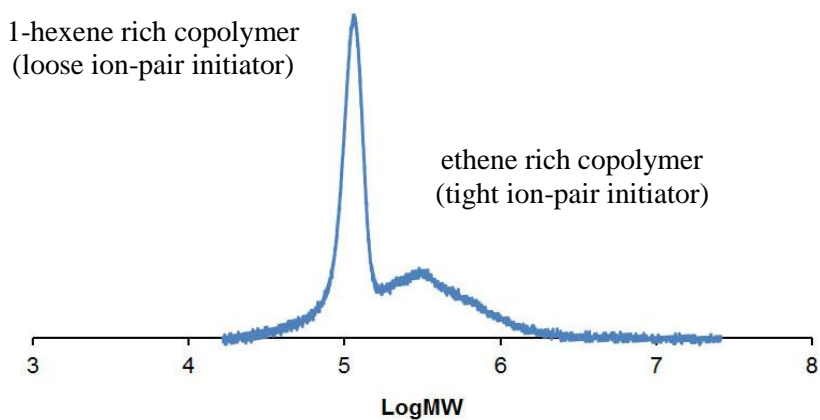
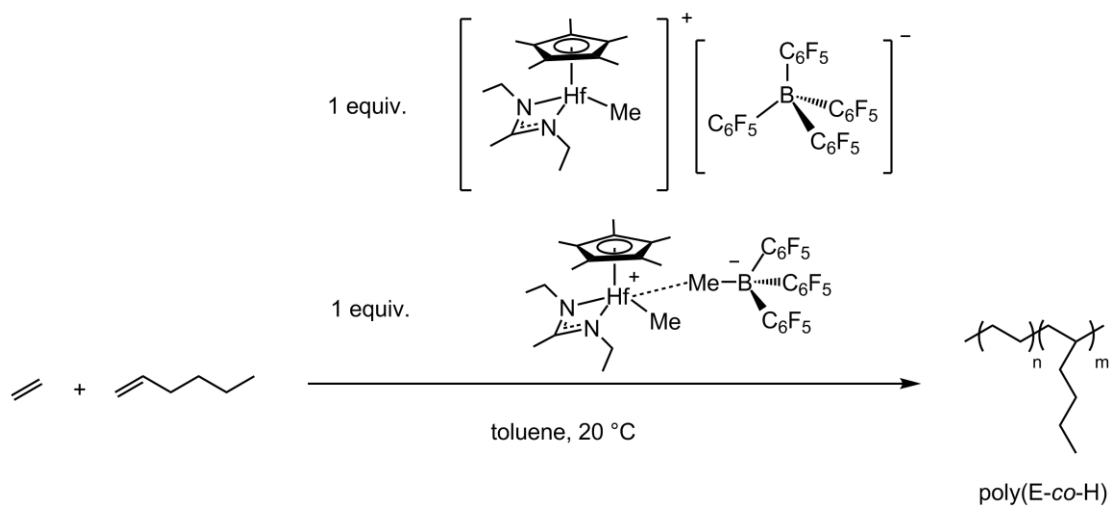
Scheme 25. Synthesis of “loose” and “tight” ion-pair initiators



Now with the ability to generate two different ion-pair initiators from a single transition metal precatalyst, the next attractive question is whether we could employ a mixture of these two ion-pairs for copolymerization and control the property of the resulting polymers. To achieve this purpose, a fast and reversible anion exchange between those two ion pairs should happen, and the rate of exchange should be faster than each of the chain propagation rate to maintain homogeneous nature of polymer's molecular weight and composition. Therefore, a copolymerization of ethene with 1-hexene using a 1 : 1 ratio of loose ion pair **07** and tight ion pair **09** was carried out in toluene at 20 °C. After 5 min, the resulting polymer was obtained after hydrolysis with acidic methanol. However, GPC

analysis of the products indicated a bimodal distribution with a lower molecular weight 1-hexene rich copolymer from loose ion pair **07** and a higher molecular weight ethene rich copolymer from tight ion pair **09** (Scheme 26). Therefore, under our polymerization conditions, absence or very slow anion exchange was observed compared to chain propagation process, which prevents us from modulating the copolymer property through employing a mixture of loose and tight ion pairs.

Scheme 26. Copolymerization of ethene with 1-hexene using mixed “loose” and “tight” ion pairs and GPC analysis of the resulting copolymers





propagation rates of each ion pair ( $k_{ct} \gg k_p, k_p'$ ), then all the polymer chains will grow at a same rate and the overall polymerization should still be living. Thus, the resulting polymer should be monomodal distributed with narrow molecular weight distribution. In the same time, the degree of co-monomer incorporation should now be set by the relative initial populations of the loose and tight ion pair as shown in Scheme 25.

In practice, different populations of the tight and loose ion pairs derived from compound **07** and **09** were readily established by activating precatalyst **08** with a mixture of the two cocatalysts **04** and **10**, whereby  $[\mathbf{08}]_0 = [\mathbf{04}]_0 + [\mathbf{10}]_0$ . Based on the strategy proposed in Scheme 27, a spectrum of different grades (compositions) of polyethene-based materials should be made from a single transition metal complex precatalyst, which achieves the goal of “one catalyst, many materials”. Since the populations of the tight and loose ion pairs could be precisely controlled, programmable modulation of copolymer compositions can be easily achieved using this strategy.

#### **4.4 Copolymerization of Ethene with $\alpha$ -Olefins in Toluene Solution**

##### **4.4.1 Kinetic studies on LCCTP using mixed ion-pair initiators**

To experimentally test the strategy proposed in Scheme 27, a kinetic study of copolymerization of ethene (E) with 1-hexene (H) using **09** and **07** mixed initiators and  $\text{ZnEt}_2$  as chain-transfer surrogate in toluene was carried out in toluene at room temperature. Aliquots were taken and quenched with methanol every 10 min for the first hour and polymerization was quenched after 90 min (Table 3). GPC and NMR analyses have been carried out for all the aliquots and the final product to verify two critical factors. First, it is important to confirm the living nature of the chain-transfer copolymerization using a mixture of loose and tight ion-pair initiators. Second, kinetic study results show the composition (1-

hexene incorporation levels) changes during the copolymerization process in order to prevent forming a gradient copolymer.

Table 3. Kinetic studies of LCCTP copolymerization of ethene with 1-hexene

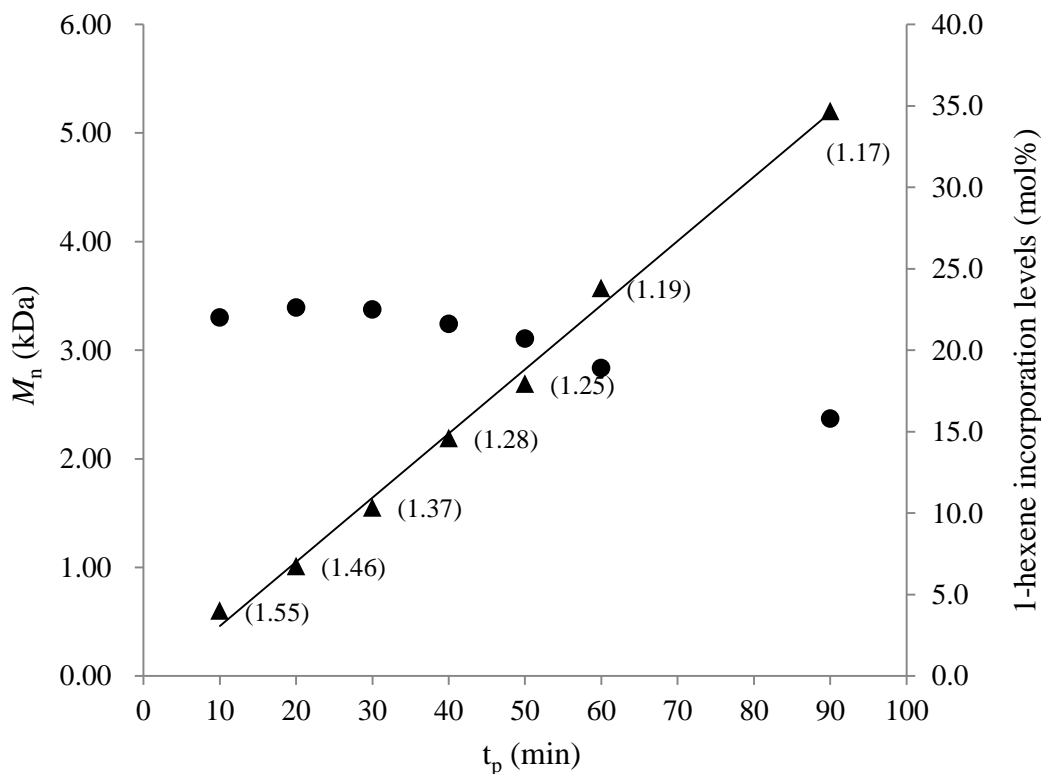
Entry	$t_p$ (min)	$M_n$ (kDa)	PDI	H contents (mol%)
4.01	10	0.60	1.55	22.0
4.02	20	1.01	1.46	22.6
4.03	30	1.55	1.37	22.5
4.04	40	2.19	1.28	21.6
4.05	50	2.69	1.25	20.7
4.06	60	3.57	1.19	18.9
4.07	90	5.20	1.17	15.8

Conditions: 40  $\mu$ mol **08**, 20  $\mu$ mol **04** and 20  $\mu$ mol **10**, 50 equiv. ZnEt<sub>2</sub> (2.0 mmol), 10.1 g 1-hexene (120 mmol), ethene (5 psi), 80 mL toluene, 25 °C

As revealed by results in Table 3, this kinetic study of LCCTP of E with H provided a highly linear relationship between  $M_n$  vs. polymerization time ( $t_p$ ) with the polydispersity index (PDI) values of all the samples remaining narrow (Figure 30). This unambiguously demonstrated the living nature of this polymerization. The broadness of PDI values for ultra-low  $M_n$  aliquots was probably due to intrinsic deficiencies in polystyrene standards and GPC columns for ultra-low-molecular weight analyses. Also, <sup>1</sup>H NMR spectra (600 MHz, 1,1,2,2-C<sub>2</sub>D<sub>2</sub>Cl<sub>4</sub>, 110 °C) provided no evidence of chain termination from  $\beta$ -hydrogen-atom transfer, which further confirmed the living character of this copolymerization. Finally, H incorporation levels for all poly(E-*co*-H) samples were calculated directly from integrations of <sup>13</sup>C {<sup>1</sup>H} NMR (150 MHz, 1,1,2,2-C<sub>2</sub>D<sub>2</sub>Cl<sub>4</sub>, 110 °C) spectra based on the method reported by Randall.<sup>163</sup> The H incorporation levels maintained between 20.7 to 22.0 mol% in the first 50 min, which indicated that the copolymer composition maintained homogeneous without

production of gradient copolymer during that time. However, after 50 min of polymerization, the H incorporation levels decreased dramatically due to the significant consumption of H and decrease of H concentration in toluene solution. The consumption rates of H were approximately 15% (after 50 min) and 26 % (after 90 min) estimated based on yield. Therefore, the total H consumption rate should be kept under 15% to maintain a homogeneous composition within the copolymer microstructures.

Figure 30. Plots of  $M_n$  vs.  $t_p$  (▲) and 1-hexene incorporation levels vs.  $t_p$  (●)

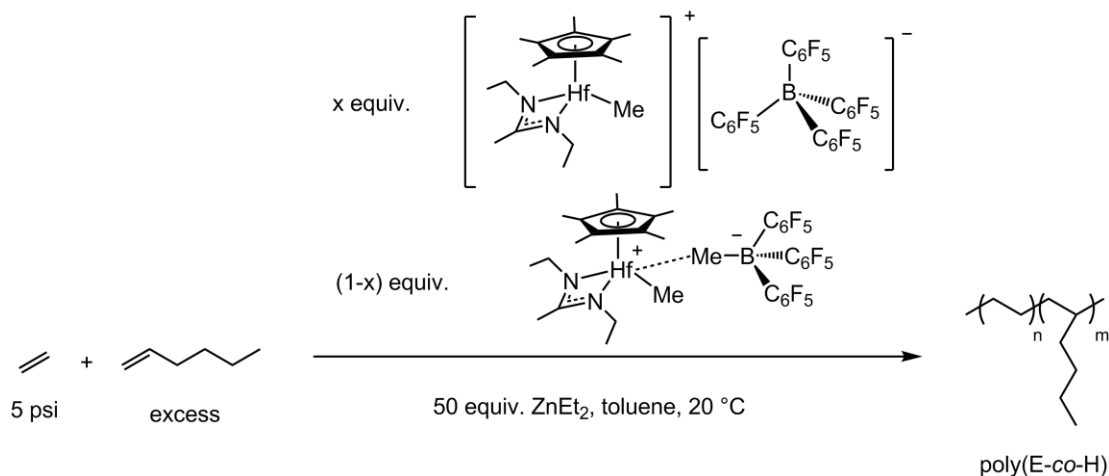


#### 4.4.2 Modulation of 1-hexene incorporation levels

With the strategy proposed in Scheme 27 been verified, the next important question is whether copolymer could be made with a spectrum of grades (composition of two components). For this purpose, LCCTP copolymerization of E with H have been carried out

in toluene using  $x$  equiv. of **07** and  $(1-x)$  equiv. of **09** as mixed loose and tight ion pairs in the presence of 50 equiv. of  $\text{ZnEt}_2$  as chain-transfer surrogate (Scheme 28). Based on previous kinetic study, initial H concentration in toluene was set as 1.5 mmol/mL and polymerization time was set for 30 min to maintain the homogeneous composition of all the samples. Polymerization temperature was set as 20 °C to allow some fluctuation. The ion pairs were generated in separated vials using 0.5 to 1.0 mL cold chlorobenzene as solvent.  $\text{ZnEt}_2$ , H and E were added/pressured to the polymerization flask for 30 min before addition of mixed ion pairs as initiators to start the polymerization.

*Scheme 28.* LCCTP copolymerization of E with H using mixed loose and tight ion pairs in the presence of  $\text{ZnEt}_2$



As shown in Table 2, when only loose ion pair **07** was used, 2.7 g of poly(E-co-H) has been obtained after hydrolysis of the initially formed  $\text{Zn}(\text{polymeryl})_2$  intermediate (Entry 4.08). GPC analysis showed a monomodal molecular weight distribution, with  $M_n = 3.50$  kDa and PDI ( $M_w/M_n$ ) = 1.21. Detailed copolymer compositional analysis of a  $^{13}\text{C}$  NMR spectrum (150 MHz, 1,1,2,2- $\text{C}_2\text{D}_2\text{Cl}_4$ , 110 °C) indicated a random composition ( $r_H \times r_E = 1.07$ ) of E and H, with H incorporation level of 17.0 mol%. Next, when a 1 : 1 ratio of loose **07** and tight **09** ion pairs were used under the identical LCCTP conditions, the poly(E-co-H) material

(Entry 4.09) was obtained with a little less yield (2.1 g) with lower  $M_n$  (2.61 kDa), which agrees with the lower activity of tight ion pair. Importantly, both the H relative reactivity  $r_H$  and incorporation level of H decreased as the tight ion pair ratio increased.

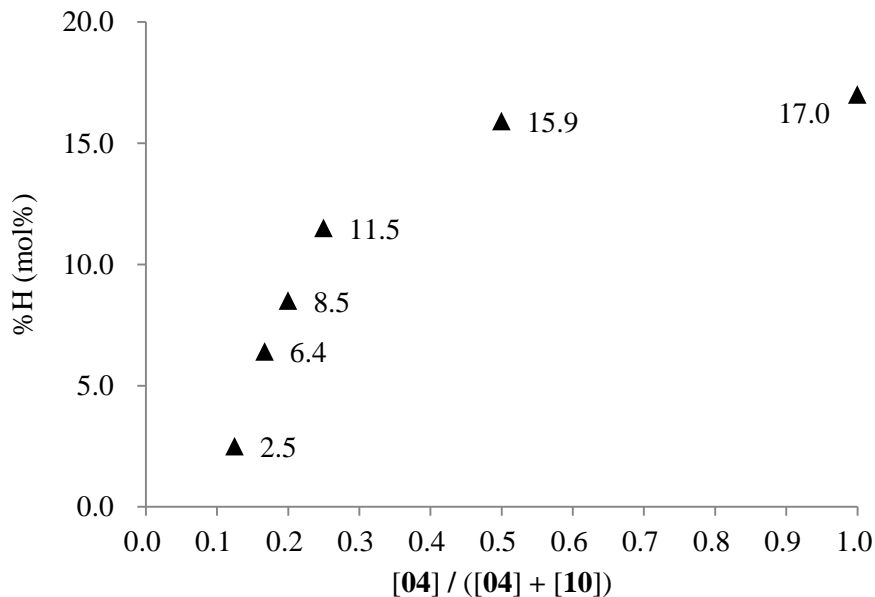
Table 4. LCCTP copolymerization results of ethene with 1-hexene in toluene

Entry	Cocatalyst <b>04 : 10</b>	Yield (g)	$M_n$ (kDa)	PDI	%H (mol%)	$r_H$	$r_E$	$r_H \times r_E$
4.08	1 : 0	2.7	3.50	1.21	17.0	0.0196	54.6	1.07
4.09	1 : 1	2.1	2.61	1.25	15.9	0.0148	58.3	0.86
4.10	1 : 3	1.4	2.18	1.27	11.5	0.0112	98.1	1.10
4.11	1 : 4	1.2	1.95	1.35	8.5	0.0078	122.1	0.95
4.12	1 : 5	1.1	1.97	1.25	6.4	0.0050	165.7	0.83
4.13	1 : 7	0.5	--	--	2.5	0.0000	434.5	--

Conditions: 20  $\mu\text{mol}$  **08**, [**04**]<sub>0</sub> + [**10**]<sub>0</sub> = [**08**]<sub>0</sub>, 50 equiv.  $\text{ZnEt}_2$  (1.0 mmol), 5.05 g 1-hexene (60 mmol), ethene (5 psi), 40 mL toluene, 20  $^\circ\text{C}$

Further decreasing the ratio of loose to tight ion pair from 1 : 3 to 1 : 7 led to a series of poly(E-co-H) materials (Entry 4.10 to 4.13) with the values of yield,  $M_n$ ,  $r_H$  and molar percentage of H all decreasing in the predicted fashion. The physical properties of those materials changed from viscous greases to non-viscous powders as H incorporation levels decreased to lower than 8.0 mol%. GPC analysis of all six poly(E-co-H) materials confirmed the monomodal distributions of molecular weight and narrow molecular weight distributions as living polymerizations. Also, product of relative reactivity,  $r_H \times r_E$ , values determined by  $^{13}\text{C}$  NMR spectroscopy confirmed the random composition of all the materials, which should be close to 1 for a random copolymer.<sup>163</sup>

Figure 31. Plot of H molar percentage vs. loose ion pair concentration



As shown in Figure 31, the trend to H molar percentage vs. loose ion pair concentration is not linear. Instead, the increasing of H incorporation level saturates after the loose ion pair reached about 50%. The reason is probably due to the limit of concentration of H in toluene. If the initial concentration of H is higher, the copolymerization with mainly loose ion pair will have more H incorporated. Therefore, the trend should be more resemble a linear shape, and the range of H incorporation level that can be tuned will be larger. This problem has been addressed in section 4.4 of this chapter.

#### 4.4.3 Modulation of propene incorporation levels

To establish the generality of applying LCCTP with mixed loose and tight ion pairs to obtain a range of different grades of polyethylene-based materials, we conducted a similar investigation of ethene and propene copolymerization in toluene. According to Table 5, three poly(E-co-P) materials were synthesized by the LCCTP copolymerization of E and P with three different populations of loose and tight ion pairs derived from 1 : 0 (entry 4.14), 1 : 1

(entry 4.15) and 0 : 1 (entry 4.16) of compound **07** and compound **09**, respectively. In each case, the LCCTP copolymerization was performed under a 1 : 9 feeding ratio of E to P mixed gas (5 psi) with 50 equiv. of ZnEt<sub>2</sub> and in toluene at 20 °C.

Table 5. LCCTP copolymerization results of ethene with propene in toluene

Entry	Cocatalyst <b>04</b> : <b>10</b>	Yield (g)	$M_n$ (kDa)	PDI	$T_m$ (°C)	$T_g$ (°C)	%P (mol%)
4.14	1 : 0	1.1	3.56	1.08	--	-54	54
4.15	1 : 1	0.5	2.30	1.10	--	--	38
4.16	0 : 1	0.2	1.54	1.11	68	--	6.6

Conditions: 20 μmol **08**, [**04**]<sub>0</sub> + [**10**]<sub>0</sub> = [**08**]<sub>0</sub>, 50 equiv. ZnEt<sub>2</sub> (1.0 mmol), 1 : 9 ethene/propene mixed gas (5 psi), 40 mL toluene, 20 °C

As shown in Table 5, GPC analysis of the three poly(E-co-P) materials confirmed the monomodal distributed nature and narrow molecular weight distributions, whereby the yield (activity) and  $M_n$  values once again decreased as the concentration of tight-ion-pair propagating species increased. <sup>1</sup>H NMR spectra provided no evidence that chain termination had occurred by β-hydrogen-atom transfer, which once again validated the living character of these LCCTP copolymerization. Finally, <sup>13</sup>C {<sup>1</sup>H} NMR spectroscopic microstructural analyses revealed a similar trend of decreasing levels of propene incorporations with the population of tight-ion-pair increased. The range of P incorporation (from 54% to 6.6%) for those poly(E-co-P) materials are larger than E/H copolymers (from 17.0% to 2.5%) because the concentration of P in toluene is much higher than E in toluene at 20 °C under about 1 atm.

For both E/H and E/P copolymers, the plots of co-monomer incorporation levels vs. loose ion concentration have established the standard curves for precise modulation of co-monomer incorporation levels, and consequently the physical property of the materials.

## 4.5 Copolymerization of Ethene with 1-Hexene in Neat 1-Hexene

### 4.5.1 Synthesis of poly(E-co-H) materials

Even though the ion-pair strategy proposed in Scheme 27 has been validated, the concentration of co-monomer in toluene solution is still a limit for the controllable range of copolymer compositions. Therefore, our next goal is to test if the LCCTP copolymerization can be carried out in neat 1-hexene instead of toluene. To the best of our knowledge, there is no literature report of using olefin monomers as polymerization solvent for coordinative chain-transfer polymerization. It seems that toluene is always the perfect solvent for chain-transfer process.<sup>85, 88-96</sup> Therefore, it is important to verify whether 1-hexene, which is also a non-polar solvent, could be used as the solvent for LCCTP as toluene. Using 1-hexene as a polymerization solvent could also avoid the problem of toluene dispersal or recycle that may cause environment issues or increase in the cost of production.

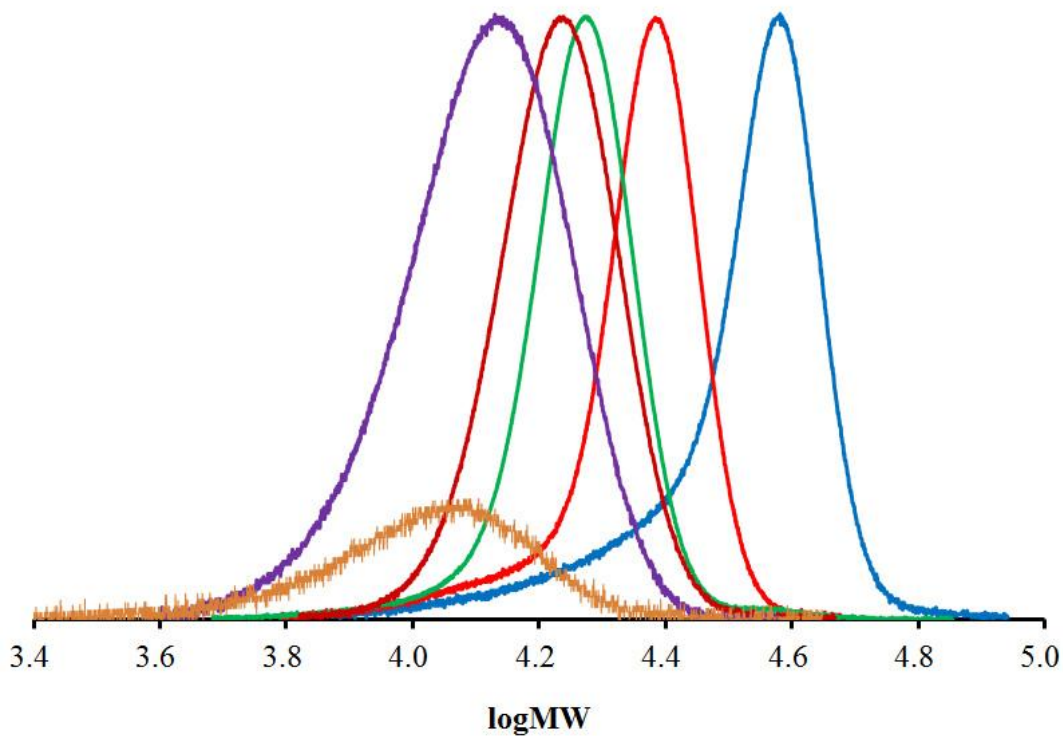
In the present study, we conducted the LCCTP copolymerization of E and H at an ethene pressure of 5 psi at 25 °C in *neat* 1-hexene to expand the range of copolymer compositions. Also, using neat 1-hexene could completely avoid the formation of a gradient-copolymer microstructure. With ZnEt<sub>2</sub> as the surrogate and a polymerization time of 30 min, the poly(E-co-H) materials (entry 4.17 to 4.22 of Table 6) obtained after hydrolysis of the initially formed Zn(polymeryl)<sub>2</sub> intermediate were all analyzed by GPC to have monomodal molecular weight distributions (Figure 32) with narrow polydispersity indexes (PDI ≤ 1.15). No evidence of vinyl end-groups from β-hydrogen-atom transfer confirmed the living nature of those copolymerizations in neat 1-hexene. The key values of yield (activity) and  $M_n$  were both found to decrease as tight-ion-pair ratio increased.

Table 6. LCCTP copolymerization of ethene with 1-hexene in neat 1-hexene

Entry	Cocatalyst <b>04 : 10</b>	Yield (g)	$M_n$ (kDa)	PDI	$T_m$ ( $^{\circ}\text{C}$ )	$T_c$ ( $^{\circ}\text{C}$ )	$T_g$ ( $^{\circ}\text{C}$ )	%H (mol%)
4.17	1 : 0	10.0	30.0	1.13	--	--	-46.3	74.4
4.18	2 : 1	4.5	21.5	1.07	--	--	-52.3	62.6
4.19	1 : 1	3.7	17.6	1.06	--	--	-61.2	38.5
4.20	1 : 2	3.0	16.3	1.05	--	20.4	--	17.8
4.21	1 : 4	1.5	12.0	1.10	82.8, 67.3	73.5	--	8.0
4.22	0 : 1	1.2	9.7	1.15	90.5, 72.0	80.7	--	6.9

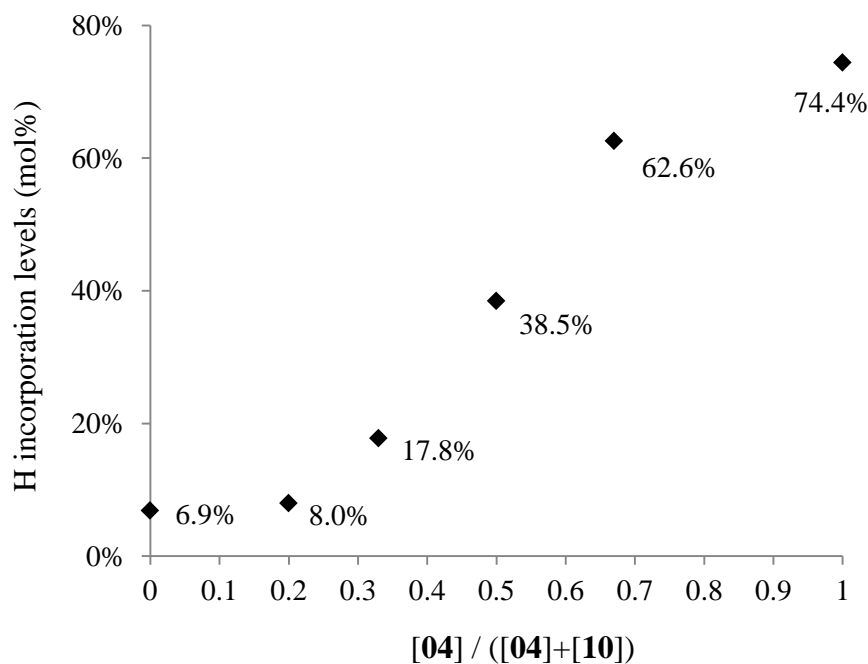
Conditions: 20  $\mu\text{mol}$  **08**,  $[\mathbf{04}]_0 + [\mathbf{10}]_0 = [\mathbf{08}]_0$ , 10 equiv.  $\text{ZnEt}_2$  (0.2 mmol), 13.4 g 1-hexene (20 mL), ethene (5 psi), 25  $^{\circ}\text{C}$ , polymerization time 30 min.

Figure 32. Molecular weight distributions of poly(E-co-H) samples of entries 4.17 to 4.22 (from right to left) of Table 6



Importantly, with only loose ion pair **07**, poly(E-*co*-H) material (entry 4.17) had a H incorporation level of 74.4%, which was a remarkably high value in comparison to that of 17.0 % from entry 4.08 in Table 4, as well as literature reported values.<sup>161</sup> On the other hand, when only the tight ion pair **09** was used as the active initiator, the poly(E-*co*-H) material (entry 4.22) that was obtained has only 6.9% H incorporation level regardless the fact that the copolymerization was carried out in neat H. Having set those two limiting cases, with different populations of the loose and tight ion pairs of **07** and **09** been used as mixed initiator, four poly(E-*co*-H) materials with 62.6% (entry 4.18), 38.5% (entry 4.19), 17.8% (entry 4.20) and 8.0% (entry 4.21) H incorporation levels were made with increasing ratio of tight-ion-pair. As show in Figure 33, the plot of H contents vs. loose ion pair concentration is symmetric which perfectly confirms the theoretical prediction of the two-state copolymer system. Also, the curve is nearly linear in around 1 : 1 ration of loose and tight ion pairs as predicted by a random two-state copolymer system.

Figure 33. H incorporation levels vs. loose ion pair concentrations.



#### 4.5.2 Compositional characterization of poly(E-co-H) materials

Table 7. Diads analysis and calculated relative reactivities of ethene and 1-hexene

Entry	[H]	[HH]	[HE]	[EE]	$r_H$	$r_E$	$r_H \times r_E$
4.17	0.744	0.628	0.232	0.140	0.102	50.9	5.20
4.18	0.626	0.432	0.387	0.181	0.0464	41.7	1.93
4.19	0.385	0.143	0.484	0.373	0.0148	75.1	1.11
4.20	0.178	0.022	0.312	0.666	0.00443	207	0.917
4.21	0.080	0.003	0.155	0.842	0.00159	523	0.832
4.22	0.069	0.001	0.136	0.863	0.000980	605	0.593

Detailed diads and triads analysis based on  $^{13}\text{C} \{^1\text{H}\}$  NMR (150 MHz, 1,1,2,2- $\text{C}_2\text{D}_2\text{Cl}_4$ , 110 °C) spectra revealed the microstructures and confirmed the random copolymer composition of all those poly(E-co-H) materials (Table 7 and Figure 35). According to the methods of Spiz et al.,<sup>162</sup> the co-monomer feed ratio at this temperature and pressure was determined to be:  $x_E/x_H = 0.0216$  for  $x_E = 0.0211$  and  $x_H = 0.979$ ;  $x_E$  and  $x_H$  are the molar fractions of E and H, respectively. Randall<sup>163</sup> and others<sup>164</sup> have shown that, for a copolymer made by a single-site catalyst at constant co-monomer concentrations, and ignoring diffusion or mixing effects, reactivity ratios can be used to relate the relative molar monomer concentration in the feedstock to the relative molar monomer concentration incorporated into the copolymer.<sup>165</sup> Therefore, the reactivity of E ( $r_E$ ) and reactivity of H ( $r_H$ ) in the E/H copolymer could be calculated based on the following equations,<sup>165</sup> where  $P_{x/y}$  represents the probability of adding a X monomer to a growing chain in which Y was the last monomer.

$$P_{E/H} = \frac{[HE + EH]}{2[E]}; P_{H/E} = \frac{[HE + EH]}{2[H]}$$

$$r(E) = \frac{x(H)}{x(E)} \cdot \frac{1 - P_{E/H}}{P_{E/H}} = \frac{x(H)}{x(E)} \cdot \frac{1 - \frac{[HE + EH]}{2[E]}}{\frac{[HE + EH]}{2[E]}}$$

$$r(H) = \frac{x(E)}{x(H)} \cdot \frac{1 - P_{H/E}}{P_{H/E}} = \frac{x(H)}{x(E)} \cdot \frac{1 - \frac{[HE + EH]}{2[H]}}{\frac{[HE + EH]}{2[H]}}$$

$$r(E) \cdot r(H) = \frac{4 \cdot [EE] \cdot [HH]}{[HE + EH]^2}$$

According to Figure 34, it is now clear that modulation of co-monomer incorporation levels is achieved through the manipulation of  $r_E$  and  $r_H$  values of the copolymerization. With the increase of loose-ion-pair, which favors the incorporation of H co-monomer in neat H, the  $r_H$  values increase dramatically (~104 times from entry 4.22 to 4.17) while the  $r_E$  values decrease a little bit (~1/12 from entry 4.22 to 4.17). The relative change of  $r_E$  and  $r_H$  values determines the overall H incorporation levels of the poly(E-co-H) materials, as well as the overall activities, yields, and molecular weights of the resulting copolymers.

Figure 34. Co-monomer relative reactivities,  $r_H$  and  $r_E$  vs. loose ion pair concentrations

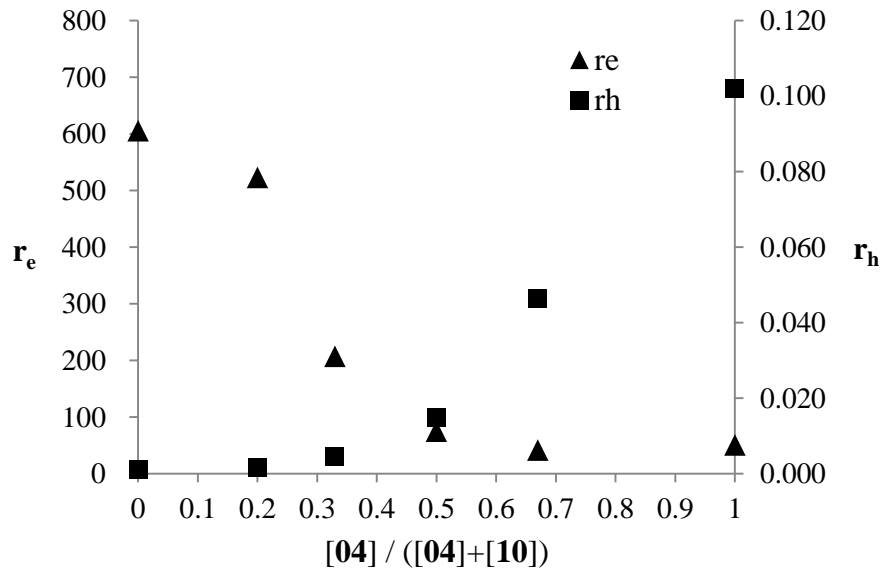
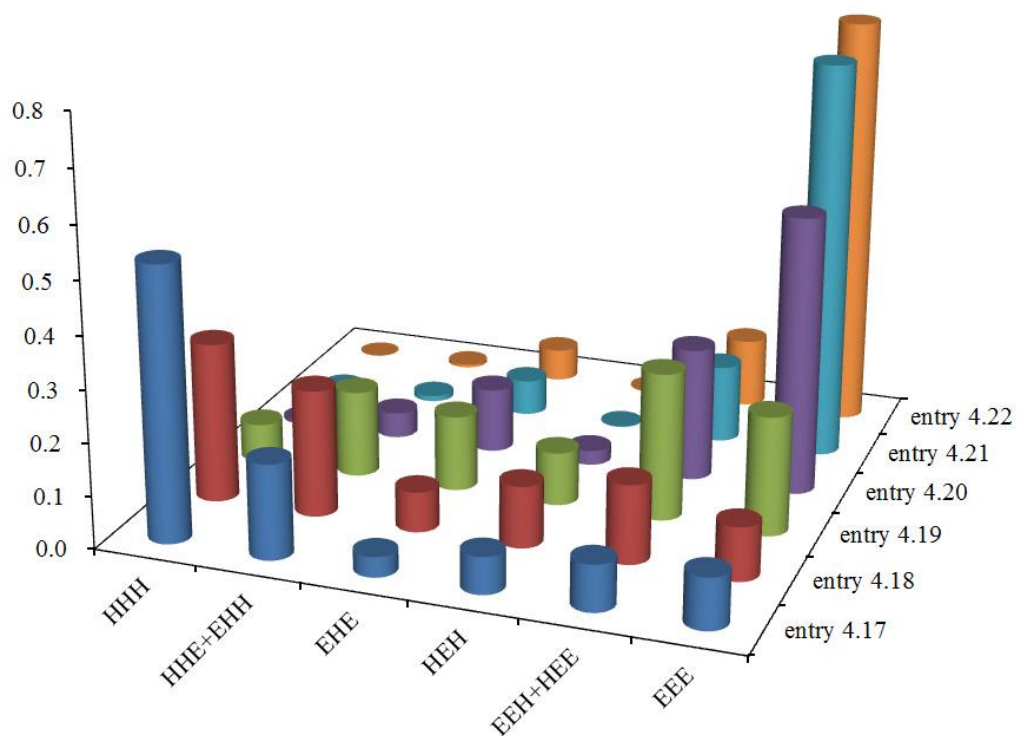


Figure 35.  $^{13}\text{C}$  NMR triads analysis of poly(E-co-H) samples in Table 6



Furthermore, the physical properties of the isolated poly(E-co-H) materials varies with different copolymer compositions. The physical differences between these materials are perhaps best captured by a side-by-side comparison of six samples (Figure 36). With increasing of E contents, the materials gradually change from viscous grease (entry 4.17, 4.18) to clear liquids (entry 4.19, 4.20) to finally white powders (entry 4.21, 4.22).

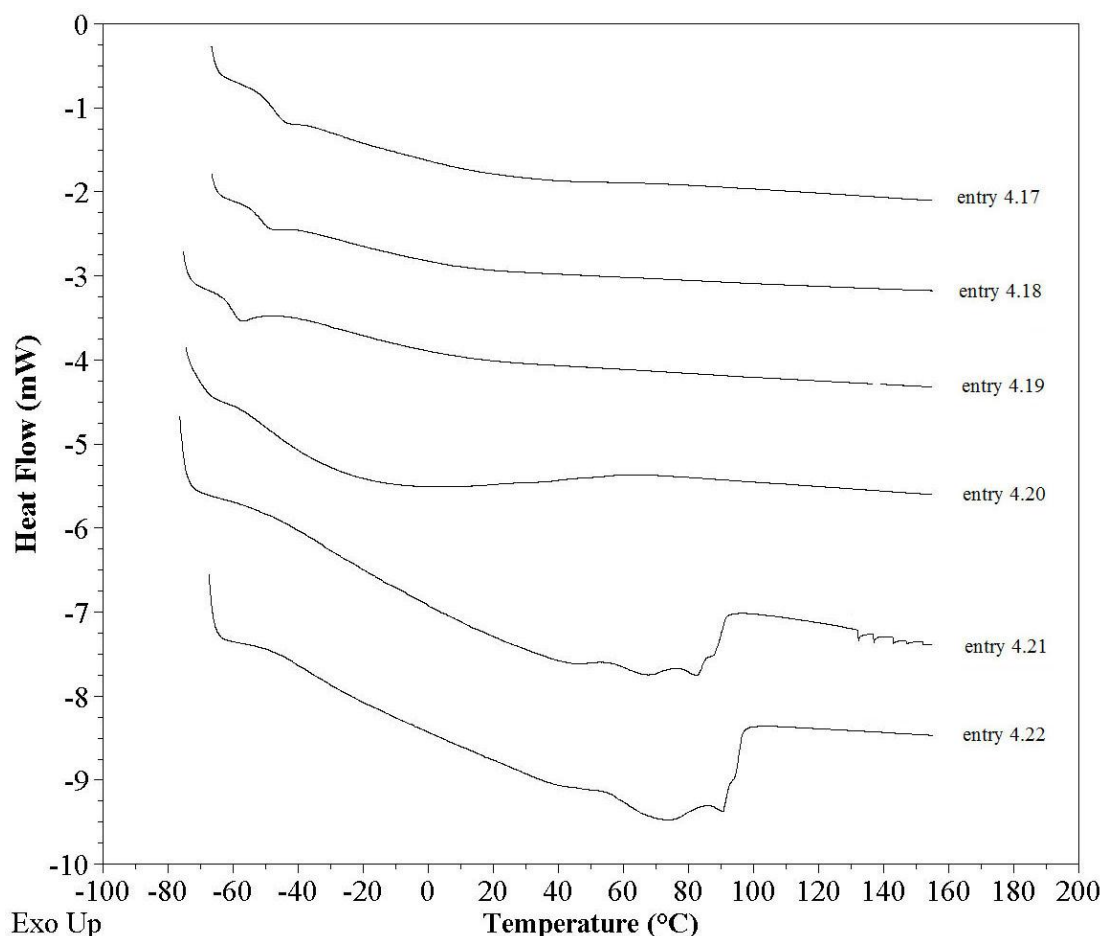
Figure 36. Photos of poly(E-co-H)s of entries 4.17 to 4.22 (from left to right) of Table 6



### 4.5.3 Thermal analysis of poly(E-co-H) materials

Thermal analysis results through differential scanning calorimetry (DSC) (2<sup>nd</sup> heating cycle, 10 °C/min) agreed with the physical properties of those materials. Characterization of poly(E-co-H) material of entry 4.17 revealed an amorphous state over a broad temperature range that was further associated with a very low  $T_g$  value of  $-46.3$  °C (Table 6). In contrast, the significantly more ethene rich material (entry 4.22) exhibited a high degree of crystallinity, with two associated melting endotherms,  $T_m = 72.0$  and  $90.5$  °C, and a single crystallization exotherm,  $T_c = 80.7$  °C. All the other samples having H incorporation levels between those two limits show the thermal behaviors between those two (Figure 37).

Figure 37. DSC traces for poly(E-co-H) materials of entry 4.17 to 4.22 of Table 4.



## 4.6 Copolymerization of Ethene with Cyclopentene

### 4.6.1 Synthesis and characterization of 1-iodo-poly(E-co-CPE) materials

To establish the possible generality of applying LCCTP with loose and tight ion pairs derived from different types of transition metal precatalysts, we conducted a similar investigation of ethene (E) and cyclopentene (CPE) copolymerization, which required a more sterically open precatalyst, CpZrMe<sub>2</sub>[N(Cy)C(Me)N(Cy)] (**13**), for the insertion of cyclic olefins. We have shown the successful LCCTP copolymerization of E and CPE using precatalyst **13** and cocatalyst **04** with ZnEt<sub>2</sub> as the surrogate to yield exclusively poly(E-co-1,2-cyclopentane) (poly(E-co-CPE)).<sup>166</sup> Furthermore, as we discussed in Chapter 3, 1-iodo-poly(E-co-CPE) can be obtained in quantitative yield through iodinolysis of Zn-C bonds of the initially formed Zn(polymeryl)<sub>2</sub> intermediate upon the addition of a slight excess I<sub>2</sub> as a solution in toluene.

Table 8. Results of the 1-iodo-poly(E-co-CPE) materials

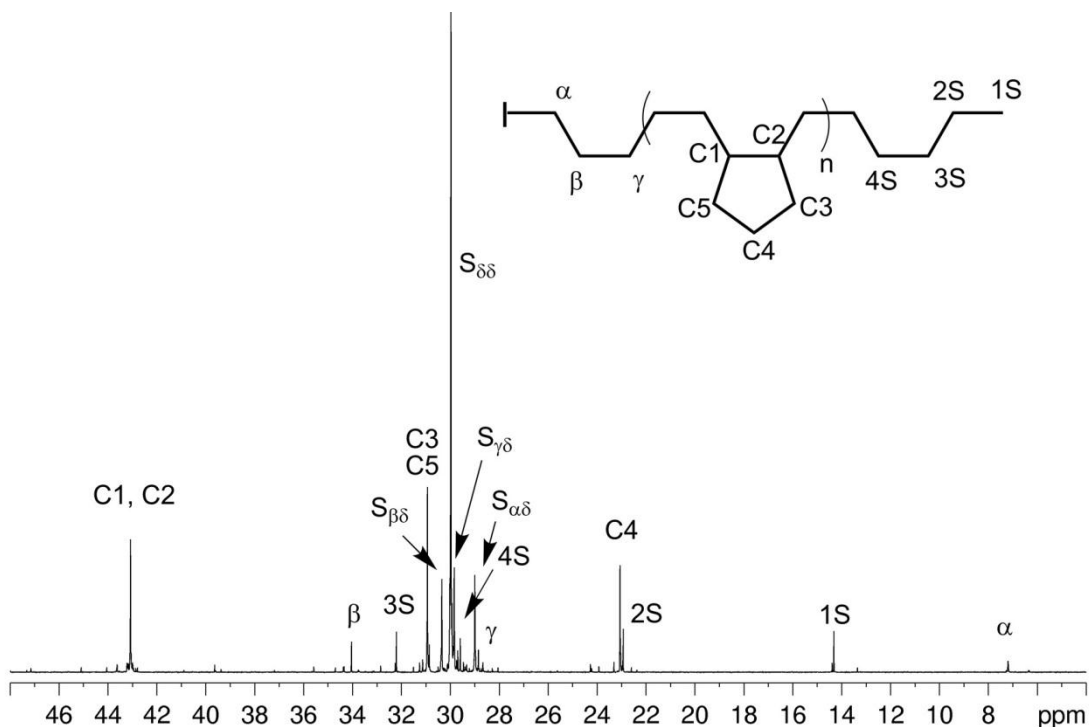
Entry	Cocatalyst <b>04</b> : <b>10</b>	Yield (g)	$M_n^{[a]}$ (kDa)	PDI <sup>[a]</sup>	$M_n^{[b]}$ (kDa)	% CPE <sup>[b]</sup> (mol%)
4.23	1 : 0	2.3	2.58	1.22	1.35	15.6
4.24	1 : 1	2.1	2.46	1.14	1.11	11.4
4.25	0 : 1	1.7	2.32	1.10	0.99	8.7

Conditions: 20  $\mu$ mol **13**, [**04**]<sub>0</sub> + [**10**]<sub>0</sub> = [**13**]<sub>0</sub>, 50 equiv. ZnEt<sub>2</sub> (1.0 mmol), 4.08 g cyclopentene (60 mmol), ethene (5 psi), 40 mL toluene, 25 °C. [a] Determined by GPC analysis. [b] Determined by <sup>13</sup>C NMR spectroscopic end-group analysis.

Three 1-iodo-poly(E-co-CP) materials were synthesized by the LCCTP copolymerization of E and CPE with three different populations of loose and tight ion pairs derived from precatalyst **13** by activation with: 1) only the borate catalyst **04** (Table 8, entry

4.23), 2) a 1:1 mixture of the two cocatalysts **04** and **10** (entry 4.24), and 3) only the borane cocatalyst **10** (entry 4.25). In each case, the LCCTP copolymerization of E and CPE was performed with 50 equiv. of  $\text{ZnEt}_2$  and 3000 equivalents of CPE (relative to **13**) in toluene at 25 °C and at an ethene pressure of 5 psi. GPC analysis of the three isolated  $\alpha$ -I-poly(E-co-CP) materials confirmed monomodal and narrow molecular-weight distributions, whereby the yield (activity) and  $M_n$  values once again decreased as the concentration of the tight-ion-pair propagating species increased.  $^1\text{H}$  NMR spectra provided no evidence that chain termination had occurred by  $\beta$ -hydrogen-atom transfer, which once again validated the living character of these LCCTP copolymerizations. Also,  $^{13}\text{C}$  NMR (150 MHz,  $1,1,2,2\text{-C}_2\text{D}_2\text{Cl}_4$ , 90 °C) spectroscopic microstructural and end-group analyses revealed that CPE was enchainment exclusively in a 1,2-fashion, and the level of CPE incorporation decreased as the population of tight ion pairs increased (Figure 38).

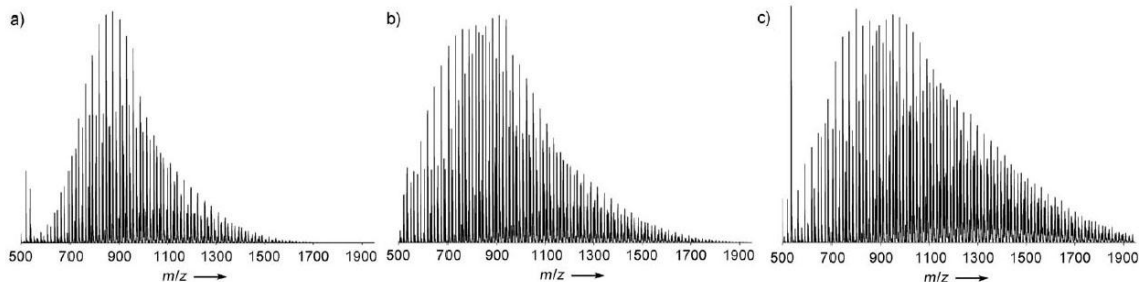
Figure 38.  $^{13}\text{C}$  { $^1\text{H}$ } NMR analysis of 1-iodo-poly(E-co-CPE) of entry 4.24 in Table 8



#### 4.6.2 MALDI-TOF-MS analysis of 1-iodo-poly(E-co-CPE) materials

To better characterize the difference of the those samples, these 1-iodo-poly(E-co-CPE) samples were further converted into the corresponding triphenylphosphonium-terminated materials,  $\alpha$ -[I][Ph<sub>3</sub>P]-poly(E-co-CPE), by heating as a solution in dimethylformamide (DMF) with an excess of PPh<sub>3</sub> at 110 °C for 3 days.<sup>167-168</sup> A significant advantage of the  $\alpha$ -[I][Ph<sub>3</sub>P]-poly(E-co-CPE) products is that an excellent qualitative picture of copolymer composition can be readily obtained through the use of matrix-assisted laser-desorption time-of-flight (MALDI-TOF) mass spectrometric analysis.<sup>169-171</sup> As originally demonstrated by Byrd et al.,<sup>167</sup> the attachment of a terminal cationic triphenylphosphonium moiety greatly enhances the utility of MALDI-TOF for characterization of the molecular-weight distributions and molecular-weight indices of polyolefin samples. On the other hand, without extensive standardization, it is not possible to extract quantitative values for molecular-weight indices and copolymer compositions from these MALDI-TOF data.<sup>169-171</sup>

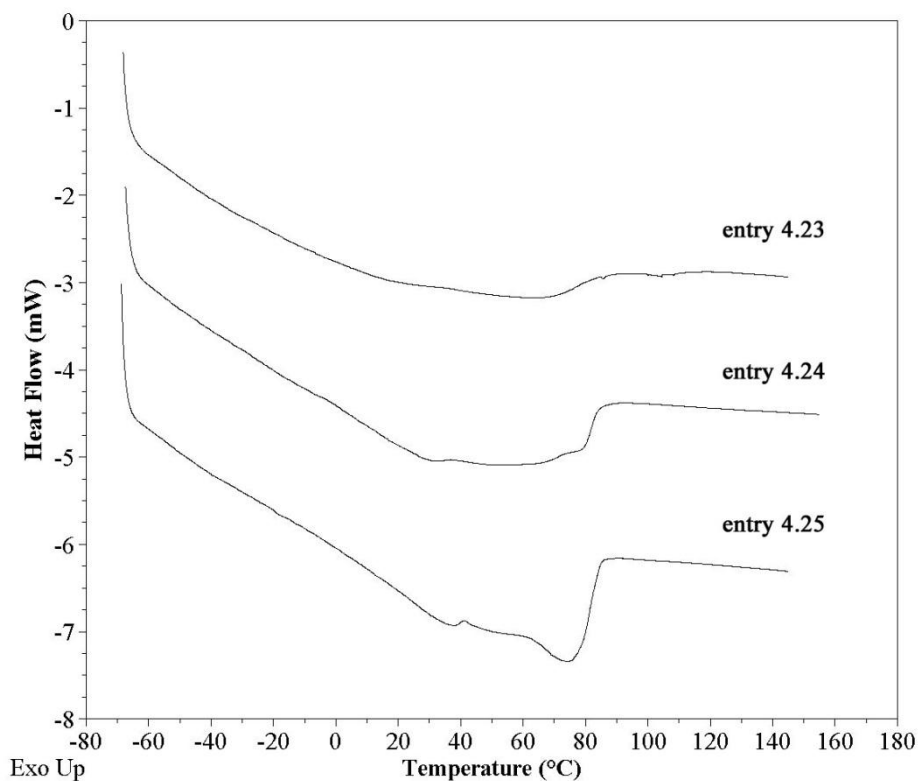
*Figure 39.* MALDI-TOF-MS spectra of the  $\alpha$ -[I][Ph<sub>3</sub>P]-poly(E-co-CPE) materials described in Table 8, a) entry 4.25, b) entry 4.24, and c) entry 4.23.



The observed discrepancies between the GPC-based  $M_n$  values and those obtained by <sup>13</sup>C NMR spectroscopic end-group analysis are probably due to intrinsic deficiencies in polymer standards and GPC columns for low-molecular-weight analyses. Indeed, the

MALDI-TOF data obtained for the three  $\alpha$ -[I][Ph<sub>3</sub>P]-poly(E-co-CPE) samples showed molecular-weight distributions that were very much in line with the  $M_n$  values derived by NMR spectroscopy. Significantly, however, these MALDI-TOF data also established unequivocally that LCCTP involving tight and loose ion pairs can indeed be used to modulate E and CPE co-monomer relative reactivities in a programmed fashion, as evidenced by the qualitative increase in the molar percentage of CPE incorporation as the population of the loose ion pair increased relative to the population of the tight ion pair (Figure 39a-c). Also, the size of the melting endotherm (proportional to the percentage of crystallinity) from DSC (2<sup>nd</sup> heating cycle, 10 °C/min) analysis confirmed the decrease of CPE incorporation levels as the tight-ion-pair concentration increases (Figure 40).

Figure 40. DSC traces for 1-iodo-poly(E-co-CPE) materials



## **4.7 Conclusions**

LCCTP copolymerization coupled with fast and reversible chain-transfer between mixed tight- and loose-ion-pair initiators mediated *via*  $\text{ZnEt}_2$  as a chain-transfer mediator has been validated as a successful strategy for greatly expanding the range of polyolefin copolymer compositions. Only a single transition metal precatalyst is needed in this strategy in combination with varying populations of cocatalysts to make infinite possibilities of copolymers, such as poly(E-*co*-H), with programmable modulated co-monomer incorporation levels.

Also, generality of this strategy has been verified to be able to expand to different transition-metal-based ion pairs, as well as a variety of polyethene-based copolymers, such as poly(E-*co*-H), poly(E-*co*-P) and poly(E-*co*-CPE). Additional investigations are currently in progress to explore the extent and limits of this new methodology, including the synthesis polyolefin materials with programmed “blocky” copolymer architectures.

# Chapter 5: Preparation of Precision Polyolefin Waxes through LCCTP Copolymerization of Ethene with Long Chain $\alpha$ -Olefin Co-monomers

## 5.1 Background

Linear low density polyethene (LLDPE) obtained by copolymerization of ethene or propene with longer chain  $\alpha$ -olefins stands a remarkable part of commercial plastics and is estimated to have over 15% annual increase in production.<sup>172-174</sup> Given the vast amount of research of LLDPE based on propene, 1-butene, 1-hexene and 1-octene as short chain branches, few have been reported using even longer  $\alpha$ -olefins as co-monomers to achieve better mechanical and rheological properties.<sup>175-178</sup> Compared to short branches of 1 to 6 carbon atoms, longer branches with over 8 carbon atoms can better lower the melting temperature, density and crystallinity as a distortion of the polymer chain.<sup>179-180</sup> More importantly, long side-chains can crystallize with one another to form side-chain crystalline units which will lead to remarkable material properties different from conventional LLDPE.<sup>181-182</sup>

In 2000, Mülhaupt and co-workers<sup>183</sup> observed side-chain crystallization behaviors from ethene/1-eicosene copolymers with 1-eicosene incorporation level exceeding 5.9 mol%. The intensity of side-chain melting peaks was depended on the incorporation levels of 1-eicosene co-monomer. Later, Piel et al.<sup>184</sup> found that side-chain crystallized even at low branch levels (2.7 mol%) when using hexacosene as a co-monomer with ethene. The density and crystallinity of the copolymer increased because of the crystallization of long side-chains,

which also resulted in a specific relaxation in the dynamic mechanical analysis (DMA). However, in both cases, the main-chain crystallinity still dominated and side-chain crystallization showed as an additional peak with lower melting temperature from differential scanning calorimetry (DSC) analysis. Unfortunately, to the best of our knowledge, no literature has been reported on side-chain crystallization predominant ethene/long chain  $\alpha$ -olefin copolymers which require very high incorporation levels of long chain  $\alpha$ -olefins. The increase on the length of  $\alpha$ -olefins often leads to the decrease of polymerization reactivity, thus high incorporation level of long chain  $\alpha$ -olefins towards ethene is extremely hard. Even though great efforts have been put on increasing catalyst activities and  $\alpha$ -olefin incorporation levels by modification of steric bulk of ligand, bite angle, configuration and conformation of transition metal catalysts, rare examples have been demonstrated to achieve high long chain  $\alpha$ -olefin incorporation levels as well as controlled macromolecular architectures.<sup>185-191</sup>

Recently, our group has achieved the successful LCCTP copolymerization of ethene (E) with 1-hexene (H), 1-octene (O) and 1,5-hexadiene (HD) using compound **07** as an initiator in combination with excess equivalents of  $\text{ZnEt}_2$  as a surrogate to yield copolymers with tunable molecular weights and narrow polydispersity (PDI) index, as well as high co-monomer incorporation levels (above 15 mol%).<sup>88-89</sup> It was then of particular interest to determine whether this same system would be capable of the living CCTP copolymerization of E with longer chain  $\alpha$ -olefins, such as 1-decene (DE), 1-tetradecene (TDE), 1-hexadecene (HDE), 1-octadecene (ODE) and 1-docosene (DCE), while still maintaining the high incorporation level of co-monomers. With the accomplishment of this goal, a novel class of ethene-based copolymers with predominant side-chain crystallization behavior could be synthesized with unique crystalline behaviors and novel physical properties.

## 5.2 LCCTP Copolymerization of Ethene with 1-Hexadecene

### 5.2.1 Synthesis of poly(E-co-HDE)s with varying molecular weights

Diethyl hafnium compound **07** was selected as the active catalyst to deliver the LCCTP copolymerization of E with long chain  $\alpha$ -olefins, such as 1-hexadecene (HDE), because of its high activity and relative thermostability at room temperature. Importantly, the sterically opened diethyl amidinate ligand environment on **07** ensured the high co-monomer reactivity and consequently high incorporation level of  $\alpha$ -olefin co-monomers.<sup>89</sup>  $\text{ZnEt}_2$  was chosen in light of that it engaged in rapid and reversible chain-transfer process with transition metal active species, such as **07**, without adverse influence on the activity or co-monomer incorporation level of the copolymerization. Copolymerization was carried out in toluene with co-monomer concentrations of 1.12 to 1.45 mmol/ml, which were required to maintain homogeneous compositional microstructure of the copolymers based on previous literature.<sup>89</sup>

Scheme 29. LCCTP copolymerization of E with long chain  $\alpha$ -olefins

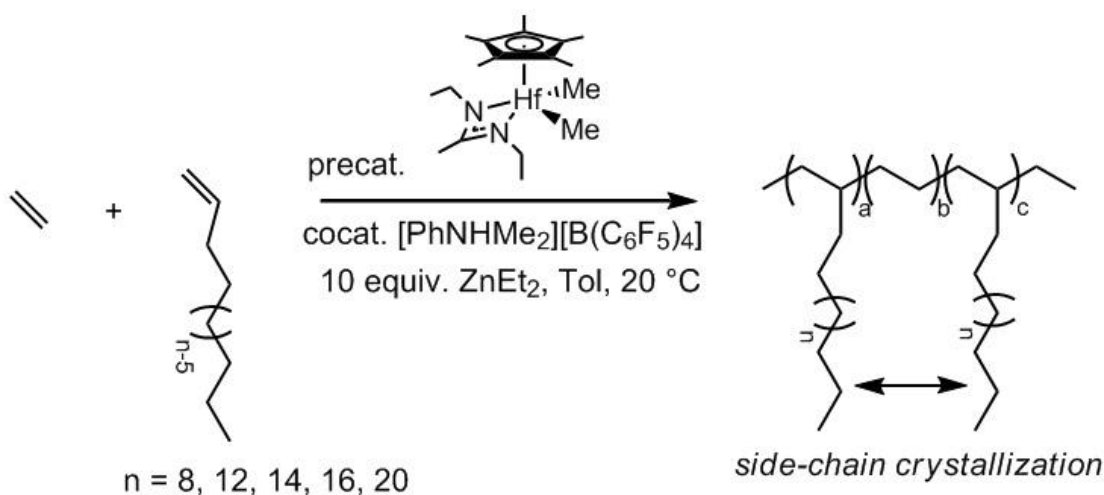


Table 9. Results of LCCTP copolymerization of ethene with 1-hexadecene

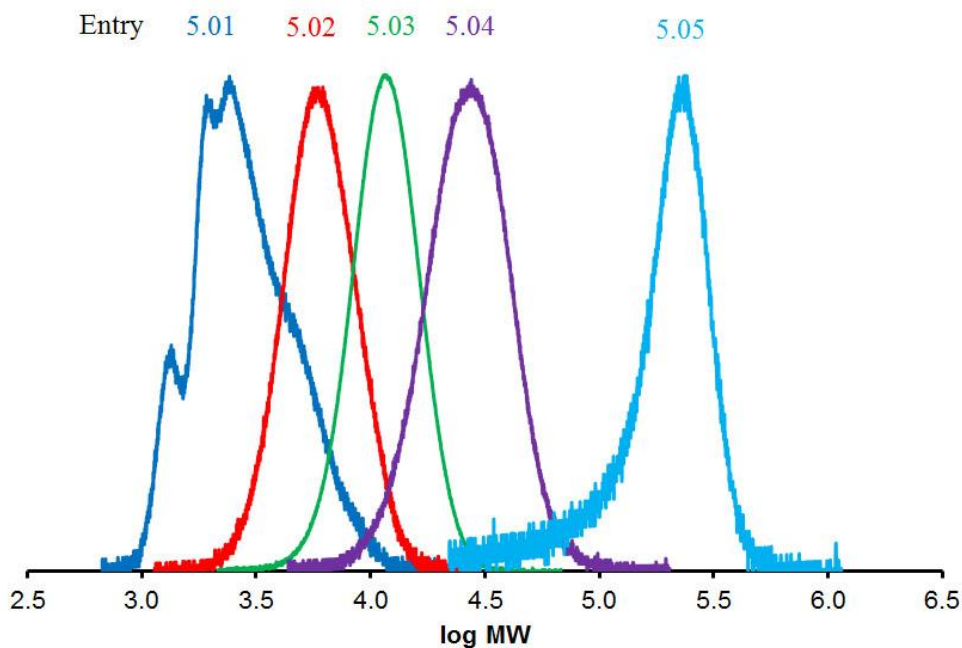
Entry	Monomers	ZnEt <sub>2</sub> (equiv.)	Yield (g)	<i>M<sub>n</sub></i> (kDa)	PDI	<i>T<sub>m</sub></i> <sup>[a]</sup> (°C)	<i>T<sub>c</sub></i> <sup>[a]</sup> (°C)	%HDE <sup>[b]</sup>
5.01	E/HDE	50	0.7	2.58	1.27	5.5	-2.3	--
5.02	E/HDE	20	1.1	4.00	1.13	11.8	-1.0	26.3
5.03	E/HDE	10	1.8	10.8	1.12	16.9	13.8	32.0
5.04	E/HDE	5	2.1	23.4	1.19	17.5	12.1	30.7
5.05	E/HDE	0	0.7	145.1	1.40	18.0	20.2	29.4

Conditions: 10 μmol **08**, 10 μmol **04**, 20.0 mmol HDE, ethene (5 psi), 10 mL toluene, 20 °C.

[a] Small main-chain melting endotherms and crystalline exotherms were omitted for clearance. [b] Determined by <sup>13</sup>C NMR structural analysis

As Scheme 29 and Table 9 illustrate, a series of LCCTP copolymerization of ethene with HDE have been accomplished by using precatalyst **08** and cocatalyst **04** with equiv. of ZnEt<sub>2</sub> varying from 50 to 0 in toluene at room temperature. In order to demonstrate the capability of LCCTP on the control of molecular weights, polymerization time was carefully chosen in combination with the amount of ZnEt<sub>2</sub> used. After hydrolysis, a series of poly(E-co-HDE) materials were obtained with *M<sub>n</sub>* values ranging from 2.58 kDa to 145.1 kDa. As shown by the overlay of GPC curves in Figure 41, molecular weights distributions were narrow (PDI < 1.2) within a large range of *M<sub>n</sub>* (4.0 to 23 kDa); the broadness of molecular weight distribution at low *M<sub>n</sub>* is caused by the limit of gel permeation chromatography (GPC) standards and columns while the broadness at high *M<sub>n</sub>* is due to slow mass transfer effect caused by high viscosity of the polymerization solution. <sup>1</sup>H and <sup>13</sup>C NMR end-group analysis confirms the living nature of the copolymerization based on the absence of chain-termination by β-hydride elimination, which is in keeping with the narrow PDI index.

Figure 41. Molecular weight distributions of poly(E-co-HDE) samples of Table 9

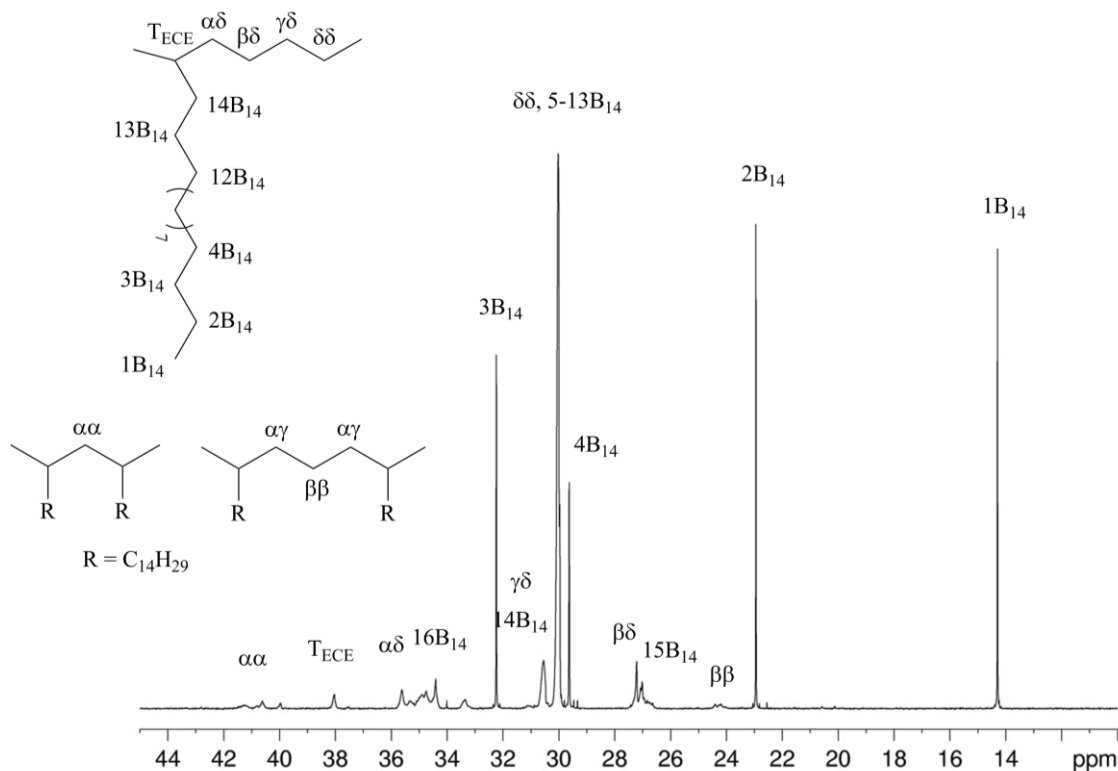


### 5.2.2 Structural and thermal analysis of poly(E-co-HDE)s

$^{13}\text{C}$   $\{^1\text{H}\}$  NMR (150 MHz, 1,1,2,2- $\text{C}_2\text{D}_2\text{Cl}_4$ , 90  $^\circ\text{C}$ ) spectroscopy was carried out to determine the chain architecture and composition of those copolymers. All poly(E-co-HDE)s were found to be random copolymers with isolated branches from HDE co-monomer (e.g., Figure 42). HDE incorporation levels were calculated based on previous literature.<sup>163</sup> Due to the ultra-low  $M_n$  (2.58 kDa) of poly(E-co-HDE) of entry 5.01, it was difficult to calculate the HDE incorporation level because of the high content of chain-end groups that overlapping with the HDE co-monomer resonances. For copolymers with  $M_n$  higher than 4.0 kDa, the HDE incorporation levels were independent of the molecular weights and maintained higher than 26 mol% (entry 5.02 to 5.05) which were much larger compared to the values in previous literatures.<sup>175-178, 185-191</sup> Those results indicated that initiator **07** maintained high

activities and incorporation levels towards bulky long chain  $\alpha$ -olefins over a board range of molecular weights, even though the length of co-monomers increased to 16 carbons.

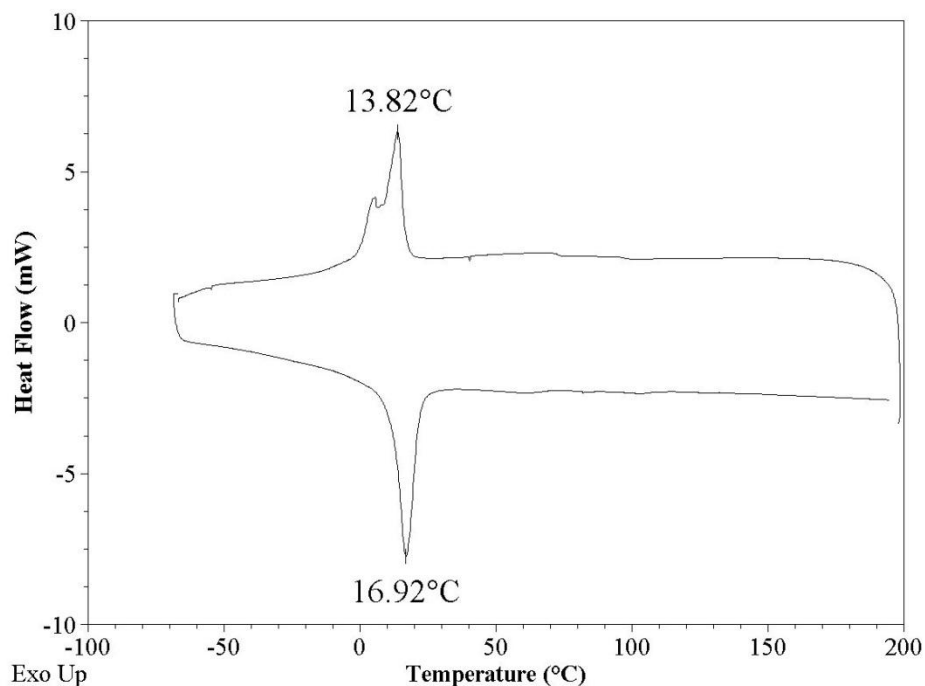
Figure 42.  $^{13}\text{C}$   $\{^1\text{H}\}$  NMR spectrum and assignments of poly(E-co-HDE) of entry 5.03 in Table 9



Thermal analysis by DSC (2<sup>nd</sup> heating and 3<sup>rd</sup> cooling cycle, 10  $^{\circ}\text{C}/\text{min}$ ) has been taken out to study the crystalline behavior of the resulting copolymers. For poly(E-co-H) and poly(E-co-O) samples with co-monomer incorporation levels over 15 mol%, no melting endotherm was observed due to the high concentration of short chain branches.<sup>89</sup> However, thermal analyses of poly(E-co-HDE)s of Table 9 by DSC reveal strong melting endotherms for all five samples with melting temperatures ( $T_m$ ) between 5.5 and 18.0  $^{\circ}\text{C}$ , and during cooling, they all undergoes crystallization between -2.3 to 20.2  $^{\circ}\text{C}$ . Figure 43 shows the heating and cooling cycles of DSC thermograms of poly(E-co-HDE) from entry 5.03 in Table

9. The possibility of residue HDE monomer in poly(E-co-HDE) samples is eliminated by the comparison with pure HDE monomer ( $T_m = 4.3\text{ }^\circ\text{C}$  and  $T_c = 1.6\text{ }^\circ\text{C}$ ). Also compared to most PE-based copolymers ( $T_m \sim 110\text{--}120\text{ }^\circ\text{C}$ ),<sup>175-184</sup> small or absence of PE main-chain melting endotherms and crystallization exotherms are observed for those poly(E-co-HDE)s, which are probably due to the high incorporation level of HDE that interrupts the packing from main-chains. As we expected, the high content of HDE branches leads to the packing of 14-carbon side-chains, and the strong melting endotherms and crystallization exotherms are caused by side-chain crystallinity. The side-chain melting temperatures of these poly(E-co-HDE)s are slightly lower than poly(HDE) (side-chain  $T_m = 35.5\text{ }^\circ\text{C}$ ),<sup>181</sup> which is due to the low side-chain contents in copolymers compared to homopolymer. Importantly, because of the negligible main-chain crystallinity, the sizes of the side-chain crystalline units are uniform and only determined by the length of the side-chains, thus leading to very narrow melting endotherms and moderate crystallinity.

Figure 43. DSC thermograms of poly(E-co-HDE) of entry 5.03 in Table 9



Architectures of the poly(E-co-HDE)s also influence the  $T_m$  values. For low  $M_n$  samples (entry 5.01 and 5.02), high contents of long 14-carbon branches make the architecture of the copolymer resemble spherical or elliptical dendrite. In this case,  $T_m$  value increases as the  $M_n$  increases because  $M_n$  has a significant influence on the architecture of the copolymer. For higher  $M_n$  samples (entry 5.03, 5.04 and 5.05), the architecture of the copolymers resembles linear brush-like copolymer which is not greatly influenced by  $M_n$ . Therefore,  $T_m$  maintains round 17 °C which is correspond with the length of the 14-carbon side-chains rather than the molecular weights of the copolymers.

These linear brush-like poly(E-co-HDE)s are quite different from LLDPE in two ways. First, the branch contents for poly(E-co-HDE)s are much higher than those from LLDPE, so that small or absence of PE main-chain crystallinity was observed. Second, all branches have the same length (14 carbon atoms) so that the side-chain crystalline units have very similar size thus leading to very narrow melting endotherms. Since the limit of the length of side-chains, the  $T_m$  is much lower and the side-chain crystallinity (crystalline size) maintains low or moderate compared to LLDPE. Therefore, these linear brush-like polyolefin copolymers are excellent candidate for precision PO wax materials instead of plastic and elastomeric materials from LLDPE.

### **5.3 Modulation of Side-Chain Lengths**

#### **5.3.1 Synthesis of copolymers with varying side-chain lengths**

With successful LCCTP copolymerization of E with HDE accomplished yielding poly(E-co-HDE)s with unique side-chain melting endotherms with  $T_m$  around 17 °C, it is intriguing to study the correlation between side-chain lengths and  $T_m$  values. It is reasonable to propose that by increasing the length of side-chains,  $T_m$  values could be tuned to slightly above room temperature, fulfilling the requirements for polyolefin waxes.<sup>192</sup> There is no

simple definition of a wax, scientists prefer to use technique criteria include: (1) a wax normally melts between 40 to 90 °C without decomposition; (2) above  $T_m$ , the viscosity of a wax is low and exhibits a strongly negative temperature dependence; (3) waxes are usually kneadable or hard to brittle, coarse to finely crystalline, transparent to opaque at 20 °C; (4) waxes usually have poor conductors of heat and electricity.<sup>192</sup>

Table 10. Results of LCCTP copolymerization of ethene with long chain  $\alpha$ -olefins

Entry	Monomers	ZnEt <sub>2</sub> (equiv.)	Yield (g)	GPC		DSC			NMR
				$M_n$ (kDa)	PDI	$T_m$ (°C)	$\Delta h_m$ (J/g)	$T_c$ (°C)	%Co
5.06	E/DE	10	2.3	17.1	1.11	--	--	--	24.2
5.07	E/TDE	10	2.4	12.1	1.15	-3.2	37.0	-8.3	22.9
5.08	E/HDE	10	1.8	10.8	1.12	16.9	60.6	13.8	32.0
5.09	E/ODE	10	2.2	10.8	1.13	34.3	63.2	30.1	25.2
5.10	E/DCE	10	1.7	13.9	1.11	46.0	75.8	39.1	20.6
5.11 <sup>[a]</sup>	E/ODE	100	18.2	5.01	1.10	30.0	61.8	26.8	31.3

Conditions: 10  $\mu$ mol **08**, 10  $\mu$ mol **04**, 20.0 mmol co-monomers, ethene (5 psi), 10 mL toluene, 20 °C. [a] Conditions: 20  $\mu$ mol **08**, 20  $\mu$ mol **04**, 2.0 mmol ZnEt<sub>2</sub>, 200 mmol ODE, ethene (5 psi), 100 mL toluene, 20 °C.

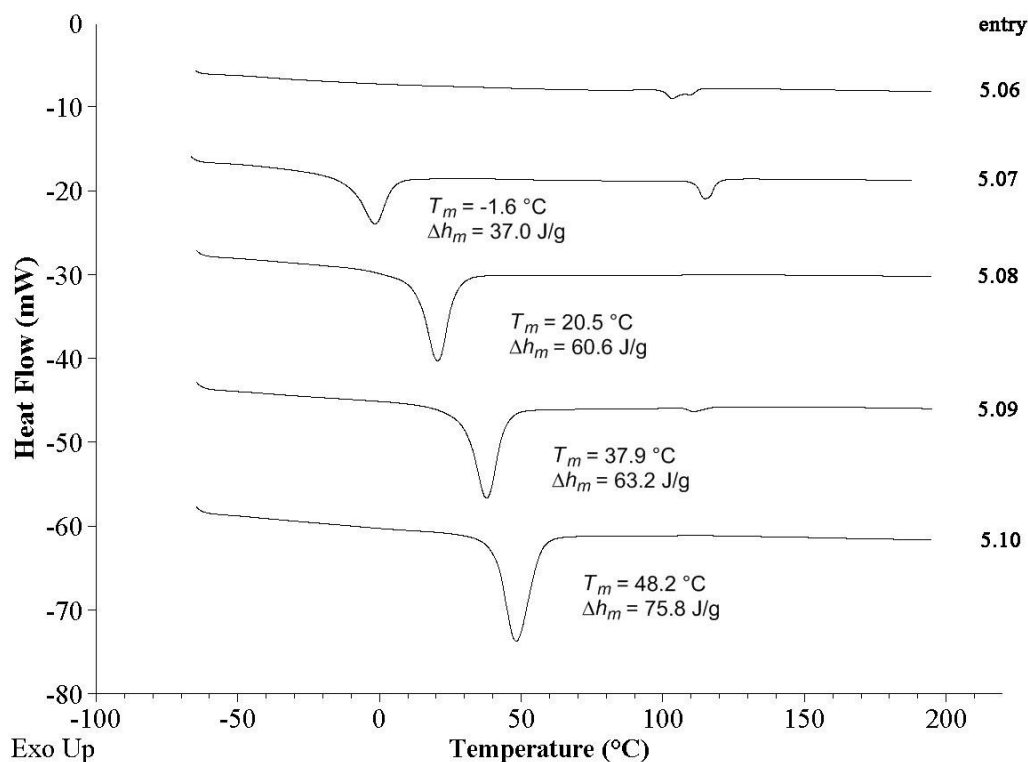
With the aim of preparing polyolefin waxes, LCCTP has been extended to copolymerization of ethene with 1-decene (DE), 1-tetradecene (TDE), 1-octadecene (ODE) and 1-docosene (DCE) to study their side-chain crystallization behaviors. In order to rule out the influence of polymer chain architecture, copolymers were made with  $M_n$  higher than 10 kDa (11 to 17 kDa) using cationic initiator **07** with 10 equivalents of ZnEt<sub>2</sub> in toluene at 20 °C for 15 to 30 min (Table 10). The absence of vinyl end-group by NMR analysis again confirms the living nature of the copolymerization, which is in keeping with the narrow PDI index ( $PDI \leq 1.15$ ). Statistically random distribution of co-monomers along PE backbone

has been revealed by  $^{13}\text{C}$  NMR triads analysis for all five copolymers. Co-monomer incorporation levels have been estimated based on  $^{13}\text{C}$  NMR spectra and found to be high in all cases (22.9 to 32.0 mol%), which suggests the possibilities for predominant side-chain crystallization for all five copolymers.

### 5.3.2 Influence of side-chain length on polyolefin wax property

For homopolymers of long chain  $\alpha$ -olefins, it is generally agreed that side-chain crystallization occurs when the length of side-chain exceeds 8 carbon atoms, for example poly(DE) has a  $T_m$  of 12.5  $^{\circ}\text{C}$ .<sup>181</sup> However, poly(E-co-DE) (entry 5.06) is a completely amorphous grease with no obvious side-chain melting endotherm by DSC (Figure 44). In contrast, poly(E-co-TDE) (entry 5.07) clearly shows a narrow side-chain melting endotherm with  $T_m = -3.2$   $^{\circ}\text{C}$ , which suggests that the minimum packing length of copolymer side-chains is 10 carbon atoms. It is also worth mention that alkanes with 9-16 carbons are medium-viscosity liquid.<sup>193</sup> However, for polymers, the main-chain probably restricts the movements of the side-chain so that the threshold for crystallinity is reduced. When increasing the side-chain to 14 carbons, poly(E-co-HDE) has an increased  $T_m$  (16.9  $^{\circ}\text{C}$ ) but still lower than room temperature. So both poly(E-co-TDE) and poly(E-co-HDE) appear as amorphous gels at room temperature. In order to obtain polyolefin waxes, LCCTP copolymerization of E with ODE (entry 5.09) and DSE (entry 5.10) were carried out, and satisfactorily both poly(E-co-ODE) and poly(E-co-DSE) are white waxes with  $T_m$  above room temperature (34.3 and 46.0  $^{\circ}\text{C}$ , respectively). Therefore 16 carbon length of side-chain with incorporation level above 20 mol% are the threshold for this E and long chain  $\alpha$ -olefin copolymer type of waxes. Figure 44 also presents the increase of heat of fusion ( $\Delta h_m$ ) as the length of side-chain increases, which agrees with that longer side chains have larger crystalline sizes and higher crystallinities.

Figure 44. DSC thermograms of entries 5.06 to 5.10 in Table 10



### 5.3.3 A scaled-up copolymerization to produce poly(E-co-ODE) wax

A highly attractive feature of LCCTP is the ability to significantly increase the bulk quantity of the product polymers without increasing the amount of transition metal catalyst. As an illustrative example, a scaled up LCCTP copolymerization of E with ODE has been accomplished by using 100 equivalents of  $\text{ZnEt}_2$  to initiator **07** in toluene solution at 20 °C for 100 min to yield 18.2 g of poly(E-co-ODE) (entry 5.11 in Table 10). Here only 9.1 mg of precatalyst **08** was required, whereas 1.82 g of this transition metal catalyst would have been necessary to provide the same amount of product through traditional living coordination polymerization. The resulting poly(E-co-ODE) appears as a white wax, and interestingly, this wax melts when rolling between the fingers, which is probably because of the closeness of its melting temperature ( $T_m = 30.0$  °C) to human skin temperature. This poly(E-co-ODE) wax

has been molded to three stars with slight heating; two of them have been dyed to blue and red (Figure 45). These wax stars stays stable at room temperature for several months without any deformation or degradation.

Figure 45. Poly(E-co-ODE) wax stars of entry 5.11 in Table 10



## 5.4 Modulation of Co-monomer Incorporation Levels

### 5.4.1 Synthesis of poly(E-co-HDE)s with varying HDE incorporation levels

In chapter 4, it has been successfully demonstrated that programmable modulation of  $\alpha$ -olefin relative reactivities and co-monomer incorporation levels to PE-based copolymers could be achieved by using two populations of loose and tight ion pair initiators coupled with  $\text{ZnEt}_2$  as a chain transfer reagent. With the ability to modulate the co-monomer incorporation levels, it is now able to study the influence of long chain  $\alpha$ -olefin incorporation levels on the side-chain and main-chain crystallization behaviors.

First of all, a homopolymer of HDE (entry 5.12 in Table 11) has been synthesized using initiator **07** under LCCTP conditions as a standard for 100% HDE incorporation sample. The poly(HDE) sample appears as white powder with  $T_m = 27.9$  °C that agrees with reported atactic poly(HDE).<sup>182,194</sup>  $^1\text{H}$  and  $^{13}\text{C}$  NMR spectra further confirm that this homopolymer is mostly *atactic* with slightly richness of *mmmm* pentad percentage which is

probably due to chain-end control mechanism. Then, four poly(E-*co*-HDE) samples have been synthesized under CCTP conditions, and the incorporation levels of HDE have been modulated by varying the ratios of two populations of ‘loose’ and ‘tight’ ion pairs, **07** and **09**, respectively (Table 11). Loose-ion-pair **07** favors chain propagation of both E and HDE, thus leading to higher incorporation level of HDE (26.3 mol%, entry 5.13). In contrast, tight-ion-pair **09** favors incorporation of E rather than HDE, thus leading to low incorporation level of HDE (4.2 mol%, entry 5.16) under the same polymerization conditions. Poly(E-*co*-HDE)s with 16.4 and 9.2 mol% of HDE were obtained when employing a mixture of **07** and **09** at ratios of 1 : 2 and 1 : 4 (entry 5.14 and 5.15, respectively). The key values of yield (activity),  $M_n$ , molar percentage of HDE incorporation were all found to decrease in the predicted fashion with an increase in the population of the tight-ion-pair **09** relative to loose-ion-pair **07**.  $^{13}\text{C}$  {1H} NMR (150 MHz, 1,1,2,2- $\text{C}_2\text{D}_2\text{Cl}_4$ , 90 °C) spectra show that all four poly(E-*co*-HDE)s are statistically random copolymers with same polymer chain architectures.

Table 11. Modulation of HDE incorporation levels

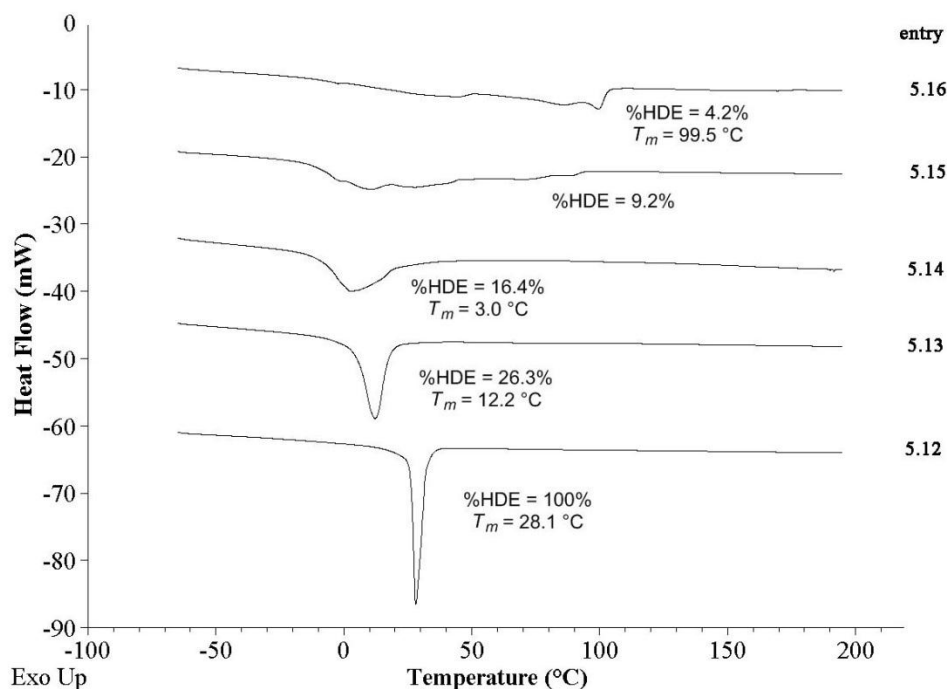
Entry	Monomers	Initiators <b>07</b> : <b>09</b>	ZnEt <sub>2</sub> (equiv.)	Yield (g)	GPC		DSC		NMR
					$M_n$ (kDa)	PDI	$T_m$ (°C)	$T_c$ (°C)	%HDE
5.12	HDE	1 : 0	10	0.9	5.32	1.1	27.9	19.9	100
5.13	E/HDE	1 : 0	20	1.1	4.00	1.13	11.8	9.0	26.3
5.14	E/HDE	1 : 2	20	0.8	3.54	1.16	3.6	-3.5	16.4
5.15	E/HDE	1 : 4	20	0.6	3.26	1.24	broad	broad	9.2
5.16	E/HDE	0 : 1	20	0.3	2.72	1.18	98.7	92.1	4.2

Conditions: 10  $\mu\text{mol}$  **08**, [**04**]<sub>0</sub> + [**10**]<sub>0</sub> = [**08**]<sub>0</sub>, 20.0 mmol HDE, ethene (5 psi), 10 mL toluene, 20 °C.

### 5.4.2 Influence of HDE incorporation level on wax property

As illustrated by Figure 46, thermal analysis by DSC (2<sup>nd</sup> heating cycle, 10 °C/min) reveals a decrease in  $T_m$  from 28.1 °C (entry 5.12) to 3.0 °C (entry 5.14) and an increase of broadness of side-chain melting endotherms by reducing the HDE incorporation levels from 100% (entry 5.12) to 16.4% (entry 5.14). This indicates that lowering the incorporation level of HDE leads to less efficient packing of side-chains and thus decreased crystallinities. By further decreasing the HDE incorporation level to 9.2% (entry 5.15), a very broad melting endotherm ( $T_m = -10$  to 90 °C) appears which is probably due to both side-chain and main-chain crystallinities. When the HDE incorporation level decreases to 4.2% (entry 5.16), main-chain melting behavior now dominates and a  $T_m$  up to 99.5 °C is observed which resembles most of the LLDPE materials.<sup>181-182</sup> This trend demonstrates that a threshold of incorporation level of side-chain branches, such as 16 mol% HDE for poly(E-co-HDE), is necessary for a predominate side-chain crystallinity relative to main-chain crystallinity.

Figure 46. DSC thermograms of samples in Table 11



## 5.5 ODE-based Homo-, Co- and Ter-polymers and Diblock Copolymers

### 5.5.1 Synthesis of ODE-based homo-, co- and ter-polymers

Table 12. Results of homo-, co- and ter-polymer based on ODE

Entry	Monomers	ZnEt <sub>2</sub> (equiv.)	Yield (g)	GPC		DSC		NMR	
				<i>M<sub>n</sub></i> (kDa)	PDI	<i>T<sub>m</sub></i> ( °C)	<i>T<sub>c</sub></i> ( °C)	%ODE (mol%)	%H (mol%)
5.17	ODE	10	1.0	4.43	1.08	42.4	35.5	100	--
5.18	E/ODE	20	1.8	5.49	1.12	32.2	27.7	24.7	--
5.19	E/H/ODE	20	2.0	6.42	1.10	20.0	18.9	16.2	7.0

Conditions: 10 μmol **08**, 10 μmol **04**, toluene, 20 °C.

To further explore the influence of polymer chain compositions on the side-chain crystallinity, a homopolymer of ODE, a copolymer of E and ODE and a terpolymer of E, H and ODE have been made using initiator **07** with ZnEt<sub>2</sub> in toluene at 20 °C as shown in Table 12. Physical appearance of Poly(ODE) (entry 5.17) is a white powder, and DSC analysis shows a single narrow melting endotherm (*T<sub>m</sub>* = 42.4 °C) and a crystallization exotherm (*T<sub>c</sub>* = 35.5 °C) as shown in Figure 47. Similar as poly(HDE), poly(ODE) is mostly atactic with slightly richness in mmmm pentad percentage determined by <sup>13</sup>C NMR spectroscopy (Figure 48). Copolymer of poly(E-co-ODE) (entry 5.18) appears as a white wax with 24.7% ODE incorporation level and a broader melting endotherm with lower *T<sub>m</sub>* (32.2 °C) compared to poly(ODE). Terpolymer of poly(E-co-H-co-ODE) (entry 5.19) has a jelly like appearance with 16.2 mol% ODE and 7.2 mol% H incorporation levels, as well as the broadest melting endotherm and lowest *T<sub>m</sub>* (20.0 °C). <sup>13</sup>C NMR analysis supports the statistically random distributions for both Poly(E-co-ODE) and Poly(E-co-H-co-ODE) (Figure 49 and 50, respectively). The difference of physical appearance agrees with the compositional change of

homo, co and terpolymers, which results in a decrease of ODE contents and increase in difficulties for side-chains to pack well in order to form crystalline units.

Figure 47. DSC thermograms of samples in Table 12

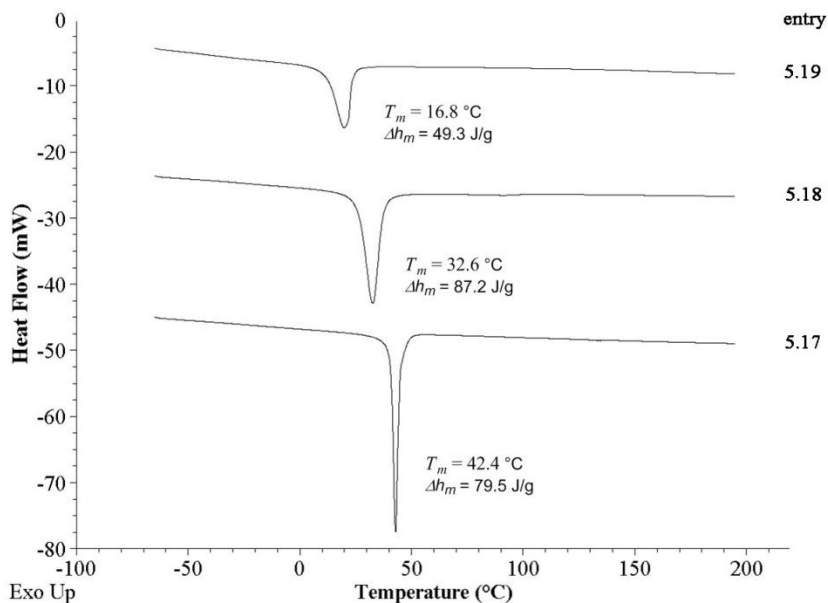


Figure 48.  $^{13}\text{C}\{^1\text{H}\}$  NMR spectrum and assignments of poly(ODE) of entry 5.17

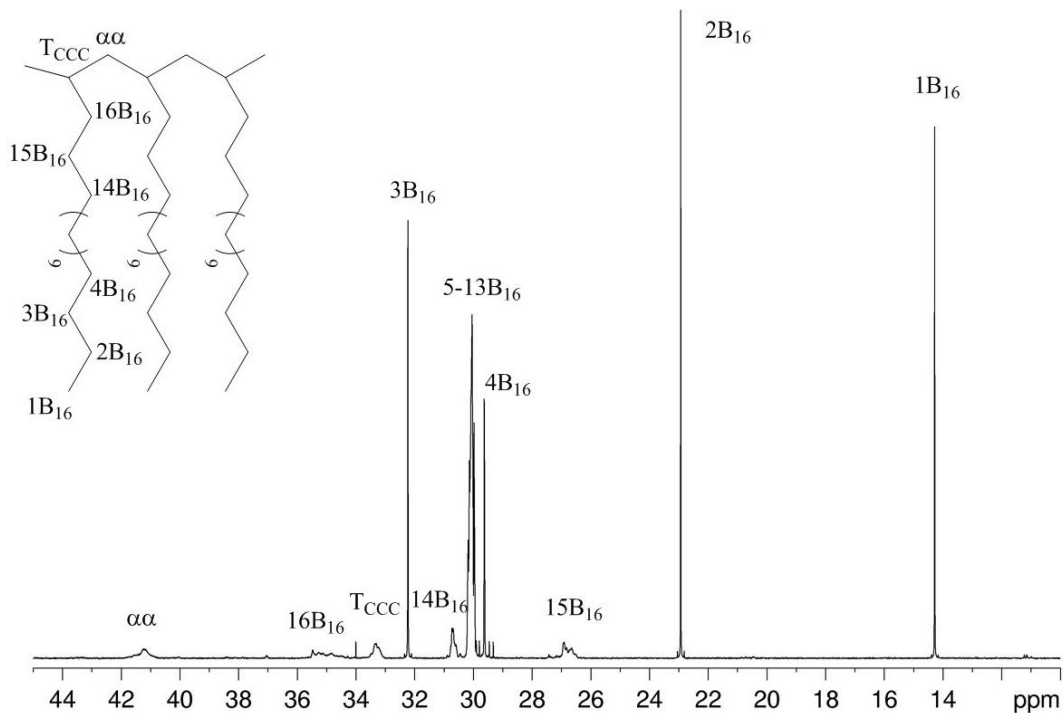


Figure 49.  $^{13}\text{C}$   $\{^1\text{H}\}$  NMR spectrum and assignments of poly(E-co-ODE) of entry 5.18

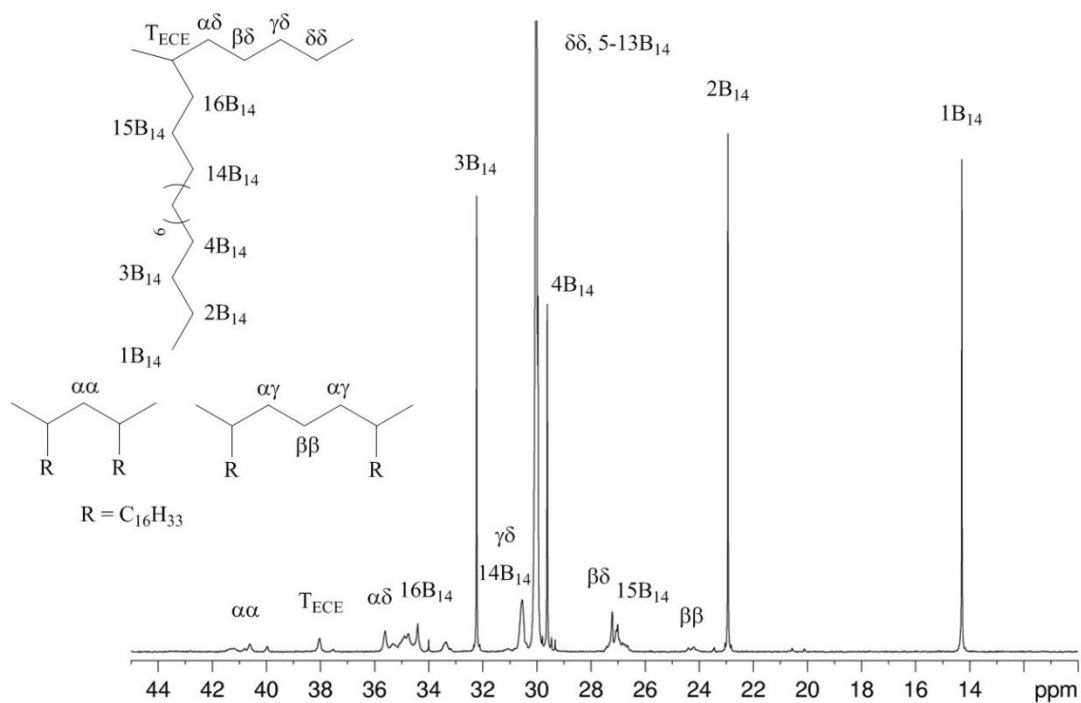
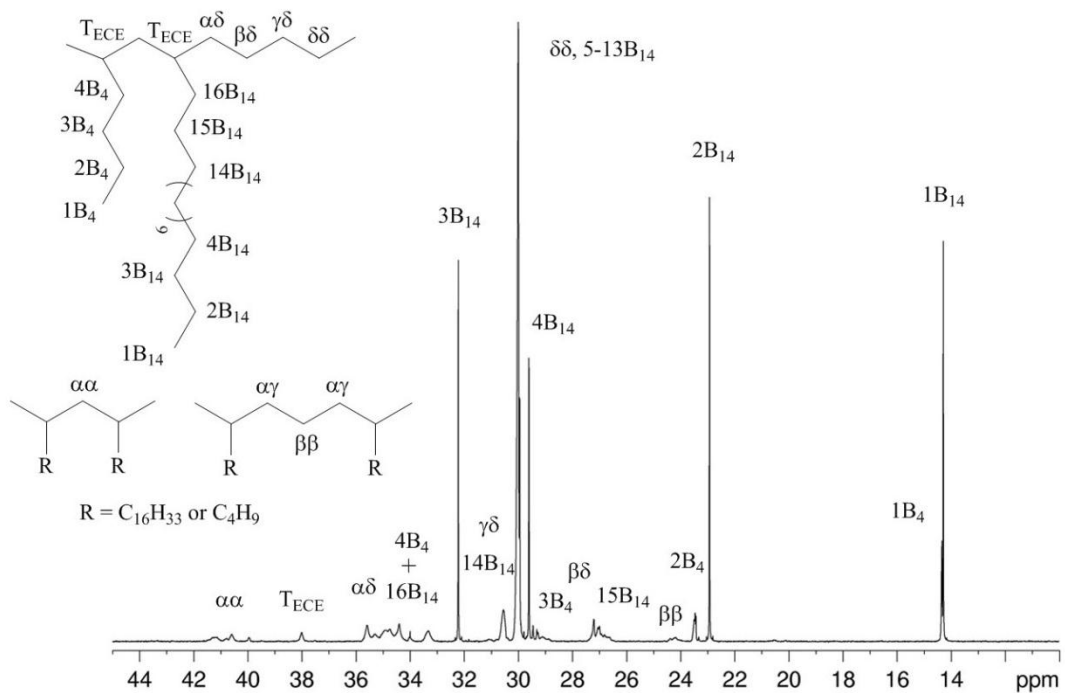


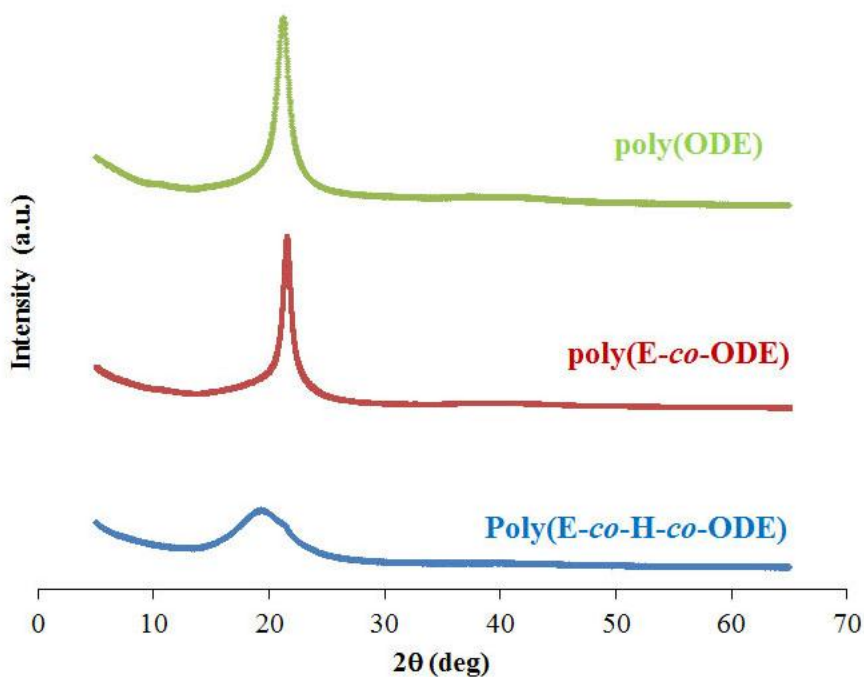
Figure 50.  $^{13}\text{C}$   $\{^1\text{H}\}$  NMR spectrum and assignments of poly(E-co-H-co-ODE) of entry 5.19



### 5.5.2 WAXD study on ODE-based homo-, co- and ter-polymers

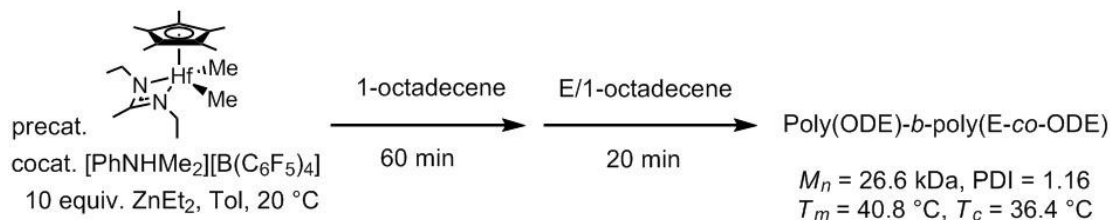
Wide angle X-ray diffraction (WAXD) measurements were carried out to further explore the difference in the size of side-chain crystalline units for the homo, co and terpolymers in Table 12. As shown in Figure 51, poly(ODE) has almost twice broader peaks than poly(E-co-ODE) which means that latter has much larger crystallite size and a decrease of crystallinity. That also explains the difference of physical appearance of poly(ODE) as a powdery solid and poly(E-co-ODE) as a hard waxy solid. Poly(E-co-H-co-ODE) is practically amorphous, which does show tiny bump in the same position as large crystalline peak in poly(ODE) and poly(E-co-ODE) but major feature is amorphous peak at lower angle. This explains the jelly like appearance of the Poly(E-co-H-co-ODE) sample.

Figure 51. WAXD Data of ODE-based homo-, co- and ter-polymers of Table 12



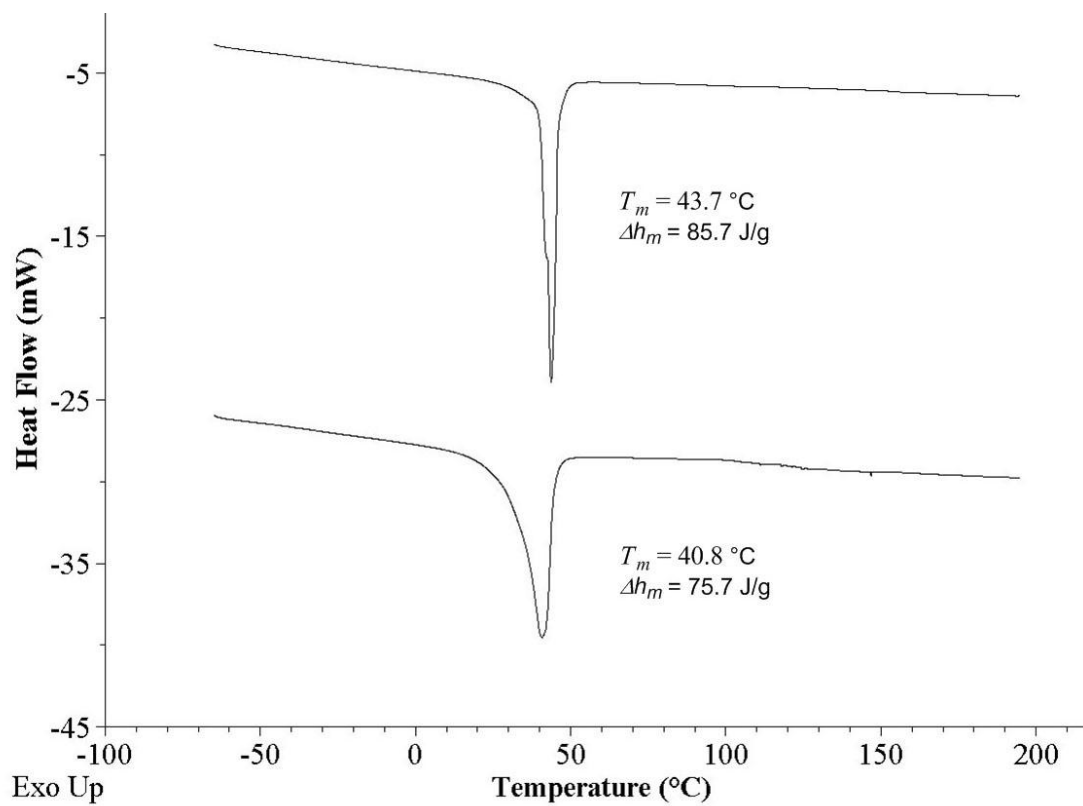
### 5.5.3 Synthesis and characterization of ODE-based diblock copolymers

Scheme 30. Synthesis of poly(ODE)-*block*-poly(E-co-ODE)



In 1996, Brookhart and co-workers<sup>195</sup> reported the preparation of  $\alpha$ -olefin based elastomeric 'hard-soft-hard' triblock copolymers with semicrystalline poly(ODE) as hard block and amorphous propene/ODE copolymer as soft block through sequential addition of monomers. Using the same method, poly(ODE)-*block*-poly(E-co-ODE) has been synthesized to couple a higher crystalline 'powder-like' poly(ODE) block and a lower crystalline 'wax-like' poly(E-co-ODE) block (Scheme 30). As shown Figure 52, the first block of poly(ODE) ( $M_n = 11.0 \text{ kDa}$ , PDI = 1.30) has a very narrow melting endotherm with  $T_m = 43.5 \text{ }^\circ\text{C}$ , which agrees with previous poly(ODE) sample (entry 5.17 in Table 12). The diblock poly(ODE)-*block*-poly(E-co-ODE) ( $M_n = 26.6 \text{ kDa}$ , PDI = 1.16) has a  $T_m$  of  $40.8 \text{ }^\circ\text{C}$  which indicates lower crystallinity caused by poly(E-co-ODE) block with less ODE incorporation level. Interestingly, the melting endotherm of diblock copolymer has a big tail compared to poly(ODE) block, which means the second block brings a disorder to the side-chain crystallite sizes. Different from either poly(ODE) or poly(E-co-ODE), the physical appearance of this poly(ODE)-*block*-poly(E-co-ODE) sample is a brittle white wax. This brittle wax appearance is probably attributed to the combination of higher crystalline powder-like poly(ODE) block and less crystalline wax-like poly(E-co-ODE) block.

Figure 52. DSC thermograms of 1<sup>st</sup> block (top) and diblock (bottom) of poly(ODE)-*block*-poly(E-co-ODE).



## **5.6 Conclusions**

The results presented in this chapter have established that LCCTP copolymerization of E with long chain  $\alpha$ -olefins, such as DE, TDE, HDE, ODE and DCE, is capable of providing a wide range of materials in a scalable fashion with high incorporation levels of long chain  $\alpha$ -olefins and predominant side-chain crystallinity. Relations of side-chain crystallinities with molecular weights, side-chain lengths and side-chain incorporation levels have been thoroughly investigated by structural and thermal analyses. A new class of polyolefin waxes based on E/ODE and E/DCE copolymers has been made with moderate side-chain crystallinity, desirable melting temperatures and very narrow melting endotherms. At last, ODE-based wax materials with varying polymer chain compositions and macromolecular architectures have been synthesized to further reveal the structure and wax property relationships. We are presently exploring the full range of opportunities provided by these findings, including end-group functionalization and well-defined block copolymer waxes.

# Chapter 6: Synthesis and Characterization of Ethene/Propene Multi-Block Copolymers through “Regional” Steric- Control Mechanism using a Binuclear Hafnium Catalyst

## 6.1 Background

### 6.1.1 Polyolefin-based Block Copolymers

By far, the most important application of living olefin polymerization is the production of block copolymers, which is typically achieved by sequential monomer addition.<sup>39</sup> There are two major advantages for polyolefin block copolymers. First, even though the types of olefin monomers are limited, materials derived from copolymerization of these monomers, particularly block copolymerization, are nearly limitless. Second, block copolymer often furnish materials whose mechanical properties are superior to the sum of their parts.<sup>54</sup> This unique behavior is due to microphase separation of the different segments of the block copolymer into discrete domains which give rise to otherwise unattainable morphologies and properties.<sup>196-197</sup>

One of the most highly sought goals in the field of olefin polymerization is the synthesis of block copolymers containing both hard semicrystalline end-blocks (e.g., PE, *iso*PP, *s*PP) and soft amorphous middle-blocks (e.g., *a*PP, poly(E-*co*-P), linear low-density polyethylene (LLDPE)). Triblock copolymers of the hard-soft-hard type have been shown to behave as thermoplastic elastomers, such as the *iso*PP-*block*-*a*PP-*block*-*iso*PP materials

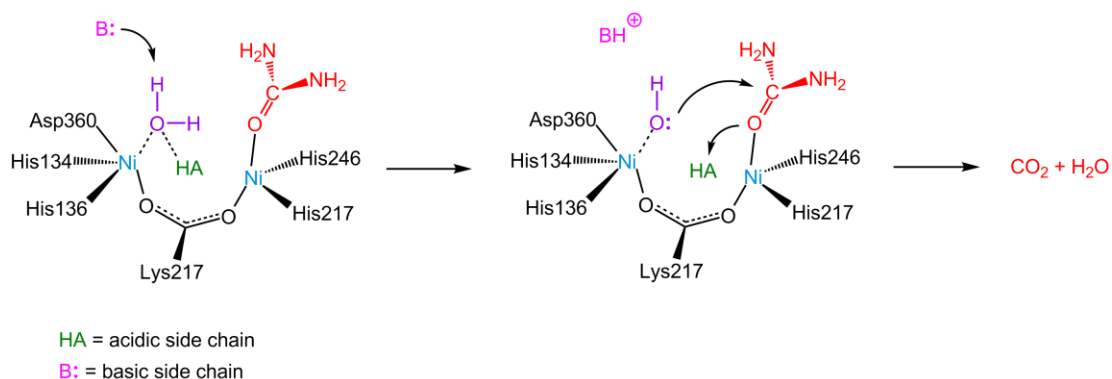
reported by our group.<sup>81-83</sup> Other types of hard-soft polyolefin block copolymers includes *iso*PVCH-*block-iso*PH-*block-iso*PVCH reported by Sita and co-workers,<sup>78</sup> PE-*block*-poly(E-*co*-H) reported by Fujita and co-workers,<sup>198</sup> PE-*block*-poly(1-octadecene) reported by Gottfried and Brookhart<sup>199</sup> and *syndio*-rich-PP-*block*-PH reported by Marques and Gomes.<sup>200</sup>

Ethene and propene are two of the most widely used chemicals nowadays to produce HDPE, LDPE, PP, LLDPE as well as their copolymers, such as EPR (ethene propene rubber).<sup>9</sup> However, block copolymers based on those two monomers are very limited, in both commercial products and academic research. In 1991, Hlatky and Turner<sup>201</sup> reported on the synthesis of diblock copolymers of ethene and propene using  $[(\eta^5\text{-C}_5\text{H}_5)\text{HfMe}(\text{PhNMe}_2)][\text{B}(\text{C}_6\text{F}_5)_4]$  to give an *aPP-block*-PE diblock *via* sequence monomer addition. Later, in 2003 Busico and co-workers<sup>202</sup> reported the first synthesis of an *iso*PP-*block*-PE copolymer ( $M_w/M_n$  as low as 1.2 when  $M_n = 6500$  g/mol) *via* the same method at polymerization durations greater than 1 min. Another example of E/P block copolymers made through sequential monomer addition was reported by Fujita and co-workers<sup>203</sup> in the synthesis of a PE-*block*-poly(E-*co*-P) diblock and a PE-*block*-poly(E-*co*-P)-*block*-PE triblock copolymers. There are two main reasons that limit the preparation of E/P block copolymers. On one hand, there are only a few transition metal catalysts that can carry out living polymerizations of both E and P under the same conditions (e.g., solvent, temperature and pressure). Second, the polymerization durations for E (and sometime P) are usually so short (less than 1 min) that sequential monomer addition method is technically difficult. Therefore, it will be very attractive to find a different strategy to make E/P block copolymers, especially in an environment that both E and P are present.

## 6.1.2 Multi-nuclear olefin polymerization catalyst systems

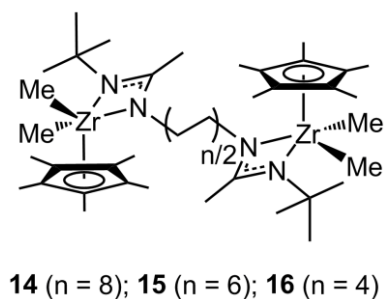
In many enzymes, such as ureases (Scheme 31), two or more metal centers are placed in close proximity to activate both electrophilic and nucleophilic reactants, in which superior activity and selectivity are achieved.<sup>204</sup> In order to mimic this nature process, multi-nuclear olefin polymerization catalyst systems have been explored to afford unique polymerization activities and polyolefin microstructures, which are usually not achievable *via* the mononuclear analogues. For example, binuclear transition metal catalysts have been studied to enhance activity and/or selectivity through creation of high local monomer concentrations to make high levels of polyolefin branching.<sup>205</sup> Also, multi-nuclear catalyst systems, generated from binuclear transition metal precatalysts and/or binuclear borate cocatalysts, has been shown to create conformationally advantageous active-site-monomer proximities<sup>206-207</sup>, as well as introduce the cooperative effect from agostic interactions that provide extra stabilization of certain olefin monomer.<sup>208-210</sup> Nevertheless, the design and synthesis of multi-nuclear olefin polymerization catalysts is not necessarily straightforward, and structures which optimize cooperative effects between catalytic centers require both rational design and empiricism.<sup>204</sup>

*Scheme 31.* Proposed mechanism of urea hydrolysis into carbon dioxide and ammonia mediated by the urease enzyme.<sup>5</sup>



Our group's recent contribution to this area was started by Wei in 2008.<sup>211</sup> A series of alkyl-linked CpAm zirconium binuclear complexes,  $[(\eta^5\text{-C}_5\text{Me}_5)\text{Zr}(\text{Me})_2]_2[\text{N}(\text{tBu})\text{C}(\text{Me})\text{N}(\text{CH}_2)_n\text{NC}(\text{Me})\text{N}(\text{tBu})]$  (**14**;  $n=8$ ), (**15**;  $n=6$ ), and (**16**;  $n=4$ ) were designed and prepared according to CpAm zirconium analogue of compound **02** (Figure 53). Compounds **14–16** have been used to carry out highly isoselective living polymerization of propene upon 100% activation using 2 equiv. of the borate cocatalyst **04**, with the degree of stereoselectivity decreasing slightly as the two metal centers were brought closer together.

Figure 53. Structure of binuclear compounds **14–16**



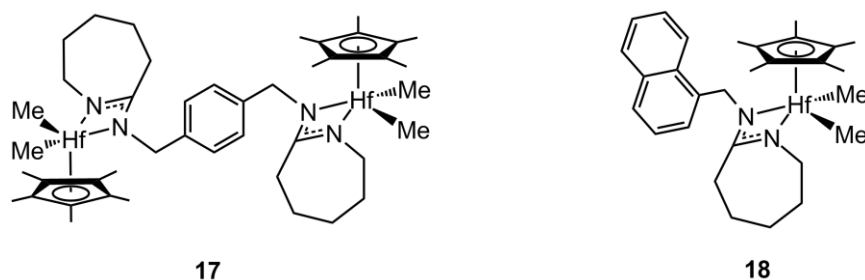
Interestingly, compounds **14–16** were found to carry out LCCTP of propene with  $\text{ZnEt}_2$  to give PP materials with much higher isotactic contents ( $[mmmm] = 0.444\text{--}0.577$ ) compared to those made from mononuclear analogue **02** ( $[mmmm] = 0.253$ ) under the same conditions. Slow chain-transfer rate between the zirconium metal centers and polymeric zinc surrogates was observed, which was supported by the broadness of molecular weight distributions of the resulting PP ( $\text{PDI} = 1.60\text{--}1.22$ ). We proposed that the steric hindrance of those binuclear catalytic species, which carry two polymer chains on one catalyst molecule, caused the higher energy barrier for  $\delta$ -bond metathesis of polymer-chain-transfer process and consequently slower chain-transfer rate. This example shows the unique polymerization behaviors of binuclear catalysts compared to their mononuclear analogues, and inspires us to explore more of the uniqueness raised by steric hindrance.

## 6.2 A Novel Binuclear Catalyst and Proposed Steric-Control Mechanism

### 6.2.1 Design and synthesis of a hafnium binuclear catalyst

Based on those interesting findings regarding multi-nuclear olefin polymerization catalysts, we decided to explore the possibility of designing a binuclear catalyst that is capable of making ethene/1-hexene multi-block copolymers with alternating “hard” (ethene-rich) and “soft” (1-hexene-rich) segments. As discussed in Chapter 4, fast chain-transfer rate compared to chain propagation rate will lead to a random copolymer. In order to make block copolymers, the chain-transfer rate between the binuclear catalyst and  $\text{ZnEt}_2$  should be much slower than the chain propagation rate. Thus, segments of ethene-rich or 1-hexene-rich blocks are allowed to grow on the “tight” binuclear ion pair or “loose” binuclear ion pair, respectively, and the resulting copolymer will maintain those segments. The tight and loose binuclear ion pairs could be generated from activating neutral binuclear precatalyst with varying ratios of cocatalysts as discussed in Chapter 4.

Figure 54. Structures of binuclear compound **17** and mononuclear analogue **18**

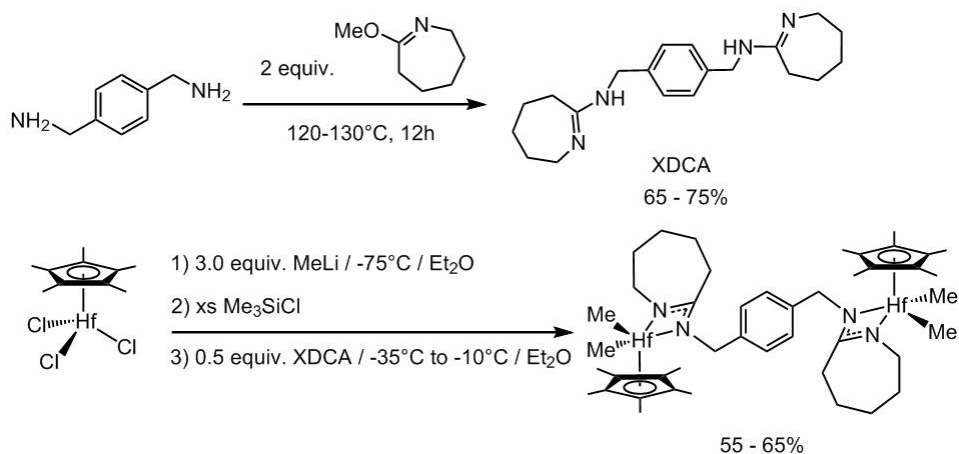


In order to achieve this goal, a *p*-xylylene-linked Cp\*-caproamidinate-based hafnium binuclear precatalyst,  $[\text{Cp}^*\text{Hf}(\text{Me})_2]_2[\text{N}(\text{CH}_2)_5\text{CN}-(\text{CH}_2)(\text{C}_6\text{H}_4)(\text{CH}_2)-\text{NC}(\text{CH}_2)_5\text{N}]$  (**17**), was designed and synthesized as shown in Figure 54. The “local” ligand environment of compound **17** is similar to that of compound **08**, which is diethyl type with widely sterically

opened vacancy site for high activity and high  $\alpha$ -olefin incorporation levels. Also, the two metal centers have a rigid *p*-xylylene linkage in order to secure the slow chain-transfer rate between the transition metal chain propagation centers and the chain-transfer surrogate. On the other hand, a mononuclear analogue  $[\text{Cp}^*\text{Hf}(\text{Me})_2][\text{N}(\text{CH}_2)_5\text{CN}(\text{CH}_2)(\text{C}_{10}\text{H}_7)]$  (**18**) was synthesized with similar “local” steric hindrance to compare the polymerization behaviors with binuclear catalyst **17**.

Binuclear precatalyst **17** was synthesized through a two-step reaction according to Scheme 32. First of all, a *p*-xylylenediamine caprolactim amidine (XDCA) ligand was made through neat reaction of *p*-xylylenediamine with 2 equiv. of *o*-methylcaprolactim. Then this ligand was added in situ to the  $\text{Cp}^*\text{HfMe}_3$  generated from  $\text{Cp}^*\text{HfCl}_3$  and 3 equiv. of MeLi at  $-75\text{ }^\circ\text{C}$  in diethyl ether, followed by slowly warming up to  $-10\text{ }^\circ\text{C}$  and then pumping away all the volatiles. The final recrystallization yield of compound **17** was around 55 to 65%. The mononuclear analogue **18** was synthesized according to the same method from a 1-naphthylmethylamine caprolactim amidine ligand. The yield was also around 50 to 65%.

Scheme 32. Two-step synthesis of binuclear compound **17**



When copolymerizations of ethene with 1-hexene or propene were carried out using binuclear precatalyst **17** and cocatalyst **04** in toluene at room temperature, ethene/1-hexene or

ethene/propene copolymers were obtained which showed different physical properties, such as  $T_m$ ,  $T_c$  and  $T_g$ , compared with random copolymers. Further structural analyses based on  $^{13}\text{C}$  NMR spectroscopy revealed the block copolymer natures of both ethene/1-hexene and ethene/propene copolymers made from compound **17**. This unexpected discovery is important because compound **17** is the first Ziegler-Natta catalyst that allows the production of ethene/ $\alpha$ -olefin block copolymers from a mixed source of ethene and  $\alpha$ -olefin co-monomers. To the best of our knowledge, all the other ethene/ $\alpha$ -olefin block copolymers were made from sequential monomer addition method.

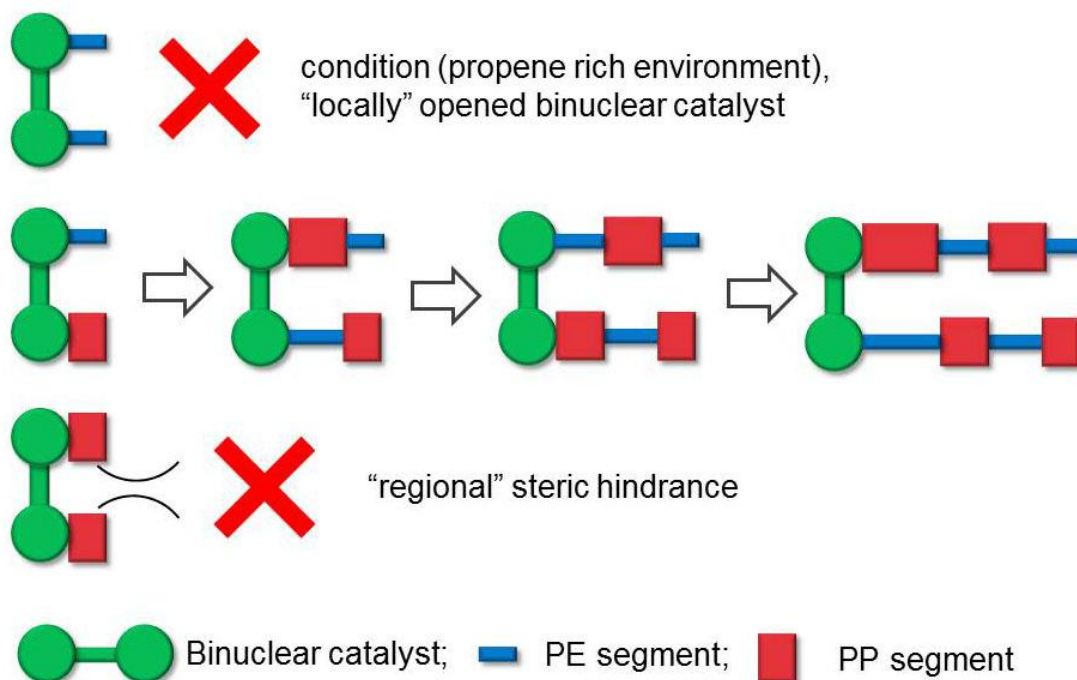
In contrast, the mononuclear analogue **18**, when activated with cocatalyst **04**, produced random ethene/ $\alpha$ -olefin copolymers under the exact same polymerization conditions. Also, mononuclear pre-cursor **04** and all the other binuclear catalysts we synthesized in our group gave same type of random ethene/ $\alpha$ -olefin copolymers under the same conditions. The details of those polymerizations will be discussed in later part of this chapter. Therefore, only binuclear pre-catalyst **17** demonstrates the unique polymerization behavior that is different than all the other known Ziegler-Natta catalysts (for homogeneous 1-alkene polymerization).

### **6.2.2 Proposed steric-control mechanism for block copolymer synthesis**

The discovery of this unexpected polymerization behavior of binuclear pre-catalyst **17** drove our research interests to study the mechanism behind this phenomenon. Based on the unique structure of binuclear pre-catalyst **17**, the proposed mechanism of its unique catalytic behavior is raised from steric hindrance around the binuclear molecule. Although it is “locally” open for high activity and high  $\alpha$ -olefin incorporation levels, the “regional” steric hindrance prevents the growing of two bulky polymer chains on the same binuclear catalyst molecule (Scheme 33). According to this proposal, if one bulky polymer chain (e.g., PP, PH)

is growing on one metal of the binuclear catalyst, then the other metal cannot grow the same polymer chain because of “regional” steric hindrance. Thus, a much less bulkier polymer chain (e.g., PE) has to grow on the other metal center. Also, since the copolymerization was carried out in a propene or 1-hexene rich environment, the “locally” opened nature of binuclear catalyst **17** will allow the incorporation of a high level of propene or 1-hexene co-monomers. Therefore, the possibility of one binuclear catalyst carries two PE chains is disfavored. As a result, one binuclear catalyst can only carry one bulky chain (e.g., PP, PH) and one less bulkier chain (e.g., PE) at the same time. The metal center having a bulky chain growing prefers insertion of a  $\alpha$ -olefin co-monomer due to the polymerization conditions, while the other metal center having a less bulkier chain now has to insert the ethene monomer because of the “regional” steric hindrance.

*Scheme 33.* Proposed “regional” and “local” steric-control mechanism of copolymerization of ethene with propene using binuclear precatalyst **17**



In order to synthesis multi-block copolymers instead of making a mixture of two homopolymers, a switch of the bulkiness of the growing polymer chain should happen at the same time on both metal centers of the same binuclear catalyst (Scheme 33). When this switch process happens, several ethene monomers insert after the bulky PP segment and the “regional” steric hindrance releases on this metal center. At the same time, the other metal center responds to this steric-change by inserting several propene monomers after the PE segment. As a result, a PE segment grows after the PP segment on one metal center; while at the same time a PP segment grows after the PE segment on the other metal center. This process keeps switching the bulkiness of the polymer chains and statistical multi-block copolymer is produced. The rate of this switching process is critical to the final microstructure of the resulting ethene-based copolymer. If the rate of the switching process is too fast, then the copolymer will be more random. If the rate of the switching process is too slow, then the copolymer will show bimodal distributed molecular weights with ethene-rich populations and  $\alpha$ -olefin-rich populations.

### **6.3 Mechanistic Study using E/H Polymerization System**

To verify the proposed mechanism in Scheme 33, mechanistic studies were carried out through polymerization of 1-hexene (H) and ethene (E) using cocatalyst **04** activated binuclear precatalyst **17** and mononuclear precatalyst **18**. First of all, H homo-polymerization was carried out using both binuclear catalyst system **17/04** and mononuclear catalyst system **18/04** in toluene at 0 °C for 1 h to complete the conversion of 50 equiv. of H to PH. According to Figure 55, PH made by **18/04** (entry 6.02 in Table 13) has a  $M_n$  of 4.67 kDa, which is close to the theoretical  $M_n$  (4.21 kDa) based on a degree of polymerization of 50. Interestingly, PH made by **17/04** (entry 6.01 in Table 13) has a  $M_n$  of 10.9 kDa, which is almost double of theoretical value of 4.21 kDa. The reason is that in a pure H monomer solution, only one metal center on the binuclear catalyst can propagate the PH chain-growth,

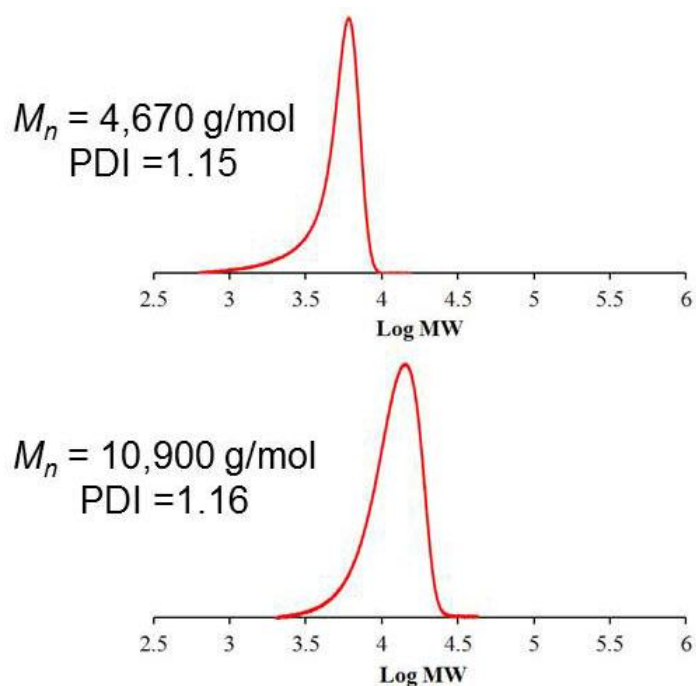
because the “regional” steric hindrance prevents the growth of two PH chains on both metal centers (Scheme 33).

Table 13. Mechanistic study on binuclear and mononuclear catalyst systems

Entry	Monomers ( $t_p$ )	Cat. system	$M_n$ (kDa)	PDI	Resulting polymer
6.01	H (1 h)	<b>17/04</b>	10.9	1.16	PH
6.02	H (1 h)	<b>18/04</b>	4.67	1.15	PH
6.03	H (1 h) + E (1 min)	<b>17/04</b>	13.9, 129	1.16, 1.13	PH-block-PE, PE
6.04	H (1 h) + E (1 min)	<b>18/04</b>	7.04	1.16	PH-block-PE

Conditions: 20  $\mu$ mol of **04**, 10  $\mu$ mol of **17** or 20  $\mu$ mol of **18**, 10 mL toluene, 0  $^{\circ}$ C

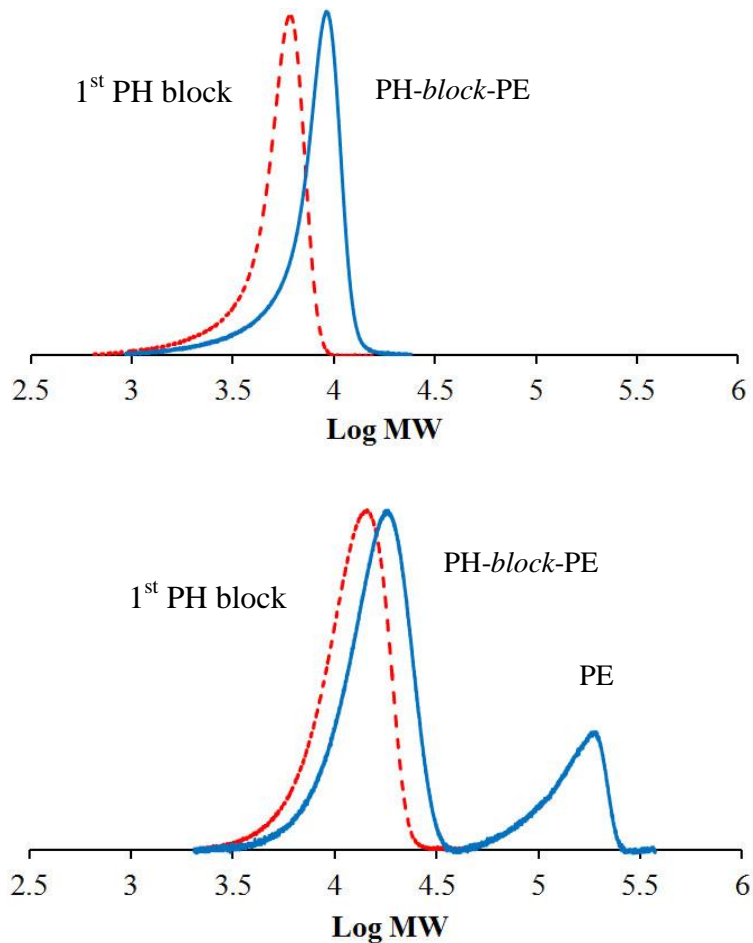
Figure 55. Molecular weight distributions of PHs using mononuclear catalyst **18/04** (top) and binuclear catalyst **17/04** (bottom)



Furthermore, the metal center on the binuclear catalyst that can not grow a PH chain should be available for the growth of a less bulky chain, such as PE (Scheme 33). Therefore,

sequential addition of E followed by H was used to further study the difference of polymerization behaviors of **17/04** and **18/04**. As expected, upon the addition of the second E monomer, both metal centers on the binuclear catalyst **17/04** carried out the chain-growth of PE, and produced a mixture of PH-*block*-PE diblock and PE homopolymer as products (Figure 56, bottom). The molecular weight of PE homopolymer is much higher than the second PE block from PH-*block*-PE diblock probably because of the influence of existing PH chain that add steric hindrance to E insertion. In comparison, mononuclear system **18/04** only made PH-*block*-PE diblock as a typical living catalyst should behave (Figure 56, top).

Figure 56. Molecular weight distributions of sequential monomer addition of E followed by H using mononuclear catalyst **18/04** (top) and binuclear catalyst **17/04** (bottom)



With successful demonstration of “regional” steric hindrance of the binuclear system **17/04**, we next carried out the copolymerization of E and H in the presence of both monomers using **17/04** in toluene at 0 °C to explore if E/H multi-block copolymer can be made through the steric-control mechanism (Scheme 33). Unfortunately, the resulting materials showed a bimodal distributed molecular weights, which indicated that the rate of the switching process was probably too slow to maintain the homogeneous architecture of the copolymers. If the size difference of E and H monomers is the main reason for the slow switching process, then using E/P copolymerization system might be able to solve this problem and yield homogeneous E/P multi-block copolymers.

#### **6.4 Copolymerization of E/P using Binuclear and Mononuclear Catalysts**

##### **6.4.1 Results of E/P copolymerization**

A series of copolymerizations using E/P mixed gas *via* either binuclear catalyst system **17/04** or mononuclear catalyst system **18/04** have been taken out in toluene at 0 °C (Table 14). The polymerization flask was purged every 5 min with fresh E/P mixed gas to maintain the desired E/P ratio during the polymerization lifetime. According to the activity difference of the two catalyst systems, polymerization time for mononuclear system **18/04** were set to be double of those for binuclear system **17/04** in order to maintain similar molecular weights of the resulting copolymers.

When a 1: 9 (E : P) ratio of mixed gas was used for the copolymerization, binuclear catalyst system **17/04** yielded 0.84 g poly(E-*co*-P) copolymer (entry 6.05 in Table 14) after 8 min with absence of  $\beta$ -hydrogen-elimination products determined by  $^1\text{H}$  NMR spectroscopy which confirmed the living nature of this catalyst system. Importantly, monomodal molecular weight distributed copolymer ( $M_n = 60.9$  kDa; PDI = 1.18) was obtained which demonstrated that the switching process of PE and PP blocks of this E/P copolymerization was fast enough

to maintain the homogeneity of the resulting E/P copolymer. For comparison, same copolymerization of E and P was performed using mononuclear catalyst system **18/04** under that same conditions to yield 0.72 g poly(E-co-P) copolymer after 16 min with  $M_n$  of 64.8 kDa and PDI of 1.16 (entry 6.08 of Table 14).

Table 14. Copolymerization of E/P using binuclear and mononuclear catalysts

Entry	E/P	Cat. system	Yield (g)	GPC		DSC			NMR
				$M_n$ (kDa)	PDI	$T_m$ (°C)	$T_c$ (°C)	$T_g$ (°C)	%E
6.05	1/9	<b>17/04</b>	0.84	60.9	1.18	105.2	63.3	-16.2	40.4
6.06	1/4	<b>17/04</b>	0.60	51.0	1.17	111.6	92.2	-25.1	67.4
6.07	1/2	<b>17/04</b>	0.36	37.8	1.10	119.4	106.5	-38.6	86.5
6.08	1/9	<b>18/04</b>	0.72	64.8	1.16	93.6	39.3	-35.8	49.1
6.09	1/4	<b>18/04</b>	0.72	90.2	1.08	97.2	61.9	-61.3	74.2
6.10	1/2	<b>18/04</b>	0.46	36.0	1.11	109.8	91.8	-43.8	89.3
6.11	1/9	<b>15/04</b>	0.40	37.7	1.18	81.7	59.6	-49.6	65.0
6.12	1/9	<b>19/04</b>	0.38	37.2	1.40	84.8	50.8	-44.6	44.4

Conditions: 20  $\mu$ mol of **04**, 10  $\mu$ mol of **17**, **15**, **19** or 20  $\mu$ mol of **18**, 25 mL toluene, 0 °C

The propene incorporation level of sample made from binuclear catalyst system (entry 6.05, %E = 40.4%; %P = 59.6%) is higher than the sample from mononuclear catalyst system (entry 6.08, %E = 49.1%; %P = 50.9%), which means binuclear catalyst system **17/04** is more “locally” opened than mononuclear catalyst system **18/04** probably due to the binuclear nature that push the counterions more away from the transition metal cations. Therefore, binuclear catalyst system **17/04** should have higher activity and higher  $\alpha$ -olefin incorporation levels compared to both the mononuclear analogue **18/04** and diethyl hafnium

analogue **08/04**, which agrees with the proposed mechanism in Scheme 33 that two PE chains growing on one binuclear molecule is disfavored.

According to thermal analysis through DSC, the values of  $T_m$ ,  $T_c$  and  $T_g$  of the copolymer made by **17/04** (entry 6.05) are significantly higher compared to the material made by **18/04** (entry 6.08). Usually, higher  $T_m$  and  $T_c$  values are indicators of higher crystallinity of the E/P copolymer resulted from higher percentage of E incorporation levels. However, detailed copolymer compositional analysis of  $^{13}\text{C}$  NMR spectra (150 MHz,  $1,1,2,2\text{-C}_2\text{D}_2\text{Cl}_4$ ,  $110\text{ }^\circ\text{C}$ ) indicated a lower E incorporation level for the sample of entry 6.05 (40.4%) than that of entry 6.08 (49.1%). The difference in  $T_g$  values is probably due to the contribution of P distribution along the polymer main chain, which means the the distribution of P unit is also not random for sample of entry 6.05. Thus, the E/P copolymer of entry 6.05 should have a unique microstructure other than traditional random E/P copolymer. In order to have higher crystallinity from low ethene content, it is highly possible for copolymer of entry 6.05 to have blockier structure than the copolymer of entry 6.08.

Further investigation of copolymerization using 1 : 4 and 1 : 2 E/P mixed gases through binuclear catalyst system **17/04** (entry 6.06 and 6.07) and mononuclear system **18/04** (entry 6.09 and 6.10) led to the E/P copolymers with similar yields, molecular weights and molecular weight distributions, but increasing incorporation levels of E. Also, copolymers from binuclear catalyst **17/04** (entry 6.06 and 6.07) always show higher P incorporation levels than those from mononuclear system **18/04** (entry 6.09 and 6.10). Again, similar differences on physical properties were obtained from copolymers made by binuclear and mononuclear catalyst systems, in which binuclear catalyst **17/04** always produce E/P copolymers with higher  $T_m$ ,  $T_c$  and  $T_g$  than the copolymers made from its mononuclear analogue.

## 6.4.2 Study on monomer sequence distributions and relative reactivities

Table 15. Results of diads analysis, relative reactivities and average sequence lengths of E/P copolymers

Entry	Cat. system	[PP]	[EP+PE]	[EE]	$r_E$	$r_P$	$r_E \times r_P$	n(E)	n(P)
6.05	<b>17/04</b>	0.527	0.138	0.335	284	0.1305	37.1	5.7	9.4
6.06	<b>17/04</b>	0.256	0.140	0.604	225	0.1405	31.6	9.6	5.3
6.07	<b>17/04</b>	0.055	0.160	0.784	128	0.0528	6.7	10.6	2.0
6.08	<b>18/04</b>	0.319	0.380	0.301	93	0.0287	2.7	2.5	3.0
6.09	<b>18/04</b>	0.075	0.367	0.558	79	0.0156	1.2	3.9	1.8
6.10	<b>18/04</b>	0.006	0.205	0.79	100	0.0034	0.3	8.7	1.1

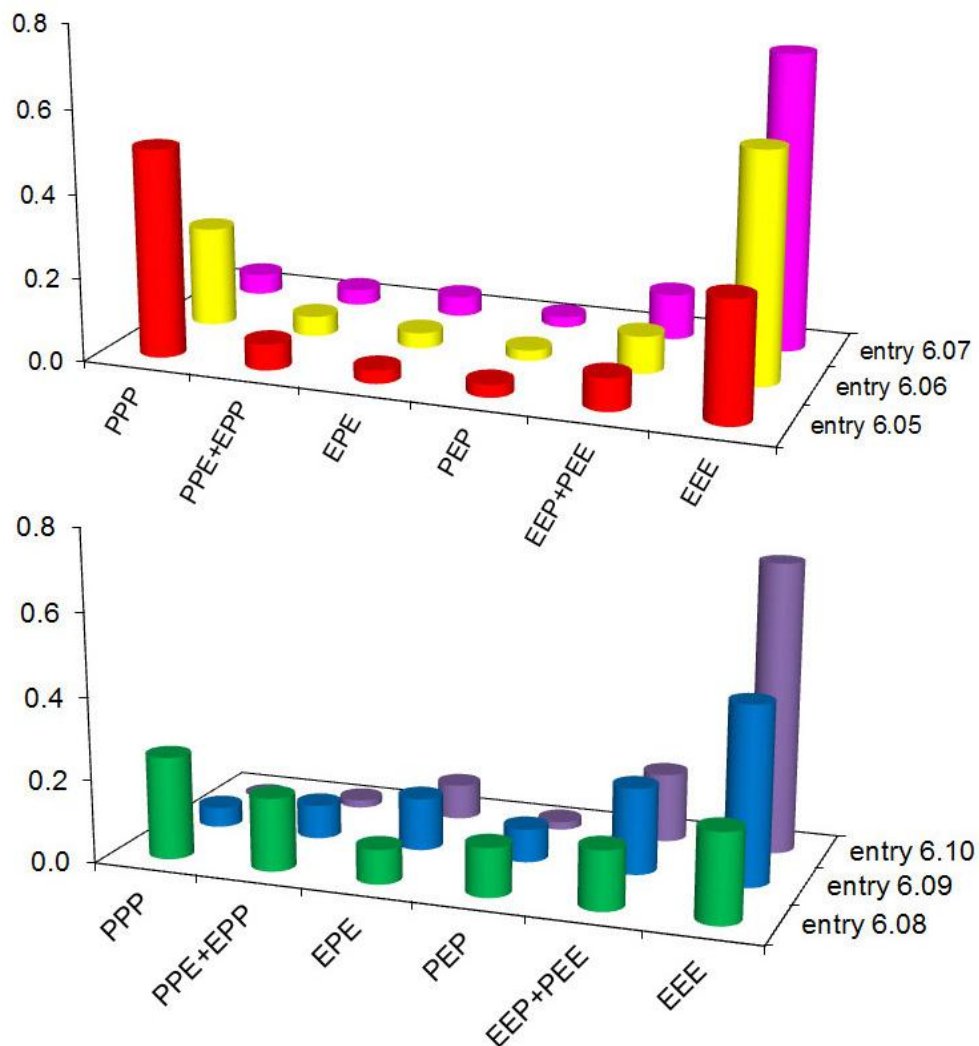
Moreover, the product of relative reactivities ( $r_P \times r_E$ ) determined by diads analysis from  $^{13}\text{C}$  NMR spectra is another indicator of the microstructure of a copolymer. Value closed to 1 indicates a random copolymer, while higher value means block copolymer and lower value shows an alternating copolymer. As shown in Table 15, the  $r_P \times r_E$  value for copolymer made from **17/04** (entry 6.05–6.07) are much higher than those made from **18/04** (entry 6.08–6.10), which confirms the blocky nature of copolymer made from binuclear catalyst. Another indicator of copolymer blockiness is the average monomer sequence length (e.g., n(E) = average E sequence length; n(P) = average P sequence length). Larger n(E) and n(P) values indicate the blocky nature of the copolymer. Again, the E/P copolymers made from binuclear catalyst always have both higher n(E) and n(P) values than those made from its mononuclear analogue under the same source of E/P mixed gas.

Usually, for block copolymer made through sequential monomer addition method, the relative reactivities values,  $r_E$  and  $r_P$ , should both be higher than 1, which will lead to greater  $r_P \times r_E$  value.<sup>166</sup> However, in this case, the values of  $r_P$  are all smaller than 1 (0.05–

0.14, entry 6.05–6.07). Therefore, the blockiness of the copolymer from binuclear catalyst **17/04** is not resulted from sequential monomer addition.

Further analysis of the triads distributions of all six E/P copolymers clearly indicates the higher ratios of EEE and PPP triads and lower ratios of PEP and EPE triads from blocky E/P copolymer (entry 6.05–6.07) than random E/P copolymer (entry 6.08–6.10) (Figure 57).

Figure 57. Triads analysis of E/P copolymers made from binuclear catalyst **17/04** (top) and mononuclear catalyst **18/04** (bottom)



### 6.4.3 Binuclear catalyst generality study

With the success of making E/P blocky copolymers with *p*-xylylene-linked caproamidine hafnium binuclear catalyst system, we continued to explore the generality of more binuclear catalysts with structural variations. First, binuclear zirconium catalyst **15** with a flexible C6 alkyl linkage and *t*Bu-amidate ligand was activated with cocatalyst **04** to carry out the copolymerization of E and P (entry 6.11 in Table 14). The resulting polymer is random based on GPC, DSC and <sup>13</sup>C NMR analyses. This rationalizes that flexible linkage lacks the ability to maintain “regional” steric hindrance which is crucial to the preparation of blocky materials. Next, we synthesized a *p*-xylylene-linked *t*Bu-amidate zirconium-based binuclear precatalyst, [Cp\*Zr(Me)<sub>2</sub>]<sub>2</sub>[(*t*Bu)NC(Me)N-(CH<sub>2</sub>)(C<sub>6</sub>H<sub>4</sub>)(CH<sub>2</sub>)-NC(Me)N(*t*Bu)] (**19**), as an analogue to compound **17**. However, copolymerization of E and P using **19/04** system yielded random E/P copolymer (entry 6.12) with lower  $T_m$ ,  $T_c$  and  $T_g$ , as well as value of  $r_P \times r_E$  close to 1. This indicates that the caprolactim amidine ligand is important to maintain the right “regional” steric hindrance for making blocky copolymers. Up until now, compound **17** is still the only precatalyst that produces blocky polyolefin materials in our group.

## 6.5 Characterization of E/P Block and Random Copolymers

### 6.5.1 Structural characterization of *b*-E/P and *r*-E/P copolymers

Now with the ability to make this fundamentally novel E/P blocky material with statistically distributed PE and PP segments, it is extremely interesting to study its physical and mechanical properties and compare them with random E/P material that is well-studied. First of all, according to table 16, blocky E/P copolymer (*b*-E/P) (entry 6.13) and random E/P copolymer (*r*-E/P) (entry 6.14) were synthesized in a larger scale through **17/04** and **18/04**, respectively, with extended polymerization time to achieve higher molecular weight ( $M_n >$

100 kDa) and larger quantity of materials for mechanical property tests. As we expected, even though the *b*-E/P has lower E content (50.8%) than that of *r*-E/P (59.8%), *b*-E/P material shows higher crystallinity (8.6%) than *r*-E/P material (4.2%) determined by integration of DSC endotherm curves. As a result, *b*-E/P material (entry 6.13 in Table 16) shows higher  $T_m$  and  $T_c$  values, as well as higher  $T_g$  (probably due to long amorphous PP segments), due to longer  $n(E)$  and  $n(P)$  values from its blocky structure. To the best of our knowledge, the  $r_P \times r_E$  value of 284 for *b*-E/P (entry 6.13) is much higher than any reported E/P copolymers in literature.

Table 16. Large scale synthesis of *b*-E/P and *r*-E/P copolymers

Entry	Cat. system	Yield (g)	GPC		DSC			NMR			
			$M_n$ (kDa)	PDI	$T_m$ (°C)	$T_c$ (°C)	$T_g$ (°C)	%E	$r_P \times r_E$	$n(E)$	$n(P)$
6.13	<b>17/04</b>	3.4	176.0	1.68	114.8	89.2	-7.0	50.8	284	18.4	22.3
6.14	<b>18/04</b>	2.8	161.0	1.53	98.9	64.3	-34.0	59.8	5.9	4.1	2.7

Conditions: 80  $\mu\text{mol}$  of **04**, 40  $\mu\text{mol}$  of **17** or 80  $\mu\text{mol}$  of **18**, 80 mL toluene, 0 °C

$^{13}\text{C}$  NMR spectra (150 MHz, 1,1,2,2- $\text{C}_2\text{D}_2\text{Cl}_4$ , 110 °C) of *b*-E/P and *r*-E/P copolymers clearly demonstrated the difference of those two materials in E and P monomer sequence distributions. Spectrum of *b*-E/P (Figure 58) shows higher resonance intensities of PPP and EEE with relatively very low intensities of PPE+EPP, EPE, PEP and EEP+PEE. Therefore, the microstructure of *b*-E/P is composed of statistically distributed multi PE and PP segments (multi-block copolymer). In contrast, spectrum of *r*-E/P (Figure 59) shows higher resonance intensities for all kinds of triads distributions, including EPE and PEP, which is typical for a random copolymer.

Figure 58.  $^{13}\text{C}$  NMR spectrum of *b*-E/P copolymer (entry 6.13 of Table 16)

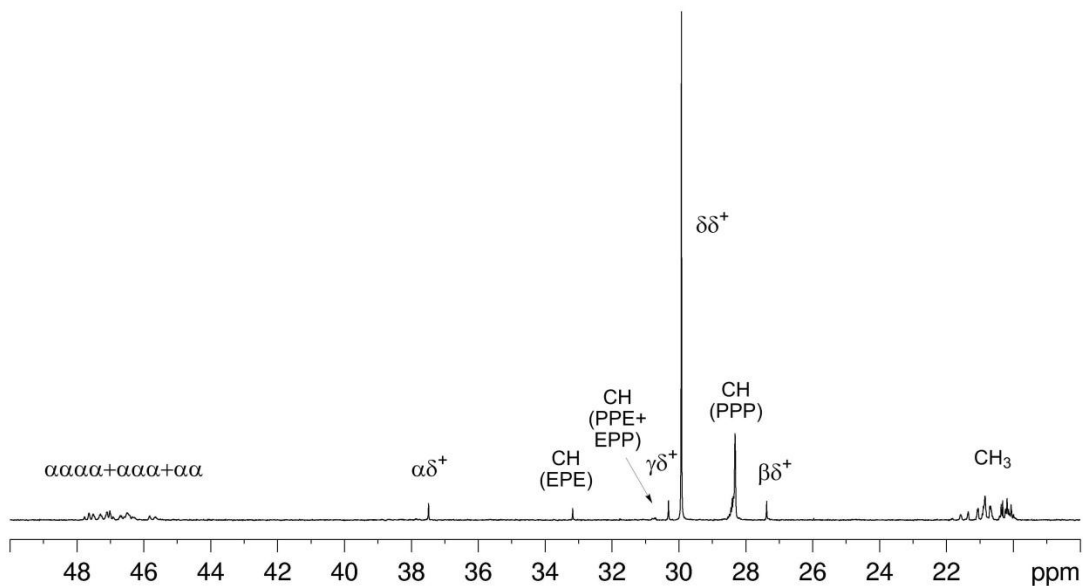
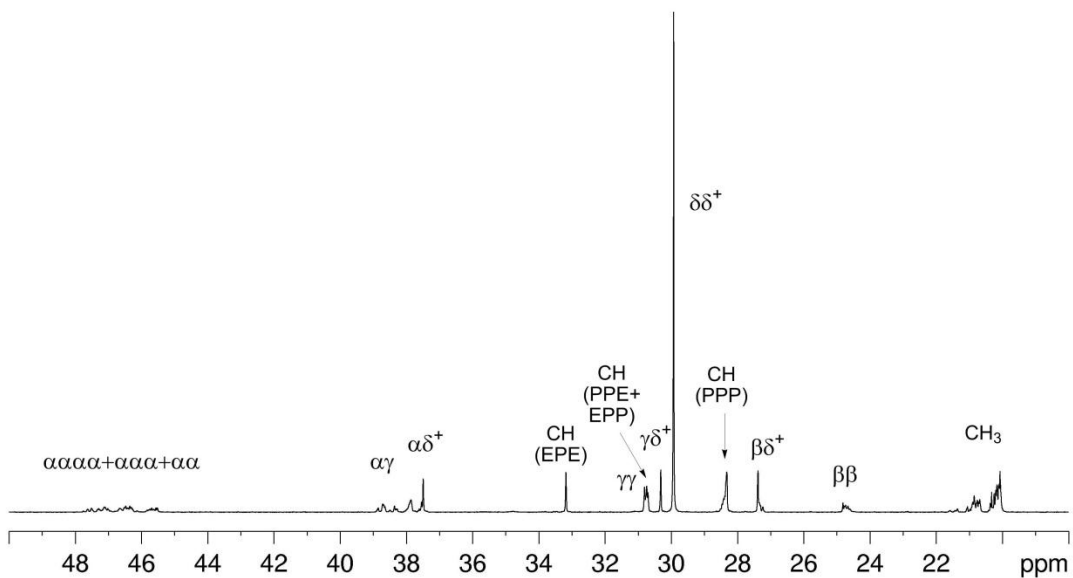


Figure 59.  $^{13}\text{C}$  NMR spectrum of *r*-E/P copolymer (entry 6.14 of Table 16)



### 6.5.2 Surface morphological characterization of *b*-E/P and *r*-E/P copolymers

Phase-sensitive, tapping mode atomic force microscopy (ps-tm-AFM) has been carried out by Wonseok in our group to study the surface morphologies of the spin-coated films of *b*-E/P and *r*-E/P materials. *b*-E/P and *r*-E/P films were annealed at 100 and 75 °C, respectively, for three day to achieve the thermodynamic equilibration of crystalline units. As shown in Figure 60. Polymer film surfaces are uniformly covered by well-dispersed crystalline PE segments (bright region) and amorphous PP segments (dark region). The total crystallinities of the two copolymer films are roughly similar, as indicated by overall bright regions, which agrees with the composition determined by <sup>13</sup>C NMR analysis. Importantly, images from *b*-E/P material (bottom right) shows a large crystalline unit size (over 200 nm), while images from *r*-E/P material (top right) shows a much smaller crystalline unit size (10–70 nm). This difference in crystalline unit sizes unambiguously confirmed the blocky structure of the *b*-E/P copolymer made from binuclear catalyst systems, which explains its higher  $T_m$  and  $T_c$  compared to *r*-E/P copolymers. Also AFM images agree with monomer sequence distribution analysis from <sup>13</sup>C NMR spectra that average E sequence length for *b*-E/P copolymer ( $n(E) = 18.4$ ) is much longer than for *r*-E/P copolymer ( $n(E) = 4.1$ ).

Also, photos of the hot-melt-pressed films of the *b*-E/P and *r*-E/P materials again demonstrated the uniqueness of the *b*-E/P copolymer from traditional *r*-E/P copolymers as the transparenance difference of these two materials. *b*-E/P (right in Figure 61) film is more opaque because of its larger the crystalline size due to the blocky structure. *r*-E/P (left in Figure 61) film is more clear due to its smaller crystalline size of the random structure, which agrees with DSC, NMR and AFM observations.

Figure 60. AFM images of *r*-E/P (entry 6.14, top) and *b*-E/P (entry 6.13, bottom)

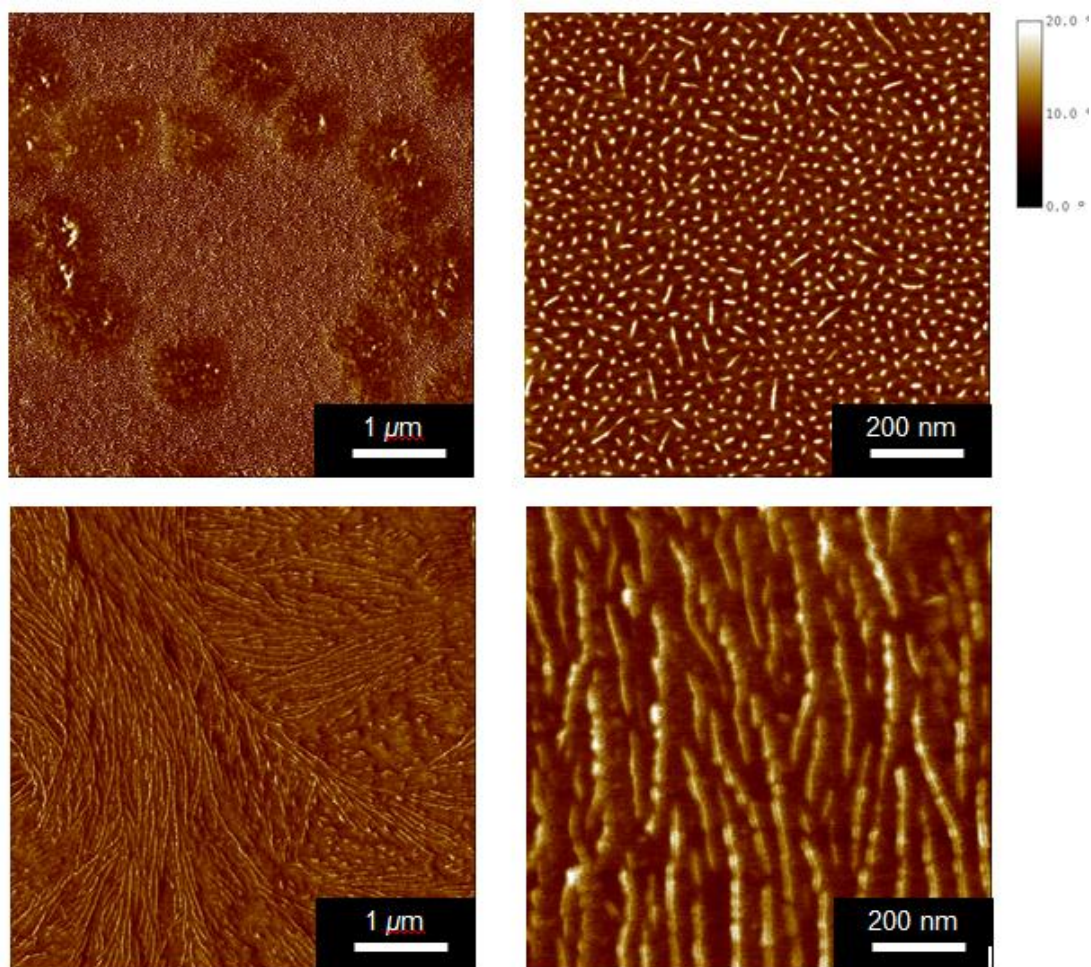


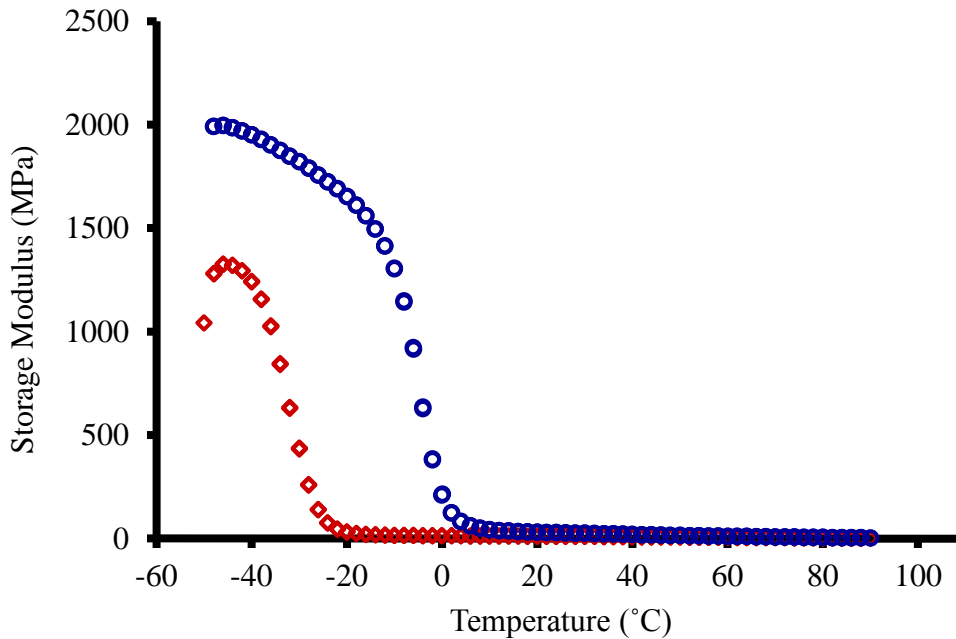
Figure 61. Photo images of *r*-E/P (left clear film) and *b*-E/P (right opaque film)



### 6.5.3 Mechanical property characterization of *b*-E/P and *r*-E/P copolymers

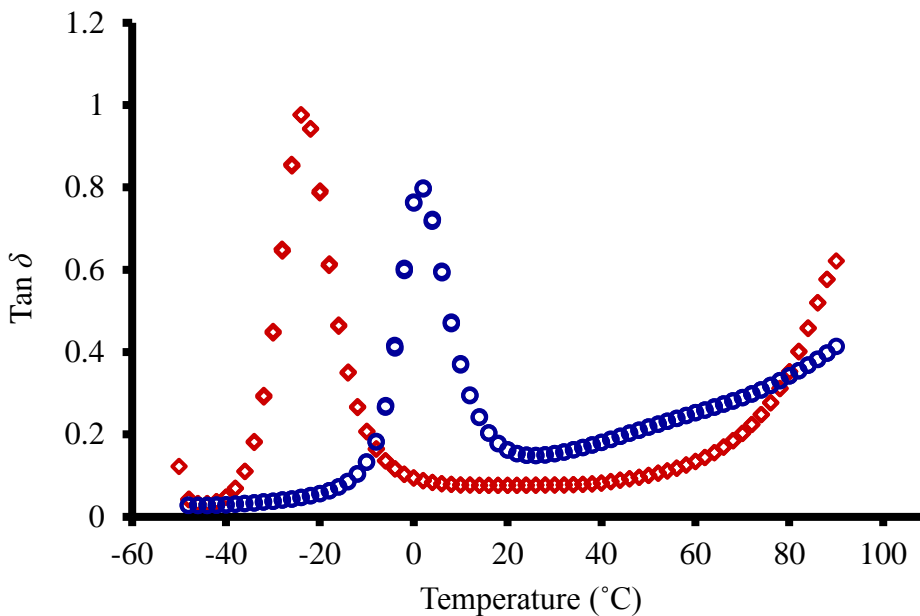
Finally, dynamic mechanical analysis (DMA) was employed to characterize the materials properties from *b*-E/P and *r*-E/P copolymers as a function of temperature with 1 Hz by Wonseok in our group. As shown in the plot of storage modulus vs. temperature (Figure 62), *r*-E/P copolymer (red triangle) has 1300 MPa of storage modulus with maximum at approximately  $-50\text{ }^{\circ}\text{C}$  and the storage modulus gradually dropped as temperature increased. *b*-E/P copolymer (blue circle), however, showed high maximum storage modulus with 2000 MPa at about  $-50\text{ }^{\circ}\text{C}$  and the storage modulus kept large value up to  $-20\text{ }^{\circ}\text{C}$  which was resulting from the long crystalline lamellar structures.

Figure 62. Plot of storage modulus vs. temperature of *r*-E/P (red diamond) and *b*-E/P (blue circle) materials



As shown in the plot of  $\tan \delta$  vs. temperature (Figure 63), the  $T_g$  of *r*-E/P copolymer (red triangle) was about  $-30$  °C which was consistent with the value from DSC ( $T_g = -34$  °C). As the temperature was closed to the glass transition, phase lag ( $\tan \delta$ ) value was sharply increased due to the increasing loss modulus and reached value a 1.0. The  $\tan \delta$  increased around  $60$  °C up to  $90$  °C which temperature range was closed to the onset melting point from DSC result. Also the obtained glass transition ( $-4$  °C) for *b*-E/P copolymer (blue circle) was well consistent with the value from DSC ( $T_g = -7$  °C). Interestingly, the phase lag was higher than that of random copolymer and kept increasing up to  $90$  °C. This tendency might due to the crystalline-crystalline slippage between relatively ethylene crystalline blocks in the presence of long propylene segments.<sup>212-213</sup>

Figure 63. Plot of  $\tan \delta$  vs. temperature of *r*-E/P (red diamond) and *b*-E/P (blue circle) materials



## 6.6 LCCTP Copolymerization of E with $\alpha$ -Olefins using Binuclear Catalysts

### 6.6.1 LCCTP copolymerization of E with P

Living coordinative chain-transfer polymerization (LCCTP) using CpAm Group 4 metal complexes with surrogate  $\text{ZnEt}_2$  has been demonstrated to produce a variety of polyolefins, especially the polyethene-based copolymer, with precisely tunable molecular weights, narrow molecular weight distributions and some degree of control on chain architectures and compositions. Also, LCCTP offers a practical solution to the “one-chain-pre-metal-center” limit on the efficiency and scalability of a living coordination polymerization. With binuclear catalyst systems, such as compound **14–16**, the slower chain-transfer rate leads to broader molecular weight distributions but higher stereoselectivity. Therefore, it is important to expand the preparation of *b*-E/P copolymers using binuclear catalyst to LCCTP strategy.

Table 17. LCCTP copolymerization of E and P using binuclear and mononuclear catalysts

Entry	E/P	Cat. system	$\text{ZnEt}_2$ (eq.)	Yield (g)	GPC	
					$M_n$ (kDa)	PDI
6.15	1/9	<b>17/04</b>	10	2.2	10.4	1.04
6.16	1/4	<b>17/04</b>	10	2.2	18.9	1.12
6.17	1/2	<b>17/04</b>	10	0.9	3.41	1.23
6.18	1/9	<b>18/04</b>	10	1.7	8.12	1.05
6.19	1/4	<b>18/04</b>	10	1.2	12.1	1.15
6.20	1/2	<b>18/04</b>	10	0.9	3.23	1.26

Conditions: 20  $\mu\text{mol}$  of **04**, 10  $\mu\text{mol}$  of **17** or 20  $\mu\text{mol}$  of **18**, 25 mL toluene, 0  $^\circ\text{C}$ .

As shown in Table 17, LCCTP copolymerization of E and P using either binuclear catalyst system **17/04** (entry 6.15–6.17) or mononuclear system **18/04** (entry 6.18–6.20) with 10 equiv. of ZnEt<sub>2</sub> as surrogate in toluene at 0 °C have been carried out with varying ratios of E/P mixed gases. First of all, all the resulting polymers showed monomodal distributed molecular weight, which indicated that chain-transfer process happened on both metal centers on the binuclear catalyst. <sup>1</sup>H NMR spectroscopy further confirmed the living nature of the chain-transfer polymerization because of the absence of vinyl group from chain termination. The PDI values of samples made from **17/04** (entry 6.15–6.17) are relative narrow and similar to those made from **18/04** (entry 6.18–6.20). This is different from what we observed for binuclear systems **14–16/04**, which indicated that the chain-transfer rate between binuclear system **17/04** and zinc metal was much faster. The reason behind these observations are not very clear now, but we could propose that rigid-link binuclear catalyst and flexible-linked binuclear behave significant different regarding to the influence of extra steric hindrance raised by two polymeric chains on one catalyst molecule.

Table 18. Results of thermal and structural analysis of E/P copolymers through LCCTP

Entry	E/P	Cat. system	DSC			NMR			
			$T_m$ (°C)	$T_c$ (°C)	$T_g$ (°C)	%P	$r_P \times r_E$	n(E)	n(P)
6.15	1/9	<b>17/04</b>	--	--	-29.5	66.4	8.6	2.7	6.4
6.16	1/4	<b>17/04</b>	103.7	91.2	-27.7	45.0	21.3	6.1	5.7
6.17	1/2	<b>17/04</b>	116.8	107.8	--	14.6	20.2	14.4	3.4
6.18	1/9	<b>18/04</b>	--	--	-38.8	66.3	2.5	1.9	4.0
6.19	1/4	<b>18/04</b>	87.8	75.8	-57.9	30.3	1.9	3.7	1.7
6.20	1/2	<b>18/04</b>	106.1	94.1	--	11.3	0.8	8.7	1.2

Importantly, all three E/P copolymers (entry 6.15–6.17 in Table 18) made from binuclear system show some degree of blockiness, represented by higher  $T_m$  and  $T_c$ , large  $r_P \times r_E$  values and longer  $n(E)$  and  $n(P)$ , compared to the copolymers made from their mononuclear analogue (entry 6.18–6.20 in Table 18). When compared the results of chain-transfer copolymerization with non-chain-transfer copolymerization (Table 14), the blockiness of the copolymer decreases for chain-transfer copolymerization. This tells us the polymeric-chain-transfer between transition metal centers and zinc metals has some influence on “regional” steric-control but could not completely randomize the distribution of the two monomers to make a random copolymer. Here the rate of chain-transfer might or might not have direct influence on the “regional” steric-control. Detailed mechanistic and polymerization behavior study is under progress to figure out a more detailed reason of those observations.

### 6.6.2 LCCTP copolymerization of E with $\alpha$ -olefins

Furthermore, LCCTP copolymerization of E with  $\alpha$ -olefins, such as 1-pentene (Pen), 1-hexene (H), 1-octene (O) and 4-methyl-1-pentene (4M1P), have been taken out using binuclear catalyst system **17/04** with  $ZnEt_2$  as surrogate in toluene to yield poly(E-co-Pen), poly(E-co-H), poly(E-co-O) and poly(E-co-4M1P). As shown in Table 19 and 20, Poly(E-co-Pen) (entry 6.21) and poly(E-co-H) (entry 6.22) materials are highly blocky ( $r_P \times r_E > 20$ ) even though the copolymerizations were carried out under chain-transfer conditions. When the size of the co-monomer increased, poly(E-co-O) (entry 6.23) materials shows more randomness ( $r_P \times r_E = 9.0$ ). Further increase the bulkiness of co-monomer to 4M1P led to poly(E-co-4M1P) (entry 6.24) materials with almost random structure ( $r_P \times r_E = 2.7$ ). The reason is under investigation, and the interaction among the binuclear catalyst,  $ZnEt_2$ , ethene and  $\alpha$ -olefin co-monomers all needs to be considered.

Table 19. LCCTP copolymerization of E and  $\alpha$ -olefins using binuclear catalyst **17/04**

Entry	Monomers	ZnEt <sub>2</sub> (eq.)	Yield (g)	GPC	
				$M_n$ (kDa)	PDI
6.21	E/Pen	10	2.0	7.85	1.41
6.22	E/H	10	2.2	18.9	1.12
6.23	E/O	10	3.5	10.0	1.80
6.24	E/4M1P	10	1.4	6.54	1.55

Conditions: 20  $\mu$ mol of **04**, 10  $\mu$ mol of **17**, 25 mL toluene, 0  $^{\circ}$ C.

Table 20. Results of thermal and structural analysis of E/ $\alpha$ -olefin copolymers

Entry	Monomers	DSC			NMR			
		$T_m$ ( $^{\circ}$ C)	$T_c$ ( $^{\circ}$ C)	$T_g$ ( $^{\circ}$ C)	%Co	$r_P \times r_E$	n(E)	n(P)
6.21	E/Pen	100-110	92.5	-53.5	44.6	21.9	6.1	4.6
6.22	E/H	103.7	91.2	-27.7	45.0	21.3	6.1	5.7
6.23	E/O	99.0	72.0	--	64.3	9.0	3.0	4.6
6.24	E/4M1P	100-110	90	-47.0	25.2	2.7	5.0	2.2

Blocky E/H copolymer has equal importance as blocky E/P materials because of the crystalline PE segment and amorphous PH segment. If high molecular weight E/H copolymer could be made through LCCTP, they could show interesting physical and mechanical properties that are unique to the conventional E/H random copolymers. In order to produce much higher molecular weight copolymers from LCCTP, less amount of ZnEt<sub>2</sub> (e.g., 2 equiv. relative to active propagation species) with extended polymerization should be employed.

## 6.7 Conclusions

A successful strategy has been proposed on steric-control mechanism using a novel hafnium binuclear catalyst to produce block E/P copolymers from E/P mixed gas. The key to this unique catalytic behavior of the binuclear catalyst system **17/04** is the combination of “locally” opened ligand environment that favors P insertion at a P rich environment with relatively high “regional” steric hindrance that disfavors the formation of two bulky chains on one binuclear catalyst molecule. With the help of a switching process that keeps changing a growing polymer chain segments from bulky one (e.g., PP) to less bulky one (e.g., PE), monodispersed statistical multi-block E/P copolymers could be made without any external dynamic control or sequential addition of monomers. NMR spectroscopy unambiguously determined the multi-block nature of *b*-E/P made from the binuclear catalyst. The unique physical and mechanical properties of *b*-E/P have been characterized and compared with the random E/P materials made from the mononuclear analogue.

Furthermore, LCCTP copolymerization based on ethene and  $\alpha$ -olefins using binuclear catalyst system **17/04** and  $\text{ZnEt}_2$  have been investigated. Preliminary results show that LCCTP copolymerization of E with P, Pen and H lead to more blocky copolymers compared to the LCCTP copolymerization of E with O and 4M1P. Therefore, it is possible to produce E/P and E/H blocky materials in a larger scale in the presence of large excess amount of  $\text{ZnEt}_2$  as a surrogate.

## Chapter 7: Conclusions

Ternary living coordinative chain-transfer polymerization (t-LCCTP) has been explored to provide previously unattainable PP oils and waxes in a scalable fashion while maintaining tight control over chain lengths and molecular weight distributions. The success of this strategy relies on a catalytic amount  $\text{ZnEt}_2$  to shuttle the polymer chains back and forth between an active hafnium chain propagation center and an excess amount of inactive aluminum surrogate for temporary holding. The  $\text{ZnEt}_2$  facilitates the overall chain-transfer rate among all three species, and ensures the catalytic chain growth on relatively inexpensive aluminum metal centers. A series of amorphous *a*PP and poly(P-*co*-O) with very narrow molecular weight distributions have been made, and the oligomerization of propene has been scaled up to yield 88 g *a*PP from only 0.11 g of hafnium metal compound.

Both LCCTP and t-LCCTP have investigated to produce block and end-group functionalized polyolefin-based materials through chemical transformation of the Zn-C or Al-C bond. *a*PP-*block*-PCL has been made through ring-opening polymerization of  $\epsilon$ -caprolactone from  $\text{Zn}(\text{O-}a\text{PP})_2$  using  $\text{Zn}(a\text{PP})_2$  as the starting material. A particularly efficient reaction of  $\text{Zn}(\text{polymeryl})_2$  with iodine in toluene solution was found to quantitatively yield iodide-terminated polyolefins, followed by further conversion to 1-carboxyl and 1-hydroxymethyl-terminated polyolefins.

Another extension of LCCTP strategy achieves the goal of "one catalyst, many materials" through a dynamic process that modulates the co-monomer relative reactivities using the chain-transfer process between the "tight" and "loose" ion-pair chain-growth centers. A broad spectrum of poly(E-*co*H) materials with controllable H incorporation levels

from 6.9% to 74.4% have been produced in a straightforward fashion through activation of a single hafnium precatalyst with varying ratios of two boron cocatalysts. The generality of this strategy has been validated by the synthesis of a series of poly(E-*co*-CPE) materials using a sterically less hindered cyclopentadienyl zirconium compound.

Furthermore, a novel class of precision polyolefin waxes has been made through copolymerization of ethene with longer  $\alpha$ -olefins with tunable side-chain lengths and incorporation levels. The predominant side-chain crystallization behaviors have been carefully investigated through structural and thermal analysis of the polyolefin waxes. Structure versatility of this type of materials has been expanded to ODE-based terpolymer and diblock copolymers.

A binuclear hafnium catalyst with “locally” opened and “regionally” hindered structure has been designed and synthesized to provide E/P multi-block copolymers with unique physical and mechanical properties. The “locally” opened chain propagation center favors the insertion of P and produce P-rich blocks, while the “regionally” hindered environment prevents the formation of two P-rich blocks from both hafnium centers on the same binuclear catalyst. Therefore, one P-rich block and one E-rich block must be grown at the same time from one binuclear catalyst, which leads to a novel class of multi-block E/P copolymers. GPC, DSC,  $^1\text{H}$  and  $^{13}\text{C}$  NMR spectroscopy have been used to confirm the multi-block structure of the copolymers. AFM and DMA have been used to reveal the surface morphological difference and mechanical property difference between this multi-block E/P copolymer with traditional random E/P copolymers. LCCTP using this binuclear hafnium catalyst with  $\text{ZnEt}_2$  has also been investigated and yielded a series of ethene/ $\alpha$ -olefin blocky materials.

## Appendix: Experimentals

**General:** All manipulations throughout this thesis were performed under an inert atmosphere of dinitrogen using either standard Schlenk techniques or a vacuum atmosphere glovebox. Dry, oxygen-free solvents were employed throughout. Diethyl ether and pentane were distilled from sodium/benzophenone (with a few milliliters of triglyme being added to the pot in the case of pentane). Toluene was distilled from sodium. Chlorobenzene and methylene chloride were distilled from calcium hydride. Benzene-d<sup>6</sup> and toluene-d<sup>8</sup> were vacuum transferred from NaK prior to use for NMR spectroscopy.

**Materials:** Polymer grade ethene and propene were purchased from Matheson Trigas, and passed through activated Q5 and molecular sieves (4 Å) before polymerization reactions. Gravimetric standard ethene and propene mixed gases were purchased from Matheson Trigas, and passed through activated Q5 and molecular sieves (4 Å) prior to polymerization. 1-hexene, 1-octene, 1-decene and 1,5-hexadiene were dried by NaK and vacuum transferred prior to use for polymerizations. 1-tetradecene and 1-hexadecene were distilled under reduced pressure from sodium. 1-octadecene and 1-docosene were distilled under 0.005 mmHg at 150 °C from sodium. Cp\*Zr(Me)<sub>2</sub>[N(Et)C(Me)N(tBu)] (**02**) and other reported precatalysts were prepared according to the literatures. Cp\*ZrCl<sub>3</sub>, Cp\*HfCl<sub>3</sub>, [Ph<sub>3</sub>C][B(C<sub>6</sub>F<sub>5</sub>)<sub>4</sub>] (**12**) and B(C<sub>6</sub>F<sub>5</sub>)<sub>3</sub> (**10**) were obtained from Strem Chemicals while [PhNHMe<sub>2</sub>][B(C<sub>6</sub>F<sub>5</sub>)<sub>4</sub>] (**04**) was purchased from Boulder Scientific and used without further purification. ZnEt<sub>2</sub> was added as a 1.1M (15% wt) solution in toluene.

**Instrumentation:** GPC analyses were performed using a Viscotek GPC system equipped with a column oven and differential refractometer both maintained at 40 °C and four

columns also maintained at 40 °C. THF was used as the eluant at a flow rate of 1.0 mL/min.  $M_n$ ,  $M_w$  and  $M_w / M_n$  values were obtained using a Viscotek GPC with OmniSEC software (conventional calibration) and ten polystyrene standards ( $M_n = 580$  Da to 3,150 kDa) (from Polymer Laboratories). DSC was performed using Q-1000 series at a heating rate of 10 °C /min, and the 2<sup>nd</sup> heating cycle was recorded.  $^{13}\text{C}$   $\{^1\text{H}\}$  NMR spectra were recorded at 150 MHz, using 1,1,2,2-tetrachloroethane- $d^2$  as the solvent at 90 °C unless otherwise noted. For wide angle X-ray diffraction (WAXD) measurements, all the samples were measured in an as-prepared state with no further thermal annealing. About 0.5 g of each sample was mounted on the sample holder and the measurement was performed on Bruker D8 Advance system with LynxEye detector. The wavelength of  $\text{CuK}_\alpha$  radiation was selected  $\lambda = 1.54$  Å and the scan angle was 5~60° with 0.05° step. The data was collected at room temperature. The obtained profiles were fitted with built-in software (Advanced TOPAS).

**t-LCCTP of propene:** The following description for entry 2.08 of Table 1 represents a typical procedure for T-LCCTP. In a 250-mL Schlenk flask, to a solution of the cocatalyst **12** (18.5 mg, 20 µmol) in 20 mL of toluene at 20 °C was added **08** (9.1 mg, 20 µmol) and stirred for 10 min.  $\text{Al}(i\text{Bu})_3$  (476 mg, 18 equiv.) as 15% wt solution in toluene and  $\text{ZnEt}_2$  (33 mg, 2 equiv.) as 15% wt (1.1 M) solution in toluene were added and stirred for 10 min. The flask was then pressurized to 5 psi with propene and the pressure was maintained for 4 h with stirring before quenching with 1.0 mL of methanol. The toluene solution was precipitated into 600 mL of acidic methanol (10% concentrated HCl) to isolate the polypropene. The final product was collected and dried overnight in *vacuo*. Yield: 3.1 g. GPC analysis:  $M_w = 4.71\text{k}$ ;  $M_n = 4.53\text{k}$ ; PDI = 1.04.

**Scaled up t-LCCTP of propene (entry 2.11 in Table 1):** In a 500-mL Schlenk flask, to a solution of the cocatalyst **12** (221.4 mg, 0.24 mmol) in 300 mL of toluene at 20 °C was added **08** (109.7 mg, 0.24 mmol) and stirred for 10 min.  $\text{Al}(i\text{Bu})_3$  (9.04 g, 190 equiv.)

and  $\text{ZnEt}_2$  (1.98 g, 10 equiv.) as 15% wt (1.1 M) solution in toluene were added and stirred for 10 min. The flask was then pressurized to 5 psi with propene and the pressure was maintained for 72 h with stirring before quenching with 10.0 mL of methanol. The toluene solution was precipitated into 1600 mL of acidic methanol to isolate the PP. The crude product was redissolved in toluene and passed through silica gel, followed by reprecipitating into 800 mL acidic methanol. The final product was collected and dried overnight in *vacuo*. Yield: 88.3 g. GPC analysis:  $M_w = 1.31\text{k}$ ;  $M_n = 1.19\text{k}$ ; PDI = 1.10.  $^{13}\text{C}$  NMR spectra analysis;  $M_n = 580$ .

**t-LCCTP copolymerization of propene with 1-octene:** The following description for entry 2.12 of Table 2 represents a typical procedure for t-LCCTP copolymerization. In a 250-mL Schlenk flask, to a solution of the cocatalyst **12** (18.5 mg, 20  $\mu\text{mol}$ ) in 20 mL of toluene at 20  $^\circ\text{C}$  was added **08** (9.1 mg, 20  $\mu\text{mol}$ ) and stirred for 10 min.  $\text{Al}(\text{iBu})_3$  (476 mg, 18 equiv.) as 15% wt solution in toluene and  $\text{ZnEt}_2$  (33 mg, 2 equiv.) as 15% wt (1.1 M) solution in toluene were added and stirred for 10 min. The flask was then added 1-octene (1.12 g, 500 equiv.) and pressurized to 5 psi with propene and the pressure was maintained for 4 h with stirring before quenching with 1.0 mL of methanol. The toluene solution was precipitated into 600 mL of acidic methanol to isolate the polypropene. The final product was collected and dried overnight in *vacuo*. Yield: 0.84 g. GPC analysis:  $M_w = 1.40$ ;  $M_n = 1.27\text{k}$ ; PDI = 1.10.

**Preparation of  $\text{Zn}(\text{aPP})_2$  stock solution:** In a 250-mL Schlenk flask, to a 41 mL toluene solution of cocatalyst **04** (48.1 mg, 0.060 mmol) at 0  $^\circ\text{C}$  were added the precatalyst **08** (27.4 mg, 0.060 mmol) and  $\text{ZnEt}_2$  in 15 wt% toluene solution (9.88 g, 12.0 mmol, 200 equiv to **08**). The flask was then pressurized to slightly above 1 atm (5 psi) with propene and the pressure was maintained for 2 h with stirring. Excess propene was then removed *in vacuo* for 30 min at 0  $^\circ\text{C}$ . An aliquot of the stock solution was taken and quenched according to the

general procedure and subjected to GPC and NMR analyses. GPC:  $M_n = 1.24$  kDa,  $M_w = 1.40$  kDa, PDI = 1.13. The bright yellow  $Zn(aPP)_2$  toluene solution was kept at  $-25$  °C in the internal freezer of the glove box and used for the following subsequent chemical reactions.

**Preparation of 1-iodo-aPP:** A saturated solution of  $I_2$  in toluene was added to 50 mL of a 200 mmol/L  $Zn(aPP)_2$  toluene solution at 0 °C until a purple color persisted in the reaction solution. The toluene solution was then extracted with  $3 \times 50$  mL 10% NaOH,  $4 \times 50$  mL 10% HCl and  $3 \times 100$  mL of distilled water. The crude product was isolated by removing all the volatiles in vacuo and then the final product was obtained after washing the crude product several times with acetone before being dried in vacuum prior to GPC and NMR analyses. Yield: 9.6 g. GPC:  $M_n = 1.19$  kDa,  $M_w = 1.31$  kDa, PDI = 1.10.

**Preparation of 1-iodo-poly(P-block-E):** In a 250-mL Schlenk flask, to a 40 mL toluene solution of cocatalyst **04** (8.0 mg, 0.010 mmol) at 25 °C were added the precatalyst **08** (4.6 mg, 0.010 mmol) and  $ZnEt_2$  in 15 wt% toluene solution (1.65 g, 2.0 mmol, 200 equiv to **08**). The flask was then pressurized to slightly above 1 atm (5 psi) with ethene and the pressure was maintained for 30 mins with stirring. After removing excess ethene in toluene by applying reduced pressure for 30 min, the stock solution of  $Zn(PE)_2$  was transferred to another glove box equipped with a propene feed. After addition of cocatalyst **04** (8.0 mg, 0.010 mmol) and precatalyst **08** (4.6 mg, 0.010 mmol) to this  $Zn(PE)_2$  / toluene stock solution, polymerization of propene was carried out at 25 °C for 2 h with a propene pressure of 5 psi. A saturated solution of  $I_2$  in toluene was then added until a purple color persisted in the reaction solution. The reaction mixture was precipitated into 600 mL acidic methanol solution ((10% HCl)) and stirred overnight. The final product was collected, washed with acidic methanol and methanol and dried in vacuum before GPC and NMR analyses. Yield: 2.2 g. GPC:  $M_n = 1.75$  kDa,  $M_w = 1.86$  kDa, PDI = 1.07.

**Preparation of 1-lithio-*a*PP:** In a 50-mL Schlenk flask, to a 3 mL Et<sub>2</sub>O solution of 1-iodo-*a*PP (580 mg,  $M_n = 1.73$  kDa, PDI = 1.05) was added 0.95 mL *t*BuLi (1.45 mmol, 2.1 equiv to 1-iodo-*a*PP, 1.55 M in pentane) at -78 °C. The reaction was allowed to stir at -78 °C for 1 h, and then warmed up to room temperature over a period of 2 h. After transferring the reaction mixture to glove box, two aliquots were taken for NMR analyses. First aliquot (0.1 mL) was allowed to remove all the volatiles via vacuum and dissolved in CDCl<sub>3</sub> prior to <sup>1</sup>H-NMR analysis. Second aliquot (0.5 mL) was quenched with 1 mL D<sub>2</sub>O and vacuumed overnight to remove volatiles before <sup>1</sup>H and <sup>13</sup>C-NMR analyses. GPC of 1-deuterio-*a*PP :  $M_n = 1.69$  kDa,  $M_w = 1.81$  kDa, PDI = 1.07.

**Preparation of 1-carboxy-*a*PP:** In a 50-mL Schlenk flask, 0.96 g of 1-iodo-*a*PP (1.04 mmol,  $M_n = 1.19$  Da, PDI = 1.10) was dissolved in a mixed solvent comprised of 4.5 mL pentane and 3.0 mL Et<sub>2</sub>O. Then 1.4 mL *t*BuLi (1.55 M in pentane) (2.2 mmol, 2.1 equiv to 1-iodo-*a*PP) was added at -78 °C within 5 min. The reaction was allowed to stir at -78 °C for 30 min and then warm up to room temperature over a period of 2 h. After cooling to -78 °C, the reaction mixture was poured onto dry ice contained within a 100 mL beaker, followed by quenching of 1 mL of 2 N HCl in methanol. After standing overnight, the top clear layer in the beaker was collected and the volatiles removed in vacuo to provide the final product that was characterized by NMR and GPC analyses. Yield: 0.72 g. GPC:  $M_n = 1.19$  kDa,  $M_w = 1.34$  kDa, PDI = 1.13.

**Preparation of 1-hydroxymethyl-*a*PP:** In a 50-mL Schlenk flask, 1.05 g of 1-iodo-*a*PP (1.13 mmol,  $M_n = 1.19$  Da, PDI = 1.10) was dissolved in a mixed solvent comprised of 4.5 mL pentane and 3.0 mL Et<sub>2</sub>O. Then 1.5 mL *t*BuLi (1.55 M in pentane) (2.4 mmol, 2.1 equiv to 1-iodo-*a*PP) was added at -78 °C within 5 min, followed by stirring the reaction at -78 °C for 30 min and warming up to room temperature over a period of 2 h. After cooling to -78 °C, 75 mg of paraformaldehyde in 1 mL pentane was added and the mixture was stirred at

-78 °C for 30 min whereupon it was allowed to warm to room temperature within 2 h. The reaction was quenched with addition of 1 mL of 2 N HCl in methanol to provide a clear yellow solution. After removing the volatiles in vacuo, the residue was dissolved in toluene and washed with 10% HCl and then distilled water. The toluene layer was dried with anhydrous Na<sub>2</sub>SO<sub>4</sub> and dried under vacuum overnight to provide the final product. Yield: 0.75 g. GPC:  $M_n = 1.20$  kDa,  $M_w = 1.38$  kDa, PDI = 1.16.

**LCCTP copolymerization of E and H (entry 4.19 of Table 6):** The following description represents a typical procedure for E and H copolymerization in neat H solvent. In a 250-mL Schlenk flask, to 20 mL H (13.4 g) at 25 °C was added ZnEt<sub>2</sub> (165 mg, 0.20 mmol) as 15 wt% (1.1 M) solution in toluene. Then the flask was pressurized to slightly above 1 atm (5 psi) with E and equilibrated for 30 min. A clear yellow mixture solution of cocatalyst **04** (8.0 mg, 0.010 mmol), cocatalyst **10** (5.1 mg, 0.010 mmol), and precatalyst **08** (9.1 mg, 0.020 mmol) in 1.0 mL chlorobenzene was then added to the reaction flask to initiate polymerization. Polymerization temperature was maintained at 25 ± 3 °C. After 30 min, polymerization was quenched with 1.0 mL of methanol. The polymer solution was then precipitated into 600 mL of acidic methanol (10% concentrated HCl) to isolate the polymer. The final product was collected and dried overnight in vacuum before GPC and NMR analyses. Yield: 3.7 g. GPC analysis:  $M_w = 18.6$ k;  $M_n = 17.6$ k; PDI = 1.06.

**Synthesis of  $\alpha$ -iodo-poly(E-co-CPE) (entry 4.24 of Table 8):** The following description represents a typical procedure for E and CP copolymerization in toluene followed by end-group functionalization using iodine. In a 250-mL Schlenk flask, to 40 mL toluene at 25 °C was added CP (4.08 g, 60.0 mmol) and ZnEt<sub>2</sub> (823 mg, 1.0 mmol) as 15 wt% (1.1 M) solution in toluene. Then the flask was pressurized to 5 psi with ethene and equilibrated for 30 min. A clear yellow mixture solution of cocatalyst **04** (8.0 mg, 0.010 mmol), cocatalyst **10** (5.1 mg, 0.010 mmol), and precatalyst **13** (8.2 mg, 0.020 mmol) in 1.0 mL chlorobenzene

was added to the reaction flask to initiate polymerization. Polymerization temperature was maintained at  $25 \pm 3$  °C. After 30 min, a slightly excess of iodine (558 mg, 2.2 mmol) was added until a purple color persisted in the reaction solution. The reaction solution was then precipitated into 600 mL basic methanol (10% NaOH) to isolate the polymer. The final product was collected, washed with acidic methanol and methanol and dried in vacuum before GPC and NMR analyses. Yield: 2.1 g. GPC analysis:  $M_w = 2.78k$ ;  $M_n = 2.46k$ ; PDI = 1.14.

**Synthesis of  $\alpha$ -[I][PPh<sub>3</sub>]-poly(E-co-CPE):** The following description represents a typical procedure for synthesis of  $\alpha$ -[I][PPh<sub>3</sub>]-poly(E-co-CP) from  $\alpha$ -iodo-poly(E-co-CP). In a 50-mL Schlenk flask, to 15 mL dry DMF was added 0.6 g of triphenylphosphine and 0.3 g  $\alpha$ -iodo-poly(E-co-CP) dissolved in 1 mL hot toluene. The reaction mixture was allowed to reflux at 110 °C for 3 days under N<sub>2</sub>. The crude product was collected via removing all the volatiles under vacuum, followed by washing with chloroform twice and then pumping away chloroform to remove residual DMF. The final product was collected and dried overnight in vacuum before NMR and MALDI-TOF-MS analyses. Yield: 0.4 g.

**LCCTP copolymerization of E with long chain  $\alpha$ -olefins (entry 5.09 of Table 10):** In a 250-mL Schlenk flask, to 10 mL toluene at 20 °C was added 5.05 g 1-octadecene (20.0 mmol) and ZnEt<sub>2</sub> (82.3 mg, 0.10 mmol) as 15 wt% (1.1 M) solution in toluene. Then the flask was pressurized to slightly above 1 atm (5 psi) with ethene and equilibrated for 30 min. A clear yellow solution of cocatalyst **04** (8.0 mg, 0.010 mmol) and precatalyst **08** (4.6 mg, 0.010 mmol) in 0.5 mL chlorobenzene was then syringed to the flask to initiate polymerization. Polymerization temperature was maintained at  $20 \pm 3$  °C. After 10 min, polymerization was quenched with 1.0 mL of methanol. The polymer solution was then precipitated into 600 mL methanol to isolate the crude produce. The final product was

collected by washing with 10 mL  $\times$  5 boiling isopropanol to remove remaining 1-octadecene and dried overnight in vacuum before GPC, NMR and DSC analyses. Yield: 2.2 g.

**LCCTP terpolymerization of E, H and ODE (entry 5.19 of Table 12):** In a 250-mL Schlenk flask, to 7.5 mL toluene at 20 °C was added 1.68 g 1-hexene (20.0 mmol), 5.05 g 1-octadecene (20.0 mmol) and ZnEt<sub>2</sub> (164.5 mg, 0.20 mmol) as 15 wt% (1.1 M) solution in toluene. Then the flask was pressurized to slightly above 1 atm (5 psi) with ethene and equilibrated for 30 min. A clear yellow solution of cocatalyst **04** (8.0 mg, 0.010 mmol) and precatalyst **08** (4.6 mg, 0.010 mmol) in 0.5 mL chlorobenzene was then syringed to the flask to initiate polymerization. Polymerization temperature was maintained at 20  $\pm$  3 °C. After 10 min, polymerization was quenched with 1.0 mL of methanol. The polymer solution was then precipitated into 600 mL methanol to isolate the crude produce. The final product was collected by washing with 10 mL boiling isopropanol 5 times to remove remaining 1-octadecene and dried overnight in vacuum before GPC, DSC and NMR analyses. Yield: 2.0 g.

**Synthesis of poly(ODE)-*block*-poly(E-*co*-ODE):** In a 250-mL Schlenk flask, to 10.0 mL toluene at 20 °C was added 5.05 g 1-octadecene (20.0 mmol) and ZnEt<sub>2</sub> (82.3 mg, 0.10 mmol) as 15 wt% (1.1 M) solution in toluene. A clear yellow solution of cocatalyst **04** (8.0 mg, 0.010 mmol) and precatalyst **08** (4.6 mg, 0.010 mmol) in 0.5 mL chlorobenzene was then added to the flask to initiate polymerization. After 1 h, 1 mL aliquot of 1<sup>st</sup> block was quenched with 0.1 mL MeOH and purified before GPC and DSC analyses. The reaction flask was then pressurized to slightly above 1 atm (5 psi) with ethene to initiate the growth of 2<sup>nd</sup> block. Polymerization temperature was maintained at 20  $\pm$  3 °C. After 20 min, polymerization was quenched with 1.0 mL of methanol. The polymer solution was then precipitated into 600 mL methanol to isolate the crude produce. The final product was collected by washing with

10 mL boiling isopropanol 5 times to remove remaining 1-octadecene and dried overnight in vacuum before GPC, DSC and NMR analyses. Final yield: 4.5 g.

**Synthesis of *p*-xylylenediamine caprolactim amidine:** In a 100 mL round bottom flask equipped with a simple distillation set-up and a magnetic stirrer were placed 0.816 g (6.0 mmol) of *p*-xylylenediamine and 1.83 g (14.4 mmol) of *o*-methylcaprolactim. The mixture was heated in an oil bath with stirring to 125 °C while distilling methanol for 16 h. After cooling the mixture to room temperature, 10 mL chloroform was added to form a clear yellow solution. This yellow solution was then precipitated into 600 mL hexane and stirred overnight. The product is isolated as a light yellow powder via filtration and washed with several portions of cold hexane before being dried under vacuum. Yield: 1.21 g (62 %). <sup>1</sup>H NMR (400 MHz, CDCl<sub>3</sub>, 293 K): δ = 7.29 (4H, s), 4.24 (4H, s), 3.36 (4H, br), 2.37 (4H, br), 1.73 (4H, m), 1.59 (8H, m).

**Synthesis of 1-naphthylmethylamine caprolactim amidine:** In a 100 mL round bottom flask equipped with a simple distillation set-up and a magnetic stirrer were placed 3.40 g (21.6 mmol) of 1-naphthylmethylamine and 3.30 g (25.9 mmol) of *o*-methylcaprolactim. The mixture was heated in an oil bath with stirring to 125 °C while distilling methanol for 16 h. After cooling the mixture to room temperature, 15 mL hexane was added with manually stirring for 20 min until solid precipitation was formed. The product was isolated as a white powder via filtration and washed with several portions of cold hexane before being dried under vacuum. Yield: 5.45 g (83%). <sup>1</sup>H NMR (400 MHz, CDCl<sub>3</sub>, 293 K): δ = 8.07 (1H, d), 7.87 (1H, d), 7.78 (1H, d), 7.54-7.40 (4H, m), 4.71 (2H, s), 3.45 (2H, br), 2.35 (2H, br), 1.75 (2H, m), 1.65 (4H, m).

**Synthesis of  $[(\eta^5\text{-C}_5\text{Me}_5)\text{Hf}(\text{Me})_2]_2[\text{N}(\text{CH}_2)_5\text{CN}-(\text{CH}_2)(\text{C}_6\text{H}_4)(\text{CH}_2)\text{-NC}(\text{CH}_2)_5\text{N}]$  (**17**):** In a 250 mL Schlenk flask, to a solution of 0.840 g (2.00 mmol) ( $\eta^5\text{-C}_5\text{Me}_5$ )HfCl<sub>3</sub> in 40

mL Et<sub>2</sub>O at -75 °C was added a solution of 4.2 mL of MeLi (1.6 M in Et<sub>2</sub>O) via syringe over 10 min. The mixture was stirred and let to warm up slowly to -10 °C for 2 h. After cooling down to -30 °C, 0.20 mL Me<sub>3</sub>SiCl was added via syringe and stirred for 10 min. After cooling to -60 °C, the reaction solution was transferred via cannula to a solution of 0.326 g (1.00 mmol) *p*-xylylenediamine caprolactim amidine in 20 mL of Et<sub>2</sub>O at -60 °C within 10 min. The mixture was stirred and allowed to warm up slowly to 0 °C for 4 h. At this point, the volatiles were removed under vacuum at room temperature. The resulting white residue was extracted with 6 mL (2 mL × 3) toluene and filtered through a pad of Celite in a glass frit. The toluene solution was concentrated to 2 mL and kept in -20 °C freezer to let product precipitate out over 1 to 3 days. yield: 0.46 g (46% yield). <sup>1</sup>H NMR (400 MHz, C<sub>6</sub>D<sub>6</sub>, 293 K): δ = 7.20 (4H, s), 4.36 (4H, s), 3.05 (4H, m), 2.03 (4H, m), 2.01 (30H, s), 1.38 (8H, m), 1.21 (4H, m), 0.04 (12H, s).

**Synthesis of [(η<sup>5</sup>-C<sub>5</sub>Me<sub>5</sub>)Hf(Me)<sub>2</sub>][N(CH<sub>2</sub>)<sub>5</sub>CN-(CH<sub>2</sub>)(C<sub>10</sub>H<sub>7</sub>)] (18):** In a 250 mL Schlenk flask, to a solution of 0.840 g (2.00 mmol) (η<sup>5</sup>-C<sub>5</sub>Me<sub>5</sub>)HfCl<sub>3</sub> in 80 mL Et<sub>2</sub>O at -75 °C was added a solution of 4.2 mL of MeLi (1.6 M in Et<sub>2</sub>O) via syringe over 10 min. The mixture was stirred and let to warm up slowly to -10 °C for 2 h. After cooling down to -30 °C, 0.20 mL Me<sub>3</sub>SiCl was added via syringe. A solution of 0.505 g (2.00 mmol) 1-naphthylmethylamine caprolactim amidine in 15 mL of Et<sub>2</sub>O was then added via cannula at -30 °C for 45 min. The mixture was stirred for 1 h at -30 °C and then was allowed to warm up to -10 °C for 1 h. At this point, the volatiles were removed under vacuum at room temperature. The resulting white residue was extracted with 8 mL (2 mL × 4) pentane and filtered through a pad of Celite in a glass frit. The pentane solution was concentrated to 2 mL and kept in -20 °C freezer to let product precipitate out over 1 to 3 days. yield: 0.59 g (50% yield). <sup>1</sup>H NMR (400 MHz, C<sub>6</sub>D<sub>6</sub>, 293 K): δ = 7.88 (1H, d), 7.69 (1H, d), 7.59 (1H, d), 7.53

(1H, d), 7.39-7.29 (3H, m), 4.87 (2H, s), 3.10 (2H, m), 2.02 (15H, s), 1.88 (2H, m), 1.44 (2H, m), 1.34 (2H, m), 1.18 (2H, m), 0.08 (6H, s).

**Typical procedure for polymerization with E and P mixed gases:** To a 0.020 mmol co-catalyst **04** was added a solution of 0.020 mmol **18** or 0.010 mmol **17** in 1.0 mL of cold chlorobenzene and mixed until a clear light yellow solution formed. This solution was then rapidly added to a 250-mL Schlenk flask loaded with 25 mL of toluene at 0 °C, which was previously pressurized to 5 psi with ethene and propene mixed gases. The flask was then repressurized and the pressure maintained for the desired reaction time while stirring before quenching with 0.5 mL of methanol. Purge the flask every 5 min to maintain the desired ethene and propene ratio. Polymerization temperature was maintained at  $0 \pm 3$  °C. The polymer solution was then precipitated into 600 mL methanol to isolate the crude produce. The final product was collected by filtration and washed with 5 mL  $\times$  4 methanol before being dried under vacuum.

**Mechanistic study (synthesis of diblock PH-*block*-PE via 17/04):** To a 0.020 mmol co-catalyst **04** was added a solution of 0.010 mmol **17** in 1.0 mL of cold chlorobenzene and mixed until a clear light yellow solution formed. This solution was then rapidly added to a 20-mL vial loaded with 10 mL of toluene at 0 °C and stirred for 10 min. 84.2 mg (1.0 mmol) precooled 1-hexene was added to the vial and stirred at 0 °C for the growth of the 1<sup>st</sup> block. After 1 h, 2 mL aliquot #1 was taken out, quenched with 0.1 mL MeOH and precipitated into 10 mL MeOH for GPC analysis. The polymerization vial was then pressurized to 5 psi with ethene and maintained for 1 min for the growth of the 2<sup>nd</sup> block before 2 mL aliquot #2 was taken out for GPC analysis. GPC: aliquot #1:  $M_w = 10.9$  kDa,  $M_n = 12.6$  kDa, PDI = 1.16; aliquot #2:  $M_w = 16.2$  kDa,  $M_n = 13.9$  kDa, PDI = 1.16 and  $M_w = 146$  kDa,  $M_n = 129$  kDa, PDI = 1.13.

**Mechanistic study (synthesis of diblock PH-*block*-PE via 18/04):** To a 0.020 mmol co-catalyst **04** was added a solution of 0.020 mmol **18** in 1.0 mL of cold chlorobenzene and mixed until a clear light yellow solution formed. This solution was then rapidly added to a 20-mL vial loaded with 10 mL of toluene at 0 °C and stirred for 10 min. 84.2 mg (1.0 mmol) precooled 1-hexene was added to the vial and stirred at 0 °C for the growth of the 1<sup>st</sup> block. After 1 h, 2 mL aliquot #1 was taken out, quenched with 0.1 mL MeOH and precipitated into 10 mL MeOH for GPC analysis. The polymerization vial was then pressurized to 5 psi with ethene and maintained for 1 min for the growth of the 2<sup>nd</sup> block before 2 mL aliquot #2 was taken out for GPC analysis. GPC: aliquot #1:  $M_w = 5.37$  kDa,  $M_n = 4.67$  kDa, PDI = 1.15; aliquot #2:  $M_w = 7.04$  kDa,  $M_n = 8.19$  kDa, PDI = 1.16.

## References:

- (1) Pino, P.; Mülhaupt, R. *Angew. Chem., Int. Ed.* **1980**, *19*, 857-875.
- (2) Böhm, L. L. *Angew. Chem., Int. Ed.* **2003**, *42*, 5010-5030.
- (3) Ziegler, K.; Holzkamp, E.; Breil, H.; Martin, H. *Angew. Chem.* **1955**, *67*, 426.
- (4) Natta, G.; Pino, P.; Corradini, P.; Danusso, F.; Mantica, E.; Mazzanti, G.; Moraglio, G. *J. Am. Chem. Soc.* **1955**, *77*, 1708-1710.
- (5) Kashiwa, N. *Polym. J. (Tokyo, Jpn.)* **1980**, *12*, 603.
- (6) Kashiwa, N. *J. Polym. Sci., Part A: Polym. Chem.* **2004**, *42*, 1-8.
- (7) Cossee, P. *J. Catal.* **1964**, *3*, 80-88.
- (8) Arlman, E. J.; Cossee, P. *J. Catal.* **1964**, *3*, 89-98.
- (9) Chum, P. S.; Swogger, K. W. *Prog. Polym. Sci.* **2008**, *33*, 797-819.
- (10) Busico, V. *Dalton Trans.* **2009**, 8794-8802.
- (11) Hustad, P. D. *Science* **2009**, *325*, 704-707.
- (12) Hillman, M.; Weiss, A. J.; Hahne, R. M. A. *Radiochimica Acta* **1969**, *12*, 200.
- (13) Herrmann, W. A.; Cornils, B. *Angew. Chem., Int. Ed.* **1997**, *36*, 1048.
- (14) Natta, G.; Pino, P.; Mazzanti, G.; Giannini, U. *J. Am. Chem. Soc.* **1957**, *79*, 2975-2976.
- (15) Breslow, D. S.; Newburg, N. R. *J. Am. Chem. Soc.* **1959**, *81*, 81-86.
- (16) Long, W. P.; Breslow, D. S. *Liebigs Ann. Chem.* **1975**, 463.
- (17) Andresen, A.; Cordes, H. G.; Herwig, J.; Kaminsky, W.; Merck, A.; Mottweiler, R.; Pein, J.; Sinn, H.; Vollmer, H. J. *Angew. Chem., Int. Ed.* **1976**, *15*, 630.
- (18) Sinn, H.; Kaminsky, W. *Adv. Organomet. Chem.* **1980**, *18*, 99.

- (19) Sinn, H.; Kaminsky, W.; Vollmer, H. J.; Woldt, R. *Angew. Chem., Int. Ed.* **1980**, *19*, 390-392.
- (20) Kaminsky, W.; Arndt, M. *Adv. Polym. Sci.* **1997**, *127*, 143.
- (21) Giannetti, E.; Nicoletti, G.; Mazzocchi, R. *J. Polym. Sci. Polym. Chem.* **1985**, *23*, 2117.
- (22) Kaminsky, W. *Macromol. Chem. Phys.* **1996**, *197*, 3907-3945
- (23) Ewen, J. A. *J. Am. Chem. Soc.* **1984**, *106*, 6355.
- (24) Kaminsky, W.; K lper, K.; Brintzinger, H.; Wild, F. *Angew. Chem., Int. Ed.* **1985**, *24*, 507.
- (25) Brintzinger, H. H.; Fischer, D.; M lhaupt, R.; Rieger, B.; Waymouth, R. M. *Angew. Chem., Int. Ed.* **1995**, *34*, 1143-1170.
- (26) De Rosa, C.; Auriemma, F.; Di Capua, A.; Resconi, L.; Guidotti, S.; Camurati, I.; Nifant'ev, I. E.; Laishevtsev, I. P. *J. Am. Chem. Soc.* **2004**, *126*, 17040-17049.
- (27) Britovsek, G. J. P.; Gibson, V. C.; Wass, D. F. *Angew. Chem. Int. Ed.* **1999**, *38*, 428-447.
- (28) Canich, J. A. M.; Turner H. W. (Exxon) WO-A 92/12162, **1992** [*Chem. Abstr.* **1993**, *118*, 81615j].
- (29) Stevens, J. C.; Timmers, F. J.; Wilson, D. R.; Schmidt, G. F.; Nickias, P. N.; Rosen, R. K.; Knight, G. W.; Lai, S.-Y. (Dow Chemical Co.) EP-B 0416815, **1990** [*Chem. Abstr.* **1991**, *115*, 93163m].
- (30) Chen, Y.-X.; Marks T. J. *Organometallics* **1997**, *16*, 3649-3657.
- (31) Emrich, R.; Heinemann, O.; Jolly, P. W.; Kr ger, C.; Verhovnik, G. P. J. *Organometallics* **1997**, *16*, 1511.
- (32) Johnson, L. K.; Killian, C. M.; Brookhart, M. *J. Am. Chem. Soc.* **1995**, *117*, 6414-6415.
- (33) Britovsek, G. J. P.; Gibson, V. C.; Kimberley, B. S.; Maddox, P. J.; McTavish, S. J.; Solan, G. A.; White, A. J. P.; Williams, D. J. *Chem. Commun.* **1998**, 849-850.

- (34) Small, B. L.; Brookhart, M.; Bennett, A. M. A. *J. Am. Chem. Soc.* **1998**, *120*, 4049.
- (35) Szwarc M. *J. Polym. Sci., Part A: Polym. Chem.* **1998**, *36*, IX–XV.
- (36) Muller, A. H. E.; Matyjaszewski, K. *Controlled and Living Polymerizations: From Mechanisms to Applications*, **2009**, Wiley-VCH Verlag GmbH & Co. KGaA
- (37) Webster, O. W. *Science* **1991**, *251*, 887-893.
- (38) Szwarc, M. *Nature* **1956**, *178*, 1168-1169.
- (39) Szwarc, M.; Levy, M.; Milkovich, R. *J. Am. Chem. Soc.* **1956**, *78*, 2656-2657.
- (40) Hsieh H. L.; Quirk R. P. *Anionic Polymerization: Principles and Practical Applications*, Marcel Dekker, New York, **1996**.
- (41) Matyjaszewski, K. *Cationic Polymerizations: Mechanisms, Synthesis, and Applications*, Marcel Dekker, New York, **1996**.
- (42) Hawker, C. J.; Bosman, A. W.; Harth, E.; *Chem. Rev.* **2001**, *101*, 3661-3688.
- (43) Kamigaito, M.; Ando, T.; Sawamoto, M.; *Chem. Rev.* **2001**, *101*, 3689-3746.
- (44) Braunecker, W. A.; Matyjaszewski, K. *Prog. Polym. Sci.* **2007**, *32*, 93-146.
- (45) Wang, J.-S.; Matyjaszewski, K. *J. Am. Chem. Soc.* **1995**, *117*, 5614-5615.
- (46) Kato, M.; Kamigaito, M.; Sawamoto, M.; Higashimura, T. *Macromolecules* **1995**, *28*, 1721-1723.
- (47) Matyjaszewski, K.; Xia, J. H.; *Chem. Rev.* **2001**, *101*, 2921-2990.
- (48) Chiefari, J.; Chong, Y. K.; Ercole, F.; Krstina, J.; Jeffery, J.; Le, T. P. T.; Mayadunne, R. T. A.; Meijs, G. F.; Moad, C. L.; Moad, G.; Rizzardo, E.; Thang, S. H. *Macromolecules* **1998**, *31*, 5559-5562.
- (49) Lowe, A. B.; McCormick, C. L. *Prog. Polym. Sci.* **2007**, *32*, 283-351.
- (50) Bielawski, C. W.; Grubbs, R. H. *Prog. Polym. Sci.* **2007**, *32*, 1-29.
- (51) Coates, G. W.; Hustad, P. D.; Reinartz, S. *Angew. Chem., Int. Ed.* **2002**, *41*, 2236-2257.

- (52) Quirk, R. P.; Lee, B. *Polym. Int.* **1992**, *27*, 359-367.
- (53) Matyjaszewski, K. *J. Phys. Org. Chem.* **1995**, *8*, 197-207.
- (54) Domski, G. J.; Rose, J. M.; Coates, G. W.; Bolig, A. D.; Brookhart, M. *Prog. Polym. Sci.* **2007**, *32*, 30-92.
- (55) Resconi, L.; Cavallo, L.; Fait, A.; Piemontesi, F. *Chem. Rev.* **2000**, *100*, 1253-1345.
- (56) Chen, E. Y. X.; Marks, T. J. *Chem. Rev.* **2000**, *100*, 1391-1434.
- (57) Doi, Y.; Ueki, S.; Keii, T. *Macromolecules* **1979**, *12*, 814-819.
- (58) Doi, Y.; Watanabe, Y.; Ueki, S.; Soga, K. *Makromol. Chem. Rapid Commun.* **1983**, *4*, 533-537.
- (59) Doi, Y.; Keii, T. *Adv. Polym. Sci.* **1986**, *73-4*, 201-248.
- (60) Doi, Y.; Murata, M.; Soga, K. *Makromol. Chem. Rapid Commun.* **1984**, *5*, 811-814.
- (61) Doi, Y.; Hizal, G.; Soga, K. *Makromol. Chem.* **1987**, *188*, 1273-1279.
- (62) Ueki, S.; Furuhashi, H.; Murakami, N.; Murata, M.; Doi, Y. *Stud. Surf. Sci. Catal.* **1995**, *92*, 359-362.
- (63) Ueki, S.; Doi, Y.; Keii, T. *Makromol. Chem. Rapid Commun.* **1981**, *2*, 403-406.
- (64) Doi, Y.; Ueki, S.; Keii, T. *Makromol. Chem. Rapid Commun.* **1982**, *3*, 225-229.
- (65) Doi, Y.; Koyama, T.; Soga, K. *Makromol. Chem. Macromol. Chem. Phys.* **1985**, *186*, 11-15.
- (66) Scollard, J. D.; McConville, D. H. *J. Am. Chem. Soc.* **1996**, *118*, 10008-10009.
- (67) Scollard, J. D.; McConville, D. H.; Payne, N. C.; Vittal, J. J. *Macromolecules* **1996**, *29*, 5241.
- (68) Baumann, R.; Davis, W. M.; Schrock, R. R. *J. Am. Chem. Soc.* **1997**, *119*, 3830-3831.
- (69) Mehrkhodavandi, P.; Schrock, R. R. *J. Am. Chem. Soc.* **2001**, *123*, 10746-10747.

- (70) Jayaratne, K. C.; Sita, L. R. *J. Am. Chem. Soc.* **2000**, *122*, 958.
- (71) Keaton, R. J.; Jayaratne, K. C.; Fettinger, J. C.; Sita, L. R. *J. Am. Chem. Soc.* **2000**, *122*, 12909.
- (72) Tshuva, E. Y.; Goldberg, I.; Kol, M.; Weitman, H. Goldschmidt, Z. *Chem. Commun.* **2000**, 379-380.
- (73) Tshuva, E. Y.; Goldberg, I.; Kol, M. *J. Am. Chem. Soc.* **2000**, *122*, 10706-10707.
- (74) Matsui, S.; Tohi, Y.; Mitani, M.; Saito, J.; Makio, H.; Tanaka, H.; Nitabaru, M.; Nakano, T.; Fujita, T. *Chem. Lett.* 1999, 1065.
- (75) Matsui, S.; Mitani, M.; Saito, J.; Tohi, Y.; Makio, H.; Tanaka, H.; Fujita, T. *Chem. Lett.* 1999, 1263.
- (76) Tian, J.; Coates, G. W. *Angew. Chem., Int. Ed.* **2000**, *39*, 3626-3629.
- (77) Tian, J.; Hustad, P. D.; Coates, G. W. *J. Am. Chem. Soc.* **2001**, *123*, 5134-5135.
- (78) Jayaratne, K. C.; Keaton, R. J.; Henningsen, D. A.; Sita, L. R. *J. Am. Chem. Soc.* **2000**, *122*, 10490-10491.
- (79) Zhang, Y.; Keaton, R. J.; Sita, L. R. *J. Am. Chem. Soc.* **2003**, *125*, 9062-9069.
- (80) Sita, L. R. *Angew. Chem. Int. Ed.* **2009**, *48*, 2464-2472.
- (81) Harney, M. B.; Zhang, Y.; Sita, L. R. *Angew. Chem., Int. Ed.* **2006**, *45*, 2400-2404.
- (82) Harney, M. B.; Zhang, Y.; Sita, L. R. *Angew. Chem., Int. Ed.* **2006**, *45*, 6140.
- (83) Giller, C.; Gururajan, G.; Wei, J.; Zhang, W.; Hwang, W.; Chase, D. B.; Rabolt, J. F.; Sita, L. R. *Macromolecules* **2011**, *44*, 471-482.
- (84) Britovsek, G. J. P.; Cohen, S. A.; Gibson, V. C.; Maddox, P. J.; Van Meurs, M. *Angew. Chem., Int. Ed.* **2002**, *41*, 489-491.
- (85) Kempe, R. *Chem. Eur. J.* **2007**, *13*, 2764-2773.

- (86) Ziegler, K.; Gellert, H. G.; Kühnhorn, H.; Martin, H.; Meyer, K.; Nagel, K.; Sauer, H.; Zosel, K. *Angew. Chem.* **1952**, *64*, 323-329.
- (87) Ziegler, K. *Adv. Organomet. Chem.* **1968**, *6*, 1-17.
- (88) Zhang, W.; Sita, L. R. *J. Am. Chem. Soc.* **2008**, *130*, 442-443.
- (89) Zhang, W.; Wei, J.; Sita, L. R. *Macromolecules* **2008**, *41*, 7829-7833.
- (90) Britovsek, G. J. P.; Cohen, S. A.; Gibson, V. C.; van Meurs, M. *J. Am. Chem. Soc.* **2004**, *126*, 10701-10712.
- (91) Kretschmer, W. P.; Bauer, T.; Hessen, B.; Kempe, R. *Dalton Trans.* **2010**, *39*, 6847-6852.
- (92) Pelletier, J.-F.; Mortreux, A.; Olonde, X.; Bujadoux, K. *Angew. Chem., Int. Ed. Engl.* **1996**, *35*, 1854-1856.
- (93) Rogers, J. S.; Bazan, G. C. *Chem. Commun.* **2000**, 1209-1210.
- (94) Bazan, G. C.; Rogers, J. S.; Fang, C. C. *Organometallics* **2001**, *20*, 2059-2064.
- (95) Ganesan, M.; Gabba i F. P. *Organometallics* **2004**, *23*, 4608-4613.
- (96) Mani, G.; Gabba i F. P. *Angew. Chem., Int. Ed.* **2004**, *43*, 2263-2266.
- (97) Arriola, D. J.; Carnahan, E. M.; Hustad, P. D.; Kuhlman, R. L.; Wenzel, T. T. *Science* **2006**, *312*, 714-719.
- (98) Hustad, P. D.; Kuhlman, R. L.; Arriola, D. J.; Carnahan, E. M.; Wenzel, T. T. *Macromolecules* **2007**, *40*, 7061-7064.
- (99) Hustad, P. D.; Marchand, G. R.; Garcia-Meitin, E. I.; Roberts, P. L.; Weinhold, J. D. *Macromolecules* **2009**, *42*, 3788-3794.
- (100) Müller, A. H. E.; Zhuang, R.; Yan, D.; Litvinenko, G. *Macromolecules* **1995**, *28*, 4326-4333.
- (101) Ziegler, K.; Krupp, F.; Zosel, K. *Angew. Chem.* **1955**, *67*, 425-426.

- (102) Wagner, J. D.; Lappin, G. R.; Zietz, J. R. In *Kirk-Othmer Encyclopedia of Chemical Technology*; Wiley: New York, **1991**; Vol. 1, p 865-913.
- (103) Vogt, D. In *Applied Homogeneous Catalysis with Organometallic Compounds*; Cornils, B., Herrmann, W. A., Eds.; VCH: New York, **1996**; Vol. 1, p 245-258.
- (104) *Alpha Olefins Applications Handbook* (Eds.: Lappin, G. R.; Sauer, J. D.), Marcel Dekker, New York, **1989**.
- (105) Wilke, G. *Angew. Chem. Int. Ed.* **2003**, *42*, 5000-5008.
- (106) Negishi, E.; Kondakov, D. Y.; Choueiry, D.; Kasai, K.; Takahashi, T. *J. Am. Chem. Soc.* **1996**, *118*, 9577-9588.
- (107) Resconi, L.; Piemontesi, F.; Franciscano, G.; Abis, L.; Fiorani, T. *J. Am. Chem. Soc.* **1992**, *114*, 1025.
- (108) Barsties, E.; Schaible, S.; Prosenc, M.-H.; Rief, U.; Roell, W.; Weyand, O.; Dorer, B.; Brintzinger, H.-H. *J. Organomet. Chem.* **1996**, *520*, 63.
- (109) Naga, N.; Mizunuma, K. *Polymer* **1998**, *39*, 5059.
- (110) Leino, R.; Luttikhedde, H. J. G.; Lehmus, P.; Wilen, C.-E.; Sjoeholm, R.; Lehtonen, A.; Seppaelae, J. V.; Naesman, J. H. *Macromolecules* **1997**, *30*, 3477.
- (111) Kim, I.; Choi, C.-S. *J. Polym. Sci., Part A: Polym. Chem.* **1999**, *37*, 1523.
- (112) Lieber, S.; Brintzinger, H.-H. *Macromolecules* **2000**, *33*, 9192.
- (113) Lahelin, M.; Kokko, E.; Lehmus, P.; Pitkaenen, P.; Loefgren, B.; Seppaelae, J. *Macromol. Chem. Phys.* **2003**, *204*, 1323.
- (114) Kukral, J.; Lehmus, P.; Klinga, M.; Leskela, M.; Rieger, B. *Eur. J. Inorg. Chem.* **2002**, 1349.
- (115) Cai, Z.; Shigemasa, M.; Nakayama, Y.; Shiono, T. *Macromolecules* **2006**, *39*, 6321.

- (116) Alfano, F.; Boone, H. W.; Busico, V.; Cipullo, R.; Stevens, J. C. *Macromolecules* **2007**, *40*, 7736.
- (117) Knap, J. E.; Leech, R. E.; Reid, A. J.; Tamplin, W. S. *Ind. Eng. Chem.* **1957**, *49*, 874-879.
- (118) Greenwood, N. N.; Earnshaw, A. *Chemistry of the Elements*, Pergamon, New York, **1984**.
- (119) Akzo Nobel Technical Bulletin, OMS 03.322.04/August **2008**.
- (120) Hupe, E.; Knochel, P.; Szabó, K. J. *Organometallics* **2002**, *21*, 2203-2207.
- (121) Hupe, E.; Calaza, M. I.; Knochel, P. *Chem. Eur. J.* **2003**, *9*, 2789-2796.
- (122) Fabicon, R. M.; Richey, Jr. H. G. *Organometallics* **2001**, *20*, 4018-4023.
- (123) Bochmann, M.; Lancaster, S. J. *Angew. Chem. Int. Ed.* **1994**, *33*, 1634.
- (124) Bochmann, M.; Lancaster, S. J. *J. Organomet. Chem.* **1992**, *434*, C1.
- (125) Amin, S. B.; Marks, T. J. *Angew. Chem., Int. Ed.* **2008**, *47*, 2006-2025.
- (126) Yanjarappa, M. J.; Sivaram, S. *Prog. Polym. Sci.* **2002**, *27*, 1347-1398.
- (127) Kawahara, N.; Saito, J.; Matsuo, S.; Kaneko, H.; Matsugi, T.; Kashiwa, N. *Adv. Polym. Sci.* **2008**, *217*, 79-119.
- (128) Boen, N. K.; Hillmyer, M. A. *Chem. Soc. Rev.* **2005**, *34*, 267
- (129) Mülhaupt, R. *Macromol. Chem. Phys.* **2003**, *204*, 289.
- (130) Tsubaki, S.; Jin, J.; Sano, T.; Uozumi, T. Soga, K. *Macromol. Chem. Phys.* **2001**, *202*, 1757-1760.
- (131) Shiono, T.; Kurosawa, H.; Soga, K. *Macromolecules* **1994**, *27*, 2635-2637.
- (132) Shiono, T.; Kurosawa, H.; Ishida, O.; Soga, K. *Macromolecules* **1993**, *26*, 2085-2089
- (133) Yi, Q.; Fan, G.; Wen, X.; Dong, J. Y.; Han, C. C. *Macromol. React. Eng.* **2009**, *3*, 91-100.

- (134) Chung, T. C. *Prog. Polym. Sci.* **2002**, *27*, 39-85.
- (135) Han, C. J.; Lee, M. S.; Byun, D. J.; Kim, S. Y. *Macromolecules* **2002**, *35*, 8923-8925.
- (136) Kuo, J.; Lin, W.; Yu, C.; Tsai, J.; Wang, T.; Chuang, T.; Ho, R. *Macromolecules* **2008**, *41*, 7967-7977.
- (137) Tzeng, F.; Lin, M.; Wu, J.; Kuo, J.; Tsai, J.; Hsiao, M.; Chen, H.; Cheng, S. Z. D. *Macromolecules* **2009**, *42*, 3073-3085.
- (138) Kaneyoshi, H.; Inoue, Y.; Matyjaszewski, K. *Macromolecules* **2005**, *38*, 5425-5435.
- (139) Li, T.; Wang, W.; Liu, R.; Liang, W.; Zhao, G.; Li, Z.; Wu, Q.; Zhu, F. *Macromolecules* **2009**, *42*, 3804-3810
- (140) Briquel, R.; Mazzolini, J.; Le Bris, T.; Boyron, O.; Boisson, F.; Delolme, F.; D'Agosto, F.; Boisson C.; Spitz, R. *Angew. Chem., Int. Ed.* **2008**, *47*, 9311-9313.
- (141) Mazzolini, J.; Espinosa, E.; D'Agosto, F.; Boisson C. *Polym. Chem.* **2010**, *1*, 793-800.
- (142) Mazzolini, J.; Mokthari, I.; Briquel, R.; Boyron, O.; Delolme, F.; Monteil, V.; Bertin, D.; Gigmes, D.; D'Agosto, F.; Boisson C. *Macromolecules* **2010**, *43*, 7495-7503.
- (143) Labet, M.; Thielemans, W. *Chem. Soc. Rev.* **2009**, *38*, 3484-3504.
- (144) Stridsberg, K. M.; Ryner M.; Albertsson, A. C. *Adv. Polym. Sci.* **2002**, *157*, 41-65.
- (145) Khanna, A.; Sudha, Y.; Pillai S.; Rath, S. *J. Mol. Model.* **2008**, *14*, 367-374.
- (143) Labet, M.; Thielemans, W. *Chem. Soc. Rev.* **2009**, *38*, 3484-3504.
- (144) Stridsberg, K. M.; Ryner M.; Albertsson, A. C. *Adv. Polym. Sci.* **2002**, *157*, 41-65.
- (145) Khanna, A.; Sudha, Y.; Pillai S.; Rath, S. *J. Mol. Model.* **2008**, *14*, 367-374.
- (146) Szwarc, M. *Acc. Chem. Res.* **1969**, *2*, 87.
- (147) Kraus, C. A. *J. Phys. Chem.* **1956**, *60*, 129.
- (148) Bjerrum, N. K. *Dan. Vldensk. Selesk. Math. Phys. Medd.* **1926**, *7*, 3.

- (149) Macchioni, A. *Chem. Rev.* **2005**, *105*, 2039-2073
- (150) Bochmann, M. *J. Organomet. Chem.* **2004**, *689*, 3982-3998
- (151) Massey, A. G.; Park, A. J. *J. Organomet. Chem.* **1964**, *2*, 245.
- (152) Yang, X.; Stern, C. L.; Marks, T. J. *J. Am. Chem. Soc.* **1994**, *116*, 10015-10031
- (153) Yang, X.; Stern, C. L.; Marks, T. J. *Organometallics* **1991**, *10*, 840-842.
- (154) Mohammed, M.; Nele, M.; Al-Humydi, A.; Xin, S.; Stapleton, R. A.; Collins, S.; *J. Am. Chem. Soc.* **2003**, *125*, 7930-7941
- (155) Li, H.; Stern, C. L.; Marks, T. J. *Macromolecules* **2005**, *38*, 9015-9027
- (156) Song, F.; Lancaster, S. J.; Cannon, R. D.; Schormann, M.; Humphrey, S. M.; Zuccaccia, C.; Macchioni, A.; Bochmann, M.; *Organometallics* **2005**, *24*, 1315-1328
- (157) Roberts, J. A. S.; Chen, M. C.; Seyam, A. M.; Li, L.; Zuccaccia, C.; Stahl, N. G.; Marks, T. J. *J. Am. Chem. Soc.* **2007**, *129*, 12713-12733
- (158) Alonzo-Moreno, C.; Lancaster, S. J.; Wright, J. A.; Hughes, D. L.; Zuccaccia, C.; Correa, A.; Macchioni, A.; Cavallo, L.; Bochmann, M. *Organometallics* **2008**, *27*, 5474-5487.
- (159) Reybuck, S. E.; Lincoln, A. L.; Ma, S.; Waymouth, R. M. *Macromolecules* **2005**, *38*, 2552-2558
- (160) Chen, Y. X.; Metz, M. V.; Li, L.; Stern, C. L.; Marks, T. J. *J. Am. Chem. Soc.* **1998**, *120*, 6287-6305
- (161) Reybuck, S. E.; Meyer, A.; Waymouth, R. M. *Macromolecules* **2002**, *35*, 637-643
- (162) Spitz, R.; Florin, A.; Guyot, A. *Eur. Polym. J.* **1979**, *15*, 441-444.
- (163) Randall, J. C. *Polymer Sequence Determination*; Academic Press: New York, **1977**.
- (164) Cozewith, C. *Macromolecules* **1987**, *20*, 1237-1244
- (165) Seger, M. R.; Maciel, G. E. *Anal. Chem.* **2004**, *76*, 5734-5747

- (166) Wei, J.; Sita, L. R. *PMSE Prepr.* **2009**, *101*, 1757-1759
- (167) Byrd, H. C. M.; Lin-Gibson, S.; Bencherif, S.; Vanderhart, D. L.; Beers, K. L.; Bauer, B. J.; Fanconi, B. M.; Guttman, C. M.; Wallace, W. E. *Polym. Mater. Sci. Eng.* **2003**, *88*, 80-81
- (168) Guttman, C. M.; Flynn, K. M.; Wallace, W. E.; Kearsley, A. J. *Macromolecules* **2009**, *42*, 1695-1702.
- (169) Willemse, R. X. E.; Staal, B. B. P.; Donkers, E. H. D.; van Herk, A. M. *Macromolecules* **2004**, *37*, 5717-5723
- (170) Montaudo, G.; Samperi, F.; Montaudo, M. S. *Prog. Polym. Sci.* **2006**, *31*, 277-357
- (171) Crecelius, A. C.; Baumgaertel, A.; Schubert, U. S. *J. Mass Spectrom.* **2009**, *44*, 1277-1286.
- (172) Knuuttila, H.; Lehtinen, A.; Nummila-Pakarinen, A. *Adv. Polym. Sci.* **2004**, *169*, 13-27.
- (173) Severn, J. R.; Chadwick, J. C.; Duchateau, R.; Friederichs, N. *Chem. Rev.* **2005**, *105*, 4073-4147.
- (174) Busico, V. *Macromol. Chem. Phys.* **2007**, *208*, 26-29.
- (175) Pérez, E.; Benavente, R.; Quijada, R.; Narváez, A.; Galland, G. B. *J. Polym. Sci. B: Polym. Phys.* **2000**, *38*, 1440-1448.
- (176) Quijada, R.; Narváez, A.; Pizzol, M. D.; Liberman, S.; Filho, A. A.; Galland, G. B. *J. Appl. Polym. Sci.* **2001**, *79*, 221-227.
- (177) Starck, P.; Löfgren, B. *Eur. Polymer J.* **2002**, *38*, 97-107.
- (178) Kaminsky, W.; Piel, C.; Scharlach, K. *Macromol. Symp.* **2005**, *226*, 25-34.
- (179) Starck, P.; Löfgren, B. *Eur. Polymer J.* **2002**, *38*, 97-107.
- (180) Stadler, F. L.; Takahashi, T.; Yonetake, K. *Eur. Polymer J.* **2011**, *47*, 1048-1053.
- (181) henschke, O.; Knorr, J.; Arnold, M. *J. M. S. Pure Appl. Chem.* **1998**, *35*, 473-481.

- (182) Subramanyam, U.; Sivaram, S. *J. Polym. Sci. Part A: Polym. Chem.* **2007**, *45*, 191-210.
- (183) Walter, P.; Trinkle, S. Suhm, J.; Mäder, D.; Friedrich, C.; Mülhaupt, R. *Macromol. Chem. Phys.* **1900**, *201*, 604-612.
- (184) Piel, C.; Starck, P.; Seppälä J. V.; Kaminsky, W. *J. Polym. Sci. Part A: Polym. Chem.* **2006**, *44*, 1600-1612.
- (185) Leino, R.; Luttikhedde, H. J. G.; Lehmus, P.; Wilén, C.; Sjöholm, R.; Lehtonen, A.; Seppälä J. V.; Näsman, J. H. *Macromolecules* **1997**, *30*, 3477-3483.
- (186) Lehmus, P.; Härkki, O.; Leino, R.; Luttikhedde, H. J. G.; Näsman, J. H.; Seppälä J. V. *Macromol. Chem. Phys.* **1998**, *199*, 1965-1972.
- (187) Lehmus, P.; Kokko, E.; Härkki, O.; Leino, R.; Luttikhedde, H. J. G.; Näsman, J. H.; Seppälä J. V. *Macromolecules* **1999**, *32*, 3547-3552.
- (188) Yoon, J. S.; Lee, D. H.; Park, E. S.; Lee, I. M.; Park, D. K.; Jung, S. O. *J. Appl. Polym. Sci.* **2000**, *75*, 928-937.
- (189) Kakinuki, K.; Fujiki, M.; Nomura, K. *Macromolecules* **2009**, *42*, 4585-4595.
- (190) Kotzabasakis, V.; Kostakis, K.; Pitsikalis, M.; Hadjichristidis, N.; Lohse, D. J.; Mavromoustakos, T.; Potamitis, C. *J. Polym. Sci. Part A: Polym. Chem.* **2009**, *47*, 4314-4325.
- (191) Mannaborworn, M.; Prasertdam, P.; Jongsomjit, B. *Molecules*, **2011**, *16*, 373-383.
- (192) Ullmann's Encyclopedia of Industrial Chemistry, 5<sup>th</sup>, **1985**, A28.
- (193) Sperling, L. H. *Introduction to Physical Polymer Science*, 4<sup>th</sup> ed, John Wiley & Sons, Inc., Hoboken, New Jersey, **2006**, p3.
- (194) Henschke, O.; Knorr, J.; Arnold, M. *J. Macromol. Sci. Pure. Appl. Chem.* **1998**, *A35*, 473-481.

- (195) Killian, C. M.; Tempel, D. J.; Johnson, L. K.; Brookhart, M. *J. Am. Chem. Soc.* **1996**, *118*, 11664-11665
- (196) Bates, F. S. *Science* **1991**, *251*, 898-905.
- (197) Ruzette, A. V.; Leibler, L. *Nat. Mater.* **2005**, *4*, 19-31.
- (198) Furuyama R.; Mitani M.; Mohri J.; Mori R.; Tanaka H.; Fujita T. *Macromolecules* **2005**, *38*, 1546-1552.
- (199) Gottfried A. C.; Brookhart M. *Macromolecules* **2003**, *36*, 3085-3100.
- (200) Yuan J. C.; Silva L. C.; Gomes P. T.; Valerga B.; Campos J. M.; Ribeiro M. R. *Polymer* **2005**, *46*, 2122-2132.
- (201) Turner H. W.; Hlatky G. G. (Exxon) PCT Int Appl WO 9421700.
- (202) Busico V.; Cipullo R.; Friederichs N.; Ronca S.; Togrou M. *Macromolecules* **2003**, *36*, 3806-3808.
- (203) Mitani M.; Mohri J.; Yoshida Y.; Saito J.; Ishii S.; Tsuru K. *J. Am. Chem. Soc.* **2002**, *124*, 3327-36.
- (204) Delfero, M.; Marks, T. J. *Chem. Rev.* **2011**, *111*, 2450-2485.
- (205) Abramo, G. P.; Li, L.; Marks, T. J. *J. Am. Chem. Soc.* **2002**, *124*, 13966.
- (206) Noh, S. K.; Kim, S.; Yang, Y.; Lyoo, W. S.; Lee, D. H. *Eur. Polym. J.* **2004**, *40*, 227.
- (207) Sierra, J. C.; Hüerl änder, D.; Hill, M.; Kehr, G.; Erker, G.; Fröhlich, R. *Chem.—Eur. J.* **2003**, *9*, 3618.
- (208) Li, H.; Stern, C. L.; Marks, T. J. *Macromolecules* **2005**, *38*, 9015.
- (209) Li, L.; Metz, M. V.; Li, H.; Chen, M.-C.; Marks, T. J.; Liable-Sands, L.; Rheingold, A. L. *J. Am. Chem. Soc.* **2002**, *124*, 12725.
- (210) Li, H.; Li, L.; Marks, T. J. *Angew Chem., Int. Ed.* **2004**, *43*, 4937.
- (211) Zhang, W.; Sita, L. R. *Adv. Synth. Catal.* **2008**, *350*, 439-447.

(212) Stephens, C. H.; Poon, B. C.; Ansems, P.; Chum, S. P.; Hiltner, A.; Baer, E. *J. Appl. Polym. Sci.* **2006**, *100*, 1651-1658.

(213) Poon, B.; Rogunova, M.; Hiltner, A.; Baer, E. *Macromolecules* **2005**, *38*, 1232-1243.